

Design, functionalization strategies and biomedical applications of targeted biodegradable/biocompatible polymer-based nanocarriers for drug delivery

Julien Nicolas,* Simona Mura, Davide Brambilla, Nicolas Mackiewicz and Patrick Couvreur

Design and functionalization strategies for multifunctional nanocarriers (e.g., nanoparticles, micelles, polymersomes) based on biodegradable/biocompatible polymers intended to be employed for active targeting and drug delivery are reviewed. This review will focus on the nature of the polymers involved in the preparation of targeted nanocarriers, the synthesis methods to achieve the desired macromolecular architecture, the selected coupling strategy, the choice of the homing molecules (vitamins, hormones, peptides, proteins, etc.), as well as the various strategies to display them at the surface of nanocarriers. The resulting morphologies and the main colloidal features will be given as well as an overview of the biological activities, with a special focus on the main *in vivo* achievements.

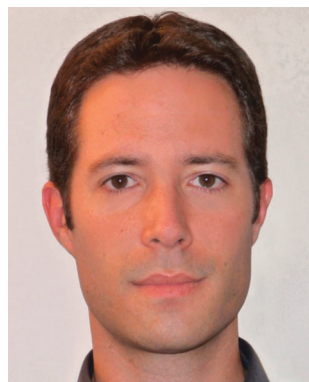
Cite this: *Chem. Soc. Rev.*, 2013, **42**, 1147

Received 16th July 2012

DOI: 10.1039/c2cs35265f

www.rsc.org/csr

Institut Galien Paris-Sud, UMR CNRS 8612, Univ Paris-Sud, Faculté de Pharmacie, 5 rue Jean-Baptiste Clément, F-92296 Châtenay-Malabry cedex, France.
E-mail: julien.nicolas@u-psud.fr; Fax: +33 1 46 83 55 11; Tel: +33 1 46 83 58 53



Julien Nicolas

Dr Julien Nicolas graduated from the Ecole Supérieure de Chimie Organique et Minérale (ESCOM), France, in 2001. He completed his PhD in 2005 under the supervision of Prof. Bernadette Charleux at the University Pierre and Marie Curie, Paris, where he studied nitroxide-mediated polymerization in homogeneous and aqueous dispersed media. He then joined the group of Prof. David M. Haddleton at the

University of Warwick, UK, for a postdoctoral fellowship to design polymer-protein bioconjugates by controlled/living radical polymerization. In 2007, he was appointed permanent CNRS researcher in the group of Prof. Patrick Couvreur, University Paris-Sud, France, where his current research activities are focused on controlled/living radical polymerization techniques and on the synthesis of novel biomaterials and functionalized, biodegradable nanoparticles for active targeting and cell imaging purposes. He is (co)author of more than 50 peer review articles in international journals, 4 patents and 7 book chapters.



Simona Mura

Dr Simona Mura gained the degree in Pharmaceutical Chemistry and Technology in 2005. In 2009, she was awarded her PhD in Chemistry and Technology of Drug at the University of Cagliari, Italy, working on the design and in vitro evaluation of novel vesicular systems for the topical delivery of drugs. In 2008 she joined the group of Pr. Elias Fattal (UMR CNRS 8612) at University Paris-Sud, Châtenay-

Malabry, France, as a post-doctoral research assistant to study the lung toxicity of biodegradable nanoparticles designed for pulmonary administration of drugs. In 2011 she was appointed Associate Professor within the framework of the << CNRS-Higher Education chairs >> program, in the group of Pr. Patrick Couvreur (UMR CNRS 8612) at University Paris-Sud, Châtenay-Malabry, France. Her research focuses on the assessment of the therapeutic activity of novel nanoparticulate systems and biopolymers for the treatment of severe neoplastic diseases.

1. Introduction

In the recent years, significant achievements have been witnessed in the field of nanotechnology, especially in material science, electronics, photonics, supramolecular assemblies and drug delivery. In particular, the medical application of nanotechnologies, usually termed nanomedicine,^{1–6} has given a crucial impulse to the development of various types of drug-loaded nanocarriers, such as liposomes, nanoparticles, micelles *etc.* A great deal of effort is now focused on the engineering of nanoparticulate systems able to serve

as efficient diagnostic and/or therapeutic tools against severe diseases, such as cancer, infectious or neurodegenerative disorders.^{7–24}

Among the numerous classes of materials employed for drug delivery purposes, colloidal systems based on polymers have attracted much attention due to the flexibility offered by macromolecular synthesis methods, the almost infinite diversity of polymers in terms of nature, properties and composition, and their ease of functionalization.^{3,7–10,12–15,25–27} Polymer-based, engineered colloids represent one of the most promising opportunities for *in vivo* diagnosis and treatment of many diseases. Indeed, the possibility to load them with a drug (which can also be covalently linked to the polymer) and to functionalize them with specific ligands, intended to be recognized by receptors overexpressed at the surface of particular cells (*e.g.*, cancer cells, brain endothelial cells *etc.*), paved the way to the so-called active targeting.^{25,27–28}

The successful design of targeted nanocarriers is usually governed by the nature of the polymer and the ligand, as well as by the selected coupling reaction. So far, a plethora of ligation strategies have been developed, each of them exhibiting benefits and drawbacks. Hence, these constructions represent a subtle equilibrium between organic chemistry, macromolecular synthesis, physico-chemistry and pharmaceutical science.

The present review will detail the different steps to construct functionalized nanoparticulate systems based on biodegradable/biocompatible polymers for targeted drug delivery (Fig. 1). More precisely, it will focus on the nature of the polymer employed for the preparation of targeted nanocarriers, the synthesis method



Davide Brambilla

Dr Davide Brambilla obtained his MSc in Experimental Medicine with honors at the University of Milano-Bicocca, Italy, in 2008. Then he moved to France in the group of Patrick Couvreur at the University of Paris-Sud where he completed his PhD in 2012. Since June 2012 he has been a post-doc in the group of Drug Formulation and Delivery headed by Prof. Jean-Christophe Leroux at the Swiss Federal Institute of Technology (ETH Zurich). In

2012 he got the ETH-VPFW/Marie Curie Post-Doctoral Fellowship. His main research interest is focused on the design of smart, brain-targeted delivery systems against Alzheimer's disease.



Nicolas Mackiewicz

Dr Nicolas Mackiewicz graduated from the Ecole Centrale Marseille (ECM), France, in 2004. He obtained his PhD in 2007 under the supervision of Prof. Charles Mioskowski at the Institute of Biology and Technologies (CEA), Paris, where he studied carbon nanotubes functionalization and potential new applications. Then, he joined the group of Dr Frederic Ducongé at the Institute of Biomedical Imaging (CEA), for

a postdoctoral fellowship to design polymerized micelles for in vivo diagnosis. In 2009, he moved to the group of Prof. Patrick Couvreur, University Paris-Sud, France, for another postdoctoral fellowship in collaboration with the pharmaceutical company Sanofi on the synthesis of novel biodegradable nanoparticles for active targeted drug delivery and imaging. In 2012, he moved to Switzerland as a R&D project manager at Vestergaard-Frandsen, to work in the field of disease control textiles to prevent and fight pests associated diseases such as malaria.



Patrick Couvreur

Prof. Patrick Couvreur is Full Professor of Pharmacy at the University Paris-Sud and holder of the chair of "Innovation Technologique" (2009–2010) at the "Collège de France". He is appointed as a Senior Member of the "Institut Universitaire de France". Prof. Couvreur's contributions in the field of drug delivery and targeting are highly recognized around the world. The major scientific contribution of Patrick Couvreur to the

Pharmaceutical Sciences is also recognized by numerous international awards, including the "2004 Pharmaceutical Sciences World Congress Award" (Kyoto, Japan), the prestigious "Host Madsen Medal" (Beijing, 2007), and very recently the "European Pharmaceutical Scientist Award" (European Federation of Pharmaceutical Sciences). In 2009, he was also awarded by the "Prix Galien", the highest French distinction in therapeutics. He has been appointed as a member of four academies (Académie des Technologies, Académie de Médecine, Académie de Pharmacie in France, and Académie Royale de Médecine in Belgium).

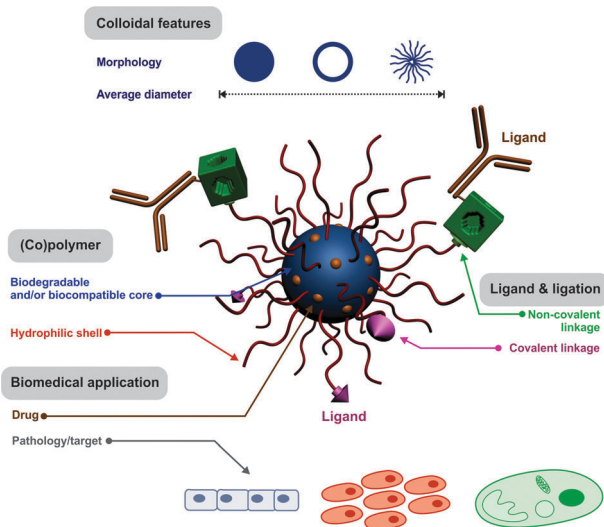


Fig. 1 Design of targeted nanoparticulate systems.

to achieve the desired macromolecular architecture, the selected coupling strategy, the choice of the homing devices (vitamins, hormones, peptides, proteins, *etc.*), as well as the various strategies to display them at the surface of nanocarriers without altering their colloidal properties. The resulting morphologies and the main colloidal features will be given as well as a general discussion about the biological activities, with a special focus on the main achievements that have been reported *in vivo*.

2. Morphology and preparation of nanocarriers

Nanoparticulate systems are colloidal-sized particles, with diameters ranging from 1 to 1000 nm. A wide variety of nanocarriers composed of different materials including lipids, polymers and inorganic materials have been developed, resulting in delivery systems that vary in their physicochemical properties and thus in their applications (Fig. 2). The following sections will describe the most used polymer-based nanoparticulate systems for drug delivery and targeting purposes.

2.1. Nanocarrier morphologies

In this review, we will focus our attention on polymer-based nanocarriers. In this regard, three classes of polymer-based

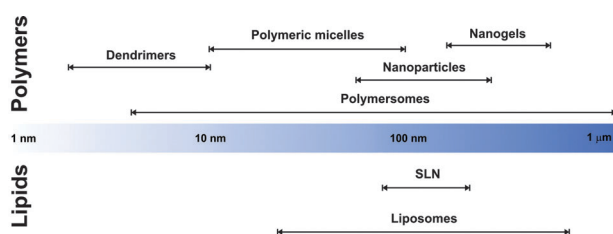


Fig. 2 Lipid and polymer-based nanoparticulate systems used in the field of drug delivery and active targeting.

colloidal systems will be discussed: (i) nanoparticles, (ii) polymeric micelles and (iii) polymersomes. The reader who would like more details about all other nanoparticulate systems (*e.g.*, liposomes, solid lipid nanoparticles, *etc.*) is referred to the adequate reviews.^{29,30} It is noteworthy that due to intense research effort in the field, most of these systems can be easily engineered, which makes them easily adjustable in terms of size, surface charge, drug loading, release mechanism, *etc.*

2.1.1. POLYMERIC MICELLES. Polymeric micelles belong to a group of nanosized colloids that can be formed by self-assembly of amphiphilic block copolymers in aqueous solution.³¹ The hydrophobic core region serves as a reservoir for hydrophobic drugs, whereas the hydrophilic shell region stabilizes the hydrophobic core, making the particle an appropriate candidate for *i.v.* administration.³² They typically present the so-called core-shell morphology and exhibit average diameters in the 5–100 nm range.³³ Contrary to nanoparticles, polymeric micelles are characterized by a critical micelle concentration (CMC). Therefore, upon dilution below the CMC, micelles disassemble into free unimers.³⁴ Nonetheless, polymeric micelles mainly show low CMC values, which make them relatively insensitive to dilution, thus leading to enhanced circulation times.³² Micelles appear to be the most advanced nanoparticulate systems for clinical trials³³ and proved already to be a relevant approach for the delivery of hydrophobic drugs and DNA, with the possibility to be functionalized by many different ligands.³⁵

2.1.2. NANOPARTICLES. Nanoparticles (NPs) are solid colloidal systems in which the drug is physically dispersed, dissolved, or chemically bounded to the polymer chains.³⁶ Depending on the method employed for their preparation, either nanospheres or nanocapsules can be obtained. Nanospheres are matrix-like systems in which the drug is dispersed within the polymer chains. On the contrary, nanocapsules are vesicular systems which are formed by a drug-containing liquid core (aqueous or lipophilic) surrounded by a single polymeric membrane.³⁷ Nanocapsules may thus be considered as a “reservoir” system. The advantage of NPs results from the ability to incorporate hydrophobic drugs at concentrations greater than their intrinsic water solubility.³⁸ Polymeric nanoparticles offer a very wide range of possibilities to greatly modify their composition, their surface (in order to have an impact on the drug loading), their circulation time or the drug release.²⁵

2.1.3. POLYMERSOMES. Polymersomes are reservoir-like systems but are opposed to nanocapsules regarding the nature of the polymer membrane, which is composed, in that case, of self-assembled amphiphilic block copolymers. They are biomimetic analogs of natural phospholipids and can be formed with sizes ranging from tens of nanometers to tens of micrometers with relatively high control of the size distribution.³⁹ The hydrophobic blocks of each copolymer tend to associate with each other in order to minimize direct exposure to water, whereas the hydrophilic blocks face inner and outer aqueous solutions and thereby delimit the two interfaces of a typical bilayer membrane.⁴⁰ The membrane is the key feature of this kind of nanocarrier. It serves to partition aqueous volumes with different compositions and concentrations, based on its selective permeability to hydrophobic

and hydrophilic molecules.⁴¹ Polymersomes have the advantage of allowing for both the encapsulation of hydrophilic components in their aqueous cavities and encapsulation of hydrophobic molecules within their membranes.⁴² The successful use of targeted polymersomes for the delivery of a wide variety of drugs will be detailed in the following chapters of this review.

2.2. Preparation methods

Several strategies can be employed in order to produce targeted nanocarriers for drug delivery. A (co)polymer can be modified with a targeting ligand either before nanocarrier formation or after by coupling it at the surface of preformed nanocarriers. The choice of the preparation method for nanocarriers mainly depends on the employed polymeric materials. For the self-assembly of (co)polymers in aqueous solution, the emulsion–solvent evaporation process and the nanoprecipitation technique are often described. When natural polymers such as albumin (BSA and HSA), gelatin or gliadin are employed, the desolvation process is the preferred method.

2.2.1. SELF-ASSEMBLY OF PREFORMED (CO)POLYMERS. Self-assembly of preformed (co)polymers is the most convenient method to prepare various nanoparticulate morphologies (*e.g.*, nanoparticles, micelles). Self-assembly of block copolymers in solution is driven by the different affinity, also referred to as block selectivity, of the solvent to each block of the copolymer. The specific size and morphology of such self-assembled structures is driven largely by thermodynamic forces.⁴³ Among the different methods that have been proposed so far, two of them are widely used: (i) the emulsion–solvent evaporation process and (ii) the nanoprecipitation technique (also called the solvent diffusion method).

The emulsion–solvent evaporation process is based on the emulsification (*e.g.*, ultra-sounds, microfluidizer *etc.*) of non-water-miscible organic solutions of a hydrophobic drug and preformed polymers into an aqueous phase containing surfactants in order to obtain nano-sized organic solvent droplets that serve as a template for nanocarrier assembly. The organic solvent is subsequently removed under reduced pressure (Fig. 3).^{44–46} To encapsulate hydrophilic drugs, a double emulsion (water-in-oil-in-water) is formed with the drug dissolved in the internal aqueous phase.

Although the emulsion–evaporation process is a widely employed technique, it usually leads to poor encapsulation yields of hydrophilic drugs.⁷ For that matter, the technique

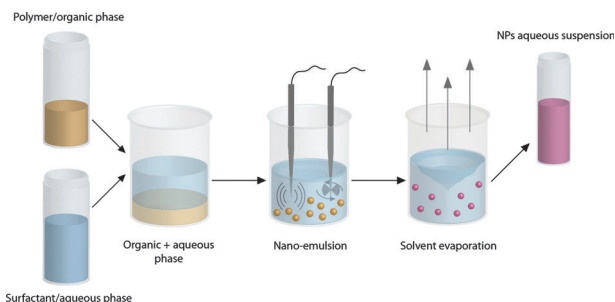


Fig. 3 Preparation of polymeric nanocarriers by emulsion–solvent evaporation.

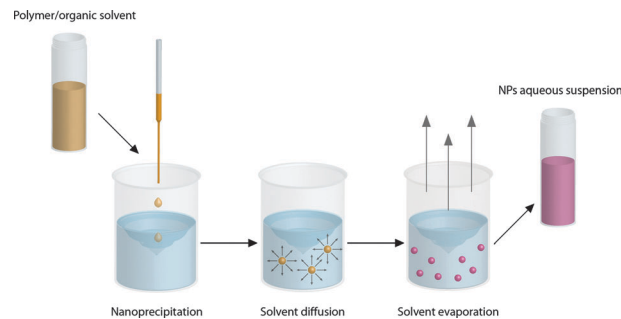


Fig. 4 Preparation of polymeric nanocarriers by nanoprecipitation.

has to be adapted with a double emulsion process. Several factors can affect the release rate of the entrapped drug such as the nanocarrier size (larger particles have a smaller initial burst release and longer sustained release than smaller particles) and the drug loading (the higher the drug loading is, the greater the burst and the faster the release rate).⁴⁷

The nanoprecipitation technique requires two solvents that are miscible. Ideally, both the polymer and the drug must be soluble in the first one (the solvent), but not in the second system (the non-solvent). Nanoprecipitation occurs by a rapid desolvation of the polymer when the polymer solution is added to the non-solvent (Fig. 4).^{48–50} Indeed, as soon as the polymer-containing solvent has diffused into the dispersing medium, the polymer precipitates, involving immediate drug entrapment. The rapid nanoparticle formation is governed by the so-called Marangoni effect, which is due to interfacial turbulences that take place at the interface of the solvent and the non-solvent and result from complex and cumulated phenomena such as flow, diffusion and surface tension variations. In contrast to emulsion–solvent evaporation, no surfactants are necessary and a broad variety of benign solvents, such as DMSO or acetone, can be used.

Another widely-employed nanocarrier formulation pathway from preformed (co)polymer is the dialysis method. In this process, the (co)polymer is dissolved in a water-miscible organic solvent and introduced into a dialysis tube. Nanocarriers are then formed upon dialysis against water.⁵¹

In order to form nanoparticles from polysaccharides, the gelation method is usually employed.⁵² In this process, polysaccharides are dissolved in water or in weak acidic medium (chitosan) and added dropwise under constant stirring to counterion solutions. Due to the complexation between oppositely charged species, polysaccharides undergo ionic gelation and precipitate into spherical (nano)particles. The nanoparticles are removed by filtration, washed with distilled water and dried. The gelation method is very simple and is performed under mild conditions. In addition, reversible physical cross-linking by electrostatic interaction instead of chemical cross-linking avoids the potential toxicity of reagents and other undesirable side effects.

The strong influence of the preparation method of polymeric micelles on the particle size, drug loading and release has been highlighted by Tyrell *et al.*⁵³ Yokoyama *et al.* studied

the drug loading efficiency of camptothecin in poly(ethylene glycol)-*block*-poly(aspartic acid) (PEG-*b*-Asp) micelles according to three different preparation methods: dialysis, oil-in-water (O/W) emulsion and solution casting. The drug loadings were found to increase from 1% to 26% to 58% respectively. When sonication was applied in conjunction with the dialysis and emulsion methods, the drug loading efficiencies increased up to 45% and 37%, respectively.⁵⁴ The solvent can also have an impact on the drug loading for a given polymer. By using a solvent evaporation process for the loading of amiodarone in poly(ϵ -caprolactone)-*block*-poly(ethylene glycol) (PCL-*b*-PEG) micelles, it was shown that acetone gave a significantly higher drug loading, compared to chloroform (87% vs. 67%).⁵⁵

For the preparation of polymersomes, a complete study reported by Mora-Huertas *et al.* gave a detailed overview of the different parameters influencing the particle size, drug loading and other factors.⁵⁶ For this kind of nanocarriers, nanoprecipitation is valued for the simplicity of its procedure, low cost, reproducible carrier size and high encapsulation efficiency. However, when the emulsion-evaporation method is employed, parameters such as the type and the volume of the organic and aqueous phases, as well as the nature and quantity of surfactants and polymers have relevant effects on particle size distribution. In addition, this parameter can be controlled by the intensity and duration of the emulsification process. The drug loading efficiency is mainly directed by the chemical nature of the drug itself and in particular its polarity. For instance, hydrophilic drugs can reach maximum encapsulation values of about 10%, whereas hydrophobic drugs can reach an encapsulation efficiency higher than 70%.⁵⁶ The drug release is governed by numerous factors, such as: (i) the conditions of the preparation method; (ii) the concentration and the physico-chemical characteristics of the active substance (particularly its solubility and oil/water partition coefficient); (iii) the nature, the degradability, the molecular weight and the concentration of the polymer, the polymer solid microstructure when re-precipitated; (iv) the nature of the oil; (v) the nanocapsule size and (vi) the conditions of the *in vitro* release test (medium pH, temperature, contact time, among others).

2.2.2. DESOLVATION OF PROTEINS. This method is applied for the design of protein-based nanoparticles and was originally developed by Marty *et al.*⁵⁷ It relies on particle formation in aqueous solution by a coacervation process and a subsequent stabilization by a cross-linking agent. The key for this approach is to use a desolvation factor such as natural salts or alcohol which should be slowly added to an aqueous protein solution. The protein ternary structure is then altered and when a certain degree of desolvation is reached, protein aggregates are formed. These aggregates are then stabilized with cross-linking agents such as glutaraldehyde or glyoxal (Fig. 5). In order to obtain dispersed protein-based nanoparticles, the turbidity has to be finely monitored to avoid particle accumulation. This process has been further optimized mainly for albumin and gelatin nanoparticles, in terms of reproducibility, colloidal features and control of surface-available amino groups.^{58,59}

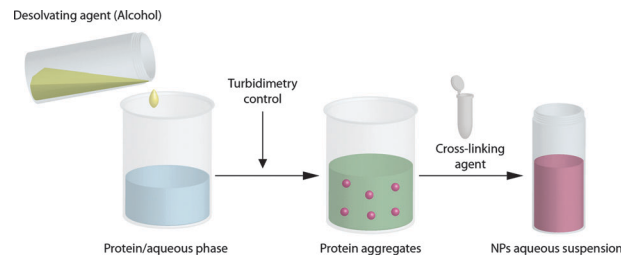


Fig. 5 Synthesis of protein-based nanoparticles by the desolvation process.

3. Design of targeted nanocarriers

3.1. Towards targeted drug delivery systems

Since Paul Ehrlich, who won the Nobel Prize for Medicine in 1908, suggested the concept of “magic bullet”: a drug that selectively destroys diseased cells but is not harmful to healthy cells,⁶⁰ a great deal of research has attempted to reach that goal, for instance for the treatment of cancer.⁶¹ In the field of tumor physiology, a crucial step forward was achieved with the discovery of the enhanced permeability and retention (EPR) effect,^{62–65} that allows for passive tumor targeting. This explains why the PEGylation strategy (*i.e.*, the covalent linkage of poly(ethylene glycol) (PEG) chains to a substrate) appeared to be a key nanotechnological advance, allowing PEGylated nanocarriers to exhibit a prolonged circulation time, thus leading to an increased opportunity to reach its site of action. This approach was employed for the preparation of drug-loaded PEGylated liposomes with doxorubicin that became the first therapeutic nanomedicine to reach the market with the FDA approval of DOXIL in 1995.⁶⁶ For polymer nanocarriers, Paclitaxel-loaded poly(lactic acid)-*block*-poly(ethylene glycol) (PLA-*b*-PEG) micelles (Genexol-PM) were marketed in 2007.⁶⁷ Nevertheless, the EPR effect is not suited for low vascular permeability cancers (*e.g.*, pancreatic cancer) and the occurrence of the so-called “accelerated blood clearance (ABC) phenomenon” (repeated injections of PEGylated liposomes may lose their long-circulating characteristic due to the production of anti-PEG IgM induced by the first dose)⁶⁸ explains the urgent need for targeted drug delivery systems able to selectively recognize specific cells or tissues. The first examples deriving from such strategy were described in 1980 with the development of ligand-conjugated liposomes. Since then, many researchers and companies worked on the design of even more efficient drug delivery by active targeting.^{25,31,61,69}

3.2. General considerations about ligation strategies

In order to perform active targeting, the strategy is to position, at the periphery of the nanoconstruct, a biologically active ligand that will interact with the surrounding biological environment. The active targeting is achieved by molecular recognition of the targeted cells/tissues by various signature molecules overexpressed at the diseased site either *via* the ligand–receptor, antigen–antibody interactions or by targeting by means of aptamers. When bio(macro)molecules such as peptides represent the target, a similar strategy is employed

by using molecules or antibodies with specific affinity toward the targeted peptides.

The ligand can either be linked to the (co)polymer prior to self-assembly into the resulting ligand-decorated nanocarrier or directly coupled at the surface of preformed nanocarriers in aqueous solutions. The choice of the synthetic route is usually governed by the size of the ligand to be attached to: whereas small ligands (*e.g.*, small organic molecules or small peptides) can be linked either to the copolymer prior to nanocarrier formation or at the surface of preformed nanocarriers, the linkage of bulky ligands (*e.g.*, polypeptides, proteins or antibodies) occurs, but not exclusively,⁷⁰ *via* the second pathway for self-assembly and hydrophilic/lipophilic balance reasons. This pathway is also preferred because the secondary structure of proteins and antibodies can be denatured by solubilization in organic solvents.⁷¹

An undeniable advantage of conjugating the ligand prior to nanocarrier formation relies on the possibility to control the reaction yield and to thoroughly characterize the resulting conjugate by routine methods. Consequently, by its simple mix with the non-conjugated (co)polymer, it is then possible to tune the density of ligands on the surface of the nanocarriers, and therefore to control the binding efficiency for a given target. This is of high importance regarding the so-called multivalency feature of the nanocarriers.⁷² However, a drawback of this method lies in the fact that the physicochemical properties of the original copolymer will be altered, especially with (bio)macromolecules. Indeed, after ligands conjugation, the hydrophilic/hydrophobic balance will be changed together with the charge and therefore the conditions to obtain nanocarriers will need to be adapted.

When conjugation occurs after the nanocarrier formation, some difficulties may arise from its purification and chemical characterization. Indeed, purification processes such as centrifugation, dialysis or filtration can degrade/modify the nanocarriers. Besides, proving the covalent linkage will necessitate more advanced surface characterization methods (*e.g.*, XPS, ToF-SIMS) whereas NMR can appear limited.⁷³ Surface characterization using surface plasmon resonance (SPR) spectroscopy can also be employed but will lead to indirect proofs and will not give the possibility to distinguish between covalent linkage or simple adsorption.

Several studies compared both approaches using small peptides as a ligand, but led to opposite results.^{74,75}

3.3. Ligands employed for targeted delivery

A broad range of ligands have been used for targeted nanocarriers and belong to the families of small molecules, carbohydrates, peptides, proteins or antibodies (Table 1).

3.3.1. SMALL MOLECULES. Molecular ligands are often readily available, inexpensive, easy to handle, to be chemically modified and to be characterized. Among biologically active small molecules, vitamins such as folic acid (FA, vitamin B9),^{76,77} and biotin (vitamin B7)⁷⁸ are widely employed for the targeting of cancer cells. Indeed, FA binds with a low affinity to the reduced folate carrier virtually present in all cells, but with a high

affinity (in the nanomolar range) to the glycosylphosphatidylinositol-linked folate receptor, which exhibits very limited distribution but is overexpressed at the surface of many types of cancer cells including ovarian, breast, brain, and lung cancer cells.⁷⁹ The expression levels in tumors have been reported to be 100–300 times higher than those observed in normal tissues.⁸⁰ In the case of biotin, which is a cell growth promoter, its content in tumors is significantly higher than in normal tissue. Due to the rapid proliferation of cancer cells, a higher quantity of biotin is needed, and therefore, biotin receptors are often overexpressed on their surface.⁸¹ Biotin has also the advantage of binding to (strept)avidin with an extremely high affinity constant and this feature is commonly employed to link (strep)avidin-antibody constructs at the surface of biotinylated nanocarriers. Cobalamin (vitamin B12), known to promote the intestinal adsorption of associated molecules, was recently employed for the development of an oral delivery system of insulin in order to bypass subcutaneous administration drawbacks.⁸²

Other small molecules such as curcumin, selegilin, selectin or alendronate have also been used as targeting ligands. Curcumin, a major component of the yellow curry spice turmeric, presents potential anti-inflammatory, antioxidant, anti-ischemic, antiarthritic and anticancer properties.⁸³ It is also able to bind the β -amyloid peptide (A β) and to disaggregate A β plaques, as well as to prevent fibril and oligomer formation, which is of great interest in the field of Alzheimer's disease.^{84–86} Selegiline, a methamphetamine derivative able to selectively inhibit monoamine oxidase-B (MAO-B), is clinically employed for the treatment of Parkinson's disease⁸⁷ and has shown interesting properties for management of AD.⁸⁸ Moreover, selegiline also displays high affinity for the amyloid peptide, a key molecule in AD etiology. Selectin was used to target P-selectin and E-selectin, whose expression levels on endothelial cells are highly increased during inflammation.^{89,90} Targeting of hydroxyapatite for treatment of bone disease was achieved using alendronate as ligand.⁹¹

Although the use of small molecules as biologically active ligands is a convenient route towards targeted nanocarriers, their main downside comes from their relatively nonselective interaction.⁹² For instance, folate can indeed bind to some non-target tissues. In addition, vitamins are present in diets and can be found in significant levels in body fluids. Therefore, the free vitamin can compete for binding with the targeted nanocarriers. Structure–activity relationships of A β -aggregation using curcumin derivatives revealed that subtle changes in the curcumin structure led to severe variations of activity.⁹³

3.3.2. CARBOHYDRATES. Similarly to small molecules, carbohydrates are often readily available, inexpensive to manufacture and sugar chemistry is sufficiently well-known to allow their efficient modification and characterization. Most carbohydrate molecules used for targeting purposes (*e.g.*, galactose, lactose, mannose) bind specifically to asialoglycoprotein receptors (ASGPR), which are membrane lectin receptors commonly found in liver cells.⁹⁴ In this view, carbohydrates are interesting ligands to target hepatic and cervical cancer cells.^{95,96} Interaction of glucose and lactose with lectins was investigated to

Table 1 Structures/schemes of biologically active ligands used for targeted nanocarrier synthesis

Ligand	Structure/scheme	Pathology	Receptor(s)/target(s)	Ref.
Small molecules				
Folic acid (FA), also known as vitamin B9		Cancer	Folate receptor	76, 77
Biotin, also known as vitamin B7		Cancer	Biotin receptor (MCF7, M109 cells)	78
Cobalamin (VB12)		Intestine adsorption	Ileocyte of intestine	82
Selegiline		Neurodegenerative diseases (PD, AD)	Amyloid-beta peptide	189
Curcumin		Cancer, AD	Amyloid-beta peptide	85, 86
Selectin		Pathological inflammation	Activated endothelium	89, 90
Alendronate		Bone diseases	Hydroxyapatite (major component of bones and teeth)	91
ACUPA	<i>S,S</i> ,2-[(5-amino-1-carboxypentyl)-ureido]pentanedioic acid	Cancer	PMSA	187
Carbohydrates				
Galactose		Cancer	Asialoglycoprotein receptor	95
Galactosamine		Cancer	Asialoglycoproteins receptor	95

Table 1 (continued)

Ligand	Structure/scheme	Pathology	Receptor(s)/target(s)	Ref.
Glucose		Bioadhesion	Lectins	97
Lactose		Bioadhesion	Lectins	97
Mannose		Bioadhesion	Lectins, mannose receptor	99
Mannan	Polymer of mannose	Immunization	Mannose receptor	98
Hyaluronan		Cancer	CD44	100
Glycyrrhizin		Hepatic cancer	Specific binding sites on hepatocytes membrane	102
TMC (trimethylated chitosan)		CNS delivery	Negatively charged membranes and extracellular lectins	103
Sialic acid		CNS delivery	Siglec family (sialoadhesin) receptor	104
Peptides and proteins				
Octreotide (OCT)		Cancer	Somatostatin receptor	108

Table 1 (continued)

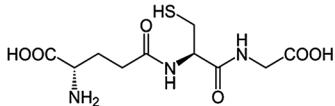
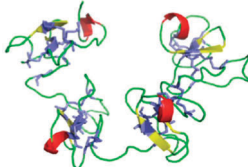
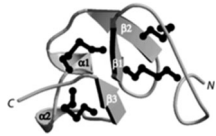
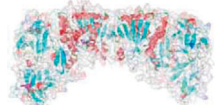
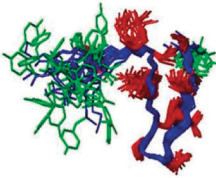
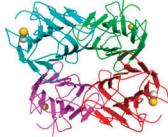
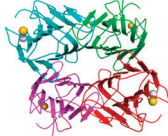
Ligand	Structure/scheme	Pathology	Receptor(s)/target(s)	Ref.
Glutathione		Membrane translocation	Tight junctions	114
WGA		Bioadhesion/cancer	<i>N</i> -Acetylglucosamine	
Solanum tuberosum lectin		CNS delivery	<i>N</i> -Acetylglucosamine	
RCA (<i>Ricinus communis</i> -120)		Bioadhesion/cancer	Galactose/ <i>N</i> -acetylgalactosamine	109–113
Odorranalectin		CNS delivery	<i>L</i> -fucose	
Con A		Infectious disease, Cancer	Con A receptor	
UEA I		Infectious disease, Cancer	Lectin UEA I receptor	
RGD peptides	GRGDS CRGDKGPDC (iRGD) Cyclo(RGDDYK)C (cyclic RGD, cRGD) Cyclo(RGDDFK) (cRGDfk) RGD4C RGD-peptidemimetic	Cancer	$\alpha_v\beta_3$ integrin receptor	115–117
K 273 peptide	HTMYHHYQHHL	Cancer	VEGF	120
TAT (CPP)	GRKKRRQRRRPQ	—	Cell membrane (translocation)	122, 123
mHph1 (CPP)	CHHHHHYARVRRRGRPRRHHHHHC	—	Cell membrane (translocation)	124
mAP (CPP)	CHHHHHRQIKIWFQNRMRMKWKHHHHHC	—	Cell membrane (translocation)	125
SynB	RGGRLSYSRRRFSTSTGR	CNS delivery	BBB (crossing <i>via</i> a caveolae-independent pathway)	128
Lyp-1 peptide	CCGNKRTRGC	Cancer	Tumor cells and tumor lymphatic vessels endothelial cells	131
LCP (lung cancer targeting peptide)	RGDLATLRQL	Cancer	$\alpha_v\beta_6$ integrins	132
XRT-cells peptide	GIRLRG	Cancer	GRP78	133
Injured vessels peptide	KLWVLPK	Injured vasculature	Collagen IV	134

Table 1 (continued)


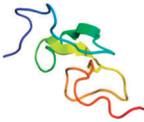
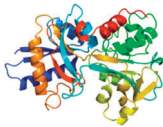
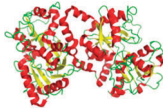
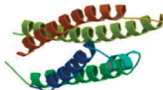
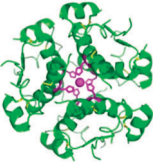
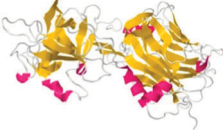
Ligand	Structure/scheme	Pathology	Receptor(s)/target(s)	Ref.
EGF1		Thrombolysis	Tissue factor	135
AP peptide	CRKRLDNR	Atherosclerosis/ cancer	IL4 receptor	136
Pep I peptide	CHVLWSTRC	Autoimmune type 1 diabetes	Pancreatic islet microvessels	137
M-cell homing peptide	CKSTHPLSC	Vaccination	Peyer's patch follicle	138
EGF		Cancer	Epidermal growth factor receptor (EGFR)	139
GE11 peptide	YHWYGYTPQNV	Cancer	Epidermal growth factor receptor (EGFR)	140
c LABL peptide	Cyclo-(1,12)-PenITDGEATDSGC	Cancer	ICAM-1	141
Transferrin (Tf)		Cancer, brain delivery	Transferrin receptor (TfR)	142, 143
Lactoferrin (Lf)		Brain delivery	Lactoferrin receptor (LfR)	144
g7 Peptide	H ₂ N-GFTGFLS(O-β-D-glucose)-CONH ₂	CNS delivery	BBB	145, 146
Similopioid peptides	H ₂ N-GFTGFLX-CONH ₂ X = S-OH, S(O-β-D-glucose), S(O-β-D-galactose), S(O-β-D-xylose), S(O-β-D-lactose)	CNS delivery	BBB	145, 146
CDX peptides	FKESWREARGTRIERG (CDX) SWREARGTRI (Pocket_CDX) CFKESWREARGTRIERGC (Cyclo_CDX)	CNS delivery	Nicotine acetylcholine receptors (nAChR)	147
Angiopep-2 TGN peptide	TFFYGGSRGKRNNFKTEEY TGNYKALHPHNG	CNS delivery/cancer CNS delivery	LRP BBB	148, 149 150
ApoE3, A-I, B-100		CNS delivery	LDL receptor (BBB)	151
Insulin		CNS delivery	Insulin receptor	152
Tetanus toxin C fragment		Cancer	Neuronal ganglioside clostridial toxin receptor GT1 _b	153
A665 and A666 peptides	LSTHTTESRSMV and LEPRWGFGWWLK	Hearing loss	Prestin receptor	154
Tet1	HLNILSTLWKYR	Hearing loss	Neuronal ganglioside clostridial toxin receptor GT1 _b	155
hNgf EE	CTFVKALTMGKQAAWR	Hearing loss	Tyrosine kinase and p75 neurotrophin receptor	156
DCL peptide	2-[[[5-Amino-1-carbox- ypentyl]carbonyl]amino}pentanedioic acid]	Cancer	PSMA	187

Table 1 (continued)








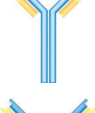




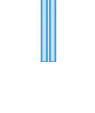





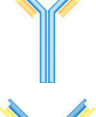
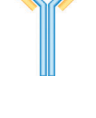

Ligand	Structure/scheme	Pathology	Receptor(s)/target(s)	Ref.
Antibodies				
Anti-CD3 Ab		Cancer	T cell antigen receptor (TCR)	159
Anti HER-2, also called Trastuzumab or Herceptin		Cancer	Human epidermal growth factor receptor 2 (HER2)	160
EGFRMab		Cancer	Epidermal growth factor receptor (EGFR)	161
DI17E6 MAb		Cancer	α_v integrins expressed on tumor and endothelial cells	162
Anti Fas (CD95/Apo-1) MAb		Cancer	Fas (CD95/Apo-1) receptor	163
Anti antigen rich MCF7 cells Mab		Cancer	Soluble membrane proteins of MCF-7 human invasive ductal breast carcinoma	164
AMB8LK Mab		Cancer	H-ferritin	165
Anti CD20 Mab, also called MabThera [®] or Rituximab		Cancer	CD20 tetraspan surface molecule expressed in B lymphocytes	166
Anti CEA Mab		Cancer	CEA	167
Anti A β_{1-42} Mab		Alzheimer's disease	A β_{1-42} peptide	168
29B4		CNS delivery	Insulin receptor	169
OX26		CNS delivery	Transferrin receptor (TfR)	170
R17217		CNS delivery	Transferrin receptor (TfR)	171

Table 1 (continued)

Ligand	Structure/scheme	Pathology	Receptor(s)/target(s)	Ref.
Anti CD44 mAb		CNS delivery	Glial cells	172
Anti NCAM1 mAb		CNS delivery	Neurons	173
Anti CD4 ⁺ Mab		Immunomodulation	T lymphocytes	174
Anti VCAM-1 Mab		Pathological inflammation	Vascular cell adhesion molecules	
Anti ICAM-1 Mab		Pathological inflammation	Intracellular adhesion molecules	175
Anti E-selectin Mab		Pathological inflammation	E-selectin	
Anti P-selectin Mab		Pathological inflammation	P-selectin	
ScFvEGFR	mAb variable fragment of anti-EGFR mAb	Cancer	Epidermal growth factor receptor (EGFR)	176
ScFvCD7	mAb variable fragment of anti-T cells mAb	Infectious disease	T-cell CD7	177
Anti HER2 affibody		Cancer	HER2	180
Aptamers				
A10RNA aptamer	57 base pair nuclease-stabilized 2'-fluoropyrimidine RNA molecule with a single 5'-CG-3' sequence	Cancer	PMSA	182
XEO2 mini aptamer	5'-CAC GAC GCU GAU GGA UCG UUA CGA CUA	Cancer	PMSA	181
2'-O-methyl RNA aptamer	GCA UCG C-3'			
AS1411 DNA aptamer	5'-d(GGTGGTGGTGGTTGGTGGTGGTGG)-3'	Cancer	Nucleolin protein	183

design bioadhesive systems.⁹⁷ In another way, mannose and mannan were used to target mannose receptors at the surface of antigen-presenting cells in order to achieve an improvement of the antigen specific response.^{98,99} Hyaluronan, a polysaccharide, was employed as a ligand for its high affinity to the CD44 receptor in the field of cancer.^{100,101} Glycyrrhizin, one of the main compounds extracted from the root of *Glycyrrhiza glabra* (licorice) was selected to decorate nanocarriers for hepatic targeting.¹⁰² Interaction with the positively charged trimethylated chitosan (TMC) and negatively

charged cell membranes was explored as a strategy to promote the passage across the BBB.¹⁰³ Controlled delivery of drugs to the brain was achieved also by targeting the sialoadhesins receptors with sialic acid residues.¹⁰⁴ Beyond their targeting abilities, another advantage of polysaccharides is the stealth properties they can confer to nanocarriers.¹⁰⁵

3.3.3. PEPTIDES AND PROTEINS. Peptides have numerous benefits in their use as targeting moieties. For instance, their production cost is rather low and they have a high activity per mass unit.

They are also stable; therefore, long-term storage and easy manipulation are possible. Moreover, the associated risk of undesired effects on the immune system is reduced, and their small size is not likely to change the physicochemical properties of the resulting decorated nanocarriers.^{106,107} Besides, their sequence can be modified in order to optimize their biological activity and/or to introduce functional groups.

The octapeptide octreotide (somatostatin analogue) was used to target the somatostatin receptors, largely expressed in tumor tissue.¹⁰⁸ Lectins (*e.g.*, WGA, *solanum tuberosum* lectin, *ricinus communis* lectin, odorranalectin, Con A and UEA-I) are proteins of non-immunological origin able to specifically recognize sugar molecules and bind glycosylated membrane components. They have been used to prepare bioadhesive systems and promote drug delivery following nasal administration or bioavailability of orally administered drugs.^{109–113} Glutathione (GSH), a small tripeptide formed by glutamic acid, cysteine and glycine, was used as a peptide ligand to promote cell adhesion and achieve a permeation-enhancing effect.¹¹⁴

Various (poly)peptides and proteins have also been used as homing devices in the fields of cancer, brain delivery and several other diseases. Among them, the tri-peptide Arg-Gly-Asp (RGD) and its derivatives appeared extremely attractive as tumor and vascular targeting ligands. Indeed, they were shown to bind to the $\alpha_v\beta_3$ integrin receptor which is highly expressed at the surface of malignant cells and in tumor proliferating neovascular endothelial cells while it is minimally expressed in normal quiescent endothelial cells.^{115–117} cRGD has been developed by Kessler *et al.* and its specific binding to $\alpha_v\beta_3$ integrins was 170 times more active than the linear form.^{118,119} The small peptide K237 has been conjugated at the surface of NPs to target the vascular endothelial growth factor receptor (VEGFR).¹²⁰ This peptide enabled a receptor-mediated internalization of functionalized NPs in endothelial cells as well as a therapeutic function by inhibition of the VEGFR signaling pathway to be achieved.

Cell penetrating peptides (CPPs), such as TAT (GRKKRRQRRRPQ, deriving from the transcriptional activator protein encoded by HIV-1), protein transduction domain (PTD) of TAT, mHph1 and mAP represent a specific class of active ligands that actually do not recognize a specific receptor but demonstrate ability in membrane translocation.^{121–127} Therefore, their combination with other ligands has usually been employed in order to achieve selective receptor recognition. The SynB peptides (RGGRLSYSRRRFFSTSTGR) are a family of CPPs that shows charge-mediated blood–brain barrier selectivity occurring *via* a caveolae-independent pathway.¹²⁸

The extensive application of phage display technology has enabled identification of novel peptide sequences that bind with high affinity to specific molecules.^{129,130} These peptides, which allow the number of potential available targets to be increased, have been investigated to functionalize nanocarriers used for the treatment of cancer and other diseases. Among them we can find: (i) the Lyp-1 peptide, which specifically home to tumor and their lymphatics;¹³¹ (ii) the LCP peptide targeted to the $\alpha_v\beta_6$ integrins overexpressed in non-small cells lung

cancer;¹³² (iii) the GIRLRG sequence that recognizes the GRP78 receptors overexpressed by ionizing radiation-treated cells;¹³³ (iv) the KLWVLPK peptide which shows high affinity for the collagen IV;¹³⁴ (v) the EGF1 peptide which interacts with the tissue factor involved in coagulation and thrombus formation;¹³⁵ (vi) the AP peptide that has a specific binding affinity to IL4 receptors;¹³⁶ (vii) the pep I peptide that binds the pancreatic islet microvessel¹³⁷ and (viii) the CKSTHPLSC sequence that specifically recognizes M-cells.¹³⁸

Targeting of the epidermal growth factor receptor (EGFR), whose overexpression is observed in several cancer cells, was achieved using the epidermal growth factor (EGF, natural ligand) as well as specific peptides such as the GE11 peptide.^{139,140} Selective targeting of ICAM-1 was achieved with the cLABEL peptide.¹⁴¹

Due to the overexpression of the transferrin receptor (TfR) both in solid tumors and on the endothelial cells of the blood–brain barrier (BBB), transferrin was used to target cancer cells and to achieve brain delivery.^{142,143} Same results were obtained for the targeting the lactoferrin receptors (LfR) with lactoferrin moieties (Lf).¹⁴⁴ The large variety of peptides which has been explored to enable nanocarriers to pass through the BBB and reach the CNS includes: (i) simi-opioid peptides (g7 peptides) able to bind the opioid receptors;^{145,146} (ii) candotoxin derived peptides (CDX) that bind the nicotine acetylcholine receptors;¹⁴⁷ (iii) the Angiopep-2 which interacts with the low-density lipoprotein receptor-related protein;^{148,149} and (iv) the TGN peptide.¹⁵⁰ CNS delivery was achieved also with apolipoproteins (Apo) such as ApoE3, ApoA-I and ApoB-100, which are also recognized by low-density lipoprotein receptors (LDLR) of the endothelial cells of the BBB.¹⁵¹ BBB crossing can also be performed by using insulin as a ligand in order to target the insulin receptor (IR), which seems to have a 10-fold higher BBB transport efficacy compared to the transferrin receptor.¹⁵²

Efficient targeting to neurons was realized using the tetanus toxin C fragment, which demonstrates high affinity binding to the neuronal ganglioside receptor.¹⁵³

Several peptides were used as targeting ligands for the management of hearing loss: (i) A665 and A666, (ii) Tet1 and (iii) hNgf EE that bind to prestin receptors, neuronal ganglioside receptors (GT1b), and tyrosine kinase receptors as well as p75 neurotrophin receptors, respectively.^{154–156}

3.3.4. ANTIBODIES. Antibodies, which are large Y-shaped proteins, perhaps represent the most efficient ligands due to their high affinities and their ability to recognize a specific part of their target. They were actually the first class of tumor targeting ligands used to deliver drugs encapsulated in micelles.¹⁵⁷ Antibodies are typically made of basic structural units, each with two large heavy chains and two smaller light chains (Fig. 6). Although the general structure of all antibodies is very similar, a small region at the tip of the protein is extremely variable, allowing millions of antibodies with different tip structures, or antigen binding sites, to exist. Even if these ligands are bulky (~ 150 kDa) they can be adapted to specifically bind to a large variety of targets with high affinities ($K_d \sim 0.1$ nM) even with a low density at the surface of

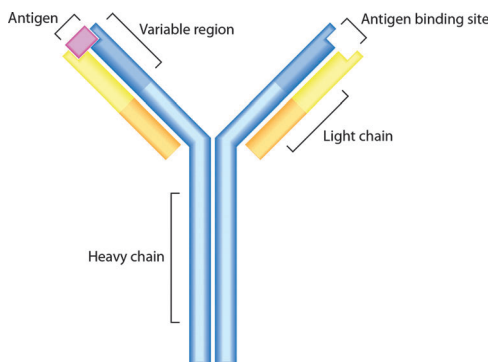


Fig. 6 General structure of an antibody.

nanocarriers.⁷⁴ It has indeed been shown that micelles slightly surface modified by antibodies accumulated in tumors, showing a better anti-tumor efficacy.¹⁵⁸

Antibodies-decorated nanoparticulate systems have been employed in the field of cancer (anti-CD3 Mab,¹⁵⁹ anti-HER2 Mab (also called trastuzumab or Herceptin),¹⁶⁰ EGFR Mab,¹⁶¹ DI17E6 Mab,¹⁶² anti FAS Mab,¹⁶³ anti antigen rich breast cancer cells Mab,¹⁶⁴ AMB8LK Mab,¹⁶⁵ anti-CD20 mAb,¹⁶⁶ anti-CEA Mab¹⁶⁷), Alzheimer's disease (anti-A β ₁₋₄₂ Mab),¹⁶⁸ brain delivery (29B4,¹⁶⁹ OX26,¹⁷⁰ R17217,¹⁷¹ anti-CD44 mAb,¹⁷² anti-NCAM1 Mab¹⁷³) and autoimmune diseases (anti CD4⁺).¹⁷⁴ A specific target to inflamed endothelium (generally observed in various pathological settings such as cancer, cardiovascular disease and arthritis) which is characterized by overexpression of endothelial cell adhesion molecules, was achieved using anti-ICAM-1 Mab, anti VCAM-1 Mab, anti E-selectin Mab as well as anti P-selectin Mab.¹⁷⁵ In some cases, the nanocarriers have been decorated only with variable chains of the Ab, allowing a drastic reduction of total MW and of adverse immune reactions (ScFvEGFR, ScFvCD7).^{176,177}

However, antibodies remain expensive and time-consuming to produce. Although antibody fragments including antigen-binding fragments (Fab), dimers of antigen-binding fragments (F(ab')₂), single-chain fragment variables (scFv) and other engineered fragments are less stable and have a lower binding avidity than whole antibodies (two binding sites), they are considered safer when injected systemically owing to reduced non-specific binding.^{92,178} Under certain conditions, the presence of antibodies at the surface of nanocarriers appeared to compromise the shielding effect of the PEG layer.¹⁷⁹ As an alternative to overcome limitations associated to antibodies, the use of affibody (anti-HER2)¹⁸⁰ was explored.

3.3.5. APTAMERS. Aptamers or mini-aptamers represent another class of efficient ligands for targeted drug delivery, for instance to bind to prostate specific membrane antigen (PSMA) using A10RNA and XEO2,^{181,182} or to nucleolin (AS1411) for the treatment of brain cancer.¹⁸³ Aptamers are short single-stranded DNA or RNA oligonucleotides that can bind specifically to small and large molecule targets. They are identified mainly by *in vitro* screening of a random sequence library (~10¹⁴–10¹⁵) for their binding ability to specific molecular targets.¹⁸⁴ They can be selected to bind to a wide variety of

targets, including intracellular proteins, transmembrane proteins, soluble proteins, carbohydrates, and small molecule drugs.³¹ Even though the selection process is complex, their high binding specificity to their target molecules and their lack of immune response due to their small size make them potential candidate ligands for targeting purposes.¹⁸⁵ A drawback associated to their use is the presence of enzymes that can degrade DNA or RNA in the blood following intravenous administration. However, their initial promise warrants exploration of methodologies that can increase their *in vivo* stability.^{74,186}

High affinity and specificity similar to antibodies and aptamers was also shown by the pseudomimetic dipeptide DCL¹⁸⁷ as well as with the ACUPA molecule (currently evaluated in clinical trials),¹⁸⁸ which were used to selectively bind PSMA.

3.4. Synthetic strategies for targeted nanocarriers

In this section, targeted nanocarriers will be discussed and gathered in different tables according to the nature of the main polymer constituent:

- Polyesters:
 - Poly(lactic acid) and poly(lactic-co-glycolic acid) (Table 2, section 3.4.2.1);
 - Poly(ϵ -caprolactone) (Table 3, section 3.4.2.2);
 - Boltorn H40 (Table 4, section 3.4.2.3);
 - Other polyesters (Table 5, section 3.4.2.4);
- Polysaccharides:
 - Chitosan (Table 6, section 3.4.3.1);
 - Cyclodextrin (Table 7, section 3.4.3.2);
 - Other polysaccharides (Table 8, section 3.4.3.3);
- Poly(amino acid)s, polypeptides and proteins:
 - Poly(amino acid)s and polypeptides (Table 9, section 3.4.4.1);
 - Proteins, (Table 10, section 3.4.4.2);
- Poly(alkyl cyanoacrylate) (Table 11, section 3.4.5).

In each table, the ranking is achieved according to the ligand coupling method and the nature of the employed ligand, which follow the order reported in the ligand table (Table 1). For each case, if the nanoparticulate system is composed of more than one (co)polymer, then each species will be independently described following Roman numerals.

3.4.1. BRIEF OVERVIEW OF MAIN LIGATION STRATEGIES

3.4.1.1. Carbodiimide chemistry. This method is the most used for the ligation of small molecules and biomolecules for targeted drug delivery purposes. The advantage of this strategy is based on its simplicity and on the native presence on both the nanocarriers and the ligand of the required functional groups (*e.g.*, carboxylic acid, amine, *etc.*) to achieve the coupling. This results in a lower probability to lose ligand specific activity.¹⁹⁰ However, the presence of multiple functional groups in the ligand can also represent a drawback in an attempt to limit multi-site attachment or to control the ligand orientation at the surface of the nanocarrier. The *o*-acylisourea intermediate formed during the activation of the carboxylic acid is susceptible to quick hydrolysis.¹⁹¹ Consequently, an excess of carbodiimide must be used to complete the reaction, which can alter the

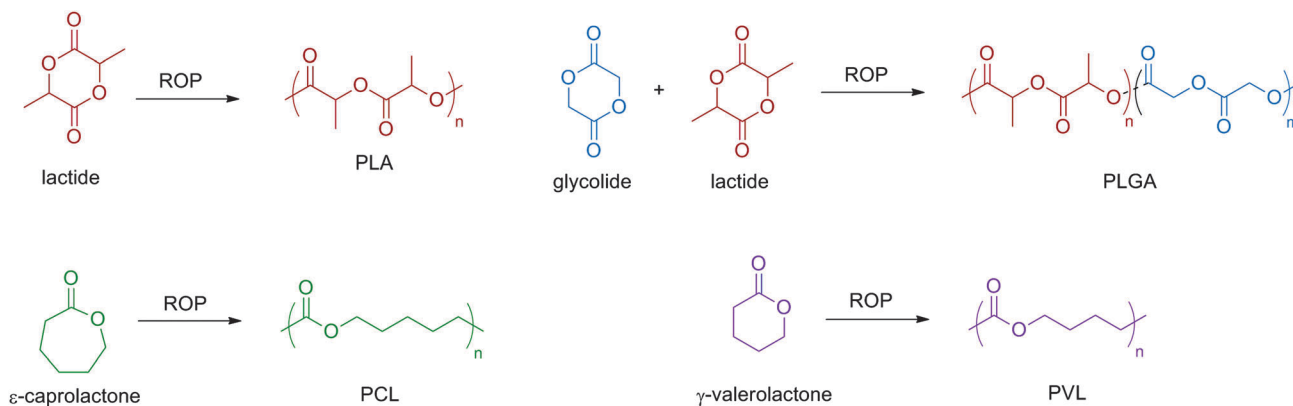


Fig. 7 Synthesis of polylactide (PLA), poly(lactide-co-glycolide) (PLGA), poly(ϵ -caprolactone) (PCL) and poly(γ -valerolactone) (PVL) by ring-opening polymerization (ROP).

colloidal stability of the resulting nanocarriers due to the poor solubility of the *o*-acylisourea. This can be solved using *N*-hydroxysuccinimide (NHS) or *N*-hydroxysulfosuccinimide (sulfo-NHS). The ester intermediate of the latter has a better solubility. Although still susceptible to hydrolysis (which is however slower than the *o*-acylisourea intermediate), NHS-esters usually lead to higher coupling efficiencies.

3.4.1.2. Michael addition. Michael addition, and in particular thiol-maleimide coupling strategy, is the second most used pathway to functionalize nanocarriers. One advantage over carbodiimide coupling is that maleimides exhibit a slower hydrolysis rate than *o*-acylisourea intermediates. Besides, maleimides react with thiols in a highly selective and efficient way at near neutral pH giving a stable thioether bond.¹⁹⁰ Nonetheless, even if native thiol groups are present in some proteins (usually to a low extent), they are hardly accessible or even absent from many others. To circumvent this limitation, thiol groups can be obtained either by reducing existing disulfide bonds (which can be however detrimental for ternary structures of certain peptides/proteins) or by using heterobifunctional cross-linking agents (see Fig. 14).¹⁹² Even if more chemical steps are needed, this coupling strategy enables a better control over biomolecular orientation and mainly avoids issues related to unwanted cross-linking or side reactions.¹⁹³ It also allows the structural, biological and binding properties of a protein to be maintained.¹⁹⁴

3.4.1.3. COPPER-CATALYZED LIGATION METHOD. Copper(I)-catalyzed Huisgen 1,3-dipolar cycloaddition reaction between an azide and an alkyne (CuAAC) recently received tremendous interest in many different fields such as dendrimers, bioconjugates, therapeutics and functionalized polymers.¹⁹⁵ This cycloaddition belongs to the class of chemical reactions, often referred to as click chemistry, that share several very important features: (i) a very high efficiency in terms of both conversion and selectivity; (ii) mild experimental conditions; (iii) a simple workup and (iv) little or no byproducts. The CuAAC ligation method can be used to control the display of biomolecules at the surface of nanocarriers.¹⁹³ The principal drawback of the CuAAC reaction is the necessary removal of the Cu-based catalyst after the coupling.

The use of copper ligands and organic scavengers is however possible to remove most of the catalyst.¹⁹⁶

3.4.1.4. Biotin-(strep)avidin ligation strategy. The biotin-(strep)-avidin ligation strategy is a very advantageous and flexible tool for active targeting. The bond between the two moieties is the strongest non-covalent biological interaction known, with a dissociation constant, K_d , in the order of 4.10^{-14} M. This sandwich strategy can be easily applied in multistep approaches.¹⁹⁷ Furthermore, biotinylated antibodies can be easily obtained¹⁹⁸ and protocols describing the synthesis of (strep)avidin-antibodies have also been reported.¹⁹⁹

3.4.2. POLYESTERS. Polyesters certainly represent the most widely employed family of polymers in this field thanks to their biodegradable and biocompatible features. Among them, one can find polylactide (PLA), polyglycolide (PGA), poly(ϵ -caprolactone) (PCL) and poly(γ -valerolactone) (PVL). They are usually synthesized by ring-opening polymerization (ROP) of lactide (LA), lactide/glycolide (LA/G), ϵ -caprolactone (ϵ CL) and γ -valerolactone (γ VL), respectively (Fig. 7). Noteworthy, copolymers of lactide and glycolide (poly(lactide-co-glycolide), PLGA) have been approved by the Food and Drug Administration (FDA) for drug delivery.

Polyesters mainly undergo bulk erosion and the mechanism of degradation is largely due to hydrolysis of ester functions present in the (co)polymer backbone, eventually leading to water and carbon dioxide as degradation products. Interestingly, by varying the lactide/glycolide ratio, tunable degradation and release rates can be achieved.

3.4.2.1. Poly(lactide) and poly(lactide-co-glycolide). Poly(lactic acid) (L, D or D, L), poly(glycolic acid) and their copolymers poly(lactic-co-glycolic acid) have been largely investigated for drug delivery purposes. In this category amphiphilic PLGA-*b*-PEG or PLA-*b*-PEG copolymers which consist of a hydrophobic PLGA or PLA block and a hydrophilic PEG have been synthesized and employed to formulate nanoparticles, micelles or polymersomes in which the hydrophobic PLGA (or PLA) and the hydrophilic PEG form the core and the shell of the resulting nanocarriers, respectively. In general, these

Table 2 Main characteristics and applications of targeted poly(lactide) and poly(lactide-co-glycolide)-based nanocarriers

Structural parameters			Colloidal parameters			Application				
Architecture	Ligand	Synthetic method	Ligand coupling method	Formulation	Morphology	Diameter (nm)	Pathology/target	Drug	Cells/tissues/organs ^d	Ref.
Ligand coupling by carbodiimide chemistry										
PLA-g3-FA	FA	ROP of LA from 6-arm hydroxy initiator; divergent synthesis	Carbodiimide (FA-NH ₂ + PLA-g3-COOH/DCC/NHS) ^a	Dialysis method	Micelles (dendrimer-like star polymer)	18	Cancer (pharynx)	—	KB	241
(i) PLA-TGPS (ii) TGFS-FA	FA	(i) ROP of LA from TGFS (ii) see ligand coupling method	Carbodiimide (TGFS-COOH/EDC/NHS + FA-NH ₂) ^b	Emulsion-solvent evaporation	Nanoparticles	300–330	Cancer (breast, glioma)	Ptx	MCF7, C6	244
(i) MePEG- <i>b</i> -PLA (ii) TGFS-FA	FA	(i) ROP of LA from MePEG-OH (ii) see ligand coupling method	Carbodiimide (TGFS-COOH/EDC/NHS + FA-NH ₂) ^a	Emulsion-solvent evaporation	Nanoparticles	300	Cancer (cervical, glioma)	Ptx ^c	Hela, C6	245
PLGA- <i>b</i> -PEG-FA	FA	Carbodiimide (PLGA-COOH/DCC/NHS + H ₂ N-PEG-NH ₂) ^a	Carbodiimide (PLGA-PEG-NH ₂ + FA-COOH/DCC) ^a	Emulsion-solvent evaporation	Nanoparticles	120–220	Cancer (ovary)	Dtx	SK-OV-3	217
PLGA/DLPC/ DSPE-PEG/ DSPE-PEG-FA	FA	Carbodiimide (DSPE/H ₂ N-PEG-FA)	Carbodiimide (H ₂ N-PEG-NH ₂ + FA-COOH/DCC/NHS) ^a	Emulsion-solvent evaporation	Nanoparticles	200–300	Cancer (breast)	Dtx	MCF7	218
(i) PLGA (ii) PL- <i>b</i> -PEG-FA	FA	(i) ROP of LA/G (ii) Carbodiimide (PL-L-NH ₂ + FA-PEG-COOH/DCC/NHS)	Carbodiimide (COOH-PEG-NH ₂ + FA-COOH/DCC/NHS) ^b	Emulsion-solvent evaporation; coating (PLGA NPs + PL- <i>b</i> -PEG-FA)	Nanoparticles	110–125	Cancer (pharynx, lung)	—	KB, A549	216
PLA- <i>b</i> -PEI-FA	FA	Carbodiimide (PLA-COOH/DCC + H ₂ N-PEI-NH ₂) ^a	Carbodiimide (PLA- <i>b</i> -PEI-NH ₂ + FA-COOH/DCC/DMAP) ^a	Emulsion-solvent evaporation; coating (PLGA NPs + PL- <i>b</i> -PEG-FA) Polyplex formation with pDNA	Micelles	100	Cancer	pDNA	Hela	239
(i) PLGA (ii) PL- <i>b</i> -PEG-FA	FA	(i) Commercial (ii) Carbodiimide (PL-L-NH ₂ + FA-PEG-COOH/DCC/NHS)	Carbodiimide (COOH-PEG-NH ₂ + FA-COOH/DCC/NHS) ^b	Emulsion-solvent evaporation; coating (PLGA NPs + PL- <i>b</i> -PEG-FA)	Nanoparticles	260	Cancer (pharynx)	Dox	KB	219
(i) P(His-co-Phe)- <i>b</i> -PEG (ii) PLA- <i>b</i> -PEG-FA	FA	(i) NCA polym. of Bz-His-NCA/ <i>L</i> -Phe-NCA; carbodiimide (P(His-co-Phe)-NH ₂ + PEG-COOH/DCC/NHS) (ii) ROP of LA from HOOC-PEG-OH	Carbodiimide (PLA- <i>b</i> -PEG-COOH/DCC/NHS + FA-NH ₂) ^a	Dialysis	Micelles	110–170	Cancer (ovary)	Dox	A2780/DOX ^R , A2780/WT	226
(i) P(His-co-Phe)- <i>b</i> -PEG (ii) PLA- <i>b</i> -PEG-FA	FA	(i) NCA polym. of Bz-His-NCA/ <i>L</i> -Phe-NCA; carbodiimide (P(His-co-Phe)-NH ₂ + PEG-COOH/DCC/NHS) (ii) ROP of LA from HOOC-PEG-OH	(i) Carbodiimide (PLA- <i>b</i> -PEG-COOH/DCC/NHS + FA-NH ₂) ^a (ii) Carbodiimide (PLA- <i>b</i> -PEG-COOH/DCC/NHS + FA-NH ₂) ^a	Dialysis	Micelles	150	Cancer (ovary)	Dox	A2780/DOX ^R	243

Table 2 (continued)

Structural parameters			Colloidal parameters			Application				
Architecture	Ligand	Synthetic method	Ligand coupling method	Formulation	Morphology	Diameter (nm)	Pathology/target	Drug	Cells/tissues/organs ^d	Ref.
PLGA- <i>b</i> -PEG-FA	FA	<i>Carbodiimide</i> (PLGA-COOH/DCC/ NHS + H ₂ N-PEG-FA)	<i>Carbodiimide</i> (H ₂ N-PEG-NH ₂ + FA-COOH/DCC) ^a	Dialysis	Micelles	85–100	Cancer (pharynx, glioma, breast)	Dox	KB, C6	220
(i) PLGA	FA	(i) <i>Commercial</i>	(i) <i>Commercial</i>	Lipid film	Polymeric	440	Cancer (breast)	Dox, pDNA	MDA-MB-231	238
(ii) OQLCS-PEG		(ii) <i>Carbodiimide</i>	(ii) <i>Carbodiimide</i>	hydration and	liposomes					
(iii) OQLCS-FA		(OQLCS-NH ₂ + PEG-NHS) ^a	(OQLCS-NH ₂ + FA-COOH/DCC/ NHS) ^a	sonication						
		(iii) see ligand coupling method	(iii) see ligand coupling method							
(i) PLGA-TGFS	FA	(i) <i>ROP</i> of LA from TGFS	(i) <i>Carbodiimide</i> (TGFS-COOH/EDC/ NHS + FA-NH ₂) ^b	Emulsion-solvent evaporation	Nanoparticles	320–360	Cancer (breast, glioma)	Dox ^c	MCF7, C6	246
(ii) TGFS-FA		(ii) see ligand coupling method	(ii) see ligand coupling method							
PLA-g3-FA/PEG	FA	<i>ROP</i> of LA from 6-arm hydroxy initiator; <i>divergent synthesis</i> ; <i>carbodiimide</i> (PLA-g3-COOH/DCC/ NHS + H ₂ N-PEG) ^a	<i>Carbodiimide</i> (FA-NH ₂ + PLA-g3-COOH/DCC/ NHS) ^a	Dialysis	Micelles (dendrimer- like star polymer)	15	Cancer (pharynx)	Dox	KB	242
(i) PHis- <i>b</i> -PEG-FA	FA	(i) <i>Carbodiimide</i> (PEG-COOH/DCC + PHis-NH ₂)	(i) <i>Carbodiimide</i> (PHis- <i>b</i> -PEG-OH + FA-COOH/DCC) ^a	Diafiltration	Micelles	50–80	Cancer (breast)	Dox	MCF7	227
(ii) PLA- <i>b</i> -PEG-FA	FA	(ii) <i>ROP</i> of LA from HOOC-PEG-OH	(ii) <i>Carbodiimide</i> (PLA- <i>b</i> -PEG-COOH/ DCC/NHS + FA-NH ₂) ^a							
PLGA- <i>b</i> -PEG-FA	FA	<i>Carbodiimide</i> (PLGA-COOH/DCC/ NHS + H ₂ N-PEG- NH ₂) ^b	<i>Carbodiimide</i> (PLGA- <i>b</i> -PEG-NH ₂ + FA-COOH/DCC) ^a	Double emulsion- solvent evaporation	Nanoparticles	155–245	Cancer (cervical)	pDNA	Hela	221
(i) PLGA	FA	(i) <i>Commercial</i>	(i) <i>Commercial</i>	Nanoprecipitation	Nanoparticles	65–85	Cancer (ovary)	Ptx	SK-OV-3, SW626	223
(ii) DMPE-DTPA		(ii) <i>Commercial</i>	(ii) <i>Commercial</i>						SK-OV-3	
(iii) DSPE-PEG		(iii) <i>Commercial</i>	(iii) <i>Commercial</i>							
(iv) DSPE-PEG-FA		(iv) DSPE/DSS + H ₂ N-PEG-FA)	(iv) <i>Carbodiimide</i> (DSPE/DSS + H ₂ N-PEG-FA)							
(i) PLGA	FA	(i) <i>Commercial</i>	(i) <i>Commercial</i>	Nanoprecipitation	Nanoparticles	70–80	Cancer (pharynx)	Dtx	KB	222
(ii) PEG-DSPE-FA		(ii) <i>Carbodiimide</i> (DSPE/DSS + H ₂ N-PEG-FA)	(ii) <i>Carbodiimide</i> (H ₂ N-PEG-NH ₂ + FA- COOH/DCC/NHS) ^a						KB	
(i) PLGA- <i>b</i> -PEG-FA	FA	<i>Carbodiimide</i> (PLGA-COOH/DCC/ NHS + H ₂ N-PEG-NH ₂)	<i>Carbodiimide</i> (PLGA- <i>b</i> -PEG-NH ₂ + FA-COOH/DCC) ^a	Dialysis	Micelles	95–130	Cancer (pharynx)	Dox ^c	KB	295
(i) PLGA	FA, biotin	(i) <i>Commercial</i>	(i) <i>Carbodiimide</i>	Emulsion-solvent evaporation	Nanoparticles	100–150	Cancer (breast)	Ptx	MCF-7, NCI-ADR, 4T1	73
(ii) PLA- <i>b</i> -PEG-FA		(ii) <i>ROP</i> of LA from FA-PEG-OH	(ii) <i>Carbodiimide</i> (HO-PEG-NH ₂ + FA-COOH/DCC/ NHS) ^a						KB	
(iii) PLA- <i>b</i> -PEG-biotin		(iii) <i>ROP</i> of LA from biotin-PEG-OH	(iii) <i>Carbodiimide</i> (HO-PEG-NH ₂ + biotin-COOH/DCC/ NHS) ^a						KB	

Table 2 (continued)

Structural parameters			Colloidal parameters			Application				
Architecture	Ligand	Synthetic method	Ligand coupling method	Formulation	Morphology	Diameter (nm)	Pathology/target	Drug	Cells/tissues/organs ^d	Ref.
(i) PLGA- <i>b</i> -PEG-RGD (ii) PLGA- <i>b</i> -PEG-FA	(i) cRGD (ii) FA	(i) <i>Carbodiimide</i> (PLGA-COOH/EDC/NHS + H ₂ N-PEG-RGD) (ii) <i>Carbodiimide</i> (PLGA-COOH/EDC/NHS + H ₂ N-PEG-FA)	(i) <i>Carbodiimide</i> (tBocNH-PEG-NHS + RGD-NH ₂) ^a (ii) <i>Carbodiimide</i> (tBocNH-PEG-NH ₂ + FA-COOH/EDC/NHS) ^a	Nanoprecipitation	Nanoparticles	50–120	Cancer (pharynx)	—	KB	225
PLA- <i>b</i> -PEG-biotin	Biotin	ROP of LA from MePEG-OH	<i>Carbodiimide</i> (biotin-NHS + H ₂ N-PEG-OH) ^a	Emulsion-solvent evaporation	Nanoparticles	220–260	Cancer (breast)	Ptx, Pgp, targeted siRNA	JC JC	224
(i) PLGA- <i>b</i> -PEG-alendronate (ii) PLGA- <i>b</i> -DCL peptide (iii) PLGA- <i>b</i> -PEG	Alendronate DCL peptide	(i) ROP of LA/G from MePEG-OH (ii) see ligand coupling method (i) <i>Carbodiimide</i> (PLGA-COOH/EDC/NHS + NH ₂ -PEG-COOH) ^a (ii) ROP of LA/G from MePEG-OH	<i>Carbodiimide</i> (PLGA-COOH/EDC/NHS + alendronate-NH ₂) ^a <i>Carbodiimide</i> (PLGA- <i>b</i> -PEG-COOH/EDC/NHS + DCL-NH ₂) ^a	Dialysis method	Nanoparticles	40–60	Bone diseases	17β estrogen	Hydroxyapatite adsorption assay	214
(i) PLGA- <i>b</i> -PEG-ACUPA (ii) PLA- <i>b</i> -PEG-ACUPA (iii) PLGA- <i>b</i> -PEG (iv) PLA- <i>b</i> -PEG	ACUPA	(i) ROP of LA/G from HO-PEG-ACUPA (ii) ROP of LA from HO-PEG-ACUPA (iii) ROP of LA/G from MePEG-OH (iv) ROP of LA from MePEG-OH	(i) and (ii) <i>Carbodiimide</i> (ACUPA-NH ₂ + HO-PEG-COOH/DCC/NHS) ^a	Nanoprecipitation	Nanoparticles	80	Cancer (prostate)	(–)-Epigallocatechin 3-gallate	LNCaP	230
PGA- <i>b</i> -PLA-Gal	Galactosamine (Gal)	<i>Carbodiimide</i> (PLA-OH/CDI + PGA-NH ₂)	<i>Carbodiimide</i> (PGA- <i>b</i> -PLA-COOH/EDC/NHS + Gal-NH ₂) ^b	Emulsion-solvent evaporation	Nanoparticles	<400	Cancer (prostate)	Dtx	LNCaP	188
PGA- <i>b</i> -PLA-Gal	Galactosamine (Gal)	<i>Carbodiimide</i> (PLA-OH/CDI + PGA-NH ₂)	(PLA- <i>b</i> -PGA-COOH/EDC/NHS + Gal-NH ₂) ^b	Emulsion-solvent evaporation	Nanoparticles	80	Cancer (liver)	Ptx	HepG2	249
PLGA-Mannan	Mannan	Commercial	(PLGA-COOH + Mannan/EDC/Sulfo-NHS) ^b	Emulsion-solvent evaporation	Nanoparticles	130	Cancer (liver)	Ptx	HepG2 HepG2	250
PLGA- <i>g</i> -HA	HA	Commercial	<i>Carbodiimide</i> (PLGA-COOH/DCC/NHS + HA-NH ₂) ^b	Double emulsion-solvent evaporation	Nanoparticles	80	Activation of immune response	Ovalbumin	DC T-cells activation	213
PLGA-TMC	TMC	Commercial	<i>Carbodiimide</i> (PLGA-COOH/EDC + TMC-NH ₂) ^b	Nanoprecipitation	Nanoparticles	80	Cancer (breast)	Dox	MDA-MB-231, ZR-75-1	212
PLGA-WGA	WGA	Commercial	<i>Carbodiimide</i> (PLGA-COOH/EDC/NHS + WGA-NH ₂) ^a	Nanoprecipitation	Nanoparticles	150	CNS delivery, Alzheimer disease (AD)	Coenzyme Q10	SH-SY5Y AD model	103
				Double emulsion-solvent evaporation	Nanoparticles	250	Oral Delivery	Thymopentin	Bioadhesion PD	203

Table 2 (continued)

Structural parameters			Colloidal parameters			Application		Ref.		
Architecture	Ligand	Synthetic method	Ligand coupling method	Formulation	Morphology	Diameter (nm)	Pathology/target		Drug	Cells/tissues/organs ^d
PLGA-WGA	WGA	Commercial	Carbodiimide (PLGA-COOH)/EDC/NHS + WGA-NH ₂ ^a	Double emulsion-solvent evaporation	Nanoparticles	150	Oral Delivery	Thymopentin	—	204
PLGA-WGA	WGA	Commercial	Carbodiimide (PLGA-COOH)/EDC/NHS + WGA-NH ₂ ^b	Emulsion-solvent evaporation	Nanoparticles	250	Cancer (lung)	—	A549	205
PLGA-WGA	WGA	Commercial	Carbodiimide (PLGA-COOH)/EDC/NHS + WGA-NH ₂ ^b	Emulsion-solvent evaporation	Nanoparticles	330	Cancer (lung)	Ptx	A549, H1299 A549	206
PLGA-lectin	WGA, RCA, Con A	Commercial	Carbodiimide (PLGA-COOH)/EDC/NHS + WGA-NH ₂ ^b	Emulsion-solvent evaporation	Nanoparticles	280–330	Cancer (lung)	Ptx	A549, H1299	207
PLGA- <i>b</i> -PEG-cRGD	cRGD	Carbodiimide (PLGA-COOH)/EDC/NHS + NH ₂ -PEG-COOH ^b	Carbodiimide (PLGA-COOH)/EDC/NHS + cRGD-NH ₂ ^b	Nanoprecipitation	Nanoparticles	400–440	Cancer (breast, skin)	Dox ^c	MDA-MB-231, MCF7, B16F10	232
(i) PLGA (ii) DSPE-PEG-RGDfR	RGDfR	Commercial	Carbodiimide (DSPE-PEG-COOH)/EDC/NHS + RGDfR-NH ₂ ^b	Nanoprecipitation	Nanocapsules	180	Cancer (breast)	Ptx, com-bretastatin A-4	MCF7	231
P(LA-co-IL)-RGD	RGD	ROP of LA/protected lysine-NCA	Carbodiimide (P(LA-co-IL)-COOH)/DCC/NHS/DMAP + RGD-NH ₂ ^a	Emulsion-solvent evaporation	Nanoparticles	170–180	Cancer (breast)	Mitoxantrone	Bacp-37 Bacp-37	296
PLGA- <i>b</i> -PEG-Pep1	Pep I peptide	Commercial	Carbodiimide (PLGA- <i>b</i> -PEG-COOH)/EDC/NHS + Pep I-NH ₂ ^a	Dialysis	Nanoparticles	150–230	Autoimmune type 1 diabetes	Genistein	Islet and skin capillary cells	202
PLA-TPGS-TF	TF	ROP of LA/G from TPGS	Carbodiimide (PLA-TPGS-COOH)/EDC/NHS + TF-NH ₂ ^b	Nanoprecipitation	Nanoparticles	140	CNS delivery, Cancer (glioma)	Dtx	C6 Biodistribution (ex vivo)	248
PLGA-peptide	Similiploid peptides	Commercial	Carbodiimide (PLGA-COOH)/DCC/NHS + peptide-NH ₂ ^a	Nanoprecipitation	Nanoparticles	160–210	CNS delivery	—	Biodistribution	200
(i) PLGA (ii) PLGA-g7 (iii) PLGA-SA	g7 Peptide, sialic acid (SA)	Commercial	Carbodiimide (PLGA-COOH)/EDC/DMAP + g7-NH ₂ or SA-NH ₂ ^a	Nanoprecipitation	Nanoparticles	150–200	CNS delivery	Loperamide	Biodistribution	201
(i) PLGA (ii) PLGA-g7	g7 Peptide	Commercial	Carbodiimide (PLGA-COOH)/DCC/NHS + g7-NH ₂ ^a	Nanoprecipitation	Nanoparticles	150–200	CNS delivery	Loperamide	Biodistribution	215
(i) PLGA (ii) PLGA-glycopeptide	Glycopeptide	Commercial	Carbodiimide (PLGA-COOH)/EDC/NHS + glycopeptide-NH ₂ ^a	Double emulsion-solvent evaporation	Nanoparticles	200	CNS delivery (depression)	Zn ²⁺	HEK293, primary hippocampal neurons	173
PLGA- <i>b</i> -PEG-cLABLE	cLABLE	Carbodiimide (PLGA-COOH)/EDC/NHS + H ₂ N-PEG-COOH ^b	Carbodiimide (PLGA- <i>b</i> -PEG-COOH)/EDC/NHS + cLABLE-NH ₂ ^b	Nanoprecipitation	Nanoparticles	175	Activated endothelium targeting	—	HUVEC	229

Table 2 (continued)

Structural parameters			Colloidal parameters			Application		Ref.
Architecture	Ligand	Synthetic method	Ligand coupling method	Formulation	Morphology	Diameter (nm)	Pathology/target	
(i) PLGA (ii) Pluronic F127-cLABL	cLABL	Commercial	<i>Carbodiimide</i> (Pluronic-COOH/ EDC/NHS + cLABL-NH ₂) ^b	Nanoprecipitation	Nanoparticles	240	Cancer (lung)	A549
(i) PLGA (ii) PLGA- <i>b</i> - PEG-anti- HER-2	anti-HER-2 Mab	(i) Commercial (ii) <i>Carbodiimide</i> (PLGA-COOH/EDC/ NHS + H ₂ N-PEG-NH ₂)	<i>Carbodiimide</i> (PLGA- <i>b</i> -PEG-NH ₂ / EDC/ SulphoNHS + Mab-COOH) ^b	Nanoprecipitation	Nanoparticles	200–250	Cancer (breast)	SK-BR-3, MCF7
(i) PLA-TGPS (ii) TGPS- anti-HER-2	anti-HER-2 Mab	(i) ROP of LA from TGPS (ii) see ligand coupling method	<i>Carbodiimide</i> (TPGS-NH ₂ /EDC/NHS + Herceptin-COOH) ^b	Nanoprecipitation	Nanoparticles	200–240	Cancer (breast)	SK-BR-3, MCF7
PLGA-anti- HER-2	anti-HER2 Mab	Commercial	<i>Carbodiimide</i> (PLGA-COOH/EDC/ NHS + Mab-NH ₂) ^b	Double emulsion- solvent evaporation	Nanoparticles	100–140	Cancer (breast)	BT-474, MDA-MB-2.3, MCF-7
PLGA-EGFR	EGFR Mab	Commercial	<i>Carbodiimide</i> (PLGA-COOH/EDC/ NHS + Mab-NH ₂) ^b	Emulsion-solvent evaporation	Nanoparticles	275	Cancer (breast)	MCF7
(i) PLA- GFLGF-PEG (ii) PLA- <i>b</i> - PEG-EGFR P(LA-co-L)- EGFR	EGFR Mab	(i) ROP of LA from PEG-GFLGF-OH (ii) ROP of LA from HOOC-PEG-OH	<i>Carbodiimide</i> (PLA- <i>b</i> -PEG-COOH/ EDC/NHS + Mab-NH ₂) ^b	Nanoprecipitation	Polysomes	120	Cancer (breast)	SK-BR-3
SMMC-7721 PLGA-anti Fas	Anti Fas (CD95/Apo-1) Mab	Commercial	<i>Carbodiimide</i> (P(LA-co-L)-COOH/ EDC/NHS + Mab-NH ₂) ^b	Emulsion-solvent evaporation	Nanoparticles	120–170	Cancer	(hepatocellular)
HCT116 PLGA-anti antigen	Anti antigen rich MCF7 cells Mab	Commercial	(PLGA-COOH/EDC/ NHS + Mab-NH ₂) ^b	Emulsion-solvent evaporation	Nanoparticles	115–190	Cancer (colorectal)	Camptothecin
(i) PLGA (ii) PLGA- <i>b</i> - PEG-anti CD44	anti CD44 Mab, anti-NCAM1 Mab	Commercial	<i>Carbodiimide</i> (PLGA-COOH/EDC/ Mab-NH ₂) ^b	Double emulsion- solvent evaporation	Nanoparticles	320–360	Cancer (breast, colorectal)	MCF-10A neoT, MCF-7, Caco-2
PLA- <i>b</i> -PEG- Aptamer	A10 RNA Aptamer	ROP of LA from HO-PEG-COOH	<i>Carbodiimide</i> (PLGA- <i>b</i> -PEG-COOH/ EDC/NHS + Aptamer- NH ₂) ^b	Double emulsion- solvent evaporation	Nano-/ microparticles	250–280	Cancer (prostate)	LNCap, PC3
PLGA- <i>b</i> - PEG-Aptamer	A10 RNA Aptamer	<i>Carbodiimide</i> (PLGA-COOH/EDC/ NHS + HOOC-PEG- NH ₂)	<i>Carbodiimide</i> (PLGA- <i>b</i> -PEG-COOH/ EDC/NHS + Aptamer-NH ₂) ^b	Nanoprecipitation	Nanoparticles	140–170	Cancer (prostate)	LNCap LNCap

Table 2 (continued)

Structural parameters			Colloidal parameters			Application				
Architecture	Ligand	Synthetic method	Ligand coupling method	Formulation	Morphology	Diameter (nm)	Pathology/target	Drug	Cells/tissues/organs ^d	Ref.
PLGA- <i>b</i> -PEG-Aptamer	A10 RNA Aptamer	<i>Carbodiiimide</i> (PLGA-COOH/EDC/NHS + HOOC-PEG-NH ₂)	<i>Carbodiiimide</i> (PLGA- <i>b</i> -PEG-COOH/EDC/NHS + Aptamer-NH ₂) ^b	Nanoprecipitation	Nanoparticles	190 (300–1200 upon Dtx encapsulation)	Cancer (prostate)	Dtx, ¹⁴ C-Ptx	LNCap	234
PLGA- <i>b</i> -PEG-Aptamer	A10 RNA Aptamer	<i>Carbodiiimide</i> (PLGA-COOH/EDC/NHS + HOOC-PEG-NH ₂)	<i>Carbodiiimide</i> (PLGA- <i>b</i> -PEG-COOH/EDC/NHS + Aptamer-NH ₂) ^b	Nanoprecipitation	Nanoparticles	160	Cancer (prostate)	Dtx	LNCap, PC3 LNCap	235
PLGA- <i>b</i> -PEG-Aptamer	A10 RNA Aptamer	<i>Carbodiiimide</i> (PLGA-COOH/EDC/NHS + HOOC-PEG-NH ₂)	<i>Carbodiiimide</i> (PLGA- <i>b</i> -PEG-COOH/EDC/NHS + Aptamer-NH ₂) ^b	Nanoprecipitation	Nanoparticles	130–175	Cancer (prostate)	CisPt	LNCaP, PC3	298
PLGA- <i>b</i> -PEG-Aptamer	A10 RNA Aptamer	<i>Carbodiiimide</i> (PLGA-COOH/EDC/NHS + HOOC-PEG-NH ₂)	<i>Carbodiiimide</i> (PLGA- <i>b</i> -PEG-COOH/EDC/NHS + Aptamer-NH ₂) ^b	Nanoprecipitation	Nanoparticles	135–165	Cancer (prostate)	CisPt	LNCap	236
PLA- <i>b</i> -PEG-Aptamer	AS1411 DNA Aptamer	<i>Carbodiiimide</i> (PLGA-COOH/EDC/NHS + HOOC-PEG-NH ₂)	<i>Carbodiiimide</i> (PLGA- <i>b</i> -PEG-COOH/EDC/NHS + Aptamer-NH ₂) ^b	Emulsion-solvent evaporation	Nanoparticles	100–200	Cancer (glioma)	Ptx	C6 C6	237
Ligand coupling by Michael addition FA-PEG- <i>b</i> -PLA-PEG- <i>b</i> -acrylate copolymer	Galactosamine (Gal)	ROP of LA from HO-PEG-Mal; see ligand coupling method; <i>Carbodiiimide</i> (FA-PEG- <i>b</i> -PLA-OH + HOOC-PEG-acrylate/DCC/DMAP) ^c (i) ROP of LA from MePEG (ii) ROP of LA from N-Boc-L-alanine-OH; thiolation; <i>Michael addition</i> (PLA-SH + H ₂ N-PEG-Mal); thiolation (iii) <i>Free radical copolymer</i> (PLA-EMA + MAA + NIPAAm)	<i>Michael addition</i> (PLA- <i>b</i> -PEG-SH + Gal-Mal) ^a	Double emulsion-solvent evaporation + cross-linking	Wormlike vesicles	20 × 100–200 (diameter × length)	Cancer (cervical)	Dox	Hela	275
(i) PLA- <i>b</i> -PEG-PEG-Gal (ii) PLA- <i>b</i> -PEG-Gal (iii) PNIPAAm- <i>g</i> -PLA	Galactosamine (Gal)	ROP of LA from N-Boc-L-alanine-OH; thiolation; <i>Michael addition</i> (PLA-SH + H ₂ N-PEG-Mal); thiolation (iii) <i>Free radical copolymer</i> (PLA-EMA + MAA + NIPAAm)	<i>Michael addition</i> (PLA- <i>b</i> -PEG-SH + Gal-Mal) ^a	Dialysis	Mixed micelles	160	Cancer (cervical)	Dox	Hela	268
(i) PLA- <i>b</i> -PEG-PEG-WGA (ii) PLA- <i>b</i> -PEG-WGA	WGA	(i) ROP of LA from MePEG-OH (ii) ROP of LA from HO-PEG-Mal	<i>Michael addition</i> (PLA- <i>b</i> -PEG-Mal + WGA-SH) ^b	Emulsion-solvent evaporation	Nanoparticles	85–90	CNS delivery (nose to brain)	—	Biodistribution	264
(i) PLA- <i>b</i> -PEG-PEG-WGA (ii) PLA- <i>b</i> -PEG-PEG-WGA	WGA	(i) ROP of LA from HO-PEG-Mal (ii) ROP of LA from MePEG-OH	<i>Michael addition</i> (PLA- <i>b</i> -PEG-Mal + WGA-SH) ^b	Emulsion-solvent evaporation	Nanoparticles	90–100	CNS delivery (nose to brain) (AD)	VIP	Biodistribution, neuroprotection	265

Table 2 (continued)

Structural parameters			Colloidal parameters			Application				
Architecture	Ligand	Synthetic method	Ligand coupling method	Formulation	Morphology	Diameter (nm)	Pathology/target	Drug	Cells/tissues/organs ^d	Ref.
(i) PLA- <i>b</i> -PEG-WGA (ii) PLA- <i>b</i> -PEG	WGA	(i) ROP of LA from HO-PEG-Mal (ii) ROP of LA from MePEG-OH	<i>Michael addition</i> (PLA- <i>b</i> -PEG-Mal + WGA-SH) ^b	Emulsion-solvent evaporation	Nanoparticles	—	CNS delivery (nose to brain)	—	Biodistribution	266
(i) PLA- <i>b</i> -PEG-STL (ii) PLA- <i>b</i> -PEG	Solanum tuberosum lectin (STL)	(i) ROP of LA from HO-PEG-Mal (ii) ROP of LA from MePEG-OH	<i>Michael addition</i> (PLA- <i>b</i> -PEG-Mal + Mal + STL-SH) ^b	Emulsion-solvent evaporation	Nanoparticles	130	CNS delivery (nose to brain)	—	Biodistribution	267
(i) PLGA- <i>b</i> -PEG-OL (ii) PLGA- <i>b</i> -PEG-OL	Odorranalectin (OL)	<i>Commercial</i>	<i>Michael addition</i> (PLGA- <i>b</i> -PEG-Mal + OL-SH) ^a	Double emulsion-solvent evaporation	Nanoparticles	115–120	CNS delivery (nose to brain)	Urocortin	Biodistribution Parkinson model	256
(i) PLA- <i>b</i> -PEG-cRGD (ii) PLA- <i>b</i> -PEG-cRGD	Odorranalectin (OL)	<i>Commercial</i>	<i>Michael addition</i> (PLA- <i>b</i> -PEG-Mal + OL-SH) ^a	Double emulsion-solvent evaporation	Nanoparticles	115–120	CNS delivery (nose to brain)	—	Ciliotoxicity Mucosa toxicity	255
(i) PLGA- <i>b</i> -PEG-cRGD (ii) PLA- <i>b</i> -PEG-cRGD	cRGD	(i) <i>Commercial</i> (ii) ROP of LA from HO-PEG-Mal	<i>Michael addition</i> (PLA- <i>b</i> -PEG-Mal + cRGD-SH) ^b	Emulsion-solvent evaporation	Nanoparticles	210	Cancer (breast)	—	NCI/ADR-RES, MCF-7, 4T1	257
(i) PLGA- <i>b</i> -PEG-cRGD (ii) PLA- <i>b</i> -PEG-cRGD	cRGD	(i) ROP of LA from HO-PEG-Mal (ii) ROP of LA from MePEG-OH	<i>Michael addition</i> (PLA- <i>b</i> -PEG-Mal + cRGD-SH) ^b	Emulsion-solvent evaporation	Micelles	100	Cancer	Dox	4T1 SKL	258
Hyper-branched HPAE- <i>g</i> -PLA-DPPE-Tf or HPAE- <i>g</i> -PLA-DPPE-cRGDfK	Transferrin (Tf) cRGDfK	ROP of LA from HPAE-OHs; PMPI + HPAE-PLA/DPPE	<i>Michael addition</i> (Mal-HPAE-PLA/DPPE + Tf-SH or RGDFK-SH) ^a	Emulsion-solvent evaporation	Nanoparticles	245–265	Cancer (cervical)	Ptx	HeLa	273
(i) PLGA- <i>b</i> -P(L)- <i>b</i> -PEG-IRGD (ii) PLGA- <i>b</i> -P(L)- <i>b</i> -PEG-CPP; PLGA- <i>b</i> -P(L)- <i>b</i> -PEG-CPP	(i) iRGD (ii) 2 CPPs (mHph1, mAP)	(i) <i>Carbodiimide</i> (PLGA-COOH/DCC + protected P(L)-NH ₂); <i>carbodiimide</i> (PEG-COOH/CDI + PLGA- <i>b</i> -P(L)) ^a (ii) <i>Carbodiimide</i> (PLGA-COOH/DCC + protected P(L)-NH ₂); <i>carbodiimide</i> (NHS-PEG-Mal) ^b	(i) <i>Carbodiimide</i> (iRGD-NH ₂ + PLGA- <i>b</i> -P(L)- <i>b</i> -PEG-COOH/CDI) ^a (ii) <i>Av/biotin</i> (PLGA- <i>b</i> -P(L) palmitic acid-Av + mHph1-biotin) ^b ; <i>Michael addition</i> (mAP-SH + PLGA- <i>b</i> -P(L)- <i>b</i> -PEG-Mal) ^b	Double emulsion-solvent evaporation	Nanoparticles	150	Cancer (lung)	TCHD + QC + ENX + siRNA	HEK293T A549	125
(i) PLA- <i>b</i> -PEG-TAT peptide (ii) PLA- <i>b</i> -PEG-TAT (iii) PSD- <i>b</i> -PEG	TAT peptide	(i) ROP of LA from MePEG-OH (ii) ROP of LA from Mal-PEG-OH (iii) <i>Carbodiimide</i> (PSD + PEG-COOH/DCC/NHS)	<i>Michael addition</i> (PLA- <i>b</i> -PEG-Mal + TAT-SH) ^b	Dialysis	Micelles	60–100	Cancer (breast)	—	MCF7	276

Table 2 (continued)

Structural parameters			Colloidal parameters			Application				
Architecture	Ligand	Synthetic method	Ligand coupling method	Formulation	Morphology	Diameter (nm)	Pathology/target	Drug	Cells/tissues/organs ^d	Ref.
(i) PLA- <i>b</i> -PEG (ii) PLA- <i>b</i> -PEG-TAT (iii) PCBS- <i>b</i> -PEG	TAT peptide	(i) ROP of LA from MePEG-OH (ii) ROP of LA from HO-PEG-Mal (iii) <i>Carbodimide</i> (PCB-NH ₂ + PEG-COOH/DCC/NHS; PEG- <i>b</i> -PCB-COOH/DCC/NHS + sulfadiazine)	<i>Michael addition</i> (PLA-PEG-Mal + TAT-SH) ^b	Dialysis	Micelles	60–100	Cancer (breast)	Dox	MCF7	277
(i) PLGA- <i>b</i> -PEG-LyP-1 (ii) PLGA- <i>b</i> -PEG	LyP-1	(i) <i>Michael addition</i> (PLGA-COOH/DCC/NHS + H ₂ N-PEG-Mal) (ii) <i>Commercial</i>	<i>Michael addition</i> (PLGA- <i>b</i> -PEG-Mal + LyP-1-SH) ^b ; <i>cyclization</i>	Emulsion–solvent evaporation	Nanoparticles	80–95	Cancer (pancreas)	—	BxPC-3 BxPC-3	252
(i) PLA- <i>b</i> -PEG (ii) PLA- <i>b</i> -PEG-LCP	LCP peptide	(i) ROP of LA from MePEG-OH (ii) ROP of LA from HO-PEG-Mal	<i>Michael addition</i> (PLA- <i>b</i> -PEG-Mal + LCP-SH) ^b	Nanoprecipitation	Micelles	45–70	Cancer (lung)	Dox	H2009, H460	253
(i) PLA (ii) DSPE-PEG-KLWVLPK	KLWVLPK peptide	(i) <i>Commercial</i> (ii) DSPE-PEG-Mal <i>commercial</i>	<i>Michael addition</i> (DSPE-PEG-Mal + peptide-GGGC-SH) ^b	Nanoprecipitation	Nanoparticles	60	Injured vessels	Ptx ^c	HaSMC Balloon angio-plasty model	134
(i) PLA- <i>b</i> -PEG (ii) PLA- <i>b</i> -PEG-EGFP EGF1	EGFP-EGF1	(i) ROP of LA from MePEG-OH (ii) ROP of LA from HO-PEG-Mal	<i>Michael addition</i> (PLA-PEG-Mal + EGFP-EGF1-SH) ^b	Double emulsion–solvent evaporation	Nanoparticles	80–110	Thrombo-embolic events	—	RAOEC Cerebral thrombosis model	254
(i) PLA- <i>b</i> -PEG-AP (ii) PAE- <i>b</i> -PEG	AP peptide	(i) ROP of LA from HO-PEG-COOH; <i>end-group thiolation</i> (via EMCS) (ii) <i>Michael-type acrylate ester/MePEG polym.</i> (diamine/bis-acrylate ester/MePEG)	<i>Michael addition</i> (PLA- <i>b</i> -PEG-NH ₂ /EMCS + AP-SH) ^c	Solvent casting	Micelles	160	Cancer (breast)	Dox	MDA-MB-231 MDA-MB-231	260
(i) PLGA- <i>b</i> -PEG-GE11 (ii) PCL	GE11 peptide	(i) <i>Michael addition</i> (PLGA-COOH/EDC/NHS + H ₂ N-PEG-Mal) (ii) <i>Commercial</i>	<i>Michael addition</i> (PLGA-PEG-Mal + GE11-SH) ^a	Nanoprecipitation	Nanoparticles	140	Cancer (ovary, breast)	Ptx, Ionidamide	SK-OV-3, MDA-MB-231, OVCAR5	251
(i) PLGA (ii) TGPS (iii) DOPE-Tf	Transferrin	<i>Commercial</i>	<i>Michael addition</i> (DOPE/MBS + Tf-SH) ^b	Nanoprecipitation	Nanoparticles	100–250	Cancer (ovary)	7α-AFTADD	SK-BR-3	272
(i) PLA- <i>b</i> -PEG-Lf (ii) PLA- <i>b</i> -PEG	Lactoferrin (Lf)	(i) ROP of LA from HO-PEG-Mal (ii) ROP of LA from MePEG-OH	<i>Michael addition</i> (PLA- <i>b</i> -PEG-Mal + Lf-SH) ^b	Double emulsion–solvent evaporation	Nanoparticles	90–130	CNS delivery	—	bEnd-3 Biodistribution	261
(i) PLA- <i>b</i> -PEG-Lf (ii) PLA- <i>b</i> -PEG	Lactoferrin (Lf)	(i) ROP of LA from HO-PEG-Mal (ii) ROP of LA from MePEG-OH	<i>Michael addition</i> (PLA- <i>b</i> -PEG-Mal + Lf-SH) ^b	Double emulsion–solvent evaporation	Nanoparticles	90	CNS delivery, Parkinson	Urocortin	bEnd-3 Biodistribution Parkinson model	262

Table 2 (continued)

Structural parameters			Colloidal parameters			Application		Ref.		
Architecture	Ligand	Synthetic method	Ligand coupling method	Formulation	Morphology	Diameter (nm)	Pathology/target		Drug	Cells/tissues/organs ^d
(i) PLA- <i>b</i> -PEG-Lf (ii) PLA- <i>b</i> -PEG	Lactoferrin (Lf)	(i) ROP of LA from HO-PEG-Mal (ii) ROP of LA from MePEG-OH	Michael addition (PLA- <i>b</i> -PEG-Mal + Lf-SH) ^b	Self-assembly	Polymersomes	90–120	GNS delivery (AD)	S14G-humanin	Biodistribution, neuroprotection	263
PLA- <i>b</i> -PEG-CDX PLA- <i>b</i> -PEG	CDX peptide	ROP of LA from HO-PEG-Mal ROP of LA from MePEG-OH Commercial	Michael addition (PLA- <i>b</i> -PEG-Mal + CDX-SH) ^a	Self-assembly	Micelles	40	Cancer (glioblastoma)	Ptx	U87	147
PLGA- <i>b</i> -PEG-Pep-TGN	Pep-TGN	Commercial	Michael addition (PLGA- <i>b</i> -PEG-Mal + peptide-SH) ^b	Emulsion-solvent evaporation	Nanoparticles	100–125	CNS delivery	—	bEnd-3 Biodistribution	150
(i) PLA/OMCCA-MAB (ii) PLA- <i>b</i> -PEG	AMBSLK MAB, anti-HER2 MAB	(i) ROP of LA (ii) ROP of LA from MePEG-OH	Anchoring (OMCCA in PLA) ^b ; Michael addition (PLA/OMCCA-Mal + MAB-SH) ^b	Nanoprecipitation	Nanoparticles	100	Cancer (prostate, pancreas, breast)	Ptx, Dex, Ptx-palmitate	PC3, Capan-1, SK-BR-3 PC3.38/luc	274
PLA-MAB	anti-HER2, HER2 MAB, anti-CD20 MAB	Commercial	Carbodiimide (PLA-COOH/EDC + cystamine); Michael addition (PLA-SH + MAB/Sulfo-MBS) ^b	Salting out	Nanoparticles	340–410	Cancer (ovary, lymphocyte)	—	SKOV-3, Daudi	194, 195
PLA-MAB	anti-HER2 MAB	Commercial	Carbodiimide (PLA-COOH/EDC + cystamine); Michael addition (PLA-SH + MAB/Sulfo-MBS) ^b	Salting out	Nanoparticles	150–190	Cancer (ovary)	Ptx	SK-OV-3	271
PLA- <i>b</i> -PEG-affibody	Anti HER-2 affibody	—	Michael addition (PLA- <i>b</i> -PEG-Mal + Affibody-SH) ^b	Nanoprecipitation	Nanoparticles	80–90	Cancer (ovary, pancreas)	—	SK-OV-3, SK-BR-3, Capan-1	259
PLGA/DSPE/PEG-MAB	anti-CEA MAB	Commercial	Michael addition (DSPE-PEG-Mal + MAB-SH) ^b	Nanoprecipitation	Lipid-polymer hybrid nanoparticles	95	Cancer (pancreas)	Ptx	BxPC-3, XPA-3	278
PLGA/DSPE/DSPE-PEG-Aptamer	XEO2 mini Aptamer	Commercial	Michael addition (DSPE-PEG-Mal + XEO2-SH) ^b	Nanoprecipitation	Nanoparticles	50–100	Cancer (prostate, cervical)	Dtx	PC3, HeLa	181
Ligand coupling by copper-catalyzed azide-alkyne cycloaddition (CuAAC)	FA	(i) ROP of LA/G from (2-bromo-2-methylpropionic acid 2-(2-hydroxyethyl-disulfanyl) ethyl ester); ATRP of PEGMA from PLGA-SS-Br; azidation (PLGA-SS-poly-PEGMA + NaN ₃) (ii) ROP of LA/G from dithiodiethanol	CuAAC (PLGA-SS-polyPEGMA-N ₃ + FA-alkyne) ^c	Nanoprecipitation	Nanoparticles	100–150	Cancer (lung)	pDNA	Calu-3	279

Table 2 (continued)

Structural parameters			Colloidal parameters			Application		Ref.		
Architecture	Ligand	Synthetic method	Ligand coupling method	Formulation	Morphology	Diameter (nm)	Pathology/target		Drug	Cells/tissues/organs ^d
P(TMCC-co-LA)-g-PEG-RGD	RGD	ROP of LA/protected TMCC; <i>carbodiimide</i> (poly(TMCC-co-LA)/EDC/sulfo-NHS + H ₂ N-PEG-N ₃)	<i>CuAAC</i> (poly(TMCC-co-LA)-g-PEG-N ₃ + alkyl- <i>RGD</i>) ^b	Dialysis	Nanoparticles	130	Eye disease	—	SIRC-rabbit corneal epithelial cells	280
Ligand coupling by biotin/avidin ligation strategy										
(i) PLGA- <i>b</i> -PEG-TTC (tetanus toxine C)		(i) <i>Carbodiimide</i> (PLGA-COOH/EDC/NHS + H ₂ N-PEG-COOH)	<i>Av/biotin</i> (PLGA- <i>b</i> -PEG-biotin + <i>Av/biotin</i> -TTC) ^b	Nanoprecipitation	Nanoparticles	250	Cancer	—	N18-RE-105, b.End3, HepG2	282
(ii) PLGA- <i>b</i> -PEG-TCC		(ii) <i>Carbodiimide</i> (PLGA-COOH/DCC/NHS + H ₂ N-PEG-biotin)								
PLGA/avidin palmitate	anti-CD4 Mab		<i>Av/biotin</i> (PLGA/avidin palmitate + biotin-anti CD4 Mab) ^b	Double emulsion-solvent evaporation	Nanoparticles	80–120	Immunome-diated diseases	Leukemia inhibitory factor (LIF)	T cell stimulation Donor specific transduction, rejection	284
PLGA/avidin lipids (butyric acid/caprylic acid/palmitic acid/stearic acid/linoleic acid)	anti-CD4 Mab		<i>Av/biotin</i> (PLGA/avidin lipids + biotin-anti CD4 Mab) ^b	Emulsion-solvent evaporation	Nanoparticles	170–270	Immunome-diated diseases	—	CD4 ⁺ T cells	283
PLA- <i>b</i> -PEG-IgG	anti-ICAM-1 Mab	ROP of LA from HO-PEG-biotin	<i>NAv/biotin</i> (PLA- <i>b</i> -PEG-biotin + <i>NAv</i>) ^b ; <i>NAv/biotin</i> (PLA- <i>b</i> -PEG- <i>NAv</i> + biotin-Mab) ^b	Emulsion-solvent evaporation	Nanoparticles	—	Inflamed endothelium	—	HUVEC	281
Ligand coupling by other ligation strategies										
(i) PLA- <i>b</i> -PEG- <i>b</i> -PLA	Selectin ligand	(i) ROP of LA from HO-PEG-OH	<i>Esterification</i> (PLA- <i>g</i> -RCOCl + selectin ligand) ^a	Double emulsion-solvent evaporation	Nanoparticles	200–250	Angiogenesis	Ptx, Endostatin	HUVEC, rat aortic ring assay	292
(ii) PLA- <i>g</i> -selectin ligand)		(ii) ROP of LA/allyl glycidyl ether; <i>pending groups modification</i>								
(i) PLA	Selectin ligand	(i) <i>Commercial</i>	<i>Esterification</i> (PLA- <i>g</i> -RCOCl + selectin ligand) ^a	Emulsion-solvent evaporation	Nanoparticles	150–200	activated vascular endothelium	Ptx, Endostatin	HUVEC, rat aortic ring assay	291
(ii) PLA-co-selectin ligand)		(ii) ROP of LA/allyl glycidyl ether; <i>pending groups modification</i>								

Table 2 (continued)

Structural parameters			Colloidal parameters			Application				
Architecture	Ligand	Synthetic method	Ligand coupling method	Formulation	Morphology	Diameter (nm)	Pathology/target	Drug	Cells/tissues/organs ^d	Ref.
(i) PLA- <i>b</i> -PEG-glucose (ii) PLA- <i>b</i> -PEG-galactose (iii) PLA- <i>b</i> -PEG-lactose (iv) PLA- <i>b</i> -PEG-mannose	Glucose, galactose, lactose, mannose	(i) ROP of EO and LA from protected glucose (ii) ROP of EO and LA from protected galactose (iii) ROP of EO and LA from protected aldehyde initiator (iv) ROP of EO and LA from protected aldehyde initiator	(i) see synthesis method (ii) see synthesis method (iii) <i>Reductive amination</i> (iv) PLA- <i>b</i> -PEG-CHO + <i>p</i> -aminophenyl-lactose ^b	Dialysis	Micelles	20–40	—	—	—	288
PLA- <i>b</i> -PEG-lactose	Lactose	ROP of EO and LA from protected aldehyde initiator	<i>Reductive amination</i> (PLA- <i>b</i> -PEG-CHO + <i>p</i> -aminophenyl-lactose) ^b	Dialysis	Micelles	30	Cancer	—	—	72
(i) PLA- <i>b</i> -PEG-glucose (ii) PLA- <i>b</i> -PEG-galactose PLGA- <i>b</i> -PEG-GRGDS	Glucose, galactose GRGDS	ROP of EO and LA from protected glucose/galactose ROP of LA/G from MePEG-OH	See synthesis method	Dialysis	Micelles	35–45	—	—	—	293
(i) PLA- <i>b</i> -PEG-RGD4C (ii) PLA- <i>b</i> -PEG-RGD4C	GRGDS RGD4C	ROP of LA/G from MePEG-OH (i) and (ii) <i>Alcohol/isocyanate coupling</i> (PLA-OH/MDI + HO-PEG-OH)	<i>Photografting</i> (PLGA- <i>b</i> -PEG + GRGDS) <i>Nucleophilic substitution</i> (PLA- <i>b</i> -PEG-OH/MSCl + RGD4C-NH ₂) ^a	Nanoprecipitation	Nanoparticles	120–130	Cancer (cervical, lymphocyte) Cancer (skin)	JNJ-7706621, Ptx Ptx	Hela TLT MDA-MB-435 MDA-MB-435	285 286
(i) PLA- <i>b</i> -PEG-K237 peptide (ii) PLA- <i>b</i> -PEG-PLA-TAT	K237 peptide TAT peptide	(i) ROP from HO-PEG-CHO (ii) ROP of LA from MePEG-OH <i>Commercial</i>	<i>Reductive amination</i> (PLA- <i>b</i> -PEG-CHO + K237-NH ₂) ^b <i>Epoxy conjugation</i> (PLA/denacol + TAT-NH ₂) ^b (PLGA/denacol + TF-NH ₂) ^b	Emulsion-solvent evaporation	Nanoparticles	80	Cancer (skin)	Ptx	MDA-MB-231	287
PLGA-Tf	Transferrin	<i>Commercial</i>	<i>Epoxy conjugation</i> (PLGA/denacol + TF-NH ₂) ^b	Emulsion-solvent evaporation	Nanoparticles	340	HIV, CNS delivery	Ritonavir	MDCK-MDR1 Biodistribution, BBB integrity PC3 PC3	290 289
P(TMCC-co-LA)- <i>g</i> -PEG-Mab	anti-HER2 Mab	ROP of LA/protected TMCC; <i>carbodiimide</i> (poly(TMCC-co-LA)- <i>g</i> -PEG-furan + anti-EDC/sulfo-NHS + H ₂ N-PEG-furan)	<i>Diels alder Reaction</i> (poly(TMCC-co-LA)- <i>g</i> -PEG-furan + anti-HER2 Mab/MPBH) ^b	Dialysis	Nanoparticles	125	Cancer (breast, endothelium)	Dox ^c	SK-BR-3	294

^a Coupling prior to nanocarrier formation. ^b Coupling post-nanocarrier formation. ^c Drug covalently linked to the (co)polymer. ^d *In vivo* experiments are written in bold.

amphiphilic copolymers were synthesized by ROP of lactide and glycolide using $\text{Sn}(\text{Oct})_2$ as a catalyst in the presence of PEG moieties acting as macroinitiators (e.g., PEG-COOH or PEG-Mal) or, alternatively, by conjugation between PEG blocks and preformed PLGA/PLA blocks.

PEGylated PLGA/PLA-based NPs were functionalized with a broad range of ligands (small molecules, peptides, antibodies) linked, almost exclusively, at the extremity of the PEG chain. However, ligands were also directly conjugated to the hydrophobic NP core, thus forming simultaneously the hydrophilic shell.

Carbodiimide-assisted coupling strategy. Ligand/(co)polymer coupling reactions performed under carbodiimide conditions were extensively employed for targeted PLA/PLGA-based nanocarriers. Indeed, it took advantage of the native carboxyl groups present at one extremity of the PLA/PLGA (co)polymer chain, either to link the ligand itself,^{103,173,200–215} a PEG block (containing another functional groups at the other extremity for further coupling with the biologically active ligand), or the PEG block already conjugated with the ligand.

In this view, when amphiphilic PLA- or PLGA-*b*-PEG block copolymers are desired, the strategy is to use (hetero) bi-functional PEGs (e.g., bis-amine-PEG, α -amine- ω -hydroxy PEG or α -amine- ω -carboxy PEG) to achieve the functionalization with the PLGA/PLA block and the ligand of interest at the other end. Alternatively, α -carboxyl- ω -hydroxyl PEGs were intensively employed as macroinitiator for the ROP of LA/G, subsequently linked to the ligand of interest *via* its remaining COOH group.

The PEG chains forming the hydrophilic shell of the NPs displayed either: (i) amine groups which were reacted with DCC/NHS-activated FA, Mab or biotin,^{73,216–224} (ii) carboxylic acid groups activated with DCC (or EDC)/NHS prior to reaction with the amino group of FA, peptides, WGA, Mab and sugars (Fig. 8)^{185,186,225–237} or (iii) hydroxyl groups which were reacted with DCC/DMAP-activated FA.²²⁷

The size of the ligands actually governs the employed synthetic pathway and the way all these building blocks were assembled. The functionalization of the (co)polymers with the desired ligands prior to self-assembly into ligand-decorated nanocarriers is the strategy of choice for small sized ligands

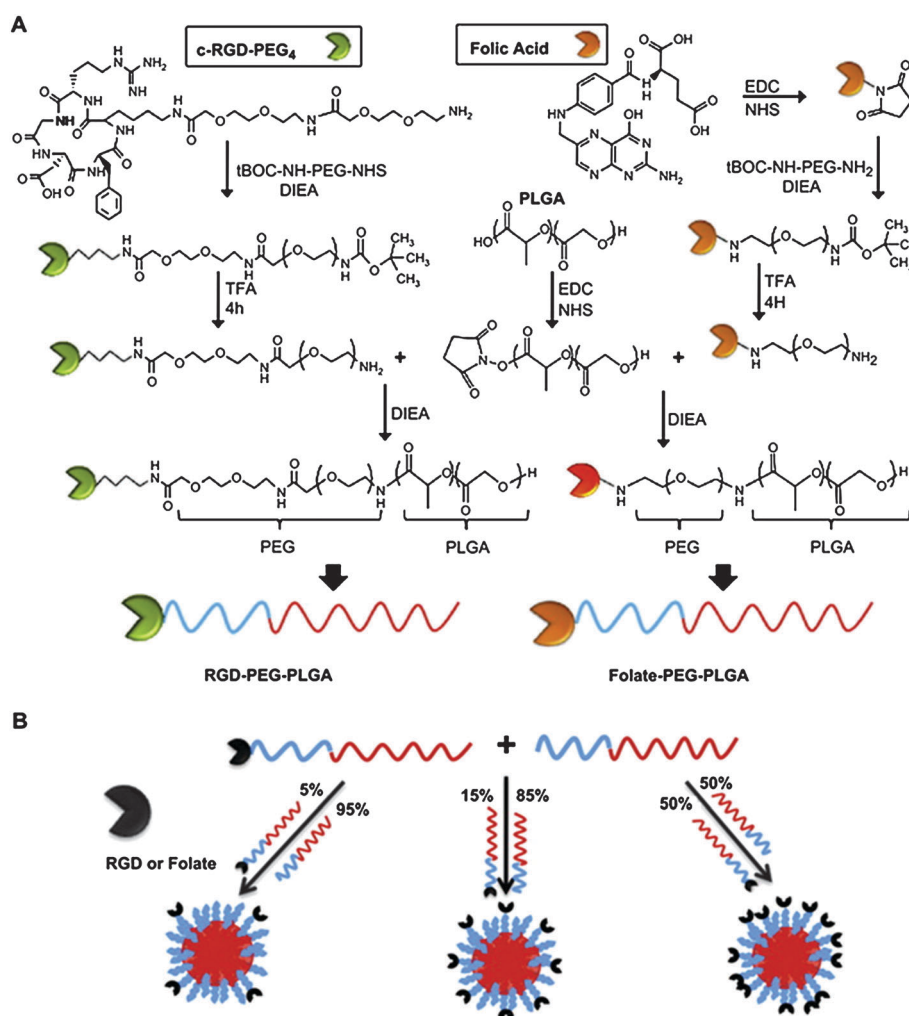


Fig. 8 (A) Synthesis of PLGA-*b*-PEG-RGD and PLGA-*b*-PEG-FA. (B) Preparation of targeted NPs with different surface ligand densities by mixing PLGA-*b*-PEG with functionalized PLGA-*b*-PEG-RGD or PLGA-*b*-PEG-FA (reprinted with permission from ref. 225. Copyright 2011, Elsevier).

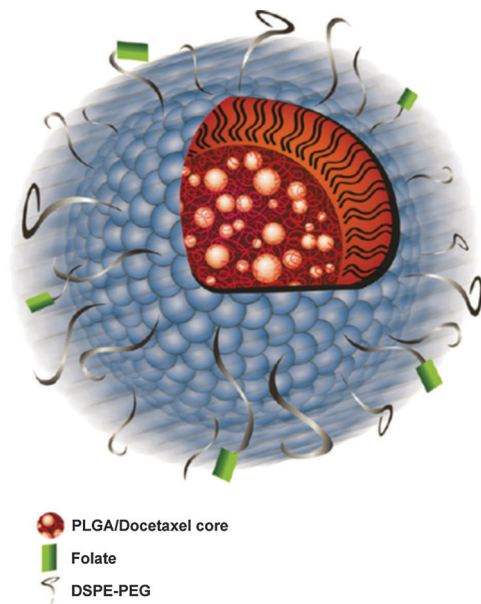


Fig. 9 Mixed lipid-shell polymer-core nanoparticles made of a core of PLGA wrapped in a lipid layer of lecithin, 1,2-distearoyl-*sn*-glycero-3-phosphoethanolamine-poly(ethylene glycol) (DSPE-PEG) and folate-DSPE-PEG (reprinted with permission from ref. 222. Copyright 2011, American Chemical Society).

such as FA. On the contrary, the post functionalization approach, which consists in the formation of PLA/PLGA or PLA-*b*-PLGA-*b*-PEG nanocarriers followed by their surface modification with the targeting moieties is largely preferred for bulky ligands such as lectins, proteins, monoclonal antibodies and aptamers. When peptides were linked, the two routes were employed.

Lipid-PEG conjugates were also used to prepare mixed lipid-shell polymer-core nanoparticles where the PLGA formed the polymeric core which was wrapped by a lipid layer made of lecithin, 1,2-distearoyl-*sn*-glycero-3-phosphoethanolamine-poly(ethylene glycol) (DSPE-PEG) and functionalized-DSPE-PEG for targeting purpose. Bis-amine-PEG was conjugated to DSPE and FA activated using DSS (Fig. 14) or EDC/NHS, respectively (Fig. 9).^{218,222–223} Alternatively, EDC/NHS activation of a hetero bifunctional

α -amine- ω -carboxy terminated PEG enabled the conjugation with the RGD peptide.²³¹ A lipid shell made of the amphiphilic PEGylated-octadecyl-quaternised lysine modified chitosan (PEG-OQLCS) was reported. The conjugation of OQLCS with a folate derivative, prepared by DCC/chemistry, allowed NP functionalization.²³⁸

DCC-mediated polycondensation has been used to conjugate PEI and PLA and FA, yielding the amphiphilic FA-PEI-*b*-PLA copolymer (Fig. 10).²³⁹ The resulting functionalized copolymer was able to condensate DNA and spontaneously formed micelles in aqueous solution and was tested to increase gene transfection efficiency.

Functionalization was also achieved using PLGA nanoparticles coated with diblock copolymer of poly(*L*-lysine)-*block*-poly(ethylene glycol)-FA (P(L-lysine)-*b*-PEG-FA) prepared from a heterobifunctional α -amine- ω -carboxy PEG used as a macroinitiator for the ROP of LA/G.^{216,219} Activated FA (DCC/NHS) was conjugated to the PEG *via* its amine group followed by its coupling with P(L-NH₂) under identical coupling conditions. This positively charged P(L-lysine)-PEG-FA allowed the coating of negatively charged PLGA NPs by ionic interaction (Fig. 11). A random P(LA-*co*-L) copolymer obtained by ring-opening copolymerization of LA and *N*^ε-(carbonylbenzoxy)-*L*-lysine was also proposed to design targeted NPs.²⁴⁰ EDC/NHS were used to conjugate EGFR Mab at the surface of P(LA-*co*-L) nanoparticles previously obtained by the solvent-emulsion evaporation method.

The carbodiimide chemistry was also used to prepare FA-functionalized dendrimer-like star polymer. A six arm star polymer synthesized by ROP of LA, using a hexahydroxy-functional initiator, was conjugated to 2,2-bis(hydroxymethyl)propionic acid-based degradable dendrons. Carboxyl end-groups of the dendrons were activated by NHS/DCC and then reacted with amino-functionalized folic acid (previously prepared by carbodiimide assisted reaction with 2,2-(ethylenedioxy) bis-ethylamine) and Hilyte488 (Fig. 12). Azido-PEG-amine was then similarly conjugated to the dendrons for PEGylation purposes.^{241,242}

Folate-mediated drug targeting was also achieved by developing pH-sensitive micelles composed of a blend of PLA-*b*-PEG-FA and either polyhistidine-*co*-phenyl alanine-*block*-poly(ethylene glycol) (P(His-*co*-Phe)-*b*-PEG)^{226,243} or PHIS-*b*-PEG-FA diblock

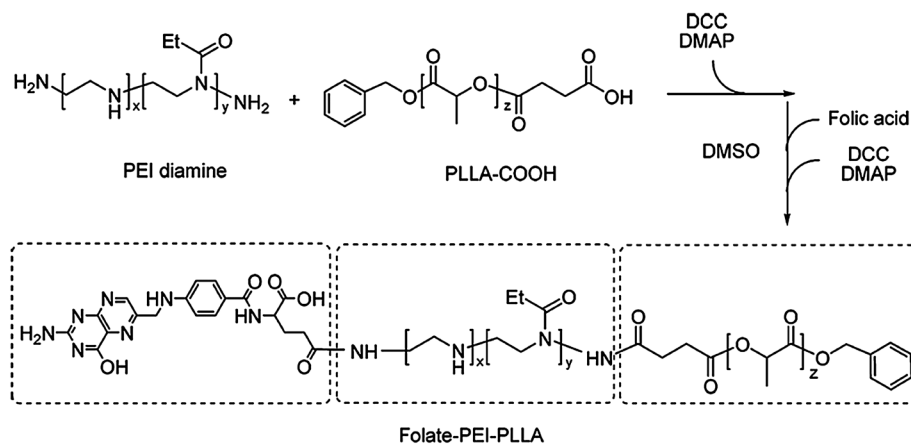


Fig. 10 Synthesis of FA-PEI-*b*-PLA by the DCC-mediated polycondensation reaction (reprinted with permission from ref. 239. Copyright 2005, American Chemical Society).

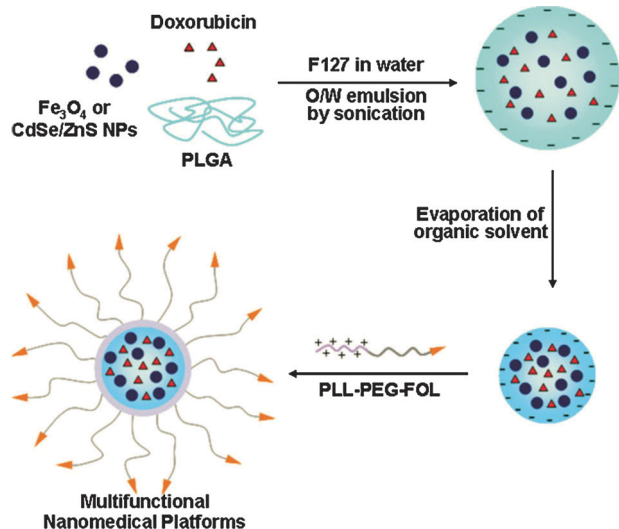


Fig. 11 Synthetic procedure for the preparation of multifunctional polymer nanoparticles using PLGA nanoparticles coated with diblock copolymer of poly(L-lysine)-*b*-poly(ethylene glycol)-FA (PLL-*b*-PEG-FA) (reprinted with permission from ref. 219. Copyright 2008, Wiley).

copolymers.²²⁷ The latter were achieved by ring-opening copolymerization of the corresponding NCA monomers (*e.g.*, Bz-His-NCA and L-Phe-NCA) followed by the DCC/NHS-assisted coupling with a monocarboxylated PEG containing or not containing the FA at the other extremity.

As an alternative to PEG, the TGPS (*D*- α -tocopheryl polyethylene glycol succinate) has been investigated by various authors. Copolymers of PLA-*b*-TGPS and PLGA-*b*-TGPS were prepared by ROP of LA or of a mixture of LA/G using HOOC-TGPS-OH as a macroinitiator. TGPS-COOH was blended with PLA- (or PLGA)-TGPS copolymer to prepare NPs at the surface of which was subsequently attached amino folate under EDC/NHS activation of the carboxyl group of TGPS.^{244–246} Alternatively, the carboxylic group of TGPS was converted to a primary amine by EDC/NHS assisted reaction with ethylene diamine and then conjugated to the carboxylic group of Herceptin by carbodiimide chemistry.²⁴⁷ Similarly, the conjugation of transferrin to the PLA-*b*-TGPS diblock copolymer was also described.²⁴⁸

Amphiphilic block copolymers were also prepared by conjugation of PLA and poly(glutamic acid) (PGA) *via* a CDI assisted coupling reaction. The amino group of galactosamine was then linked to the PGA carboxyl group *via* EDC/NHS.^{249,250}

Thiol-maleimide coupling strategy. Another robust strategy to achieve PLA/PLGA (co)polymer/nanoparticle functionalization is based on the thiol-maleimide Michael-type addition. Most of the time, a PLA-*b*-PEG (or PLGA-*b*-PEG) amphiphilic copolymer is prepared by ROP of LA (or LA/G) using a heterobifunctional α -maleimide- ω -hydroxy PEG as a macroinitiator. In turn, a H₂N-PEG-Mal was also conjugated to the DCC/NHS-activated carboxylic group of a pre-synthesized PLA/PLGA block.^{251,252}

Thiol-terminated peptides were covalently coupled to the maleimide functionality at the distal end of the PEG chain *via* thiol-ether chemistry.^{150,253–260} Reaction of lactoferrin^{261–263} or lectins,^{264–267} after their thiolation *via* with 2-iminothiolane, allowed introduction of thiol groups and the use of the same conjugation strategy. For instance, Toti and coworkers developed an interfacial activity assisted surface functionalization (IAASF) method to link, *via* thiol/maleimide coupling, the cyclic RGD peptide at the surface of PLGA NPs (Fig. 13).²⁵⁷

Alternatively, 2-iminothiolane was used to introduce sulfhydryl groups on PLA, yielding PLA-SH which was then conjugated to H₂N-PEG-Mal. The resulting PLA-*b*-PEG-NH₂ was modified by addition of 2-iminothiolane and the thiol groups at the outer end of the PEG chains were reacted with maleimide-functionalized galactosamine (*via* *N*-methoxycarbonylmaleimide).²⁶⁸

PEG was also activated at both ends with CDI and subsequently reacted with PLGA-*b*-PLL and iRGD to yield the PLGA-*b*-PLL-*g*-PEG-iRGD copolymer.¹²⁵

Thiol groups were introduced by the reaction of cystamine to surface EDC-activated carboxyl groups of PLA NPs (in this case, the reduction of disulfide bonds using tris(2-carboxyethyl)phosphine (TCEP) is required. This strategy was applied to the coupling of anti-HER2 and anti-CD20 Mab (previously reacted with sulfo-MBS to insert maleimide groups, Fig. 14).^{269–271} Similarly, MBS (Fig. 14) was used to conjugate Tf-SH to dioleoylphosphatidylethanolamine (DOPE) to prepare micelles used for post functionalization of PLGA NPs.²⁷²

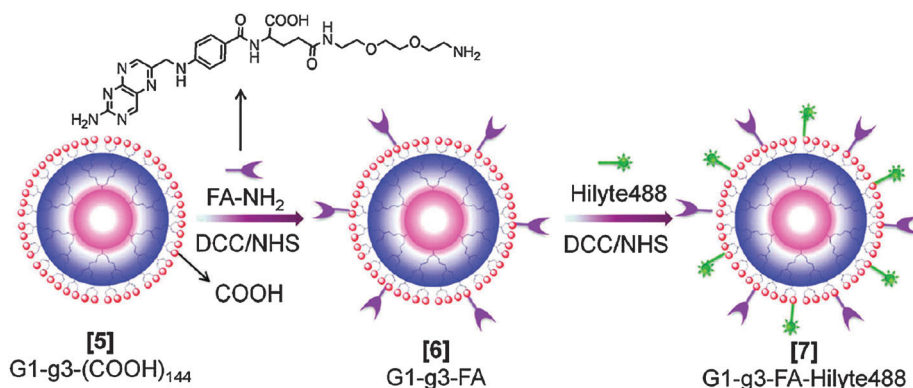


Fig. 12 Synthesis of Hilyte488-labeled folate-DLSP conjugate, G1-g3-FA-Hilyte488 (reprinted with permission from ref. 241. Copyright 2005, American Chemical Society).

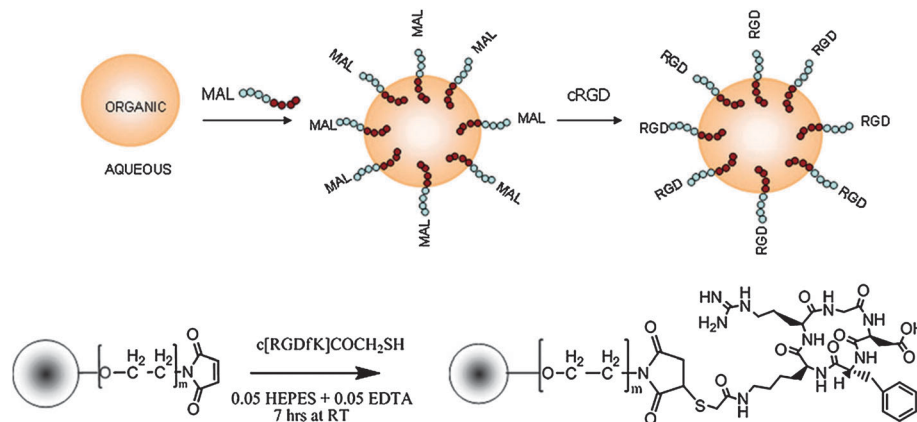


Fig. 13 Representation of the interfacial activity assisted surface functionalization (IAASF) technique (top panel) and the synthetic scheme for conjugation of cRGD peptide to PLGA nanoparticles that are surface functionalized with maleimide groups (bottom panel) (reproduced with permission from ref. 257. Copyright 2010, American Chemical Society).

The thiol-maleimide strategy was also used to functionalize hyperbranched poly(β (amino-ester)-*graft*-poly(lactic acid)-1,2-dipalmitoyl-*sn*-glycero-3-phosphoethanolamine (HPAE-*g*-PLA-DPPE) with cRGDFk and Tf prior to NP formulation (Fig. 15).²⁷³ Antibody coupling was also achieved using octadecyl-4-(maleimidomethyl)cyclohexane carboxylic acid as a linker anchored at the surface of PEGylated PLGA NPs.²⁷⁴

A FA-PEG-*b*-PLA-*b*-PEG-acrylate triblock copolymer containing FA at one end and an acrylate moiety at the other end was obtained by a three-step reaction procedure. Its self-assembly in aqueous solution conducted to wormlike polymer vesicles (Fig. 16). After the ROP of LA from a Mal-PEG-OH macroinitiator, the resulting Mal-PEG-PLA was reacted with a thiolated folate. The final triblock resulted in the coupling

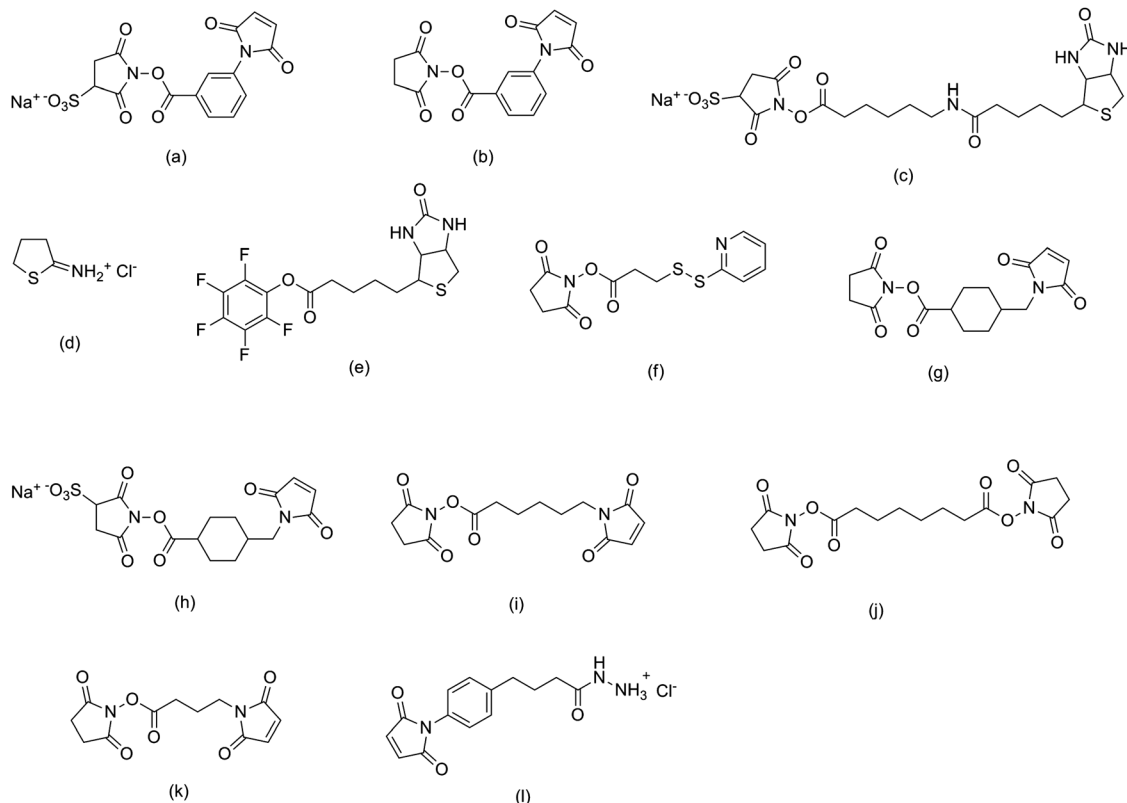


Fig. 14 Structure of *m*-maleimidobenzoyl-*N*-hydroxysulfosuccinimide ester (sulfo-MBS, a), *m*-maleimidobenzoyl-*N*-hydroxysuccinimide (MBS, b), sulfosuccinimidyl-6-[biotin-amido]hexanoate (sulfo-NHS-LC-biotin, c), 2-iminothiolane (Traut's reagent, d), pentafluorophenyl-ester biotin (PFP-biotin, e), *N*-succinimidyl-3-(2-pyridyldithio)propionate (SPDP, f), succinimidyl-4-(*N*-maleimidomethyl)cyclohexane-1-carboxylate (SMCC, g), sulfosuccinimidyl-4-(*N*-maleimidomethyl)cyclohexane-1-carboxylate (sulfo-SMCC, h), *N*- ϵ -maleimidocaproyl-oxysuccinimide ester (EMCS, i), disuccinimidyl suberate (DSS, j), 4-maleimidobutyric acid *N*-succinimidyl ester (k) and 4-(4-*N*-maleimidophenyl)butyric acid hydrazide-HCl (MPBH, l).

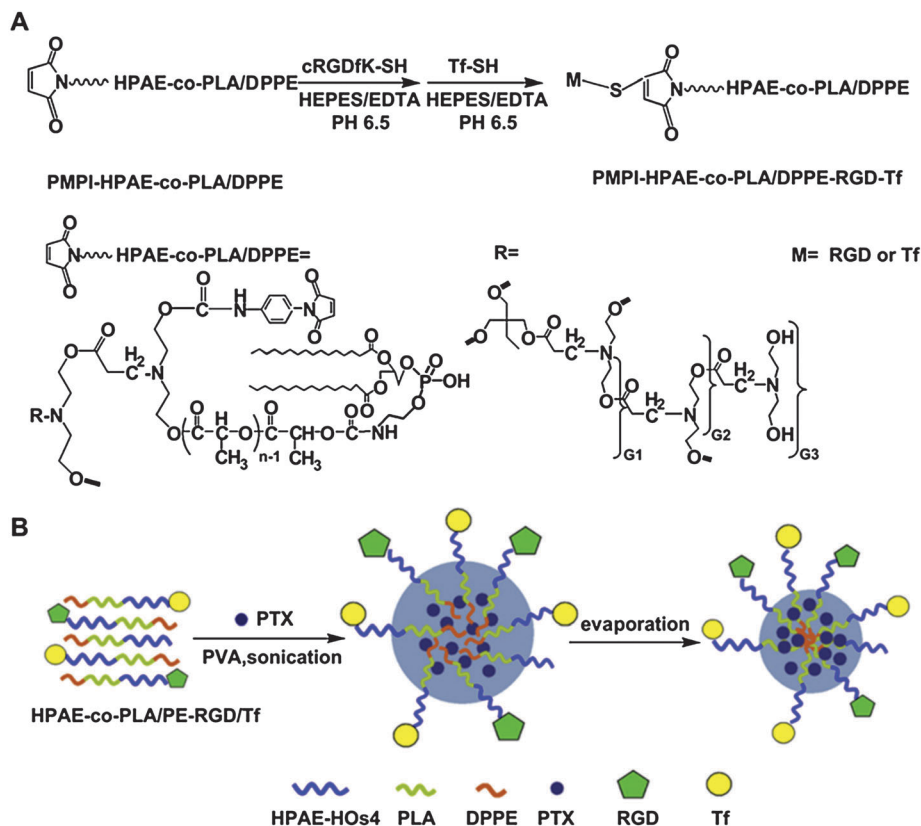


Fig. 15 Synthetic pathway to functionalize hyperbranched poly(β -amino-ester)-graft-poly(lactic acid)-1,2-dipalmitoyl-*sn*-glycero-3-phosphoethanolamine (HPAE-*g*-PLA-DPPE) with cRGDfK and Tf via thiol-maleimide ligation (adapted with permission from ref. 273. Copyright 2012, Elsevier).

between Mal-PEG-PLA-OH and the COOH-PEG-acrylate under DCC/DMAP conditions.²⁷⁵

Targeted, pH-sensitive polymeric micelles were prepared by blending PLA-*b*-PEG/PLA-*b*-PEG-Mal copolymers and a pH-sensitive diblock copolymer of poly(methacryloyl sulfadimethoxine)-*b*-PEG (PSD-*b*-PEG). Micelle functionalization was obtained by conjugating the TAT peptide to the surface maleimide groups of the micelles. Interestingly, at physiological pH (7.4), the anionic PSD complexed with cationic TAT of TAT-micelles, which shielded the TAT from the surrounding environment. However, at slightly acidic tumor pH, this TAT/PSD complexation no longer occurred and conducted to a TAT peptide exposure at the surface of the nanocarrier (Fig. 17).²⁷⁶ In a following work, the same authors replaced the non-biodegradable PSD with the PCBS, which is rapidly degraded in the presence of cysteine.²⁷⁷

Thiol-maleimide coupling was also employed for the design of aptamer-PEG-lipid-polymer hybrid NPs prepared *via* self-assembly of PLGA, lecithin and DSPE-PEG-Mal. After nanoparticle formation, surface conjugation *via* thiol-maleimide ligation was achieved with a thiol-containing RNA aptamer,¹⁸¹ or an anti-CEA MAb.²⁷⁸ Co-nanoprecipitation of DSPE-PEG-Mal with PLGA covalently linked to Ptx (obtained by a drug/alkoxide initiated ring opening polymerization of LA) was investigated to prepare functionalized nanoparticles named “nanoburrs”. Functionalization was achieved by the coupling of maleimide groups exposed on the outer shell of nanoburrs with the cysteine-terminated

KLWVLPK peptide which selectively binds the collagen IV, the most representative component of the basal membrane.¹³⁴

Copper-catalyzed azide-alkyne cycloaddition (CuAAC). The copper-catalyzed azide-alkyne cycloaddition (CuAAC), which belongs to the “click chemistry” ligation methods, was employed to synthesize FA- and RGD peptide-decorated PLA- or PLGA-based nanoparticles.^{279–280} Saeed *et al.*²⁷⁹ proposed the combination of ROP and ATRP to a PLGA-SS-P(OEGMA) diblock copolymer. Its subsequent azidation with NaN_3 and its reaction with propargyl-derivatized FA led to the desired PLGA-SS-polyPEGMA-FA copolymer (Fig. 18). In a similar way, the successful immobilization of GRGDS peptides at the surface of P(TMCC-*co*-LA)-*g*-PEG nanoparticles was reported.²⁸⁰

Biotin/avidin ligation strategy. Some authors also took advantage of the ability of biotin to strongly bind avidin/neutravidin to design targeted PLA/PLGA nanoparticles. The biotinylated diblock copolymers were prepared either by ROP of LA using hydroxyl-PEG-biotin as a macroinitiator²⁸¹ or by DCC/NHS assisted coupling of PLGA-COOH and an amino-PEG-biotin.²⁸² Biotin-decorated NPs were then incubated with avidin or neutravidin and then reacted with biotin-functionalized targeting ligand such as IgG and the tetanus toxin C fragment.^{281,282} As an alternative to PEG, an avidin-lipid anchor was prepared in order to position avidin moieties at the surface of PLGA NPs, and subsequently reacted with a biotinylated anti-CD44 Mab.^{283,284}

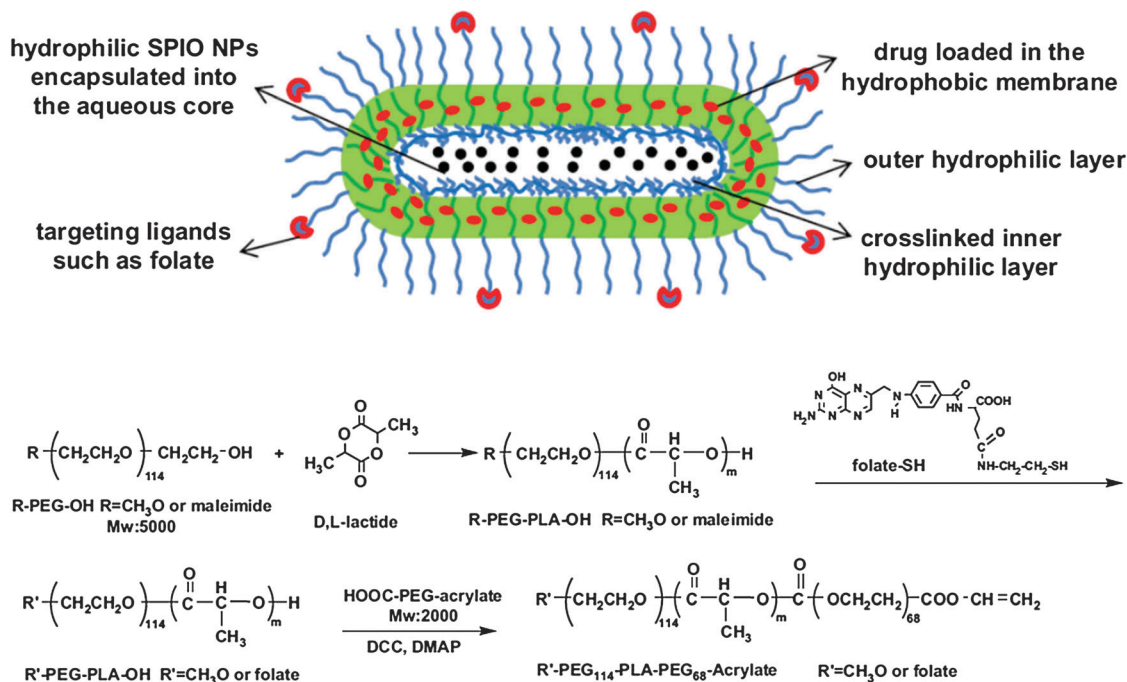


Fig. 16 Illustration of tumor-targeting multifunctional wormlike polymer vesicles formed by triblock copolymers for targeted cancer chemotherapy and imaging (top) and synthetic scheme of the R-PEG-*b*-PLA-PEG-acrylate (R = methoxy or folate) triblock copolymer (bottom) (adapted with permission from ref. 275. Copyright 2010, Elsevier).

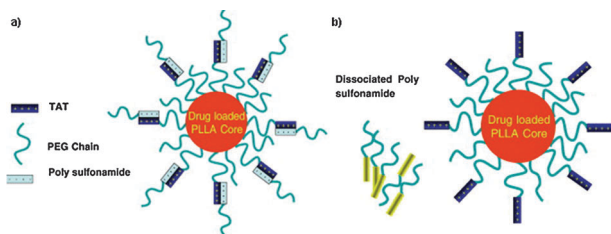


Fig. 17 Schematic model for the proposed drug delivery system: the carrier system consists of two components, a PLLA-*b*-PEG micelle conjugated to TAT and a pH-sensitive diblock polymer PSD-*b*-PEG. (a) At normal blood pH, the sulfonamide is negatively charged, and when mixed with the TAT micelle, shields the TAT by electrostatic interaction. Only PEG is exposed to the outside which could make the carrier long circulating; (b) when the system experiences a decrease in pH (near the tumor) sulfonamide loses charge and detaches, thus exposing TAT for interaction with tumor cells (reproduced with permission from ref. 276. Copyright 2007, American Chemical Society).

Other ligation strategies. Other strategies explored to prepare functionalized PLGA/PLA-based biodegradable nanocarriers, but to a lesser extent, relied on: (i) the photografting of RGD peptide on PLGA-*b*-PEG block copolymers;²⁸⁵ (ii) the nucleophilic substitution of sulfonated PLA-*b*-PEG-OMs by amino RGD4C;²⁸⁶ (iii) the reductive amination involving an aldehyde-functionalized PEG and terminal amino groups of peptides or *p*-aminophenyl derivatized sugars;^{72,287,288} (iv) the epoxy conjugation, which allowed coupling of Tf and TAT peptide at the surface of NPs;^{289,290} (v) the esterification of selectin-specific ligands with PLA functionalized with 1% pendant acid chloride groups;^{291,292} (vi) the anionic ring polymerization of ethylene oxide and LA using metalated protected sugars as initiators²⁹³ and (vii) the

Diels-Alder reaction between furan-functionalized P(TMCC-*co*-LA)-*g*-PEG and maleimide-modified anti-HER2 Mab.²⁹⁴

3.4.2.2. Poly(ϵ -caprolactone). Nanocarrier systems were also prepared using poly(ϵ -caprolactone) as the main component. PCL is a biodegradable semicrystalline polymer which, however, shows more resistance to chemical hydrolysis than the other polyesters.²⁹⁹ Moreover, the *in vitro* and *in vivo* degradation occurs very slowly in the absence of enzymes.³⁰⁰ Most of the targeted PCL-based NPs were constructed from amphiphilic PCL-*b*-PEG diblock copolymers.

Indeed, only two reports employed non-PEGylated targeted PCL NPs based on the use of either a poly(ϵ -caprolactone-*co*-4-maleate- ϵ -caprolactone) (poly(CL-*co*-MCL)) random copolymer³⁰¹ or a poly(ϵ -caprolactone)-*b*-poly(acrylic acid) (PCL-*b*-PAA) amphiphilic diblock copolymer.³⁰² In the first case, ligand functionalization was accomplished by forming an amide bond between carboxyl groups of (P(CL-*co*-MCL)) and the amino folate, in the presence of DCC and pyridine.³⁰¹ In the second one, PCL-*b*-PAA shell cross-linked (SCK) nanoparticles were prepared and functionalized by reacting activated carboxylic groups from the PAA shell with terminal amino groups of the protein transduction domain of the TAT peptide. Interestingly, successive treatment with TFA enabled cleavage of the peptide from the resin and caused hydrolysis of the core of the nanoparticles, thus leading to the formation of “nanocages”.³⁰² Fluorescent NPs were prepared by surface conjugation of FTSC (fluorescein-5-thiosemicarbazide) (Fig. 19).

Most of the PCL-*b*-PEG amphiphilic copolymers were synthesized by ROP of ϵ -caprolactone using heterobifunctional PEGs (*e.g.*, HO-PEG-COOH or HO-PEG-Mal) as macroinitiators.^{70,303–313}

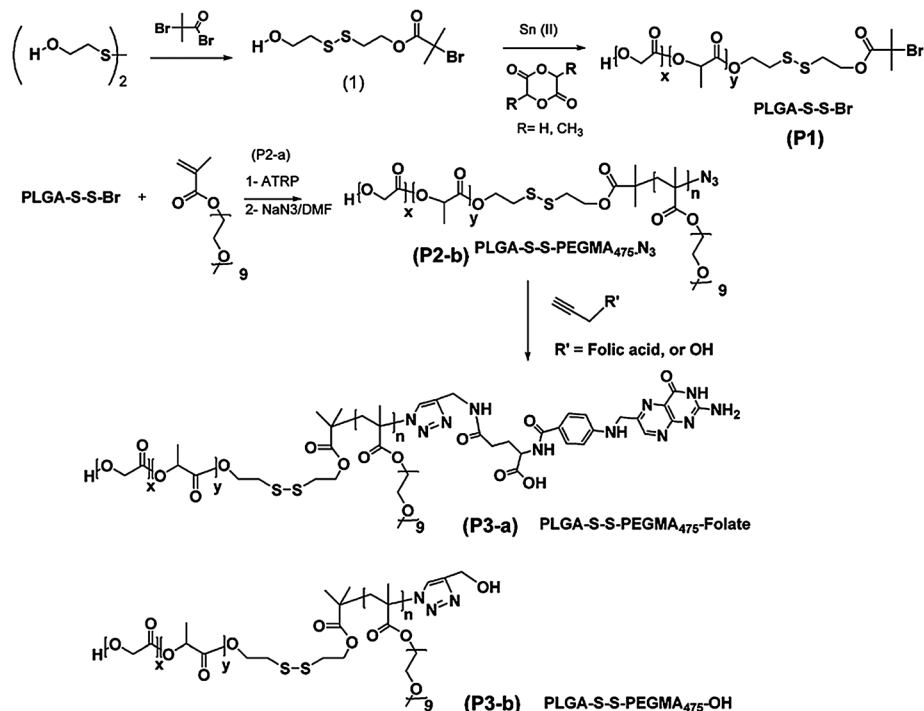


Fig. 18 Synthetic strategy for folic acid end-functional block copolymers by a combination of ROP, ATRP and click chemistry (reproduced with permission from ref. 279. Copyright 2011, American Chemical Society).

However, other strategies were also employed and different architectures were designed. Potassium alkoxide was employed as initiator and yielded an allyl-terminated PEG-*b*-PCL, which was converted into H₂N-PEG-*b*-PCL by radical addition reaction

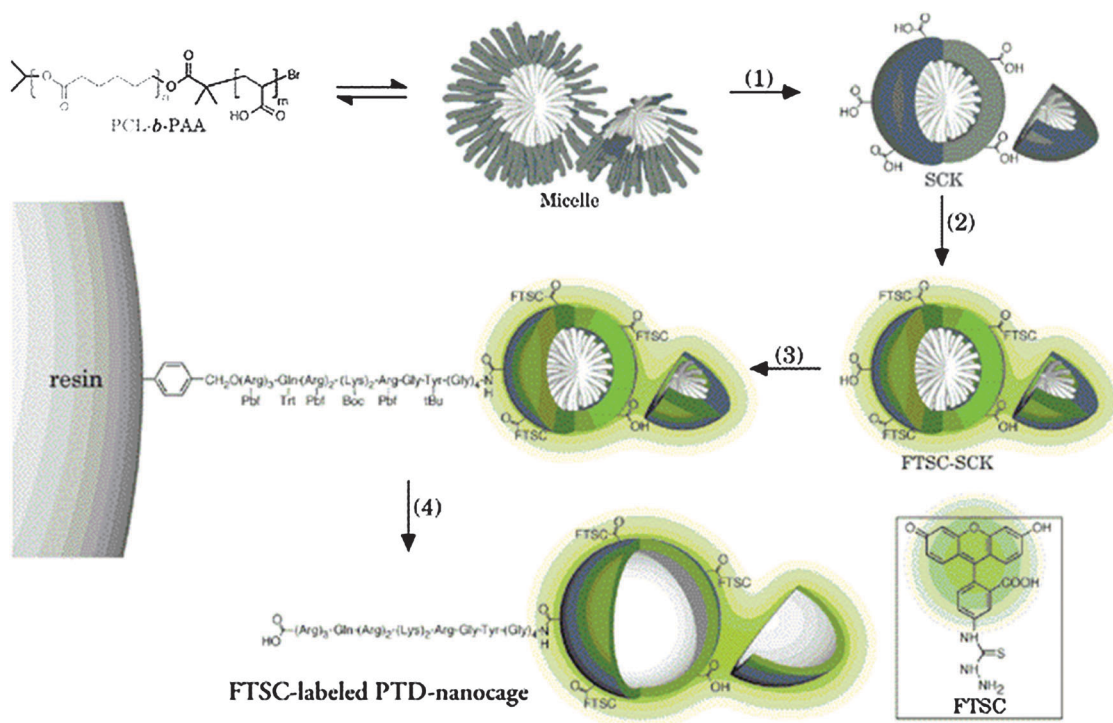


Fig. 19 Solid-phase synthesis strategy involved coupling of the protein transduction domain (PTD) with fluorescein-labeled shell cross-linked (SCK) nanoparticles, followed by cleavage from the support and excavation of the nanoparticle core domain to yield FTSC-labeled PTD-nanocage bioconjugates (reprinted with permission from ref. 302. Copyright 2001, American Chemical Society).

with 2-aminoethanethiol-HCl in the presence of potassium persulfate as catalyst.³¹⁴ A triblock PEG-*b*-PCL-*b*-PEG was prepared by conjugation of hydroxyl groups at both ends of PCL to diamino-PEG.³¹⁵ Amphiphilic block copolymer such as PCL-*b*-polyphosphoesters (PCL-*b*-PEEP)³¹⁶ and poly(ethylene glycol)-block-poly(δ -valerolactone) (PVL-*b*-PEG)⁷⁰ were also described.

Carbodiimide-assisted coupling strategy. As for previously described PLA/PLGA-based nanocarriers, the carbodiimide chemistry was a strategy of choice for ligand functionalization. DCC/NHS activated folate was reacted with the amino group at the extremity of the PEG block, yielding the corresponding FA-PEG-*b*-PCL, which was then used to prepare nanoparticles or micelles by nanoprecipitation or water/oil emulsion solvent- evaporation techniques.^{314,315,317} Alternatively, *N*-hydroxy succinimide-PEG-PCL was synthesized and conjugated to DNA aptamer,³⁰³ EGF peptide,^{70,304–306} Lf,³⁰⁷ and anti EGFR-Mab (Fig. 20)³⁰⁸ via formation of an amide bond. Galactosamine and glucosamine were conjugated to the hydroxyl end group of PCL-*b*-PEEP via *N,N'*-carbonyldiimidazole (CDI) assisted reaction.³¹⁶ Surprisingly, FA was also linked to the hydrophobic block of a PEG-*b*-PCL diblock copolymer via reaction of FA-NHS and terminal amino groups of the PCL block (obtained by conversion of hydroxyl into amino groups via the azidealkyl compound).^{317,318}

Thiol-maleimide Michael addition ligation. Maleimide-functionalized NPs were prepared using a blend of PEG-*b*-PCL and Mal-PEG-*b*-PCL block copolymers. Successful surface decoration was achieved by conjugation to thiol groups peptides such as hNgfEE,¹⁵⁶ Angiopep,^{309,310} cRGDfk,³¹³ Tf³¹¹ and OX26 Mab.³¹²

Reductive amination. Reductive amination was also exploited to synthesize RGD-functionalized NPs. First, acetal-terminated PEG-*b*-PCL was synthesized by ROP of EO and ϵ CL using 3,3-diethoxy-1-propanol as initiator. Micelles were prepared by co-solvent evaporation method followed by acetal removal to release the aldehyde group. Simple incubation of these polymeric micelles with the GRGDS enabled peptide conjugation via formation of a Schiff base, then reduced using NaBH₃CN.^{319,320} Synthesis of peptide-decorated micelles, prepared using the pre-functionalized GRGDS-PEG-*b*-PCL copolymer was also investigated by the same group.^{321,322}

Photografting. Peptide grafting on previously photoactivated PCL-*b*-PEG copolymers was proposed as alternative strategy to prepare RGD functionalized nanocarriers.^{323,324}

Other coupling methods. The other coupling approaches investigated for successful functionalization of PCL nanocarriers relied on: (i) the formation of ether bond which involved the quaternization of a tertiary amine end group of PEG-*b*-PCL with a brominated mannose derivative;³²⁵ (ii) the thioetherification of a cysteine-terminated peptide with a iodoacetate derivative of PEG-*b*-PCL;^{154,326} (iii) the use of avidin/biotin ligation strategy to conjugate biotin-WGA to Av-biotin-decorate PCL NPs³²⁷ and (iv) the click post functionalization of micelles made of amphiphilic PCL-*b*-POEGMA block copolymers.³²⁸ In this latter case, a multi-step approach was used: first, the P(OEGMA-*co*-azPMA) was synthesized by atom transfer radical polymerization (ATRP) and used as macroinitiator for the ROP of ϵ CL. The resulting

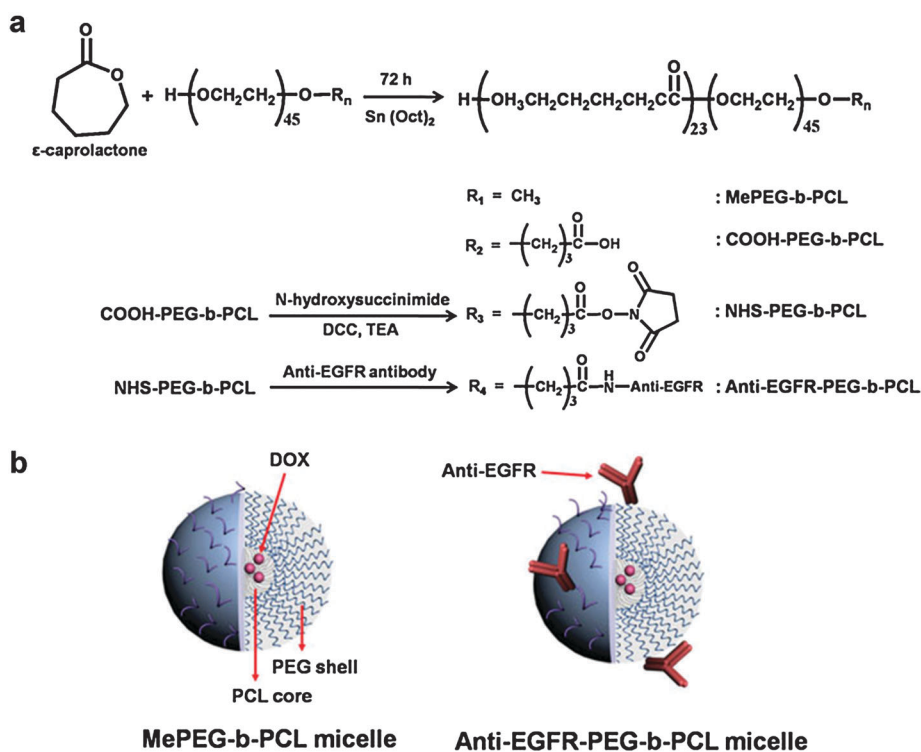


Fig. 20 (a) Synthesis of MePEG-*b*-PCL, HOOC-PEG-*b*-PCL, NHS-PEG-*b*-PCL, and anti-EGFR-PEG-*b*-PCL. (b) Schematic illustration for Dox-micelle and Dox-anti-EGFR-micelle (reprinted with permission from ref. 308. Copyright 2008, Wiley).

Table 3 Main characteristics and applications of targeted poly(ϵ -caprolactone)-based nanocarriers

Structural parameters			Colloidal parameters			Application				
Architecture	Ligand	Synthetic method	Ligand coupling method	Formulation	Morphology	Diameter (nm)	Pathology/target	Drug	Cells/tissues/organs ^d	Ref.
Ligand coupling by carbodiimide chemistry PEG- <i>b</i> -PCL-FA	FA	ROP of ϵ CL from MePEG-OH; end-group amination	Carbodiimide (PEG- <i>b</i> -PCL-NH ₂ + FA-COOH/DCC/NHS) ^a	Dialysis	Micelles	60–120	Cancer	Ptx		317
PEG- <i>b</i> -PCL-FA	FA	ROP of ϵ CL from MePEG-OH; end-group amination	Carbodiimide (PEG- <i>b</i> -PCL-NH ₂ + FA-COOH/DCC/NHS) ^a	Dialysis	Micelles	50–130	Cancer (breast, cervical)	Ptx	MCF-7, HeLa,	318
PCL- <i>b</i> -PEG-FA	FA	ROP of ϵ CL and EO; end-group amination	Carbodiimide (PCL- <i>b</i> -PEG-NH ₂ + FA-COOH/DCC/NHS) ^a	Nanoprecipitation	Micelles	50–120	Cancer (MDR)	FG020326	KBv200	314
FA-PEG- <i>b</i> -PCL-PEG-FA	FA	Nitration (O ₂ N-PCL-NO ₂ + H ₂ N-PEG-NH ₂)	Carbodiimide (H ₂ N-PEG- <i>b</i> -PCL- <i>b</i> -PEG-NH ₂ + FA-COOH/DCC/NHS) ^a	Nanoprecipitation	Nanoparticles	50–100	Cancer (ovary, lung)	Dox	OVCAR3, A549	315
(i) P(CL- <i>co</i> -MCL-FA)	FA	(i) and (ii) ROP of ϵ CL/4-carboxyl- ϵ -caprolactone; side chain modification with maleic anhydride	Carbodiimide (P(CL- <i>co</i> -MCL)/DCC/NHS + FA-NH ₂) ^a	Emulsion-solvent evaporation	Nanoparticles	80–145	Cancer (stomach)	5-FU	SGC7901/ SGC7901	301
PCL- <i>b</i> -PEEP-Gal	Galactosamine (Gal)	ROP of ϵ CL and EEP	Carbodiimide (PCL- <i>b</i> -PEEP-OH/GDI + Gal-NH ₂) ^b	Dialysis	Micelles	70	Cancer (liver)	Ptx	HepG2	316
PCL- <i>b</i> -PAA-PTD	Protein transduction domain (PTD) of TAT	ROP of ϵ CL from Al(OCH ₂ CBT ₃) ₃ ; ATRP of α BA from PCL-BI; deprotection	Carbodiimide (PCL- <i>b</i> -PAA-COOH/EDC + PTD-NH ₂) ^b	Dialysis + cross-linking	Nanoparticles (nanocages after PCL removal by TFA)	35–75	Cancer (ovary, cervical)	—	CHO, HeLa	302
(i) PCL- <i>b</i> -PEG-EGF	EGF	(i) and (ii) ROP of ϵ CL from HO-PEG-COOH	Carbodiimide (PCL- <i>b</i> -PEG-COOH/DCC/NHS + EGF-NH ₂) ^a	Dry down	Micelles	25	Cancer (breast)	Ellipticine	MCF7, MDA-MB-468	304
(ii) PCL- <i>b</i> -PEG-EGF	EGF	(i) and (ii) ROP of ϵ CL from HO-PEG-COOH	Carbodiimide (PCL- <i>b</i> -PEG-COOH/DCC/NHS + EGF-NH ₂) ^a	Dry down	Micelles	50–70	Cancer (breast)	—	MCF7, MDA-MB-468	306
(i) PCL- <i>b</i> -PEG-EGF	EGF	(i) and (ii) ROP of ϵ CL from HO-PEG-COOH	Carbodiimide (PCL- <i>b</i> -PEG-COOH/DCC/NHS + EGF-NH ₂) ^a	Dry down	Micelles	25–60	Cancer (breast)	—	MCF7, MDA-MB-468	305
(ii) PCL- <i>b</i> -PEG-EGF	EGF	(i) ROP of γ VL from MePEG-OH (ii) ROP of γ VL from HO-PEG-COOH	Carbodiimide (PCL- <i>b</i> -PEG-COOH/DCC/NHS + EGF-NH ₂) ^a	Dry down	Micelles	30–45	Cancer (breast)	—	MDA-MB-468	70
(i) PCL- <i>b</i> -PEG-EGF	Lactoferrin (Lf)	(i) ROP of ϵ CL from MePEG-OH (ii) ROP of ϵ CL from HO-PEG-COOH	Carbodiimide (PCL- <i>b</i> -PEG-COOH/DCC/NHS + Lf-NH ₂) ^b	Thin film hydration	Polymersomes	220	Brain delivery (Cancer, glioma)	Dox, tetrandrine	C6	307
(ii) PCL- <i>b</i> -PEG-EGF	Anti-EGFR Mab	(i) ROP of ϵ CL from MePEG-OH (ii) ROP of ϵ CL from HO-PEG-COOH	Carbodiimide (PCL- <i>b</i> -PEG-COOH/DCC/NHS + Mab-NH ₂) ^a	Nanoprecipitation	Micelles	25–30	Cancer (colon)	Dox	RKO	308

Table 3 (continued)

Structural parameters			Colloidal parameters			Application				
Architecture	Ligand	Synthetic method	Ligand coupling method	Formulation	Morphology	Diameter (nm)	Pathology/target	Drug	Cells/tissues/organs ^d	Ref.
(i) PCL- <i>b</i> -PEG-aptamer peptide (ii) PCL- <i>b</i> -PEG-TGN peptide	AS1411 DNA aptamer, TGN peptide	(i) ROP of εCL from HO-PEG-COOH (ii) ROP of εCL from HO-PEG-Mal	(i) <i>Carbodiimide</i> (PCL- <i>b</i> -PEG-COOH)/EDC/NHS + aptamer-NH ₂ ^b (ii) <i>Michael addition</i> (PCL- <i>b</i> -PEG-Mal + TGN-SH) ^b	Emulsion-solvent evaporation	Nanoparticles	150–170	Cancer (glioma)	Dtx	C6, bEnd.3 Biodistribution , C6	303
Ligand coupling by Michael addition PCL- <i>b</i> -PEG-cRGDfk	cRGDfk	ROP of εCL from HO-PEG-Mal	<i>Michael addition</i> (PCL- <i>b</i> -PEG-Mal + cRGDfk-SH) ^a (<i>via heterobifunctional linker</i> , 4- <i>mal-eimidobutyric acid N-succinimidyl ester</i>) <i>Michael addition</i> (PCL- <i>b</i> -PEG-Mal + Tf-SH) ^b	Emulsion-solvent evaporation	Micelles	35–45	Cancer (Kaposi's Sarcoma)	Dox	SLK	313
(i) PCL- <i>b</i> -PEG-Transferrin (ii) PCL- <i>b</i> -PEG-Tf	Transferrin	(i) ROP of εCL from PEG-OH (ii) ROP of εCL from HO-PEG-Mal	<i>Michael addition</i> (PCL- <i>b</i> -PEG-Mal + Tf-SH) ^b	Nanoprecipitation	Polymersomes	100	Cancer (glioma)	Dox	C6 Biodistribution , PK, C6	311
P(VL- <i>co</i> -EVL- <i>co</i> -AVL- <i>co</i> -OPD)-GIRLRG peptide	GIRLRG peptide	ROP of VL/OPD/AVL; epoxy formation (P(VL- <i>co</i> -OPD- <i>co</i> -AVL)/mCPBA)	<i>Thiol-ene</i> (P(VL- <i>co</i> -OPD- <i>co</i> -EVL- <i>co</i> -AVL) + GIRLRG-SH) ^b	Cross-linking in organic medium	Nanoparticles	n.d.	Cancer	Ptx	HUVEC, GL261 MDA-MB-231, GL261	133
(i) PCL- <i>b</i> -PEG-Angiopep (ii) PCL- <i>b</i> -PEG-angiopep	Angiopep	(i) ROP of εCL from MePEG-OH (ii) ROP of εCL from HO-PEG-Mal	<i>Michael addition</i> (PCL- <i>b</i> -PEG-Mal + angiopep-SH) ^b	Emulsion-solvent evaporation	Nanoparticles	100	Cancer (glioblastoma)	Ptx	U87 MG U87 MG	309
(i) PCL- <i>b</i> -PEG-Angiopep (ii) PCL- <i>b</i> -PEG-angiopep	Angiopep	(i) ROP of εCL from MePEG-OH (ii) ROP of εCL from HO-PEG-Mal	<i>Michael addition</i> (PCL- <i>b</i> -PEG-Mal + angiopep-SH) ^b	Emulsion-solvent evaporation	Nanoparticles	100	Cancer (brain capillary)	—	BCFCs Biodistribution	310
PCL- <i>b</i> -PEG-hNgf-EE peptide	hNgf-EE peptide	<i>Commercial</i>	<i>Michael addition</i> (PCL- <i>b</i> -PEG-Mal + hNgfEE-SH) ^b	Nanoprecipitation	Polymersomes	70–100	Hearing loss	—	PC-12, organotypic explant cultures	156
(i) PCL- <i>b</i> -PEG-OX26 Mab (ii) PCL- <i>b</i> -PEG-OX26	OX26 Mab	(i) ROP of εCL from MePEG-OH (ii) ROP of εCL from HO-PEG-Mal	<i>Michael addition</i> (PCL- <i>b</i> -PEG-Mal + OX26-SH) ^b	Nanoprecipitation	Polymersomes	100	Alzheimer's disease	NC-1900	Brain delivery , PK, AD model	312
Ligand coupling by reductive amination PCL- <i>b</i> -PEG-GRGDS	GRGDS	ROP of EO and εCL from 3,3-diethoxy-1-propanol	<i>Reductive amination</i> (PCL- <i>b</i> -PEO-CHO + GRGDS-NH ₂) ^b	Nanoprecipitation	Micelles	70–80	Cancer (skin)	—	B16-F10	319
PCL- <i>b</i> -PEG-GRGDS	GRGDS	ROP of EO and εBCL from 3,3-diethoxy-1-propanol	<i>Reductive amination</i> (PCL- <i>b</i> -PEO-CHO + GRGDS-NH ₂) ^b	Nanoprecipitation	Micelles	70–95	Cancer (skin)	Dox ^c	B16-F10	320

Table 3 (continued)

Structural parameters			Colloidal parameters			Application				
Architecture	Ligand	Synthetic method	Ligand coupling method	Formulation	Morphology	Diameter (nm)	Pathology/target	Drug	Cells/tissues/organs ^d	Ref.
PCL- <i>b</i> -PEG-GRGDGS	GRGDGS	ROP of EO and εBCL from 3,3-dithoxy-1-propanol	Reductive amination (PCL- <i>b</i> -PEO-CHO + GRGDS-NH ₂) ^b	Nanoprecipitation	Micelles	70–95	Cancer (breast)	Dox ^c	MDA-435/LCC6 WT, MDA-435/LCC6 MDR, MDA-435/LCC6 WT, MDA-435/LCC6 MDR	321
(i) PCL- <i>b</i> -PEO-RGD4C	RGD4C, TAT peptide	(i) ROP of EO and εBCL from 3,3-dithoxy-1-propanol	(i) Reductive amination (PCL- <i>b</i> -PEO-CHO + RGD4C-NH ₂) ^b	Nanoprecipitation	Micelles	70–95	Cancer (breast)	Dox ^c , siRNA	MDA-435/LCC6 MDR	322
(ii) PCL- <i>b</i> -PEO-TAT		(ii) ROP of EO and εCL from 3,3-dithoxy-1-propanol	(ii) Thiazolidine ring formation (PCL- <i>b</i> -PEO-CHO + TAT-SH) ^a							
Ligand coupling by photografting										
(i) PLGA	RGD	(i) ROP of LA/G from MePEG-OH	Photografting (PCL- <i>b</i> -PEG + RGD) ^a	Double emulsion-solvent evaporation	Nanoparticles	200–210	Vaccination	Albumin	Caco-2, Raji B/oral immunization	323
(ii) PLGA- <i>b</i> -PEG		(ii) ROP of LA/G from MePEG-OH								
(iii) PCL- <i>b</i> -PEG-RGD		(iii) ROP of eCL from PEG-AIEt ₂								
(i) PLGA	RGD, RGD peptide-mimetic	(i) ROP of LA/G from MePEG-OH	Photografting (PCL- <i>b</i> -PEG + RGD) ^a	Nanoprecipitation	Nanoparticles	140–150	Cancer (liver)	Ptx	HUVEC TLT	324
(ii) PLGA-PEG		(ii) ROP of LA/G from MePEG-OH								
(iii) PCL- <i>b</i> -PEG-RGD or RGD peptide-mimetic		(iii) ROP of eCL from PEG-AIEt ₂								
Ligand coupling by other coupling strategies										
PCL- <i>b</i> -P(PEGMA- <i>b</i> -co-PMA-FA)	FA	ATRP of PEGMA/AzPMA from HO-ATRP initiator; ROP of εCL from HO-P(PEGMA- <i>b</i> -AzPMA)	CuAAC (PCL- <i>b</i> -P(PEGMA- <i>b</i> -AzPMA) + alkyne-FA) ^c	Dialysis	Micelles	30	Cancer (cervical)	Ptx	HeLa	328
(i) PCL- <i>b</i> -PEG-Mannose	Mannose	(i) ROP of EO and εCL from N,N'-dimethylaminoethyl alkoxide	Quaternization (PCL- <i>b</i> -PEG-NMe ₂ + Mannose-Br) ^d	Nanoprecipitation	Nanoparticles	210–310	Vaccination			325
(ii) PLA		(ii) Commercial Nitration (H ₂ N-PEG- <i>b</i> -PCL + 4-nitrophenyl-iodoacetate)								
PCL- <i>b</i> -PEG-prestin-binding peptides (A665, A666)	Prestin binding peptides (A665, A666)		Thioether bond formation (PCL- <i>b</i> -PEG-I + peptide-SH) ^e	Nanoprecipitation	Polymersomes	85–125	Hearing loss		Rat cochlear explants, hair cells	154
PCL- <i>b</i> -PEG-Tet1 peptide	Tet1 peptide		Thioether bond formation (PCL- <i>b</i> -PEG-I + Tet1-SH) ^d	Nanoprecipitation	Polymersomes	85–125	Hearing loss		Transympnic injection and cochleostomy	326
(i) PLA	WGA	(i) Commercial ROP of LA from MePEG-OH	Av/biotin (PCL- <i>b</i> -PEG-biotin + Av + WGA-biotin) ^b	Nanoprecipitation	Nanoparticles	100	—	—	uptake by spiral ganglion cells Caco-2	327
(ii) PLA- <i>b</i> -PEG		(ii) ROP of LA from MePEG-OH								
(iii) PCL- <i>b</i> -PEG-WGA		(iii) ROP of εCL from biotin-PEG-NH ₂								

^a Coupling prior to nanocarrier formation. ^b Coupling post-nanocarrier formation. ^c Drug covalently linked to the (co)polymer. ^d *In vivo* experiments are written in bold.

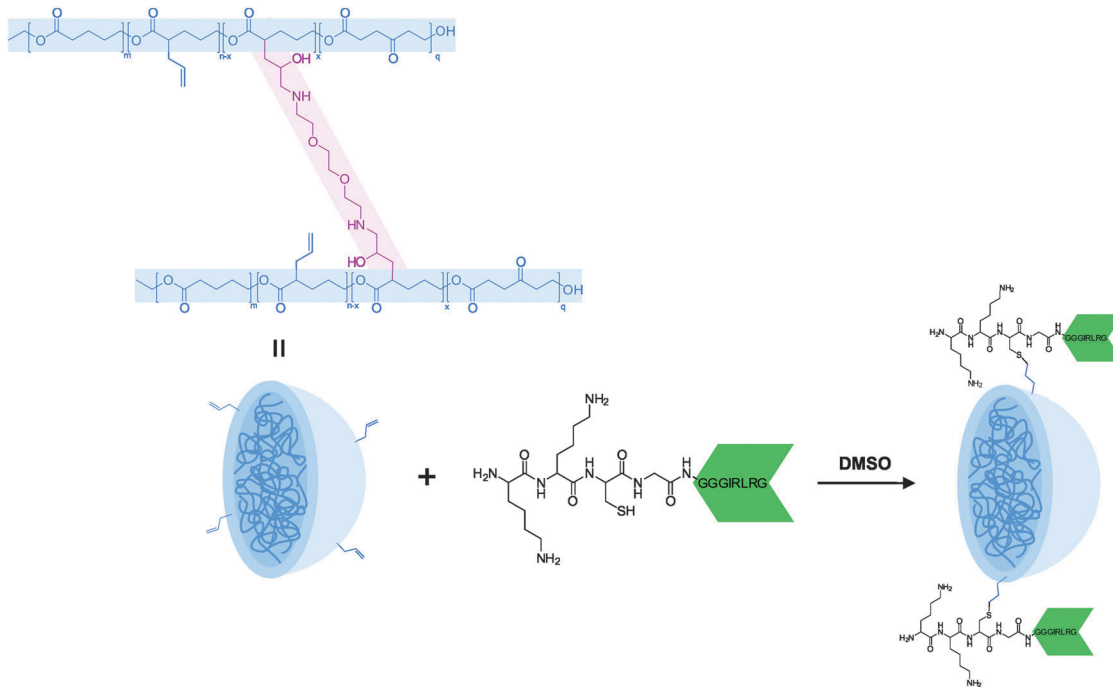


Fig. 21 Synthetic strategy to design GIRLRG-targeted poly(valerolactone-co-epoxyvalerolactone-co-allylvalerolactone-co-oxepanedione) nanoparticles.

PCL-*b*-P(OEGMA-*co*-AzPMA) was then reacted with alkyne-FA under CuAAC conditions.

Targeted PCL-based nanocarriers were prepared almost exclusively by conventional methods (*e.g.*, nanoprecipitation, emulsion-solvent evaporation, dialysis). However, another approach was proposed by the group of Passarella.¹³³ The linear poly(valerolactone-*co*-epoxyvalerolactone-*co*-allylvalerolactone-*co*-oxepanedione) containing 11% of epoxide cross-linking moieties was cross-linked in organic medium with 2,2'-(ethylenedioxy)-bis(ethylamine) to form nanoparticles of controlled size. Peptide-conjugation was then achieved by thiol-ene chemistry between the cysteine-terminated peptide and the allyl groups at the surface of NPs (Fig. 21).

3.4.2.3. Hyperbranched amphiphilic polyester block copolymers (Boltorn H40). Hyperbranched amphiphilic polyester block copolymers have also been explored to develop functionalized micelles for drug delivery applications. These unimolecular micelles have a core made of the dendritic Boltorn H40 surrounded by a hydrophobic inner shell and a hydrophilic PEG-based outer shell at the extremity of which are anchored the targeting ligands. The Boltorn H40 was selected due to its biodegradability and the presence of many functional hydroxyl end groups useful for further modifications. In practice, Boltorn H40 was used as macroinitiator for the ROP of LA or ϵ CL, leading to the formation of the inner hydrophobic shell of PLA or PCL. The ROP of ϵ CL and benzyl malolactonate was also carried out, yielding a hydrophobic layer made of random poly(caprolactone-*co*-malic acid) blocks. The hydrophilic functionalized shell was synthesized according to different reaction schemes: (i) esterification of H40-PCL-OH with the carboxyl end groups of PEG-FA (previously synthesized by DCC-assisted

reaction of FA and α -amine- ω -hydroxy PEG);³²⁹ (ii) oxidation of hydroxyl end groups to carboxyl functions by reaction with succinic anhydride and then successive DCC activation to conjugate FA-PEG-OH (previously synthesized by DCC/NHS assisted reaction of FA with α -hydroxy- ω -amine PEG);³³⁰ (iii) oxidation of hydroxyl end groups to carboxyl functions followed by carbodiimide assisted conjugation to PEG. Functionalization with FA was finally obtained by esterification of carboxylic group of FA with the remaining hydroxyl group of the PEG (Fig. 22).³³¹

The synthesis of hyperbranched polyester amphiphilic block copolymers was also reported by a combination of ROP (ϵ CL from Boltorn H40 as macroinitiator) and ATRP (copolymerization of OEGMA (oligo(ethylene glycol) monomethyl ether methacrylate)) and AzPMA (3-azidopropyl methacrylate) from H40-*g*-PCL-Br. Ligand coupling was achieved by click reaction of the resulting H40-PCL-P(OEGMA-*co*-azPMA) with an alkyne-containing folate (Fig. 23).³³² A T_1 -type MRI contrast agent was also tethered using a similar pathway.

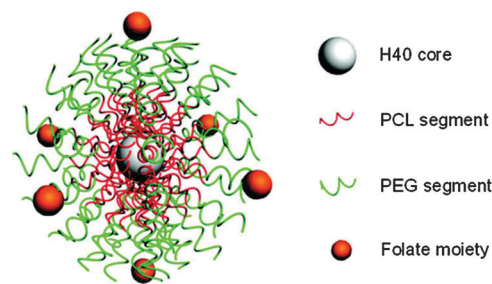


Fig. 22 Structure of amphiphilic hyperbranched polymer H40-PCL-PEG-FA (reproduced with permission from ref. 331. Copyright 2008, American Chemical Society).

Table 4 Main characteristics and applications of targeted Boltorn H40-based nanocarriers

Structural parameters		Colloidal parameters			Application				
Architecture	Ligand Synthetic method	Ligand coupling method	Formulation	Morphology (nm)	Diameter (nm)	Pathology/target	Drug	Cells/tissues/organs	Ref.
Ligand coupling by carbodiimide chemistry (i) H40-P(CL-co-MA)-FA PEG (ii) H40-P(CL-co-MA)-PEG-FA	ROP of eCL/MABz from H40-OH; <i>Carbodiimide</i> (H40-P(MABz-co-CL)-OH + MePEG-COOH/DCC or FA-PEG-COOH/DCC)	<i>Carbodiimide</i> (HO-PEG-NH ₂ + FA-COOH/DCC/NHS) or anhydride ^a	Dialysis	Micelles	25	Cancer (breast)	Dox ^b	4T1	329
H40-PLA- <i>b</i> -PEG-FA	ROP of LA from H40 + succinic anhydride; <i>Carbodiimide</i> (H40-PLA-COOH/DCC/DMAP + FA-PEG-OH)	<i>Carbodiimide</i> (HO-PEG-NH ₂ + FA-COOH/DCC/NHS) ^a	Dialysis	Micelles	100	Cancer (breast)	Dox	4T1	330
H40-PCL- <i>b</i> -PEG-FA	ROP of eCL from H40 + succinic anhydride; <i>Carbodiimide</i> (H40-PCL-COOH/DCC + HO-PEG-OH)	<i>Carbodiimide</i> (H40-PCL- <i>b</i> -PEG-OH + FA-COOH/DCC) ^a	Dialysis	Micelles	<100	Cancer (lung, cervical)	5-FU, Ptx	Hela, A549	331
Ligand coupling by copper-catalyzed azide-alkyne cycloaddition (CuAAC) H40-PCL- <i>b</i> -P(PEGMA-co-MA)-FA	ROP of eCL from H40; ATRP of PEGMA/AzPMA from H40-PCL-Br	<i>CuAAC</i> (PCL- <i>b</i> -P(PEGMA-co-alkyne-FA) ^a	Nanoprecipitation	Micelles	15–30	Cancer (cervical)	Ptx	Hela	332

^a Coupling prior to nanocarrier formation. ^b Drug covalently linked to the (co)polymer.**Table 5** Main characteristics and applications of targeted other polyester-based nanocarriers

Structural parameters		Colloidal parameters			Application				
Architecture	Ligand Synthetic method	Ligand coupling method	Formulation	Morphology (nm)	Diameter (nm)	Pathology/target	Drug	Cells/tissues/organs ^b	Ref.
Ligand coupling by carbodiimide chemistry P(HB-co-HO)- <i>b</i> -PEG-FA HBPH-FA	<i>Fermentation</i> from <i>S. freddiei</i> FA FA	<i>Carbodiimide</i> (P(HB-co-HO)-COOH/DCC + FA-PEG-NH ₂) ^a <i>Carbodiimide</i> (HBPH/CDI + FA-NH ₂) ^a	Double emulsion-solvent evaporation Emulsion-solvent evaporation	Nanoparticles Nanoparticles	240 60–65	Cancer (cervical) Cancer (breast, lung)	Dox Cytochrome C	Hela Hela MCF-7, A549	334 333

^a Coupling prior to nanocarrier formation. ^b *In vivo* experiments are written in bold.

3.4.2.4. Other polyesters. Some examples of nanocarriers made of other polyesters have been reported. The melt polymerization strategy was applied to a water soluble AB₂ type monomer (3-[bis(2-hydroxyethyl)amino]propionic acid ethyl ester) in order to synthesize a novel water soluble highly branched polyhydroxyl polymer.³³³ This led to the formation of a three dimensional polymer with amphiphilic cavities in which both the hydrophilic cytochrome C and an amphiphilic fluorescent dye were encapsulated. Moreover, the numerous hydroxyl groups at the polymer surface offered the possibility of high functionalization. This was performed under CDI activation and further conjugation to amino folate (Fig. 24).

Polyhydroxylalkanoates (PHA) are bio-polyesters synthesized and accumulated by different prokaryote species. These polymers show physico-chemical and mechanical properties similar to those of PLGA and are thus extremely attractive for potential application in the biomedical field, especially for drug delivery and imaging purposes. Among the various PHAs, the poly-(3-hydroxybutyrate-co-3-hydroxyoctanoate) (P(HB-co-HO)) copolymer, synthesized by a *S. fredii* strain, has been recently investigated by Zhang and coworkers.³³⁴ In order to prepare functionalized NPs, the natural polymer was modified by carbodiimide chemistry with introduction of a PEG block and a FA as a targeting ligand. First, DCC activated FA was reacted with diamino-PEG and the resulting FA-PEG-NH₂ was reacted with P(HB-co-HO) with DCC and pyridine as catalyst, yielding the desired P(HB-co-HO)-b-PEG-FA.

3.4.3. POLYSACCHARIDES. Polysaccharides are one of the most popular polymeric materials used to prepare nanocarriers for drug delivery because of their outstanding physical and biological properties. Polysaccharides have a large number of reactive groups, a wide range of molecular weight, varying chemical composition, which contribute to their diversity in structure and in property. The chemical structures of common polysaccharides used in this field are presented in Fig. 25.

Due to the presence of various functional groups on the polymer backbone, polysaccharides can be easily modified chemically and biochemically, resulting in many kinds of sugar-based derivatives. As natural biomaterials, polysaccharides are highly stable, safe, non-toxic, hydrophilic and some of them are biodegradable. In addition, polysaccharides have abundant resources in nature and cost less in their processing.

3.4.3.1. Chitosan. Chitosan, which derives from the partial deacetylation of chitin, is a copolymer of *N*-acetylglucosamine and glucosamine units frequently used in biomedical applications and is undoubtedly the most employed polysaccharide for targeted drug delivery. Most of the examples of targeted chitosan nanocarriers employed unmodified chitosan, however, a few reports also used trimethylated chitosan,³³⁵ hydrophobically modified glycol chitosan-cholanic acid (HGC),³³⁶ galactosylated chitosan,³³⁷ *N*-octyl-*O*, *N*-carboxymethyl chitosan (OCC)³³⁸ or octadecyl-quaternized lysine modified chitosan (OQLCS).³³⁹ The reason for the extensive use of chitosan for the design of polysaccharide-based targeted nanocarriers is partially due to the presence of naturally-occurring primary amino groups on the chitosan backbone that can be reacted with ester-activated or

aldehyde-containing compounds such as: (i) ligands;^{138,335,340–350} (ii) linkers for further coupling;^{336,337,351,352} (iii) polymer chains such as PEG;^{344,353,354} (iv) or other moieties such as octaldehyde, quaternized octadecyl lysine to finely tune its solubility.^{336,338} For similar purposes, carboxylic acid groups can also be readily inserted in chitosan structure either *via* carboxymethylation using monochloroacetic acid^{338,355} or by amidation using succinic anhydride.³⁵⁶ Radical addition can also be performed on allyl-chitosan in the presence of 4,4'-azobis (4-cyanovaleric acid) (ACVA) and a poly(PEGMA) previously synthesized by the RAFT technique to yield the corresponding grafted chitosan-poly(PEGMA).³⁵⁷

The main strategies to synthesize targeted chitosan nanocarriers relied on: (i) the direct coupling of the homing device to chitosan; (ii) the coupling of the ligands *via* a heterobifunctional linker which can be either molecular (*e.g.*, sulfo-SMCC, SMCC, SPDP, see Fig. 14) or macromolecular such as those based on PEG. Most of the time, chitosan nanocarriers were prepared by ionic gelation after chitosan functionalization with small ligands, whereas more bulky ones, such as peptides or antibodies, were linked post-nanocarrier formation. The colloidal morphologies were almost exclusively spherical nanoparticles but some examples reported the formation of chitosan-based micelles³³⁸ and polymeric liposomes.³³⁹ Bioactive drugs such as Interleukin-1 receptor antagonist (*i.e.*, pDNA),^{335,337,341,342,357} MTX,³⁴³ Dox,^{338,353,356} Oli-A,³⁴⁵ CPT,³⁴⁶ anti-caspase-3 peptide Z-DEVD-FMK,^{353,354} Gem,³⁴⁷ siRNAs^{348,349,352} and ADR³⁵⁰ were encapsulated within the chitosan matrix during nanocarrier formation. Occasionally, some drugs, such as MMC³⁴⁴ and Dox,³⁵¹ were covalently linked to the chitosan skeleton by traditional coupling strategies.

Carbodiimide-assisted coupling strategy. The vast majority of ligand coupling relied on carbodiimide chemistry, whereby COOH-containing ligands were previously activated by EDC (in the presence or absence of NHS/sulfo-NHS, see Fig. 14) and reacted with amino groups of chitosan to form an amide linkage (Fig. 26).^{138,335,340–345,347–349,354–356} This was successfully applied to FA,^{335,340–345,355,356} CK69,¹³⁸ scFvCD7,³⁴⁸ TAT and TGA peptides³⁴⁹ and the anti-HER2 antibody.³⁴⁷ However, chitosan can also be functionalized with GFFG or LGPV tetrapeptides,³⁴⁶ linear PEG chains^{353,354} by EDC/NHS at the distal end of which the ligand of interest is further installed. The radical coupling of a poly(PEGMA) polymer onto allyl-chitosan was also reported and was further linked to GSH after its activation by EDC/NHS.³⁵⁷ Octadecyl-quaternized lysine-modified chitosan (OQLCS) was both PEGylated and functionalized by FA using PEG-NHS and FA-NHS, respectively.³³⁹

Chitosan was pre-functionalized by heterobifunctional linkers (*e.g.*, sulfo-SMCC, SMCC, see Fig. 14) in order to position maleimide moieties, allowing Michael addition to proceed with thiol-bearing ligands (previously obtained by their modification with 2-iminothiolane).^{336,351} This strategy was exemplified with anti-HER2 Mab, which was linked at the surface of chitosan nanoparticles,³⁵¹ and by the atherosclerotic plaque (AP)-homing peptide which was coupled to hydrophobically modified glycol chitosan-cholanic acid (HGC) prior to nanoparticle formation.³³⁶

Table 6 Main characteristics and applications of targeted chitosan-based nanocarriers

Structural parameters		Colloidal parameters			Application		Ref.
Architecture	Ligand	Synthesis method	Ligand coupling method	Formulation	Morphology	Diameter (nm)	
Ligand coupling by carbodiimide chemistry Chitosan-FA (99%) ^d	FA	—	Carbodiimide (Chitosan-NH ₂ + FA-COOH/EDC) ^a	Ionic gelation	Nanoparticles	90–110	Cancer (diagnosis)
Chitosan-FA	FA	Depolymerization (HNO ₃)	Carbodiimide (Chitosan-NH ₂ + FA-COOH/EDC) ^a	Ionic gelation	Nanoparticles	110	Arthritis
Chitosan-FA	FA	—	Carbodiimide (Chitosan-NH ₂ + FA-COOH/EDC) ^a	Ionic gelation	Nanoparticles	100–350	Cancer (gene therapy)
Trimethylated chitosan-FA	FA	Depolymerization (NaNO ₂ /NaBH ₄); trimethylation	Carbodiimide (Chitosan-NH ₂ + FA-COOH/EDC/NHS) ^a	Ionic gelation	Nanoparticles	100	Cancer (gene therapy)
Chitosan-FA (95%) ^d	FA	—	Carbodiimide (Chitosan-NH ₂ + FA-COOH/DCC/NHS) ^a	Ionic gelation	Nanoparticles	240–370	Cancer
Chitosan-FA (85%) ^d	FA	Carboxymethylation (monochloroacetic acid + chitosan) ^a	Carbodiimide (Chitosan-COOH/EDC + FA-NH ₂) ^a	Sonication	Nanoparticles	150–180	Cancer (skin, cervical)
Chitosan-FA	FA	Amidation (chitosan + succinic anhydride) ^a	Carbodiimide (Chitosan-COOH/EDC + FA-NH ₂) ^a	Sonication	Nanoparticles	200–430	Cancer (cervical)
Chitosan-FA-g-PEG (95%) ^d	FA	Carbodiimide (Chitosan-NH ₂ + PEG-COOH/EDC) ^b	Carbodiimide (Chitosan-NH ₂ + FA-COOH/EDC) ^b	Ionic gelation	Nanoparticles	200	Cancer (cervical, liver)
Chitosan-FA (98%) ^d	FA	—	Carbodiimide (Chitosan-NH ₂ + FA-COOH/DCC/NHS) ^a	Ionic gelation	Nanoparticles	70–990	Cancer (leukemia)
Chitosan-tetra-peptides (GFFG or LGPV)-FA (95%) ^d	FA	Carbodiimide (Chitosan-NH ₂ + GFFG or LGPV tetrapeptides-COOH/NHS/EDC) ^b	Carbodiimide (Chitosan-tetra-peptide-NH ₂ + FA-COOH/NHS/EDC) ^b	Sonication in PBS/NaCl	Nanoparticles	140–160	Cancer (lung, liver)
Octadecyl-quaternized lysine modified chitosan (OQLCS)-FA/OQLCS-PEG	FA	Carbodiimide (OQLCS-NH ₂ + PEG-NHS) ^a	Carbodiimide (OQLCS-NH ₂ + PEG-FA-COOH/DCC/NHS) ^a	Lipid film hydration and sonication	Polymeric liposomes	160	Cancer (breast)
Galactosylated chitosan-spermine	Spermine, galactose	Depolymerization (NaNO ₂)	Carbodiimide (Chitosan-NH ₂ + lactobionic acid/EDC/NHS) ^a ; <i>peptidic coupling</i> (Chitosan/DSC/DMAP + spermine) ^a	Ionic gelation	Nanoparticles	240–560	Cancer (liver)
Chitosan-g-poly(PEGMA)-GSH (90%) ^d	Glutathione (GSH)	Radical addition (poly(PEGMA)-CPADB + allyl-chitosan/ACVA) ^a	Carbodiimide (Chitosan-g-poly(PEGMA)-COOH/EDC/NHS + GSH-NH ₂) ^a	Ionic-gelation	Nanoparticles	100–250	Gene vectors
Chitosan-TAT/TGA	TAT, TGA	—	Carbodiimide (Chitosan-NH ₂ + TGA-COOH/TAT-COOH/EDC/NHS) ^a	Solubilization in water	Nanoparticles	180–240	HEK293
Chitosan-CKS9 (92%) ^d	CKSTHPLSC (CKS9)	—	Carbodiimide (Chitosan-NH ₂ + CK69-COOH/EDC/NHS) ^a	Ionic gelation	Nanoparticles	190–270	Peyer's patch (vaccine)

Table 6 (continued)

Structural parameters			Colloidal parameters			Application		Ref.
Architecture	Ligand	Synthesis method	Ligand coupling method	Formulation	Morphology	Diameter (nm)	Pathology/target	
Chitosan-anti-HER2 (80–85%) ^d	Anti-HER2 Mab	—	<i>Carbodiimide</i> (Chitosan-NH ₂ + anti-HER-COOH/EDC/NHS) ^b	Ionic gelation	Nanoparticles	250–300	Cancer (pancreas)	347
Chitosan-scFvCD7 (86%) ^d	scFvCD7	—	<i>Carbodiimide</i> (Chitosan-NH ₂ + scFvCD7-COOH/EDC/sulfo-NHS) ^b	Ionic gelation	Nanoparticles	300–350	Infectious disease	348
Ligand coupling by Michael addition								
Hydrophobically modified glycol chitosan-cholic acid (HGCA)-AP peptide	Atherosclerotic plaque (AP)-homing peptide	<i>Carbodiimide</i> (Chitosan-NH ₂ + 5β-cholic acid/EDC/NHS) ^c	<i>Michael addition</i> (Chitosan-Mal + AP-SH) ^c	Sonication in PBS	Nanoparticles	300	Atherosclerosis	336
Chitosan-anti-HER2 (96%) ^d	anti-HER2 Mab	—	<i>Michael addition</i> (anti-HER2-SH + Chitosan-Mal) ^b	Self-assembly in water	Nanoparticles	230–670	Cancer (breast, ovary)	351
Chitosan-g-PEG-OX26 (70–90%) ^d	OX26 (CD71)	<i>Carbodiimide</i> (Chitosan-NH ₂ + biotin-PEG-COOH/EDC/NHS) ^c	<i>Michael addition</i> (OX26-Mal + SAV-SH); <i>Sav/biotin</i> (Chitosan-g-PEG-biotin + SAV-OX26) ^b	Ionic gelation	Nanoparticles	640	CNS delivery (ischemia)	354
Chitosan-g-PEG-OX26 (14%) ^d	OX26 (CD71)	<i>Carbodiimide</i> (Chitosan-NH ₂ + biotin-PEG-COOH/EDC/NHS) ^c	<i>Michael addition</i> (OX26-Mal + SAV-SH); <i>Sav/biotin</i> (Chitosan-g-PEG-biotin + SAV-OX26) ^b	Ionic gelation	Nanoparticles	640	CNS delivery (ischemia)	353
Ligand coupling by other ligation strategies addition								
Chitosan-RGD	RGD	—	<i>Disulfide bridge formation</i> (Chitosan-PDS + RGD-SH) ^a	Ionic gelation	Nanoparticles	200	Cancer (ovary)	352
Chitosan (>85%) ^d	Glycyrrhizin (GL)	—	<i>Imine formation</i> (CHO-GL + Chitosan-NH ₂) ^b	Solubilization in water	Nanoparticles	140–260	Cancer (liver)	350
N-octyl-O, N-carboxymethyl chitosan (OCC)-PEG-OCT	Octreotide (OCT)	<i>Carboxymethylation</i> (Chitosan-NH ₂ + chloroacetic acid); <i>reductive amination</i> (Chitosan-NH ₂ + octaldehyde) ^c	<i>Anchoring</i> (OCC + SA-PEG-OCT) ^a	Dialysis method	Micelles	100–140	Cancer (breast, lung)	338

^a Coupling prior to nanocarrier formation. ^b Coupling post-nanocarrier formation. ^c Drug covalently linked to the (co)polymer. ^d Percentage of deacetylation. ^e *In vivo* experiments are written in bold.

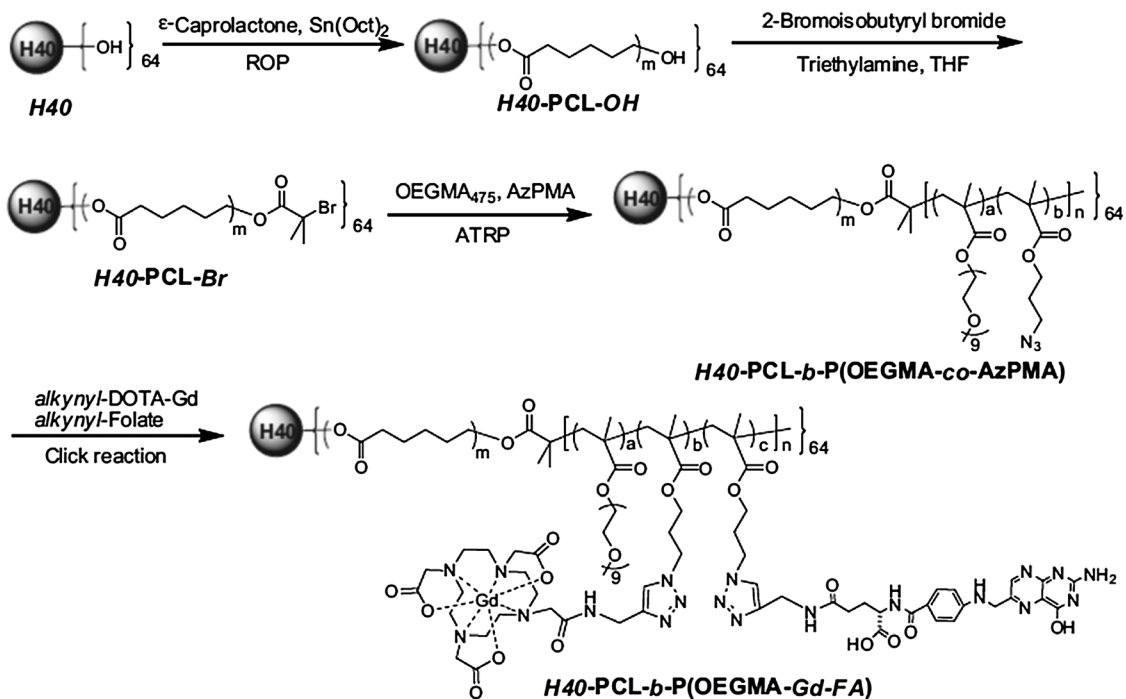


Fig. 23 Synthetic route employed for the preparation of amphiphilic multi-arm star block copolymers, H40-PCL-b-P(OEGMA-Gd-FA), by a combination of ROP, ATRP and click chemistry (reprinted with permission from ref. 332. Copyright 2011, Elsevier).

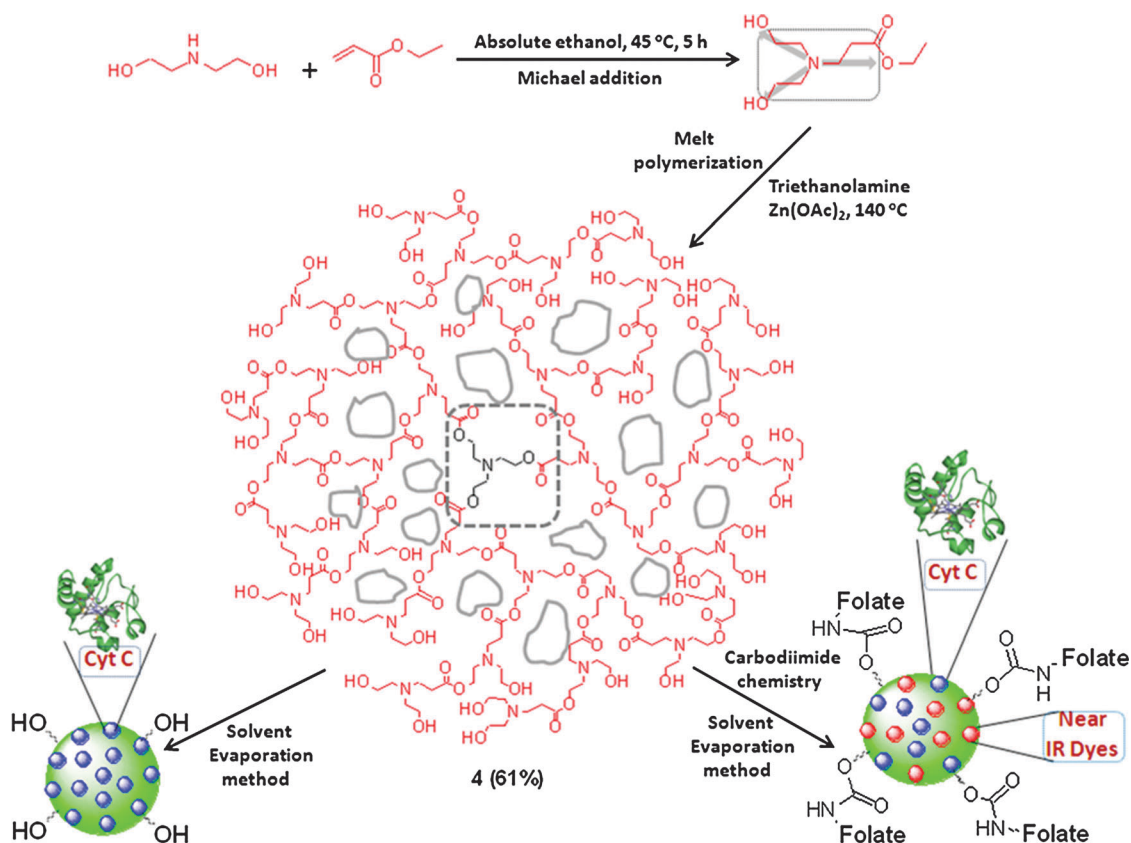


Fig. 24 Schematic representation of the synthesis of three dimensional hydrophilic HBPH polymer (4) and its functional HBPH nanoparticles (adapted with permission from ref. 333. Copyright 2010, American Chemical Society).

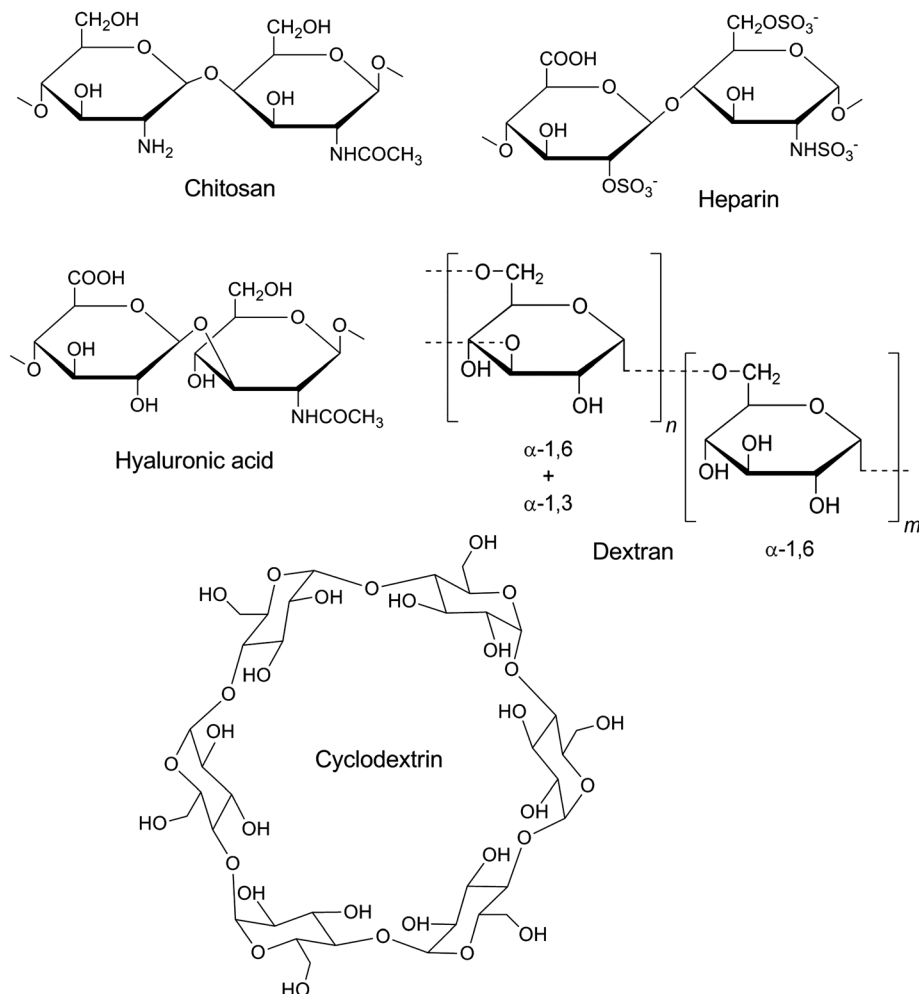


Fig. 25 Chemical structures of the main polysaccharides used for targeted drug delivery.

Thiol–maleimide Michael addition ligation. A combination of Michael addition and SAV/biotin ligation was employed in order to design chitosan-*g*-PEG-biotin-SAV-OX26 nanoparticles.^{353,354} In these studies, the OX26 antibody was reacted with MBS (Fig. 14) in order to position maleimide groups and further linked to thiol-reactive SAV obtained after thiolation of SAV by means of 2-iminothiolane. In a second step, the resulting OX26-SAV was bounded to chitosan-*g*-PEG-biotin nanoparticles, previously obtained by the coupling of chitosan and biotin-PEG-COOH *via* EDC/NHS chemistry (Fig. 27).

Other ligation strategies. Other synthetic strategies were employed and relied on: (i) imine formation between chitosan nanoparticles and aldehyde-derivatized glycyrrhizin (GL);³⁵⁰ (ii) disulphide bridge formation between a thiol-bearing RGD and chitosan bearing PDS groups, previously obtained by reaction of chitosan and SPDP (Fig. 14);³⁵² (iii) peptidic coupling after activation of chitosan with DSC/DMAP followed by its reaction with spermine³³⁷ and (iv) simple anchoring of octreotide-PEG-stearic acid (OCT-PEG-SA) in *N*-octyl-*O*, *N*-carboxymethyl chitosan (OCC).³³⁸

3.4.3.2. Cyclodextrin. The enzymatic degradation of starch by cyclodextrin-glycosyltransferase (CGT) produces cyclic oligomers called cyclodextrins (CDs, also called cycloamyloses) which are non-reducing, crystalline, water soluble, cyclic, oligosaccharides. Cyclodextrins consist of glucose monomers arranged in a donut shape ring. Three naturally occurring CDs are α -CD, β -CD and γ -CD. All the hydroxyl groups in CDs are oriented to the outside of the ring while the glucosidic oxygen and two rings of the non-exchangeable hydrogen atoms are directed towards the interior of the cavity. This combination gives to CDs a hydrophobic inner cavity and a hydrophilic exterior. The hydrophobic internal cavity provides the capability to form inclusion complexes with a variety of “guest” hydrophobic molecules such as aromatics, alcohols, fatty acids, esters, *etc.*

CDs are currently employed in pharmaceutical formulations and because of their low toxicity and the lack of immune response, they also represent an ideal starting material for drug delivery purposes.³⁵⁸

The group of Davis reported a great deal of work concerning the design of targeted CD-based nanoparticles for the delivery of nucleic acids. All their work relied on the design of a linear

Table 7 Main characteristics and applications of targeted cyclodextrin-based nanocarriers

Structural parameters		Colloidal parameters			Application		Cells/tissues/ organs ^b	Ref.
Architecture	Ligand	Synthesis method	Ligand coupling method	Formulation	Morphology	Diameter (nm)		
Ligand coupling by Michael addition βCDP-g- AD-PEG-Tf	Transferrin (Tf)	Polym. of β-CD/dimethylsuberimidate.2HCl; <i>carbodiimide</i> (4-imidazoleacetic acid/EDC/NHS + βCDP-NH ₂); <i>binding</i> (PEG-AD + βCDP)	<i>Michael addition</i> (vinylsulfone-PEG-AD + TF-NH ₂) or <i>reductive amination</i> (TF-CHO + AD-PEG-NH ₂); <i>binding</i> (AD-PEG-Tf + βCDP)	Self-assembly in water	Nanoparticles	100–150	Cancer (metastatic)	K562, PC-3 359
βCDP-g- AD-PEG-Tf	Transferrin (Tf)	Polym. of β-CD/dimethylsuberimidate.2HCl; <i>carbodiimide</i> (4-imidazoleacetic acid/EDC/NHS + βCDP-NH ₂); <i>binding</i> (PEG-AD + βCDP)	<i>Michael addition</i> (vinylsulfone-PEG-AD + TF-NH ₂); <i>binding</i> (AD-PEG-Tf + βCDP) ^a	Self-assembly in water	Nanoparticles	70	Cancer (skin)	Detection in human melanoma; siRNA-specific mRNA reduction and fragmentation HeLa 362
βCDP-g- AD-PEG-Tf	Transferrin (Tf)	Polym. of β-CD/dimethylsuberimidate.2HCl; <i>carbodiimide</i> (4-imidazoleacetic acid/EDC/NHS + βCDP-NH ₂); <i>binding</i> (PEG-AD + βCDP)	<i>Michael addition</i> (vinylsulfone-PEG-AD + TF-NH ₂); <i>binding</i> (AD-PEG-Tf + βCDP) ^a	Self-assembly in water	Nanoparticles	50–180	Cancer	siRNA (siLuc, siCON1), pDNA (pGL3-CV) HeLa 361
βCDP-g- AD-PEG-Tf	Transferrin (Tf)	Polym. of β-CD/dimethylsuberimidate.2HCl; <i>carbodiimide</i> (4-imidazoleacetic acid/EDC/NHS + βCDP-NH ₂); <i>binding</i> (PEG-AD + βCDP)	<i>Michael addition</i> (vinylsulfone-PEG-AD + TF-NH ₂); <i>binding</i> (AD-PEG-Tf + βCDP) ^a	Self-assembly in water	Nanoparticles	60–100	Cancer (neuroblastoma)	siRNA (siR2A + 5, siR2B + 5, siR2B + 6) Neuro2A Neuro2A 364
βCDP-g- AD-PEG-Tf	Transferrin (Tf)	Polym. of β-CD/dimethylsuberimidate.2HCl; <i>carbodiimide</i> (4-imidazoleacetic acid/EDC/NHS + βCDP-NH ₂); <i>binding</i> (PEG-AD + βCDP)	<i>Michael addition</i> (vinylsulfone-PEG-AD + TF-NH ₂); <i>binding</i> (AD-PEG-Tf + βCDP) ^a	Self-assembly in water	Nanoparticles	90–120	Cancer (neuroblastoma)	siRNA (against luciferase) Neuro2A 360
βCDP-g- AD-PEG-Tf	Transferrin (Tf)	Polym. of β-CD/dimethylsuberimidate.2HCl; <i>carbodiimide</i> (4-imidazoleacetic acid/EDC/NHS + βCDP-NH ₂); <i>binding</i> (PEG-AD + βCDP)	<i>Michael addition</i> (vinylsulfone-PEG-AD + TF-NH ₂); <i>binding</i> (AD-PEG-Tf + βCDP) ^a	Self-assembly in water	Nanoparticles	50	Cancer (cervical, ovary, colon)	DNazyme A2780, HT29, HeLa HT29 363
βCDP-g- AD-PEG-Tf	Transferrin (Tf)	Polym. of β-CD/dimethylsuberimidate.2HCl; <i>carbodiimide</i> (4-imidazoleacetic acid/EDC/NHS + βCDP-NH ₂); <i>binding</i> (PEG-AD + βCDP)	<i>Michael addition</i> (vinylsulfone-PEG-AD + TF-NH ₂); <i>binding</i> (AD-PEG-Tf + βCDP) ^a	Self-assembly in glucose 5%	Nanoparticles	70	Cancer	siRNA (siR2B + 5) Non-human primates 365
βCDP-g- AD-PEG-Tf	Transferrin (Tf)	Polym. of β-CD/dimethylsuberimidate.2HCl; <i>carbodiimide</i> (4-imidazoleacetic acid/EDC/NHS + βCDP-NH ₂); <i>binding</i> (PEG-AD + βCDP)	<i>Michael addition</i> (vinylsulfone-PEG-AD + TF-NH ₂); <i>binding</i> (AD-PEG-Tf + βCDP) ^a	—	Nanoparticles	50	Cancer	siRNA (siEFBP2, siEFBP2mut) Ewing's sarcoma mouse model 366

^a Coupling prior to nanoparticle formation. ^b *In vivo* experiments are written in bold.

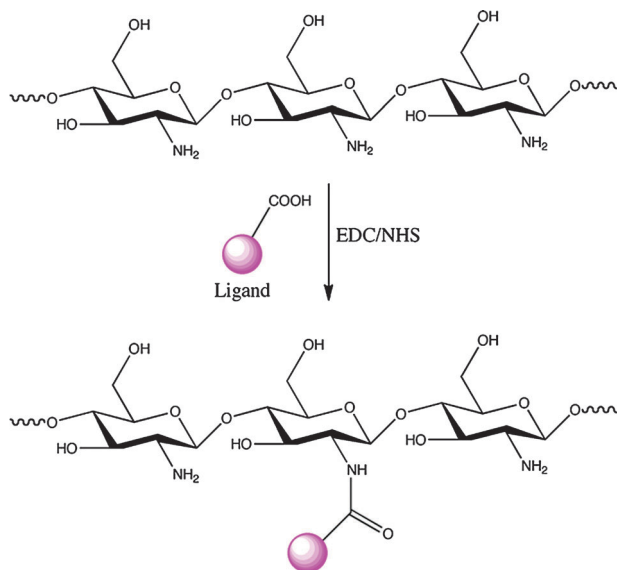


Fig. 26 Peptidic coupling between ligand-COOH and Chitosan-NH₂.

CD-containing water-soluble copolymer synthesized by the condensation copolymerization of difunctionalized β CDs with dimethyl-suberimidate-2HCl (a comonomer bearing six methylene groups separating the charges in the backbone). Typically, these polycations present ~ 5 – 6 repeating units and thus are low molecular weight polymers.³⁵⁹ Imidazole moieties were then conjugated at the extremities of the polymer by amidation (*via* EDC/NHS) of the primary amines with 4-imidazoleacetic acid (Fig. 28a). The formation and the stabilization of the CD-based nanoparticles as well as their concomitant functionalization with ligands of interest were achieved by adamantane (AD)-CD “host-guest” interactions using an AD-PEG-hTf. This heterobifunctional compound was built by the Michael addition of hTf onto vinylsulfone-PEG-AD.

In aqueous solution, the positively charged copolymer self-assembles with polyanionic nucleic acids (*i.e.*, pDNA, DNAzyme and siRNA) *via* electrostatic interactions, leading to β CDP/nucleic acids nanocarriers with variable features and sizes. Upon addition of AD-PEG₅₀₀₀-hTf, AD spontaneously forms inclusion with the β CD-units residing at the surface of the complexes,

leading to targeted CD-based nanocarriers with average diameters from 50 to 180 nm (Fig. 28b). Typically, a 70 nm nanoparticle can contain $\sim 10\,000$ CDP polymer chains, ~ 2000 siRNA molecules, ~ 4000 AD-PEG₅₀₀₀ molecules, and ~ 100 AD-PEG₅₀₀₀-Tf molecules. This represents a significant payload of siRNA and a large ratio of siRNA to targeting ligand.^{360–366}

3.4.3.3. Other polysaccharides. Several other polysaccharides have also been involved in the design of targeted nanoparticles. Among them, one can find: (i) heparin, a highly sulfonated glycosaminoglycan;^{368–370} (ii) xyloglucan, a β -(1-4)-glucan backbone partially substituted by α -(1,6)-linked xylose units³⁷¹ and (iii) dextran, a complex branched glucan.³⁷²

Targeted heparin nanoparticles were designed by a combination of amidation with succinic anhydride (in order to install carboxylic acid groups on heparin) followed by the coupling of the ligand bearing amine groups by EDC/DCC-assisted chemistry. FA (previously converted into its amino derivative) was linked prior to nanoparticle formation by self-assembly,^{369,373} whereas the ScFv EGF was coupled at the surface of preformed heparin nanoparticles using EDC/NHS activation (Fig. 29).³⁶⁸ This route was also followed to link an amino-PEG-FA onto heparin in order to yield the heparin-g-PEG-FA conjugate, further self-assembled into targeted, PEGylated heparin nanoparticles.³⁷⁰ *Cis*-diamminedichloroplatinum(II) (DDP, *CisPt*),³⁶⁸ Taxol³⁷⁰ or Pt-DNA³⁶⁸ were encapsulated into heparin nanoparticles, whereas Ptx was linked to the polymer structure *via* DCC/DMAP (Fig. 29).^{369,373}

Carboxypentyl-xyloglucan-galactose was prepared by nucleophilic substitution of 6-bromohexanoic acid by xyloglucan followed by the coupling of galactosamine *via* EDC-assisted ligation.³⁷¹ A similar procedure has been achieved with Dox. Carboxypentyl-xyloglucan-galactose nanoparticles were then obtained by the dialysis method.

In the case of dextran, its amidation with succinic acid followed by the amidation reaction with amino alkyl VB12-derivatives assisted by EDC/NHS resulted, after nanoparticle formulation including insulin entrapment, in dextran-VB12 nanoparticles.

3.4.4. POLY(AMINO ACID)S, POLYPEPTIDES AND PROTEINS

3.4.4.1. Poly(amino acid)s and polypeptides. Poly(amino acid)s (PAAs) are natural or synthetic biodegradable ionic polymers

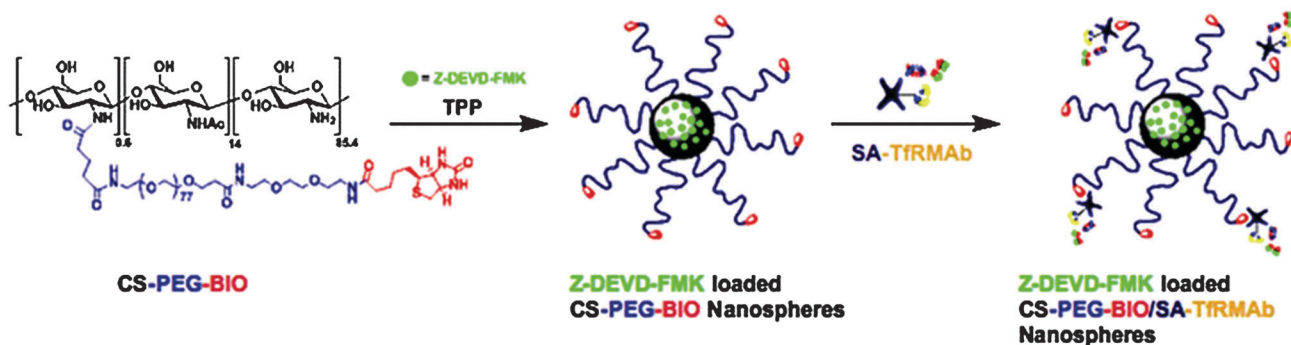


Fig. 27 Schematic view of CS-PEG-BIO nanoparticles loaded with caspase-3 inhibitor Z-DEVD-FMK by an ionic gelation procedure with TPP. The resulting nanoparticles were decorated with anti-mouse transferrin antibody by means of biotin-streptavidin technology (reproduced with permission from ref. 353. Copyright 2009, Society of Neuroscience).

Table 8 Main characteristics and applications of targeted nanocarriers based on other polysaccharides

Structural parameters			Colloidal parameters			Application				
Architecture	Ligand	Synthesis method	Ligand coupling method	Formulation	Morphology	Diameter (nm)	Pathology/target	Drug	Cells/tissues/organs ^a	Ref.
Ligand coupling by carbodiimide chemistry										
Heparin-FA	FA	—	<i>Amidation</i> (heparin + succinic anhydride); <i>carbodiimide</i> (heparin-COOH/DCC/DMAP + FA-NH ₂) ^a	Polymer (DMSO) added to NaHCO ₃ , dialysis	Nanoparticles	60	Cancer (pharynx)	Ptx ^c	KB-3-1, Tu212 Biodistribution, anti-tumor activity (KB-3-1) KB-8-5	369
Heparin-FA	FA	—	<i>Amidation</i> (heparin + succinic anhydride); <i>carbodiimide</i> (heparin-COOH/DCC/DMAP + FA-NH ₂) ^a	Polymer (DMSO) added to NaHCO ₃ , dialysis	Nanoparticles	60	Cancer (pharynx)	Ptx ^c		373
Heparin-g-PEG-FA	FA	—	<i>Amidation</i> (heparin + succinic anhydride); <i>carbodiimide</i> (heparin-COOH/EDC/NHS + FA-PEG-NH ₂) ^a	Nanoprecipitation, polymer/Taxol (DMSO) + Cold water dropwise, dialysis	Nanoparticles	160–190	Cancer (pharynx, lung)	Taxol	KB-3-1, A549	370
Dextran-VB12	VB12	—	<i>Amidation</i> (dextran + succinic anhydride); <i>carbodiimide</i> (VB12-NH ₂ + Dextran-COOH/EDC/NHS) ^a	Emulsion method in aqueous solution + crosslinking agent (epichlorohydrin)	Nanoparticles	150–280	Diabetes	Insulin	Diabetics induced mice	372
Carboxypentyl-xyloglucan-galactose	Galactose	—	<i>Nucleophilic substitution</i> (xyloglucan + 6-bromo-hexanoic acid); <i>carbodiimide</i> (galactosamine + carboxypentyl-xyloglucan-COOH/EDC) ^a	Polymer (DMSO) dialysis against water	Nanoparticles	140	Cancer (cervical, liver)	Dox ^c	HepG2, HeLa HepG2	371
Heparin-ScFvEGFR	ScFvEGFR	—	<i>Amidation</i> (heparin + succinic anhydride); <i>carbodiimide</i> (Heparin-COOH/EDC/NHS + ScFvEGFR) ^b	Self-assembly in water (72h) and purification by dialysis	Nanoparticles	150	Cancer (lung)	DDP and Pt-DNA	H292 Tumor uptake/ anti-tumor activity	368

^a Coupling prior to nanocarrier formation. ^b Coupling post-nanocarrier formation. ^c Drug covalently linked to the (co)polymer. ^d *In vivo* experiments are written in bold.

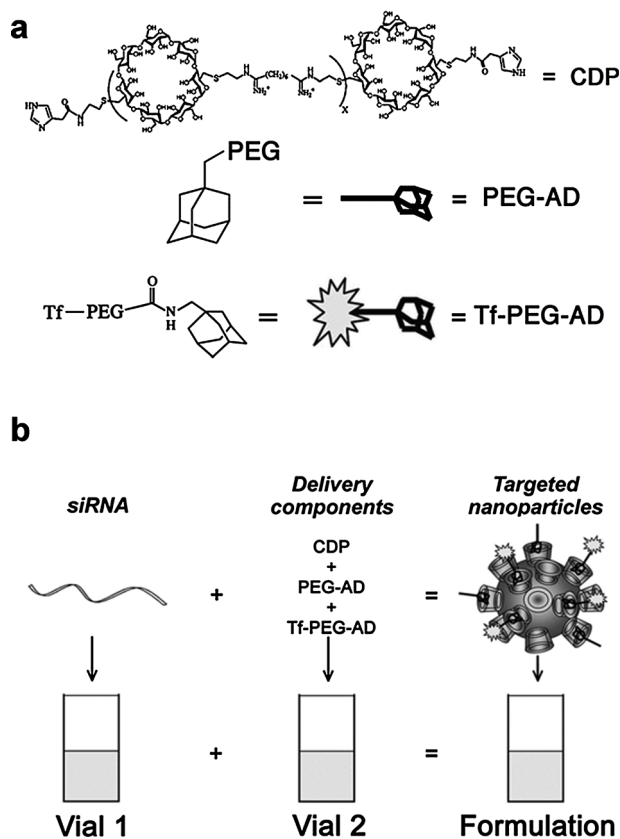


Fig. 28 Components and formulation of targeted nanoparticle-containing siRNA. (a) The delivery components are (i) a water-soluble, linear cyclodextrin-containing polymer (CDP), (ii) an adamantane (AD)-PEG conjugate, and (iii) the targeting component that is an adamantane conjugate of PEG that has human transferrin (Tf) conjugated at the end opposite to the adamantane (Tf-PEG-AD). (b) The formulation contains two vials, one with siRNA and the other with the delivery components. When the two vials are mixed together, the targeted nanoparticles form *via* self-assembly of the four components (reproduced with permission from ref. 367. Copyright 2009, American Chemical Society).

often employed for the design of targeted drug delivery systems because they are made of hydrolysable peptidic bonds and can form polyelectrolyte complexes with DNA (the polymer is highly charged at physiological pH and has been identified as a unique gene/plasmid delivery vehicle). In addition, they can be involved in the synthesis of PAA-*b*-PEG amphiphilic block copolymers to form micelles, nanoparticles or polymersomes. Synthetic PAA are usually obtained from the polymerization of *N*-carboxyanhydride (NCA) initiated by primary amino compounds (Fig. 30). If PEG-*b*-PAA is desired, ω -amino PEG is used as a macro initiator. Poly(aspartate), poly(benzyl-*L*-glutamate) (PBLG), poly(*L*-lysine) (PLL) and poly(histidine) (PHis) are the most widely used PAA in the field of drug delivery. For instance, poly(*L*-glutamic acid) has been found to be highly susceptible to degradation by lysosomal enzymes, leading to monomeric *L*-glutamic as the degradation product, which makes them ideal candidates as biodegradable biomaterials.

Most of the targeted NPs based on PAAs were made of amphiphilic block copolymers comprising a hydrophilic block (*e.g.*, PEG, heparin, hyaluronan, polygalactose *etc.*) and a polypeptidic

one, forming the shell and the core of the resulting nanocarriers, respectively. The synthesis of the amphiphilic block copolymers was achieved by ROP of the desired NCA from amino-PEG derivatives or from the coupling of the preformed PAA and the hydrophilic block by carbodiimide, Michael addition or “click” chemistry. The polypeptidic block was made of PBLG,^{96,374–378} PHis,^{227,379,380} poly(*L*-histidine-*co*-phenylalanine) (P(His-*co*-Phe)),^{226,243} poly(aspartic acid) (PAsp),³⁸¹ PLL¹²⁵ or poly(benzyl-*L*-aspartic acid) (PBLA).^{382,383}

Blending the PAA-*b*-PEG block copolymer with PLA-*b*-PEG copolymers was also often reported as an alternative for functionalization (or to introduce a second functionalization), for which the ligand is present at the extremity of the PEG chains of the PLA-*b*-PEG.^{226,227,243,379} Other synthetic strategies were achieved, such as the copolymerization of NCAs with lactide acid (*e.g.*, P(*L*-*co*-LA)),²⁴⁰ or the coupling of PBLG with polyester dendrons (PEDs) bearing PEG blocks at each of their extremities (Fig. 31).³⁸⁴ Targeted elastin-like polypeptide block copolymer (ELP_{BC}) NPs, comprising an ELP[V₁A₈G₇] hydrophobic block and an ELP[V₅] hydrophilic one, were synthesized by genetic encoding and self-assembled in water.³⁸⁵

A broad variety of ligands (small molecules, peptides, antibodies) was linked to polypeptide-based NPs, most often at the distal end of the hydrophilic block (mainly PEG). However, the ligand was also directly linked to the polypeptidic NP core, thus forming a hydrophilic shell at the same time.^{240,376,377,386} The functionalization occurred almost exclusively prior to NP formation except for the coupling of mHph1 and mAp cell penetrating peptides¹²⁵ and the EGFR antibody.³⁸⁵

Carbodiimide-assisted coupling strategy. The carbodiimide chemistry was here again a method of choice as it took advantage of functional groups present on ligand/polymer chain ends. For instance, the PEG chains forming the hydrophilic shell of the NPs exhibited either: (i) hydroxyl groups which were reacted with DCC-activated FA,^{221,227} (ii) carboxylic acid groups activated with DCC/NHS prior to reaction with amine-bearing FA (*i.e.*, FA-NH₂)³⁸⁴ or with CDI to link the iRGD peptide,¹²⁵ or (iii) amine moieties reacted with NHS-activated FA (*i.e.*, FA-NHS). Amine groups from P(LA-*co*-L) were also readily activated with EDC/NHS for their subsequent coupling with EGFR MAb that occurred at NP surface.²⁴⁰ When a PLA-*b*-PEG was blended with a polypeptide-based (co)polymer, FA was used as a targeting moiety and linked to the PEG extremity, either to its hydroxyl group after activation of FA with DCC,²²¹ or to its carboxylic acid group using FA-NH₂.^{226,227,243}

Thiol-maleimide Michael addition ligation. Several homing devices, such as FA,³⁷⁴ and two CPPs (TAT³⁷⁹ and mAP¹²⁵) were derivatized with cysteine residues and further linked *via* Michael addition to sulfhydryl-reactive polypeptide copolymers/NPs. For the cysteine-terminated CPPs, TAT was conjugated onto a PLA-*b*-PEG-*b*-Phis-Mal prior to self-assembly to form the targeted NPs,³⁷⁹ whereas mAP was reacted at the surface of preformed PLGA-*b*-PLL-*b*-PEG-Mal NPs (the latter were obtained after reaction between PLGA-PLL NPs and the NHS-PEG-Mal heterobifunctional PEG).¹²⁵ Similarly, a cysteine-functionalized FA was linked with a PBLG-PEG-Mal, which was

Table 9 Main characteristics and applications of targeted poly(amino acid)-based nanocarriers

Structural parameters			Colloidal parameters			Application				
Architecture	Ligand	Synthesis method	Ligand coupling method	Formulation	Morphology	Diameter (nm)	Pathology/target	Drug	Cells/tissues/organs ^a	Ref.
Ligand coupling by carbodiimide chemistry										
(i) PHis- <i>b</i> -PEG-FA	FA	(i) <i>Carbodiimide</i> (PEG-COOH/DCC + PHis-NH ₂)	(i) <i>Carbodiimide</i> (PHis- <i>b</i> -PEG-OH + FA-COOH/DCC) ^a	Dialysis	Micelles	50–80	Cancer (breast)	Dox	MCF7	227
(ii) PLA- <i>b</i> -PEG-FA	FA	(ii) <i>ROP</i> of LA from HOOC-PEG-OH	(ii) <i>Carbodiimide</i> (PLA- <i>b</i> -PEG-OH + FA-COOH/DCC) ^a	(i) <i>Carbodiimide</i> (PLA- <i>b</i> -PEG-COOH/DCC/NHS + FA-NH ₂) ^a (ii) <i>Michael addition</i> (PLA- <i>b</i> -PEG-COOH/DCC/NHS + FA-NH ₂) ^a	Emulsion-solvent evaporation + coating PLGA NPs + P ₁ L- <i>b</i> -PEG-FA	110–125	Cancer (pharynx, lung)	—	KB, A549	216
(i) PLGA	FA	(i) <i>ROP</i> of LA/G	(i) <i>Carbodiimide</i> (P ₁ L-NH ₂ + FA-PEG-CHOO/DCC/NHS)	Dialysis	Nanoparticles	140–190	Cancer (pharynx)	Ptx	KB	293, 294
(ii) P ₁ L- <i>b</i> -PEG-FA	FA	(ii) <i>Carbodiimide</i> (P ₁ L-NH ₂ + FA-PEG-CHOO/DCC/NHS)	(ii) <i>Carbodiimide</i> (P ₁ L-NH ₂ + FA-PEG-NH ₂) ^a	Dialysis	Nanoparticles	140–190	Cancer (pharynx)	—	KB/KB	384
PBLA- <i>g</i> -heparin-FA or PBLA- <i>g</i> -heparin- <i>g</i> -PEG-FA	FA	<i>Carbodiimide</i> (PBLA-NH ₂ + HOOC-heparin-FA/EDC or HOOC-heparin- <i>g</i> -PEG-FA/EDC)	<i>Carbodiimide</i> (heparin-COOH/EDC + FA-NH ₂ or FA-PEG-NH ₂) ^a	Dialysis	Micelles	75–90	Cancer (pharynx)	—	KB/KB	384
PBLA(PED- <i>b</i> -PEG-FA) _n	FA	<i>NCA polym.</i> of γ - <i>n</i> -dodecyl-L-glutamate-NCA from H ₂ N-PEG; <i>carbodiimide</i> (HOOC-PEG-COOH/DIC + PLGA(PED-OH)) _n	<i>Carbodiimide</i> (PBLA(PED- <i>b</i> -PEG-COOH) _n /EDC/NHS + FA-NH ₂) ^a	Dialysis	Micelles	75–90	Cancer (pharynx)	—	KB/KB	384
(i) PLGA- <i>b</i> -P ₁ L- <i>b</i> -PEG-IRGD	(i) IRGD	(i) <i>Carbodiimide</i> (PLGA-COOH/DCC + protected P ₁ L-NH ₂); (ii) 2 CPPS	(i) <i>Carbodiimide</i> (IRGD-NH ₂ + PLGA- <i>b</i> -P ₁ L- <i>b</i> -PEG-COOH/CDI) ^a	Double emulsion-solvent evaporation	Nanoparticles	150	Cancer (lung)	TCHD + QC + ENX + siRNA	HEK293T/A549	125
(ii) PLGA- <i>b</i> -P ₁ L- <i>b</i> -PEG-CPP	(ii) (mHph1, mAP)	(ii) <i>Carbodiimide</i> (PLGA- <i>b</i> -P ₁ L- <i>b</i> -PEG-COOH/DCC + protected P ₁ L-NH ₂); <i>carbodiimide</i> (NHS-PEG-Mal on NPs)	(ii) <i>Av/biotin</i> (PLGA- <i>b</i> -P ₁ L/palmitic acid-Av + mHph1-biotin) ^b ; <i>Michael addition</i> (mAP-SH + PLGA- <i>b</i> -P ₁ L- <i>b</i> -PEG-Mal) ^b	Double emulsion-solvent evaporation	Nanoparticles	150	Cancer (lung)	TCHD + QC + ENX + siRNA	HEK293T/A549	125
P(LA-co-L)-EGFR	EGFR Mab	<i>ROP</i> of LA/protected-L	<i>Carbodiimide</i> (P(LA-co-L)/EDC/NHS + EGFR-NH ₂) ^b	Emulsion/solvent evaporation	Nanoparticles	150	Cancer (liver)	—	SMMC-7721/ SMMC-7721	240
Ligand coupling by Michael addition										
PEG- <i>b</i> -PBLG- <i>b</i> -PEG-FA	FA	<i>NCA polym.</i> of BLG-NCA from Mal-PEG-NH ₂ ; <i>carbodiimide</i> (NH ₂ -PBLG-PEG-FA + acrylate-PEG-NHS)	<i>Michael addition</i> (PBLG- <i>b</i> -PEG-Mal + FA-SH) ^a	Self-assembly	Polymersomes	140	Cancer (cervical)	Dox ^c	HeLa	374
(i) PLA- <i>b</i> -PEG- <i>b</i> -PHIS-TAT	TAT	(i) <i>Michael addition</i> Mal-PHIS-Mal (NCA <i>polym.</i> of His-NCA + post-functionalization) + PLA- <i>b</i> -PEG-SH (ROP of LA from HOOC-PEG-OH + DCC/NHS/cystamine)	(i) <i>Michael addition</i> (PLA- <i>b</i> -PEG- <i>b</i> -PHIS-Mal + TAT-SH) ^a	Dialysis	Micelles	95	Cancer (breast, lung, ovary, epiderm, leukemia)	Dox	MCF7, NCI/ADR-RES, HL-60, MX2, HL-60, NCI-H69/AR, A549	A2780/AD, MCF7, A549, KB
(ii) PLA- <i>b</i> -PEG-FA	FA	(ii) <i>ROP</i> of LA from HOOC-PEG-OH	(ii) <i>Carbodiimide</i> (FA-NH ₂ + PLA- <i>b</i> -PEG-COOH/DCC/NHS) ^a	Dialysis	Micelles	95	Cancer (breast, lung, ovary, epiderm, leukemia)	Dox	MCF7, NCI/ADR-RES, HL-60, MX2, HL-60, NCI-H69/AR, A549	A2780/AD, MCF7, A549, KB

Table 9 (continued)

Structural parameters		Colloidal parameters			Application					
Architecture	Ligand	Synthesis method	Ligand coupling method	Formulation	Morphology	Diameter (nm)	Pathology/target	Drug	Cells/tissues/organs ^d	Ref.
Ligand coupling by copper-catalyzed azide-alkyne cycloaddition (CuAAC)										
Pseudo poly- <i>l</i> -alanine-FA	FA	<i>Melt polym.</i> of 3-[butyl-(2-hydroxypropyl)amino]-propionic acid; <i>Carbodiimide</i> (polyalanine-COOH)/DCC/ <i>NHS</i> + propargyl amine ^b	CuAAC (polyalanine-alkyne + FA-N ₃) ^b	Nanoprecipitation	Nanoparticles	100	Cancer (lung)	Ptx	A549, H9c2	387
PBLG- <i>b</i> -PG-galactose	Galactose	<i>NCA polym.</i> of BLG-NCA and PG	CuAAC (PBLG- <i>b</i> -PG + N ₃ galactose) ^a	Nanoprecipitation	Polymersomes	60	—	—	Lectin	386
PBLG- <i>b</i> -HA	HA	<i>NCA polym.</i> of BLG-NCA from 1-azido-3-aminopropane and; CuAAC (α -alkyne-HA + PBLG-N ₃)	CuAAC (see synthesis method) ^a	Nanoprecipitation	Polymersome	440	Cancer (glioma)	Dox	C6	377
PBLG- <i>b</i> -HA	HA	<i>NCA polym.</i> of BLG-NCA from 1-azido-3-aminopropane and; CuAAC (α -alkyne-HA + PBLG-N ₃)	CuAAC (see synthesis method) ^a	Nanoprecipitation	Polymersome	440	Cancer (breast)	Dox	MCF7	376
PBLG- <i>b</i> -HA	HA	<i>NCA polym.</i> of BLG-NCA from 1-azido-3-aminopropane and; CuAAC (α -alkyne-HA + PBLG-N ₃)	CuAAC (see synthesis method) ^a	Nanoprecipitation	Polymersome	260–280	Cancer (breast)	Dox	MCF7, U87	375
PBLG- <i>b</i> -HA	HA	<i>NCA polym.</i> of BLG-NCA from 1-azido-3-aminopropane and; CuAAC (α -alkyne-HA + PBLG-N ₃)	CuAAC (see synthesis method) ^a	Nanoprecipitation	Polymersome	350–430	Cancer (breast)	Dox	Ehrlich Ascites Tumor	378
Ligand coupling by other ligation strategies										
PLA- <i>b</i> -PEG- <i>b</i> -PHis-biotin	Biotin	<i>Carbodiimide</i> (biotin-PHis-NH ₂ , <i>NCA polym.</i> from Biotin- <i>NCA polym.</i> of N ^m -DNP-1-his-tidine) + PLA- <i>b</i> -PEG-COOH/DCC/ <i>NHS</i>)	Reductive amination (H(O)C-PEG- <i>b</i> -PBLA + FA-NHNH ₂) ^a	Dialysis	Micelles	100	Cancer (breast)	Dox	MCF7	380
PASP- <i>b</i> -PEG-FA	FA	<i>NCA polym.</i> of BLA-NCA from acetal-PEG-NH ₂	<i>Reductive amination</i> (H(O)C-PEG- <i>b</i> -PBLA + FA-NHNH ₂) ^a	Dialysis	Micelles	65	Cancer (pharynx)	Dox ^c	KB	381
PBLG- <i>b</i> -PEG-galactose	Galactose	<i>NCA polym.</i> of BLG-NCA from galactose-PEG-NH ₂	<i>Amidation</i> (lactonolactone + H ₂ N-PEG-NH ₂) ^a	Dialysis	Nanoparticles	105–325	Cancer (liver)	Ptx	HepG2	96
ELP[V ₁ A ₈ G ₇]- <i>b</i> -RGD	RGD	<i>Genetically encoded synthesis</i>	<i>Genetically encoded synthesis</i> ^a	Self-assembly with temperature	Nanoparticles	50–60	Cancer (leukemia)	—	K562	385

^a Coupling prior to nanocarrier formation. ^b Coupling post-nanocarrier formation. ^c Drug covalently linked to the (co)polymer. ^d *In vivo* experiments are written in bold.

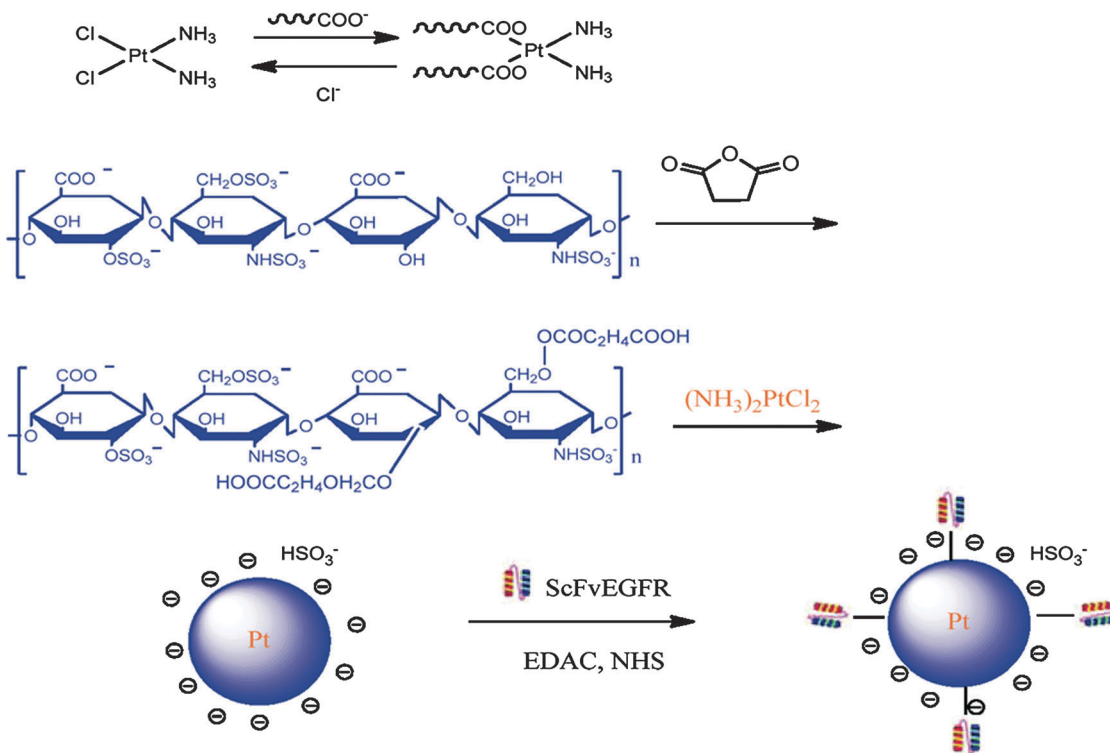


Fig. 29 Preparation of ScFv EGF-functionalized DDP-heparin nanocarriers (adapted with permission from ref. 368. Copyright 2011, American Chemical Society).

further coupled to a NHS-PEG-acrylate moiety to yield the corresponding FA-PEG-*b*-PBLG-*b*-PEG-acrylate triblock copolymer (Fig. 32).³⁷⁴ Stable polymersomes exhibiting FA at their periphery were formed by self-assembly and subsequent cross-linking *via* the acrylate functions. Interestingly, Dox was conjugated onto the polyglutamate segment using a pH-sensitive hydrazone bond to achieve pH-responsive drug release.

Copper-catalyzed azide-alkyne cycloaddition (CuAAC). Click chemistry has been used to attach hyaluronan (HA)^{375–378} and galactose³⁸⁶ as targeting moieties at the surface of PBLG polymersomes (Fig. 33). PBLG and HA were end-functionalized by an azide and an alkyne group, respectively, and reacted by CuAAC under standard conditions in organic medium.^{375–378}

In the case of galactose, a PBLG-*b*-PG was first synthesized by sequential ring opening polymerization of NCAs and the PG block was further glycosylated under CuAAC conditions using an azide-functionalized galactose (Fig. 34).³⁸⁶

Starting from mono and di-*N*-alkylated amino acids, Santra and coworkers³⁸⁷ described a one step strategy (*i.e.*, melt polymerization) to synthesize a pseudo-poly(amino acid) polymer which was able to form nanoparticles by a simple solvent evaporation method. Propargyl groups were introduced at the surface of nanoparticles *via* carbodiimide-assisted reaction and successive functionalization was performed by click chemistry using an azide-modified FA (Fig. 35). Ptx and a NIR dye were encapsulated in these NPs as therapeutic and imaging agents, respectively.

Other ligation strategies. Other methods to generate targeted polypeptide-based NPs relied on: (i) the use of biotin-NH₂

(*via* biotin-NHS) to initiate the polymerization of NCAs followed by the coupling with a PLA-*b*-PEG diblock copolymer to form a biotin-PHis-*b*-PEG-*b*-PLA triblock copolymer;³⁸⁰ (ii) the biotinylation of the mHph1 CPP and its coupling with palmitic acid-Av which acted as an anchor at the surface of PLGA-PL-PEG NPs;¹²⁵ (iii) the reductive amination between FA-hydrazide (FA-NH-NH₂) and aldehyde-PEG-*b*-PBLA diblock copolymer, followed by partial hydrolysis to form FA-*b*-PEG-*b*-PAsp;³⁸¹ (iv) the direct amidation of galactose with a PEG diamine followed by the NCA polymerization of BLG-NCA⁹⁶ and (v) the synthesis of genetically encoded RGD-ELP[V1A8G7]-ELP[V5] amphiphilic copolymer.³⁸⁵

3.4.4.2. Proteins. Due to their biocompatibility, proteins also represent an important class of natural polymers that have been widely used for targeted drug delivery.³⁸⁸ Functionalization with drugs or ligands can be readily achieved *via* the lysine residues present at their surface. One of the most employed protein as nanocarrier component is perhaps albumin, but gelatin and gliadin have also been successfully used. Protein NPs are generally obtained by the desolvation method but solvent displacement and direct solubilization or auto-assembly have also been employed.

Thiol-maleimide Michael addition ligation. A well-explored strategy to achieve functionalized proteins relied on the Michael addition (Mal/SH ligation) using ligands bearing a thiol group. In this case, the protein is first reacted, *via* its lysine residues, with a heterobifunctional NHS-PEG-Mal (PEG molar mass ranged from 2000 to 5000 Da). Then, the ligand of interest is generally thiolated (using heterobifunctional spacers

Table 10 Main characteristics and applications of targeted protein-based nanocarriers

Structural parameters			Colloidal parameters			Application			
Architecture	Ligand	Synthesis method	Ligand coupling method	Formulation	Morphology	Diameter (nm)	Pathology/target	Cells/tissues/organs ^c	Ref.
Ligand coupling by carbodiimide chemistry									
HSA-biotin	Biotin	—	<i>Carbodiimide</i> (Biotin/EDC/NHS + BSA) ^a	Cross-linked HSA <i>via</i> EDC	Nanoparticles	125–145	Cancer (breast, cervical)	T47D, HeLa	402
HSA-biotin	Biotin	—	<i>Carbodiimide</i> (Biotin/EDC/NHS + BSA) ^a	Cross-linked HSA <i>via</i> EDC	Nanoparticles	125–145	Cancer (breast)	4T1	403
BSA-Lysine-galactose	Galactose	<i>Imine formation</i> (BSA-CHO + Lysine)	<i>Carbodiimide</i> (Galactosamine + BSA-Lysine-COOH/EDC) ^a	Desolvation/cross-linking (glutaraldehyde)	Nanoparticles	180–200	Cancer (liver)	HepG2	404
Gliadin-UEA I/Con A	Ulex Europaeus Agglutinin I (UEA I) and Concanavalin A (Con A) lectins	—	<i>Carbodiimide</i> (Gliadin-COOH/EDC + UEA I/Con A) ^a	Desolvation/cross-linking (glutaraldehyde)	Nanoparticles	410	<i>H. pylori</i>	<i>H. pylori</i> strains	407
Ligand coupling by Michael addition									
HSA-PEG-cyclic RGD	Cyclic RGD	<i>Carbodiimide</i> (NHS-PEG-Mal + HSA)	<i>Michael addition</i> (cyclic RGD-SH + HSA-PEG-Mal) ^a	Auto-assembly	Micelles	30	Cancer (skin)	M21+	389
BSA-cyclic RGD	Cyclic RGD (cyclo(-Arg-Gly-Asp-D-Tyr-Lys)-Cys)	—	<i>Michael addition</i> (BSA-Mal, RGD-SH) ^a	Desolvation/cross-linking (glutaraldehyde)	Nanoparticles	130	Cancer (pancreas)	BxPC3	408
Gelatin-PEG-EGF	EGF	<i>Carbodiimide</i> (NHS-PEG-Mal + Gelatin)	<i>Michael addition</i> (EGF-SH + Gelatin-PEG-Mal) ^a	Solvent displacement method/cross-linking (glyoxal)	Nanoparticles	200	Cancer (pancreas)	Panc-1	391
HSA-PEG-Tf/OX26/R17217	Transferrin or transferrin receptor monoclonal antibodies (OX26 or R17217)	<i>Carbodiimide</i> (NHS-PEG-Mal + HSA)	<i>Michael addition</i> (Tf-SH or OX26-SH or R17217-SH + HSA-PEG-Mal) ^a	Desolvation/cross-linking (glutaraldehyde)	Nanoparticles	150–180	Brain delivery	Tail-flick test	393
HSA-PEG-ApoE3/A-1/B-100	Insulin or anti-insulin receptor monoclonal antibody (29B4)	<i>Carbodiimide</i> (NHS-PEG-Mal + HSA)	<i>Michael addition</i> (HS-ApoE3/A-1/B-100 + HSA-PEG-Mal) ^a	Desolvation/cross-linking (glutaraldehyde)	Nanoparticles	220–240	Brain delivery	Tail-flick test	392
HSA-PEG-29B4/insulin	Insulin or anti-insulin receptor monoclonal antibody (29B4)	<i>Carbodiimide</i> (NHS-PEG-Mal + HSA)	<i>Michael addition</i> (insulin-SH or 29B4-SH + HSA-PEG-Mal) ^a	Desolvation/cross-linking (glutaraldehyde)	Nanoparticles	150–190	Brain delivery	Tail-flick test	169
HSA-PEG-anti-HER-2 Mab	anti-HER-2 Mab	<i>Carbodiimide</i> (NHS-PEG-Mal + HSA)	<i>Michael addition</i> (Trastuzumab-SH + HSA-PEG-Mal) ^a	Desolvation/cross-linking (glutaraldehyde)	Nanoparticles	390–410	Cancer (breast)	SK-BR-3	396
HSA-PEG-anti-HER-2 Mab	anti-HER-2 Mab	<i>Carbodiimide</i> (NHS-PEG-Mal + HSA)	<i>Michael addition</i> (HSA-PEG-Mal + Trastuzumab-SH) ^a	Desolvation/cross-linking (glutaraldehyde)	Nanoparticles	220	Cancer (breast)	SK-BR-3, BT-474	397
HSA-PEG-DI17E6/IgG	DI17E6 Mab	<i>Carbodiimide</i> (NHS-PEG-Mal + HSA)	<i>Michael addition</i> (HS-IgG/DI17E6 + HSA-PEG-Mal) ^a	Desolvation/cross-linking (glutaraldehyde)	Nanoparticles	165–180	Cancer (skin)	M21	395
Ligand coupling by biotin/Av ligation addition									
Gelatin-EGF	EGF	—	<i>Michael addition</i> (Gelatin-SH + NAv-biotin (biotin-EGF + Gelatin-NAv) ^a)	Desolvation/cross-linking (glutaraldehyde)	Nanoparticles	220	Cancer (lung)	A549	399

Table 10 (continued)

Structural parameters		Colloidal parameters				Application				
Architecture	Ligand	Synthesis method	Ligand coupling method	Formulation	Morphology	Diameter (nm)	Pathology/target	Drug	Cells/tissues/organs ^c	Ref.
Gelatin-EGF	EGF	—	<i>Michael addition</i> (Gelatin-SH + NAV-Mal); <i>NAV/biotin</i> (biotin-EGF + Gelatin-NAV) ^a	Desolvation/cross-linking (glutaraldehyde)	Nanoparticles 230	230	Cancer (lung)	<i>CisPt</i>	A549 SCID model	400
Gelatin-EGF	EGF	—	<i>Michael addition</i> (Gelatin-SH + NAV-Mal); <i>NAV/biotin</i> (biotin-EGF + Gelatin-NAV) ^a	Desolvation/cross-linking (glutaraldehyde)	Nanoparticles 240	240	Cancer (lung)	—	A549 SCID model	398
Gelatin-CD3	CD3 Mab	—	<i>Michael addition</i> (Gelatin-SH + NAV-Mal); <i>NAV/biotin</i> (biotin-CD3 + Gelatin-NAV) ^a	Desolvation/cross-linking (glutaraldehyde)	Nanoparticles 250–300	250–300	T-lymphocytes	—	—	401
HSA-PEG-ApoE	ApoE	<i>Carbodiimide</i> (NHS-PEG-Mal + HSA)	<i>Michael addition</i> (NAV-SH + HSA-PEG-Mal); <i>NAV/biotin</i> (biotin-ApoE + HSA-PEG-NAV) ^a	Desolvation/cross-linking (glutaraldehyde)	Nanoparticles 340	340	Brain delivery	Loperamide	Tail-flick test	390
Gelatin-PEG-trastuzumab or HSA-PEG-anti-HER-2 Mab	anti-HER-2 Mab	<i>Carbodiimide</i> (NHS-PEG-Mal + HSA or Gelatin)	<i>Michael addition</i> (Gelatin-SH/HSA-SH + NAV-Mal); <i>NAV/biotin</i> (trastuzumab-biotin + Gelatin-NAV/HSA-NAV)	Desolvation/cross-linking (glutaraldehyde)	Nanoparticles 210–320	210–320	Cancer (breast)	—	MCF7, SK-BR-3, BT474	394
Ligand coupling by other ligation strategies										
Gelatin-siloxane-Tat	Tat	<i>Two-step sol-gel process</i>	<i>Disulfide bridge formation</i> (Tat-SH + Gelatin-siloxane-SH) ^a	See synthesis method	Nanoparticles 210	210	Cancer (cervical)	pDNA/pSVβ-gal	HeLa	406
Gelatin-siloxane-PEG-SynB	SynB	<i>Two-step sol-gel process</i> ; <i>carbodiimide</i> (HOOC-PEG-NH ₂ /EDC/NHS)	<i>Disulfide bridge formation</i> (SynB-SH + Gelatin-siloxane-PEG-PDS) ^a	See synthesis method	Nanoparticles 150–200	150–200	Brain delivery	—	BBB model Brain targeting	405

^a Coupling post-nanocarrier formation. ^b Drug covalently linked to the (co)polymer. ^c *In vivo* experiments are written in bold.

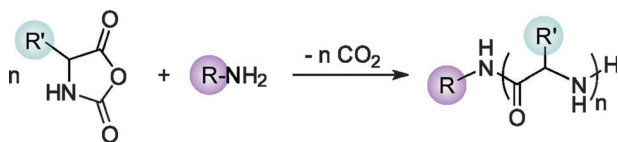


Fig. 30 Synthesis of poly(amino acid) (PAA) by the polymerization of *N*-carboxyanhydride (NCA) initiated by amino compounds.

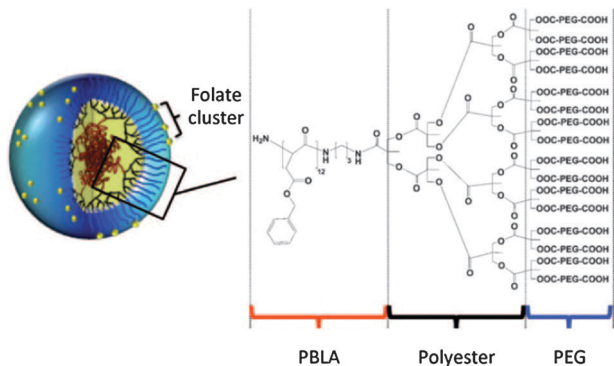


Fig. 31 Detailed chemical structure of the non-folate conjugated linear dendritic polymer and illustration of its self-assembly into "patchy" micelles presenting clusters of folate of variable sizes on the surface of the micelle (reproduced with permission from ref. 384. Copyright 2010, Wiley).

such as MBS, sulfo-MBS *etc.*) and allowed linking at the surface of the protein (see Fig. 14 for the structures of the spacers). This pathway was successfully applied to a broad variety of targeting peptides (cyclic RGD),³⁸⁹ proteins (ApoE3, A-I, B-100, EGF, insulin, Tf)^{169,390–393} or antibodies (Trastuzumab, DI17E6, IgG, 29B4, OX26, R17217, see Fig. 36)^{169,393–397} for application in cancer and brain delivery (CNS-related disease).

Encapsulation of loperamide^{169,392,393} was reported as a model drug to test the efficiency of the brain delivery whereas pDNA³⁹¹ and Dox^{395,396} were employed for cancer therapy. Dox was also covalently linked to the protein (Fig. 37).³⁸⁹

Biotin/avidin ligation. The NAv/biotin ligation strategy also represents a method of choice for targeted protein NPs. The global idea is to graft maleimide moieties at the surface of protein NPs and to use thiol-bearing ligands to form a thioether bond. Proteins were turned into sulfhydryl-reactive NPs, either by thiolation with 2-iminothiolane or by reacting with a NHS-PEG-Mal. Note that the latter pathway also leads to PEGylated NPs. NAv is activated with *m*-maleimidobenzoyl-*N*-hydroxy-succinimide (sulfo-MBS, Fig. 14), followed by its incubation with the Mal-functionalized proteins to yield NAv-decorated protein NPs. Then, the ligands were biotinylated with commercially available biotinylation reagents, such as sulfosuccinimidyl-6-[biotin-amido]hexanoate (sulfo-NHS-LC-biotin, Fig. 14) or pentafluorophenyl-ester biotin (PFP-biotin, Fig. 14) before their coupling to the NPs by simple incubation. This was efficiently applied to albumin and gelatin NPs at the surface of which ApoE,³⁹⁰ EGF,^{398–400} CD3 MAb⁴⁰¹ and trastuzumab³⁹⁴ were positioned. Drugs were either encapsulated/adsorbed (loperamide)³⁹⁰ or covalently linked to the protein (*CisPt*) (Fig. 38).⁴⁰⁰

Carbodiimide coupling strategy. HSA was also functionalized with biotin *via* EDC/NHS chemistry to target biotin receptors overexpressed at the surface of certain cancer cells.^{402,403} This was readily achieved by a one-pot reaction between HSA, biotin and EDC/NHS. The same coupling chemistry was also used to covalently link MTX as the anticancer drug to HSA. In the same spirit, galactose was tethered at the surface of doxorubicin-encapsulated albumin NPs (Fig. 39).⁴⁰⁴ In this example, glutaraldehyde was used to cross-link the NPs and to present aldehyde moieties at their surface for their further conjugation to lysine. EDC was then used to perform the conjugation between galactosamine and the exposed carboxylic acid of lysine residues.

Other ligation strategies. Interesting pathways have been reported to link cell penetrating peptides, such as TAT or SynB, to gelatin NPs by means of a disulfide bridge.^{405,406} Gelatin-siloxane NPs were first prepared by a two-step sol-gel process. In the first route, the NPs were grafted with PEG *via* EDC/NHS coupling chemistry using surface amines of the NPs.⁴⁰⁵ Then the sulfhydryl-containing SynB peptide was tethered to the NPs by using the *N*-succinimidyl-3-(2-pyridyldithio) propionate (SPDP) heterobifunctional linker (Fig. 14), through the formation of a disulfide bridge. The second route reported the surface modification of the gelatin-siloxane NPs by the Traut's reagent (Fig. 14) in order to position thiol groups at their surface.⁴⁰⁶ The Cys-containing TAT peptide was then coupled to the NPs by forming the disulfide bridge.

3.4.5. POLY(ALKYL CYANOACRYLATE). Alkyl cyanoacrylates are widely-known monomers, extremely appreciated for their very high reactivity and the excellent adhesive properties of the resulting polymers. On one hand, the famous Superglue[®], which contains short alkyl chain cyanoacrylates, is commonly employed by the general public for repairing and do-it-yourself activities whereas longer alkyl chain cyanoacrylates have been developed for biomedical purposes such as *e.g.* surgical glue for the closure of skin wounds and embolic material for endovascular surgery. Their use for the construction of nanoparticles has been discovered in the late seventies by Couvreur *et al.*⁴⁰⁹ and, since that time, a very important number of pharmaceutical applications have been reported due to the ease of preparation (in aqueous medium) and the biocompatibility of these nanoparticles. Importantly, they are currently in a phase III clinical trial for the treatment of the MDR resistant hepatocarcinoma.

Poly(alkyl cyanoacrylate) (PACA) can be synthesized according to three distinct types of polymerization: (i) anionic polymerization; (ii) zwitterionic polymerization and (iii) radical polymerization. However, due to their very high reactivity, anionic and zwitterionic polymerization mechanisms are predominant under conventional experimental conditions with respect to the radical process.

The predominant degradation mechanism, which is believed to be the main degradation pathway *in vivo*, occurs *via* the hydrolysis of their side chain ester functions, producing the corresponding alkyl alcohol and poly(cyanoacrylic acid) as

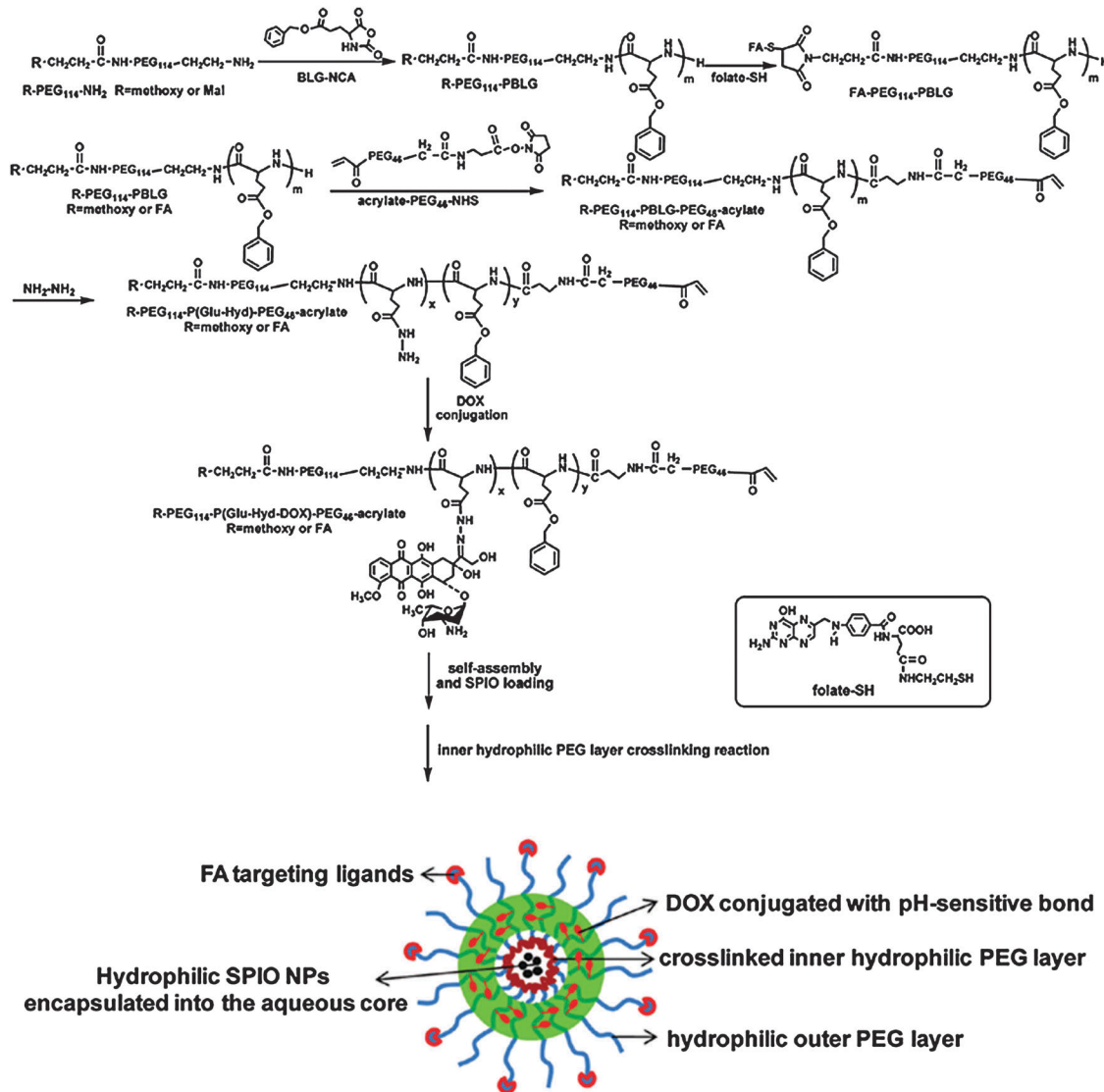


Fig. 32 Synthetic scheme of the amphiphilic triblock copolymers and the preparation process of the SPIO/DOX-loaded vesicles with cross-linked inner hydrophilic PEG layers (reproduced with permission from ref. 374. Copyright 2010, American Chemical Society).

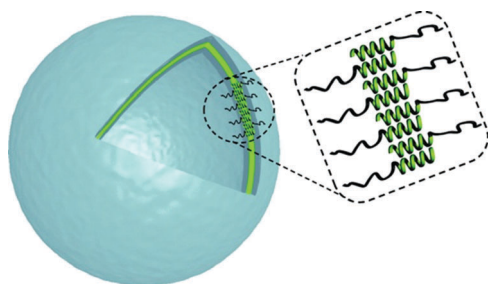


Fig. 33 Schematic representation of PBLG-*b*-HA polymersomes, with a bilayer forming membrane with PBLG packed antiparallel (reproduced with permission from ref. 378. Copyright 2012, American Chemical Society).

the degradation products, the latter being fully water-soluble and readily eliminated by kidney filtration.⁴¹⁰ PACA are one of the fastest degrading polymers having degradation times

ranging from few hours to few days. However, a complete excretion of these materials would occur only for low-molecular weight polymers, typically for a molecular weight below $10\,000\text{ g mol}^{-1}$.

In the field of PACA, examples of successful functionalizations to achieve active targeting are rather scarce because of the very high reactivity of alkyl cyanoacrylate monomers and/or the rapid degradability of PACA polymers/nanoparticles.⁴¹¹ However, the tandem Knoevenagel condensation–Michael addition, which allowed preparing PEGylated PACA NPs (Fig. 40), also represented a convenient strategy to position functional groups at the extremity of the PEG chains for further coupling, either on the copolymer in organic medium or directly at the surface of the resulting NPs.

Couvreur and coworkers synthesized targeted PACA NPs by coupling FA to P(HDCA-*co*-NH₂PEGCA) NPs *via* an amidation reaction from its NHS-ester derivative.^{412,413} During the synthesis, a *t*Boc-protected amino PEG was used and the deprotection

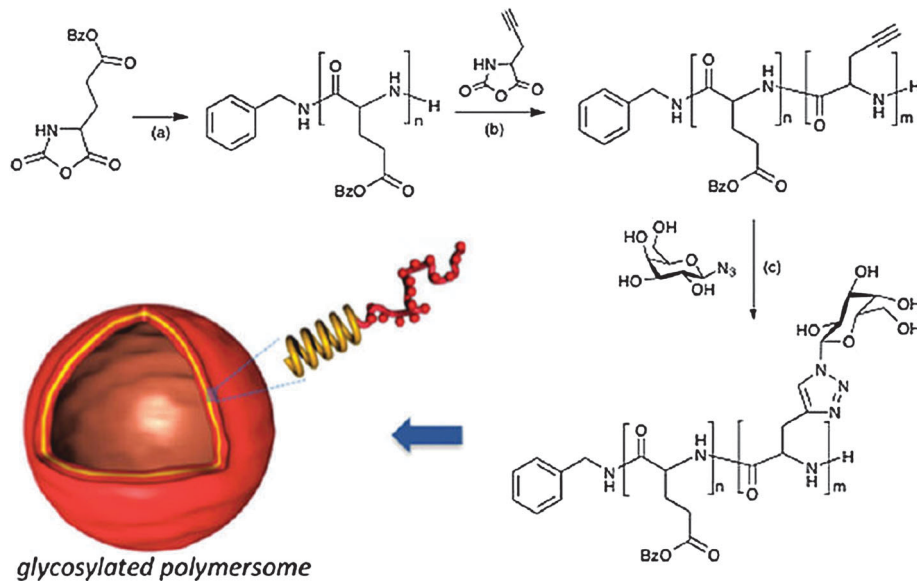
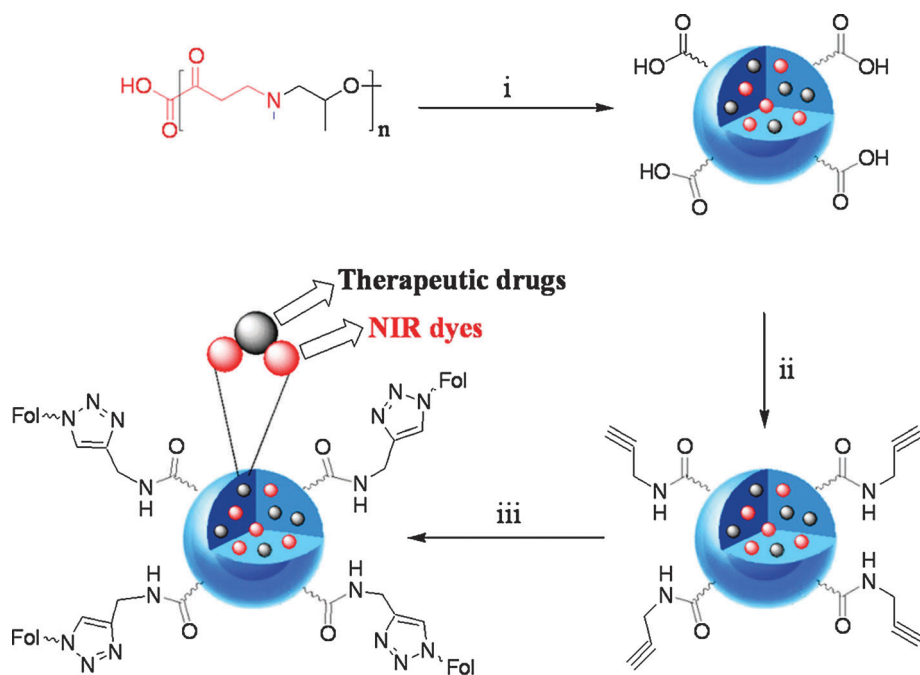


Fig. 34 Synthesis of PBLG-*b*-PGG glycopeptide block copolymers by a combination of ring-opening polymerization of NCA and click chemistry (reproduced with permission from ref. 386. Copyright 2012, Elsevier).



i. Solvent diffusion method, DMF, H₂O, DiI, Paclitaxel **ii.** Carbodiimide chemistry, propargylamine, EDC, NHS **iii.** Click chemistry, Folate-N₃, CuI

Fig. 35 Synthesis of functional poly(amino acid) based theranostic polymeric nanoparticles (reproduced with permission from ref. 387. Copyright 2011, American Chemical Society).

occurred prior to NP formation (Fig. 41). NPs exhibited an average diameter of 80–90 nm. 15% of the PEG chain-ends were functionalized with FA and SPR accounted for a significant binding with

the folate-binding protein (FBP). The same targeted system was also employed to encapsulate pDNA/PEI or pDNA/PL for transfection purposes.⁴¹⁴ In this case, bigger NPs of 260–390 nm were obtained.

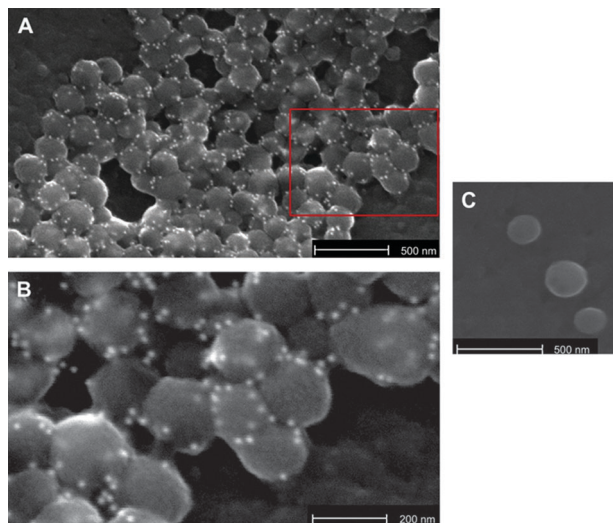


Fig. 36 Scanning electron microscopy (SEM) images showing HSA nanoparticles with D117E6 coupled on the surface (A, B = magnification of A in the red quadrangle) and nanoparticles without an antibody coupling (C) (reproduced with permission from ref. 395. Copyright 2010, Elsevier).

Periodate oxidation was also employed from P(HDCA-co-NH₂PEGCA) NPs to link the Tf protein.^{415,416} W/O/W double emulsion was used to generate the amino-functionalized NPs

containing pDNA⁴¹⁶ or pDNA/PLL.⁴¹⁵ Average diameter ranged from 130–150 nm (pDNA) to 240–290 nm (pDNA/PLL).

Click chemistry,⁴¹⁷ which has emerged as a powerful ligation strategy, was recently applied to PACA NPs.⁴¹⁸ By means of CuAAC, a versatile targeted nanoparticulate platform based on PACA has been recently proposed and exhibited stealth, fluorescent and targeting abilities. A heterobifunctional azidopoly(ethylene glycol) (N₃PEG) was first derivatized with the selected ligand by CuAAC using CuSO₄/sodium ascorbate as the catalytic system and turned into its cyanoacetate derivative under DCC-assisted chemistry (Fig. 42). Its terpolymerization with varying amount of MePEGCA (in order to tune the final surface density of ligand) and HDCA by tandem Knoevenagel condensation–Michael addition led to the corresponding ligand-containing amphiphilic copolymer. After concomitant self-assembly in aqueous solution with a rhodamine B-tagged PACA copolymer,⁴¹⁹ functionalized NPs in the 85–150 nm range displaying the ligand of interest were obtained. The versatility of this methodology was illustrated by the coupling of a small library of biologically active ligands (biotin, selegiline, curcuminoids) in order to target cancer (biotin) and Alzheimer's disease (selegiline, curcuminoids) *via* the Aβ₁₋₄₂ peptide biomarker.⁴²⁰ To perform the CuAAC coupling, the ligands were first derivatized with an alkyne group except for selegiline, which natively contains such function. Interestingly, thanks to the surface availability of biotin, a monoclonal anti-Aβ₁₋₄₂

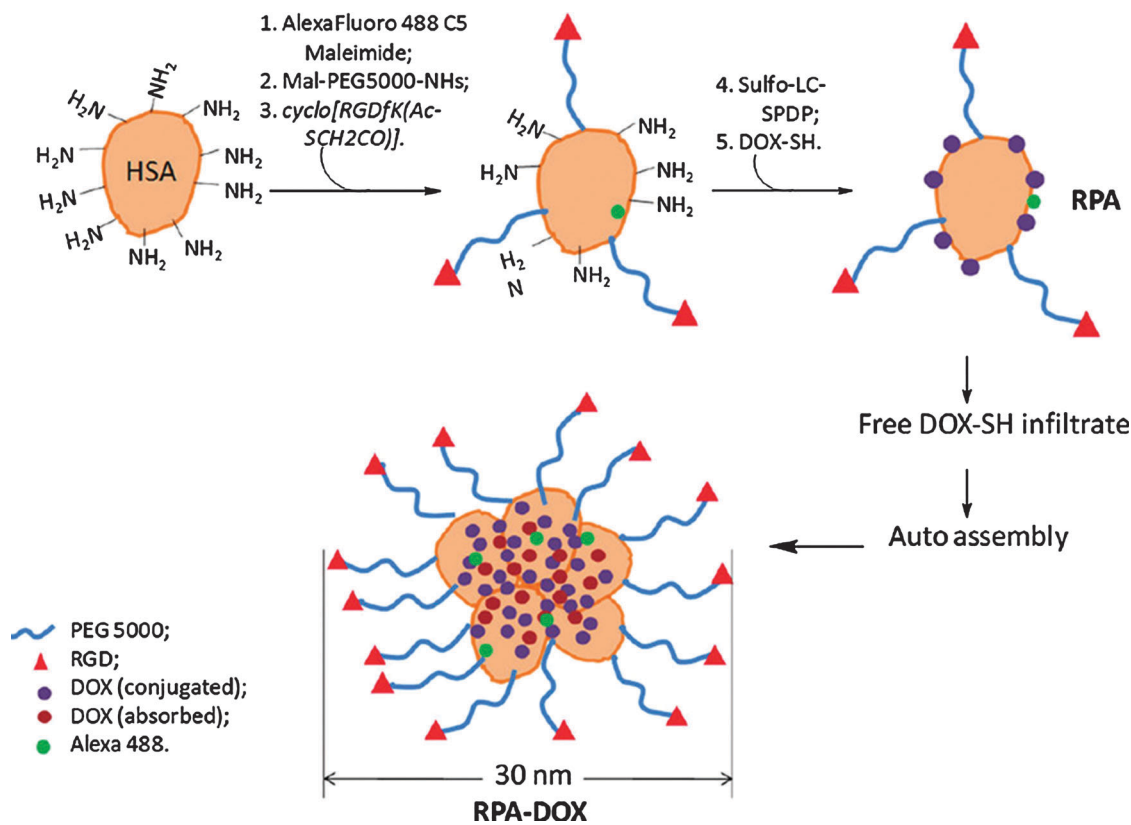


Fig. 37 Synthetic pathway for targeted albumin-based micelles for delivery of amphipathic drugs (reprinted with permission from ref. 389. Copyright 2011, American Chemical Society).

Table 11 Main characteristics and applications of targeted poly(alkyl cyanoacrylate)-based nanocarriers

Structural parameters			Colloidal parameters			Application				
Architecture	Ligand	Synthesis method	Coupling method	Formulation	Morphology	Diameter (nm)	Pathology/target	Drug	Cells/tissues/organs	Ref.
Ligand coupling by carbodiimide chemistry										
P(HDCA-co-FAPEGGA)	FA	<i>Knoevenagel condensation-Michael addition</i>	<i>Carbodiimide</i> (P(HDCA-co-H ₂ NPEGGA) + FA-NHS) ^p	Nanoprecipitation	Nanoparticles	80–90	Cancer	—	—	412
P(HDCA-co-FAPEGGA)	FA	<i>Knoevenagel condensation-Michael addition</i>	<i>Carbodiimide</i> (P(HDCA-co-H ₂ NPEGGA) + FA-NHS) ^p	Nanoprecipitation	Nanoparticles	80–90	Cancer (ovary)	—	KB3-1	413
P(HDCA-co-FAPEGGA)	FA	<i>Knoevenagel condensation-Michael addition</i>	<i>Carbodiimide</i> (P(HDCA-co-H ₂ NPEGGA) + FA-NHS) ^p	Nanoprecipitation	Nanoparticles	260–390	Cancer (ovary)	pDNA/Pi-L or pDNA/PEI	KB	414
Ligand coupling by copper-catalyzed azide-alkyne cycloaddition (CuAAC)										
P(HDCA-co-biotinPEGGA)	Biotin	<i>Knoevenagel condensation-Michael addition</i>	<i>Click chemistry</i> (azidoPEG + biotin-alkyne) ^a	Nanoprecipitation or emulsion/solvent evaporation	Nanoparticles	100	Cancer (breast, lung)	Ptx	MCF7, M109	422
P(HDCA-co-SeIPEGGA)	Selegiline (SeI)	<i>Knoevenagel condensation-Michael addition</i>	<i>Click chemistry</i> (azidoPEG + SeI-alkyne) ^a	Nanoprecipitation	Nanoparticles	90–110	Alzheimer's disease	—	Aβ _{1–42}	420
P(HDCA-co-CurPEGGA)	Curcuminoids (Cur)	<i>Knoevenagel condensation-Michael addition</i>	<i>Click chemistry</i> (azidoPEG + Cur-alkyne) ^a	Nanoprecipitation	Nanoparticles	85–105	Alzheimer's disease	—	Aβ _{1–42}	422
P(HDCA-co-biotinPEGGA)	anti-Aβ _{1–42} MAb	<i>Knoevenagel condensation-Michael addition</i>	<i>Click chemistry</i> (azidoPEG + biotin-alkyne) ^a and SAV/ <i>biotin</i> (P(HDCA-co-biotinPEGGA) + Mab-SAV) ^b	Nanoprecipitation	Nanoparticles	150	Alzheimer's disease	—	Aβ _{1–42}	422
Ligand coupling by other ligand strategies										
P(HDCA-co-MePEGGA)	PEG	<i>Knoevenagel condensation-Michael addition</i>	—	Nanoprecipitation	Nanoparticles	90–110	Alzheimer's disease	—	Aβ _{1–42}	423
P(HDCA-co-TFPEGGA)	Transferrin (TF)	<i>Knoevenagel condensation-Michael addition</i>	<i>Imine formation</i> (P(HDCA-co-H ₂ NPEGGA) + Tf-CHO) ^b	Double emulsion-solvent evaporation	Nanoparticles	130–150	Cancer (leukemia)	pDNA	K562	424
P(HDCA-co-TTPEGGA)	Transferrin (TF)	<i>Knoevenagel condensation-Michael addition</i>	<i>Imine formation</i> (P(HDCA-co-H ₂ NPEGGA) + Tf-CHO) ^b	Double emulsion-solvent evaporation	Nanoparticles	240–290	Cancer (leukemia)	DNA/Pi-L	K562	415

^a Coupling prior to nanocarrier formation. ^b Coupling post-nanocarrier formation.

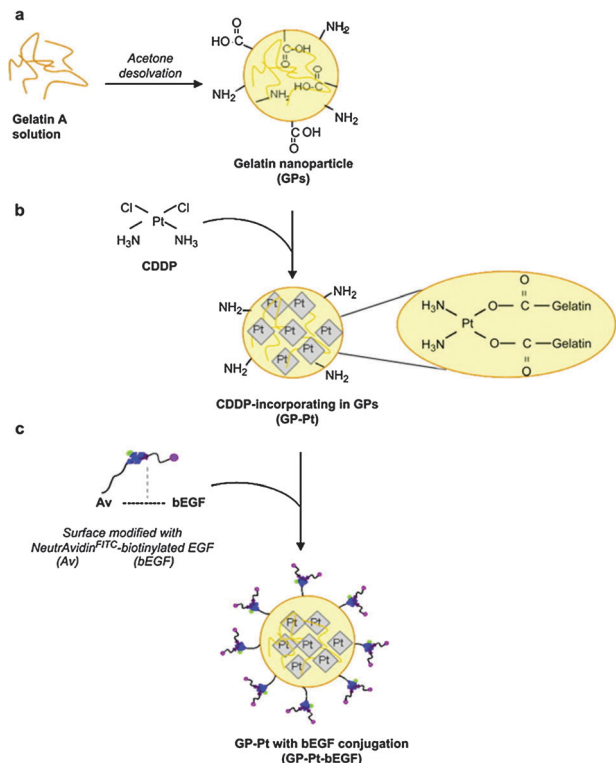


Fig. 38 Schematic representation of gelatin NP formulations (GPs). (a) GPs were prepared by desolvation method; (b) CDDP-loaded GPs (GP-Pt) were spontaneously formed via a ligand exchange reaction of Pt(II) from the chloride to the carboxyl group in the GPs; (c) surface modification of GP-Pt was performed with NeutrAvidin-FITC-biotinylated-EGF complex (reproduced with permission from ref. 400. Copyright 2009, Elsevier).

antibody was positioned by simple incubation at the surface of the NPs by means of the biotin/streptavidin ligation strategy. Note that the PEG chains exposed at the surface of the non-functionalized P(HDCA-co-MePEGCA) NPs also served as a ligand exhibiting a significant affinity for the A β ₁₋₄₂ peptide.^{421,422}

4. Biological applications of targeted nanoparticles

4.1. General considerations

The application of nanotechnologies in the biomedical field has attracted a great deal of interest in the past decades due to its potential to revolutionize the treatment of severe diseases such as cancer, neurological and cardiovascular diseases. In particular, nanocarriers targeted to specific tissues offer the advantages of improved drug therapeutic efficiency and dramatically reduced toxicity and unspecific side effects. In this perspective, in order to promote selective interactions, targeted nanocarriers have been designed taking inspiration from the specific characteristics of each disease. Due to the dramatically high number of deaths caused every year, much effort has been devoted to engineering actively targeted nanocarriers to improve the traditional treatment of cancer. Therefore, functionalized nanocarriers have been prepared using ligands able to specifically bind receptors with increased expression on malignant cells or molecules able to interfere with the signaling pathway unique to cancer cells.

Some *in vitro* proofs of concept of active targeting were provided using empty nanocarriers but mainly drug-loaded

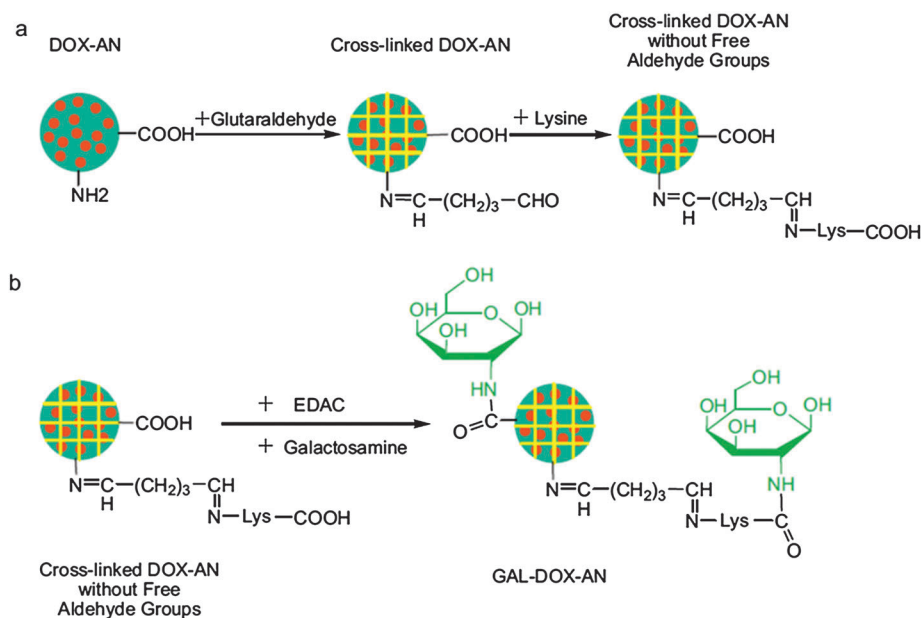


Fig. 39 Schematic illustration for the preparation of Gal-Dox-albumin: (a) preparation of cross-linked Dox-albumin nanoparticles without free aldehyde groups on surface; (b) conjugation of Gal onto the surface of Dox-albumin. The red small spheres represent Dox; the big spheres represent albumin; the yellow lines inside the big spheres represent glutaraldehyde cross-linkage (reprinted with permission from ref. 404. Copyright 2011, Elsevier).

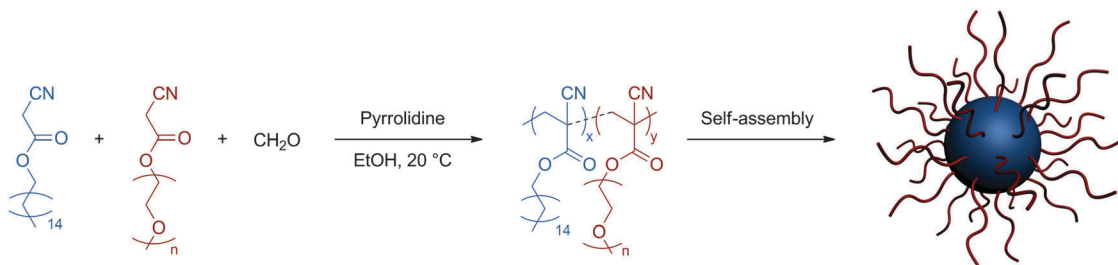


Fig. 40 Synthesis of P(HDCA-co-MePEGCA) copolymer by tandem Knoevenagel condensation–Michael addition.

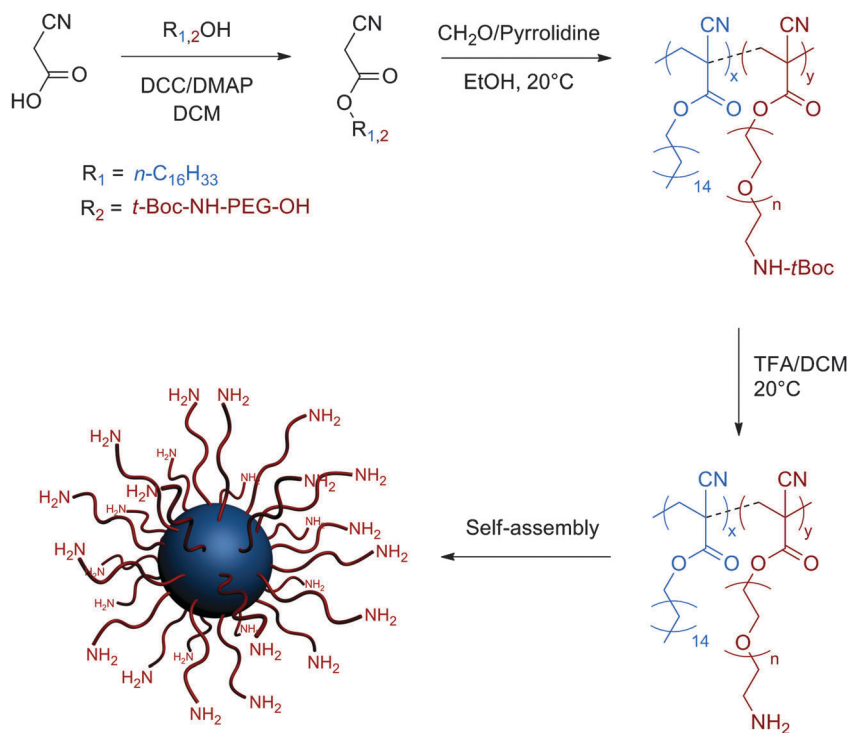


Fig. 41 Synthesis of P(HDCA-co-NH₂PEGCA) copolymer for further NP surface functionalization.

systems have been investigated in order to assess the therapeutic potential of the ligand-targeted strategy. Considering that FA is certainly one of the most represented targeting ligands, we decided to present a more detailed description of *in vitro* experiments performed using FA-functionalized nanocarriers. The feasibility of this approach was evaluated by measuring the uptake of the nanocarriers and their cytotoxicity over specific cell lines, which well exemplifies the studies carried out with other targeting molecules. Indeed, although some details were opportunely modified according to the used ligand, such *in vitro* experimental protocol was generally described by all research groups.

Therefore, in this review, we preferred to highlight *in vivo* studies by presenting the most attractive results obtained so far. Indeed, the *in vivo* pharmacological investigation is fundamental before the translation of the targeted nanomedicine concept into clinical trials and, noteworthily, the increasing number of papers dealing with the *in vivo* evaluation of ligand-targeted nanocarriers is witnessed.

Ligand-targeted nanocarriers have found application not only in the treatment of cancer but also in the management of other severe diseases. A general overview of these therapeutic applications will be proposed.

4.2. Cancer

4.2.1. VITAMIN TARGETED NANOCARRIERS

4.2.1.1. Folic acid targeted nanocarriers. A broad range of cancers are characterized by a significant overexpression of folate receptors, up to 100–300 times higher than normal tissue.^{76,80,425} Therefore, FA has been widely employed as a ligand for achieving targeted therapies of several carcinomas. Commonly used chemotherapeutic drugs (*i.e.* paclitaxel, docetaxel and doxorubicin, 5-FU and Oligomycin-A) were encapsulated in these drug delivery systems, resulting in improved cytotoxicity against cancer cells. Interesting examples of both physical entrapment and covalent coupling of the drug to the copolymers have been explored with the aim of increasing

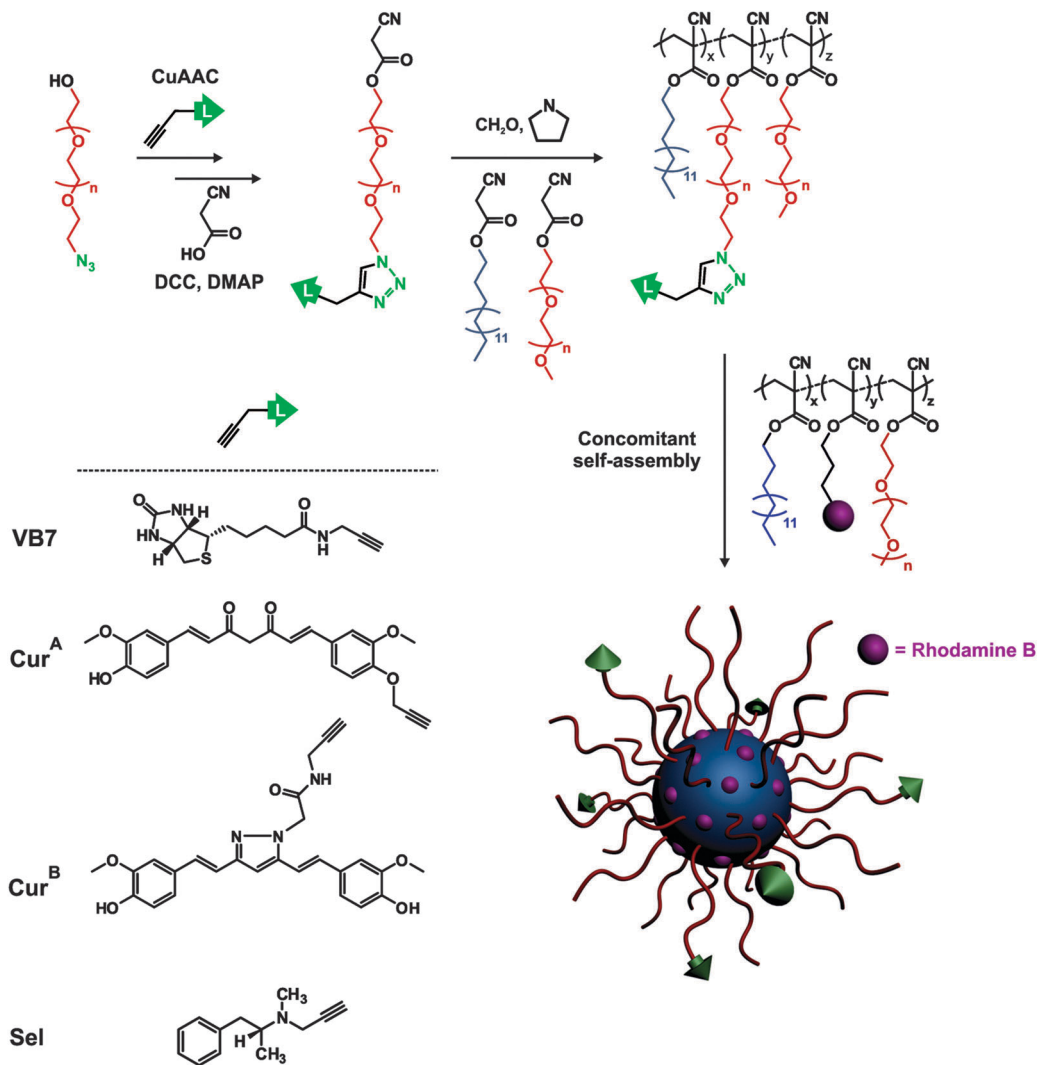


Fig. 42 Synthetic pathway to prepare fluorescent, PEGylated and biodegradable poly(alkyl cyanoacrylate) nanoparticles functionalized with biotin (VB7), selegiline (Sel) or curcuminoid derivatives (Cur^A and Cur^B).

the drug loading together with the therapeutic efficacy of the nanocarriers.^{245,246,295,329} Targeted nanocarriers were also exploited as carriers of plasmid DNA for gene therapy,^{221,238,239,335,342} The physical entrapment or the covalent conjugation of various fluorophores (*e.g.*, FITC, Hylite 488, Alexa 488, Coumarin-6) allowed their accurate traceability and the evaluation of specific *in vitro* and/or *in vivo* interactions.

The *in vitro* efficiency of folate-mediated targeting has been evaluated using cell lines, which overexpress the folate receptor. Among these cell lines, the human epidermal carcinoma (KB), the human cervical carcinoma (Hela), the human breast carcinoma (MCF7), the murine mammary carcinoma (4T1), human ovarian carcinoma (SKOV-3), human squamous carcinoma (SiHa), and the human gastric carcinoma (SGC-7901) are the most well-known. These cells were compared, in terms of uptake/targeting to folate receptor deficient cancer cells such as human alveolar carcinoma A549 and normal/healthy cells such as murine fibroblast NIH/3T3, macrophages and human endothelial EA.hy 926. Fluorescent nanocarriers allowed

monitoring and quantifying the specific folate-receptor mediated binding and internalization by flow cytometry and confocal microscopic analysis. Published results clearly demonstrated that the cellular uptake was enhanced by conjugation of FA at the surface of the NPs compared to the unspecific internalization of bare/naked nanocarriers. In addition, folate receptor overexpressing cell lines showed the highest internalization of FA-functionalized nanocarriers. Competitive binding experiments, performed in the presence of an excess of free FA confirmed the occurrence of a folate-mediated endocytosis mechanism.

The adequate targeting ligand density, which can be controlled by tuning the ratios of ligand-conjugated and ligand-lacking copolymer in the formulation, was also investigated. For instance, independently of the initial amount of PLGA-*b*-PEG-FA used (*i.e.*, from 7 to 75 mol%), only 21% of folate groups were detected by Valencia and coworkers at the surface of their nanoparticles prepared using a blend of PLGA-*b*-PEG and PLGA-*b*-PEG-FA.²²⁵ This was probably due to the interactions between the low water soluble folate molecules and the

PLGA during the formulation process, which caused the entrapment of a significant fraction of the FA into the core of the NPs. Consequently, fine tuning the initial stoichiometry of the different copolymers is a crucial parameter to assure the presence of a sufficient fraction of FA at the surface of the nanoparticles for achieving uptake on FA receptor-overexpressed cells.²²⁵ However, although the targeting capability could be compromised when a too low amount of FA is present at the surface of the nanocarriers, it was reported that an excess of FA could affect the aqueous stability of the resulting nanocarriers and cause formation of insoluble aggregates.²⁴² The manner by which FA molecules are presented to the cells (*i.e.* homogeneously or in spatially defined groupings on a nanoparticle surface) and its influence on cellular uptake was also investigated. Both *in vitro* and *in vivo* studies were performed by Poon and coworkers,³⁸⁴ using linear dendritic PBLA(PED-*b*-PEG-FA)_n polypeptide micelles with statistically similar amounts of folate in different spatial arrangements. *In vivo* results clearly showed that arrangement of FA molecules in clusters presenting an optimal size of, on average, three folate groups, enhanced the uptake of micelles owing to the resultant higher avidity and longer residence times on the cell membrane (Fig. 43).

The *in vitro* cytotoxicity of drug-loaded nanocarriers was evaluated in parallel to the assessment of their targeting features by a routine MTT viability test. Folate-decorated drug-loaded nanocarriers showed a higher toxicity compared to untargeted NPs, due to the intracellular uptake enhancement mediated by folate receptors. Noteworthy, strong cytotoxicity was also measured in multidrug resistant cell lines.^{226,314} When pDNA was encapsulated into polyester NPs, efficient gene delivery was confirmed by successful transfection results.^{221,238,239} It is

therefore evident that the ability of these NPs to bind receptors with high affinity offers the possibility of an efficient targeted delivery of drugs to cancer cells, thus enhancing their therapeutic efficacy.

The possibility to combine active targeting, therapeutic efficiency as well as imaging properties has been demonstrated by the encapsulation of Dox, quantum dots and iron oxide crystals into the hydrophobic core of folate-functionalized PLGA NPs.²¹⁹ The specific targeting ability for cells overexpressing folate receptors led to high NP uptake, which was further confirmed by T₂-weighted MR images. Moreover, the targeting properties were enhanced by application of an external magnetic field, causing the progressive increase of the signal drop and a higher cytotoxicity. Fe₃O₄ was encapsulated also within the core of chitosan-based NPs.³⁴⁶ The resulting magnetic properties allowed the guidance of the nanoparticles toward the tumor using an external magnetic field. Compared to control experiments, an approximately 50 times greater accumulation of magnetic nanoparticles was registered in S-180 sarcoma-bearing Kunming mice, 3 h after administration.

The *in vivo* validation of specific folate-mediated uptake of drug-loaded nanocarriers was provided by different groups using tumor xenograft animal models developed by transplanting folate overexpressing cancer cells. Tumor accumulation and therapeutic efficacy of chemotherapeutic-loaded nanocarriers were evaluated in KB,^{295,379} MCF7,^{73,379} HeLa,³³⁴ A549,³⁷⁹ drug resistant A2780/AD,³⁷⁹ H-22,³⁴⁴ and SGC-7901 carcinoma³⁰¹ models. In all these studies, intravenous administration of folate-decorated nanoparticulate systems resulted in a higher drug accumulation at the tumor site and a slower rate of tumor growth compared to non-functionalized counterparts and to the free drug used as controls. The enhanced permeability and

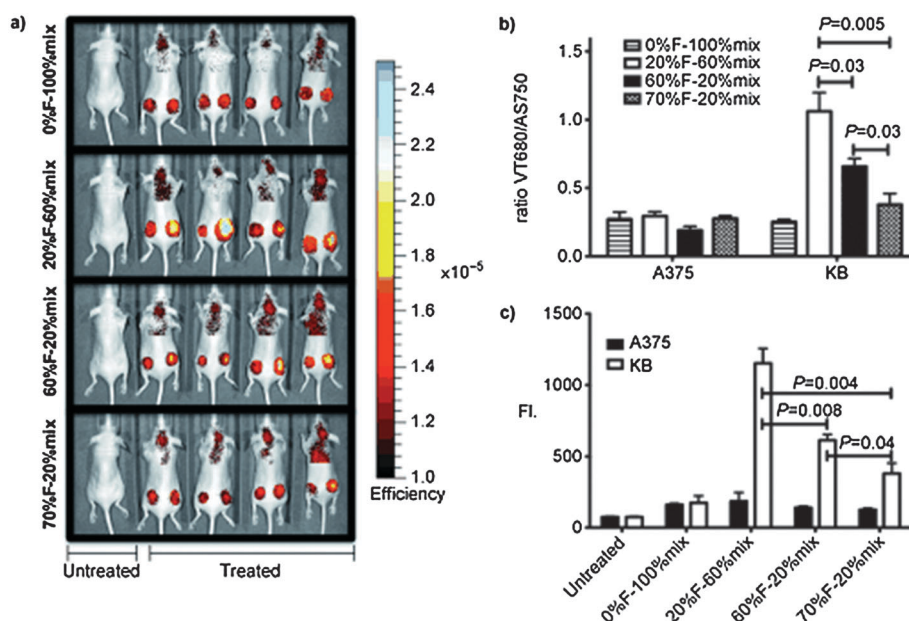


Fig. 43 *In vivo* evaluation of patchy micelles on nude mice bearing two different tumors (right flank: KB, left flank: A375). (a) Fluorescence 3D optical imaging of tumored nude mice 48 h after injection with different formulation micelles. Only fluorescence from tumors and a non-tumoral region of the mice (upper torso) is shown. (b) Normalized tumor fluorescence VivoTag680(VT680)/AngioSense 750(AS750) of tumors (n = 4) showing the highest *in vivo* targeting with 20%F-60%mix micelles. (c) Mean cell-associated micelle fluorescence (FI) (reproduced with permission from ref. 384. Copyright 2009, Wiley).

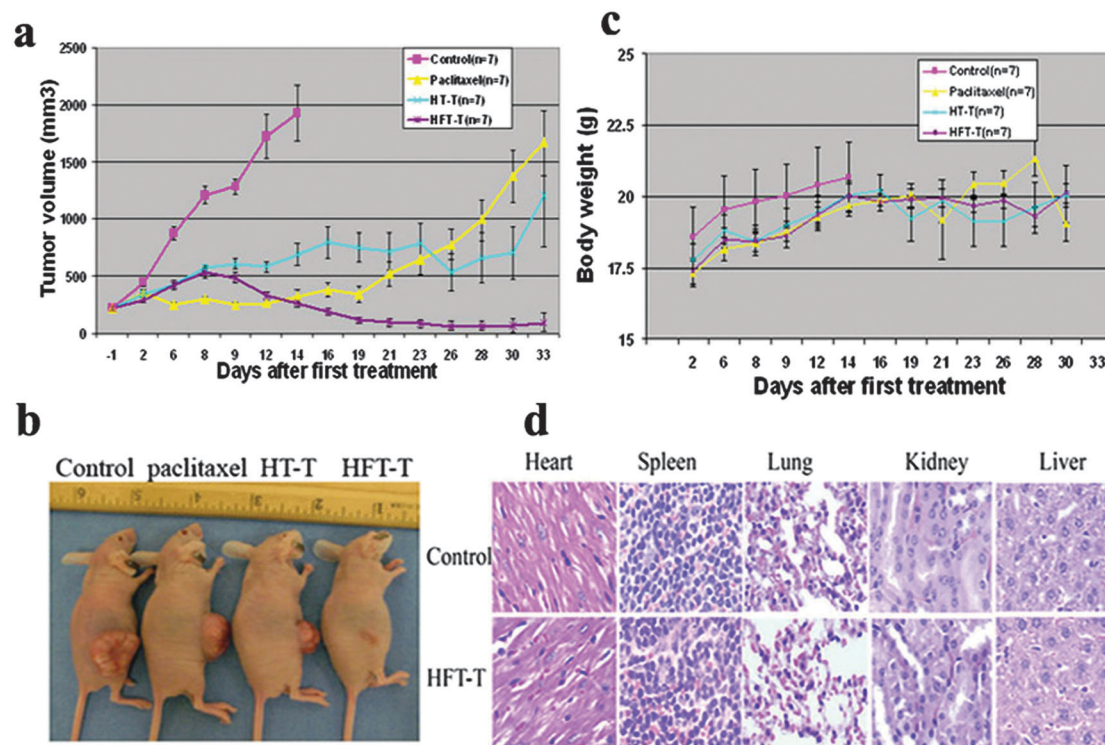


Fig. 44 Antitumor effect of FA functionalized NPs (HFT-T) in an animal model. (a) The growth curve of KB-3-1 xenografts showed that all the treatment groups including free Ptx, blank NPs (HT-t), and HFT-T significantly inhibited the growth of tumor as compared with the control ($p < 0.0001$ for each treatment). The tumor volumes were similar in HT-T and free Ptx-treated groups ($p < 0.608$), but FA-decorated NPs more potently reduced tumor growth than free Ptx ($p < 0.0001$). (b) A representative mouse from each group. (c) The body weight of the mice in all groups. (d) Representative images of H&E organ staining from control and HFT-T-treated mice (magnification 200) (reproduced with permission from ref. 369. Copyright 2009, American Chemical Society).

retention effect due to the large pores present in the tumor endothelial vessels (compared to healthy tissue) and the reduced tumor lymphatic drainage caused a passive accumulation of the nanocarriers at the tumor site. Then, the more efficient internalization of functionalized systems *via* a folate-receptor mediated endocytosis led to an improved therapeutic response. An example of such successful results is provided in Fig. 44. Therapeutic efficacy of FA-functionalized Ptx-loaded heparin nanoparticles was assessed in KB-3-1 xenograft-bearing mice.³⁶⁹ The treatment with free Ptx suppressed tumor growth only initially, and after 3 weeks of treatment, the tumor no longer responded and grew rapidly, likely due to the development of a drug resistance mechanism. Contrariwise, after the same period of treatment with targeted nanocarriers, this resurgence in tumor growth was not observed. Moreover, compared with control treatments (*i.e.* non-functionalized NPs or free Ptx) FA-targeted NPs induced a significantly higher increase of acetylated tubulin levels, marker of a pro-apoptotic stage.

Interestingly, Werner and coworkers explored the potential of folate-targeted nanoparticles, loaded with docetaxel (FT-NP Dxtl), as radiosensitizers to improve the efficacy of the radiotherapy in the tumor and to reduce the toxicity in the healthy tissues.²²² Moreover, due to the importance of timing of radiotherapy, they were the first to determine the optimal interval between chemo and radiotherapy. *In vivo* studies were performed

on mice bearing KB cells xenograft tumors, which were treated with FT-NP Dxtl and irradiation at 3, 12, 24 or 48 h post injection. Due to the specific accumulation in the tumor, systemic administration of FT-NP Dxtl caused a significant inhibition of tumor progression compared to the controls (free drug and non-targeted nanoparticles). The most important tumor growth delay was observed in mice irradiated 12 h after nanoparticles administration. These results clearly demonstrated the potential of these nanoparticles as radiosensitizer and highlighted the importance of determining the optimal time of irradiation to achieve successful treatments. The folate-targeting strategy was then enlarged leading to the development of so-called “ChemoRad” nanoparticles which offer the possibility of concurrent use of chemo and radiotherapy.²²³ Ptx and yttrium-90 were used as chemo and radiotherapeutic isotope, respectively. The effectiveness of this dual system was investigated in an ovarian peritoneal metastasis model developed by intraperitoneal injection of folate overexpressing ovarian cancer cells. Compared to mono treatments (chemotherapy or radiotherapy only), the best therapeutic outcome was achieved in mice treated with ChemoRad nanoparticles. Moreover, although not statistically significant, there was a clear trend toward longer survival in groups treated with folate-targeted nanoparticles (Fig. 45).

The design of nanocarriers combining FA receptor targeting and early endosomal pH sensitiveness was proposed by Kim and coworkers to overcome tumor multidrug resistance.^{226,243}

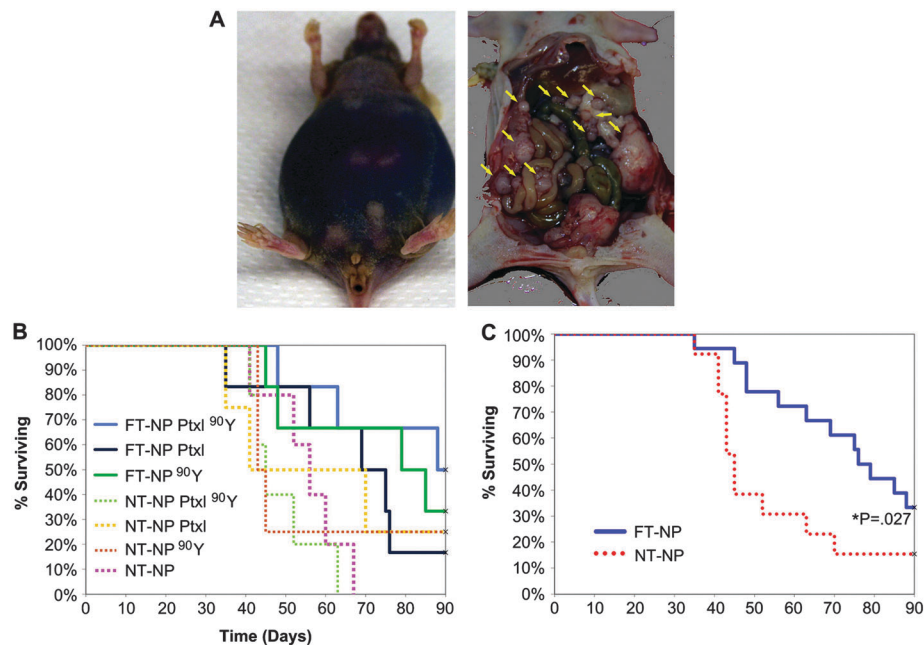


Fig. 45 *In vivo* efficacy of Chemorad NPs. (A) Example of a murine ovarian intraperitoneal metastasis model. The mouse shown in the figure has ascites and diffuse peritoneal metastasis. (B) SKOV-3 cells implanted IP in Nu/Nu female mice, 3 weeks of incubation prior to treatment with NPs. FT-NP Ptxl 90Y appears to be the most effective treatment though statistically non-significant. (C) Survival analysis comparing folate targeted NP (FT-NP) treatment arms to combined NT-NP arms (reproduced with permission from ref. 223. Copyright 2011, Elsevier).

Multidrug resistant ovarian tumor xenograft-bearing mice were used to assess the anticancer activity of Dox-loaded pH-sensitive micelles made of a blend of P(His-co-Phe)-*b*-PEG and PLA-*b*-PEG-FA. These advanced micelles were able to induce a significant inhibition of the tumor growth rate compared to control groups, which received Dox-loaded pH-insensitive micelles of free Dox. Despite the presence of the FA at their surface, which makes both pH-sensitive and pH-insensitive micelles share the same endocytosis pathway, they caused a different therapeutic effect that might be explained considering the existence of different intracellular events such as drug release and endosomal lysis. This observation was confirmed by non-invasive imaging experiments performed by using the dorsal window chamber model. The highest accumulation of Dox at the tumor site was observed 1 h after i.v. injection of pH-sensitive micelles, while, in the case of pH-insensitive ones the maximum was reached at 20 minutes, whereas at 1 h it was already in the decline phase. Therefore, pH-sensitive micelles probably induced a high cytosolic accumulation of Dox, which allowed overcoming the limited defense capacity of MDR cells.

A pH-responsive PLA-*b*-PEG-*b*-PHis targeted nanocarrier encapsulating Dox and bearing TAT and FA ligands was proposed by Lee and coworkers.³⁷⁹ This nanocarrier displayed the ability to hide TAT at its surface during circulation and to expose it at a slightly acidic tumor extracellular pH to facilitate the internalization process. When tested on MCF-7, A549, KB and drug resistant A2780/AD xenograft tumor models, a significant regression of tumor growth was observed after three bolus injections of Dox-loaded micelles (10 mg equivalent Dox per kg body weight per injection) at 3-day interval, while minimum weight loss was observed.

4.2.1.2. Biotin-targeted nanocarriers. Biotin has often been used to functionalize various targeting ligands for their further binding with avidin, neutravidin or streptavidin. This ligation strategy is useful when bulky ligands (protein, MAb *etc.*) are intended to be linked at the surface of NPs. In that case, biotinylated NPs can be either reacted with SAV/NAV/Av-ligand conjugates or with biotinylated ligands and SAV/NAV/Av are used as a sandwich moiety. However, the use of biotin as a biologically active ligand recently appeared as an elegant way to target cancer cells and represents an original alternative to the extensive use of folic acid towards tumor overexpressed folate receptors. Several authors investigated the use of biotin-functionalized biodegradable NPs to target breast cancer cells, which overexpress biotin receptors.^{224,422} Patil and coworkers co-encapsulated Ptx and P-gp-targeted siRNA into biotin-functionalized PLA-*b*-PEG NPs in order to overcome tumor drug resistance. Primary mammary carcinoma JC cells, which overexpress the P-gp and exhibit a resistant phenotype both *in vitro* and *in vivo*, were used to assess the efficacy of the dual agent functionalized NPs. *In vivo* studies demonstrated that the incorporation of biotin resulted in an improved anticancer effectiveness compared to controls. This result was probably due to a synergic effect between Ptx and P-gp-targeted siRNA simultaneously delivered by a biotin-mediated mechanism to tumor cells. Moreover, their different release profiles probably caused the inactivation of the P-gp before complete release of Ptx, thus enhancing the therapeutic effect. Noteworthy, a synergy effect between chemo and gene therapy was observed; indeed, the same dose of Ptx was not effective in the absence of gene silencing. Biotin was also positioned at the surface of HSA

NPs conjugated to methotrexate (MTX) molecules in order to target cancer cells.⁴⁰³ The anticancer efficacy of biotin targeted MTX-HSA NPs was evaluated in mice bearing 4T1 breast carcinoma whereby a single dose of biotin-targeted MTX-HSA NPs showed stronger *in vivo* antitumor activity than non-targeted MTX-HSA NPs and free MTX. After 7 days of treatment, average tumor volume in the biotin targeted MTX-HSA NPs-treated group decreased to ~18% of the initial tumor volume when the number of attached biotin molecules on MTX-HSA-NPs was the highest. The average tumor volume in non-targeted MTX-HSA NPs-treated mice grew rapidly and reached 250% of the initial tumor volume. Biotin targeted MTX-HSA NPs caused a significant increase of the median survival time of tumor-bearing mice (47.5 ± 0.7 days) compared with control groups (non-targeted MTX-HSA NPs or saline), which corresponded to an increase of their life span up to ~220%.

4.2.2. LECTIN-TARGETED NANOCARRIERS. Lipids and proteins, which constitute the membrane of cells, are often glycosylated and can be agglutinated by lectins. Different patterns of glycans are expressed by different cells. Therefore, lectin-functionalized nanocarriers can be used to selectively target specific cell types. Among the various lectins, the WGA from *Triticum vulgare*, able to specifically recognize *N*-acetyl-glucosamine and sialic acid, is the most-employed lectin for targeting purposes. WGA-targeted PLGA NPs have been proposed by Mo and coworkers^{205–207} as drug delivery systems to enhance the therapeutic efficiency of Ptx and overcome side effects associated to its conventional Cremophore[®] EL formulation.⁴²⁶ *In vitro* studies were performed using cancer and normal pulmonary cell lines expressing different glycosylation profiles to assess the selectivity of cell-nanoparticle interactions. Compared to bare nanoparticles and conventional Ptx formulations, used as controls, a higher cytotoxicity and intracellular accumulation was observed after exposure to functionalized nanoparticles, which was clearly due to an efficient WGA-receptor mediated endocytosis. The *in vivo* anti-cancer evaluation was performed on mice bearing A549 xenograft tumors treated with a single intra-tumoral injection of targeted NPs at a Ptx dose of 10 mg kg^{-1} . A single injection inhibited the progression of tumor growth for 23 days post treatment and tumor doubling time was estimated to be greater than 25 days compared to only 11 days for the free drug-treated group. Conventional formulation had a negligible effect on the tumor growth, however the failure of this treatment might be explained considering that the authors decided to work at a low Ptx dose.⁴²⁷

4.2.3. SUGAR-TARGETED NANOCARRIERS. The functionalization of nanoparticles with sugar moieties was described as a strategy to achieve an active targeting on hepatic cells, which largely express the asialoglycoprotein receptors able to bind galactose and *N*-acetylgalactosamine-terminated glycoproteins. Thus, galactosamine has been conjugated at the surface of γ -PGA-*b*-PLA nanoparticles loaded with Ptx.²⁵⁰ The antitumor efficacy of the prepared nanoparticles was investigated in a HepG2 hepatoma xenograft tumor model. Galactosamine-functionalized NPs showed the highest therapeutic activity, with a significant inhibition of tumor growth compared to saline, free Ptx and non-targeted NPs. This result was correlated to the large

accumulation of functionalized nanoparticles at the tumor site, clearly observed during the biodistribution studies. Remarkably, only the group treated with galactosamine-functionalized NPs did not show any weight loss, thus confirming a specific targeting of cancer cells without adverse effects for healthy cells. Galactosamine was also employed to decorate carboxypentyl-xyloglucan-galactose NPs, leading to similar results.³⁷¹

HA was successfully employed as a ligand in doxorubicin-loaded PBLG-*g*-HA polymersomes, which suppressed growth of breast tumor in female Sprague-Dawley (SD) rats as opposed to the control group.³⁷⁶ In addition, reduced level of serum enzymes (LDH and CPK) indicated reduced cardiotoxicity of Dox after loading in polymersomes. These results suggested that intracellular delivery of Dox-loaded PBLG-*g*-HA polymersomes was dependent on the CD44 expression level in cells due to the presence of HA on the surface of polymersomes, and could be used as a self-targeting drug delivery cargo in over-expressed CD44 glycoprotein cells of breast cancer. In this view, it was shown that these polymersomes enhanced intracellular uptake of Dox or Dtx in a murine model of Ehrlich Ascites Tumor (EAT) *via* CD44 receptor mediated endocytosis, resulting in prolonged tumor doubling time and in increasing the life span of mice (Fig. 46).^{375,378}

4.2.4. PEPTIDE TARGETED NANOCARRIERS

4.2.4.1. RGD peptide. Several PLA/PLGA-based nanocarriers functionalized by RGD or RGD-containing peptides were designed, taking advantage from their ability to selectively target the $\alpha_v\beta_3$ integrin receptor.^{125,231,232,257,258,273,285,286,296,313,321,322,324} Anticancer drugs (Ptx, mitoxantrone, Dox), vascular disrupting agents (combretastatin) as well as DNA were also encapsulated in these nanosystems. RGD-targeted theranostic PLA-*b*-PEG micelles, which combine imaging and therapeutic properties by encapsulation of both Dox and SPIO, were proposed by Nasongkla and coworkers.²⁵⁸ *In vitro* cytotoxicity and uptake studies were generally performed using the normal HUVEC cell line to mimic the angiogenic tumor vasculature cells and various malignant cell lines, all overexpressing the $\alpha_v\beta_3$ integrin receptor (B16F10 mouse melanoma cells; MDA-MB-231, Bcap-37, MCF7 human breast carcinoma cells; 4T1 murine mammary carcinoma; DU145 human prostate carcinoma cells; Hela human cervical carcinoma cells and A549 adenocarcinoma cells). Models of co-culture (normal endothelial cells and cancer cells) were also proposed to investigate selective uptake and toxicity of drug loaded systems.²³¹ *In vivo* administration of fluorescent nanocarriers in tumor-bearing mice enabled assessment of the distribution of functionalized systems by non-invasive imaging and quantification of the specific tumor accumulation.²³¹ RGD-decorated nanocarriers induced a significant enhancement of the fluorescence intensity compared to non-targeted systems, which was clearly due to the combined effect of passive accumulation and ligand-mediated active targeting mechanism. However, results of dose-response studies showed that tumor accumulation discrepancies between targeted and non-targeted nanosystems were reduced at high doses probably as a consequence of RGD receptor saturation.²⁵⁷ Variable uptake in different cell lines might be explained considering the different expression of integrins on the cell surface.⁴²⁸

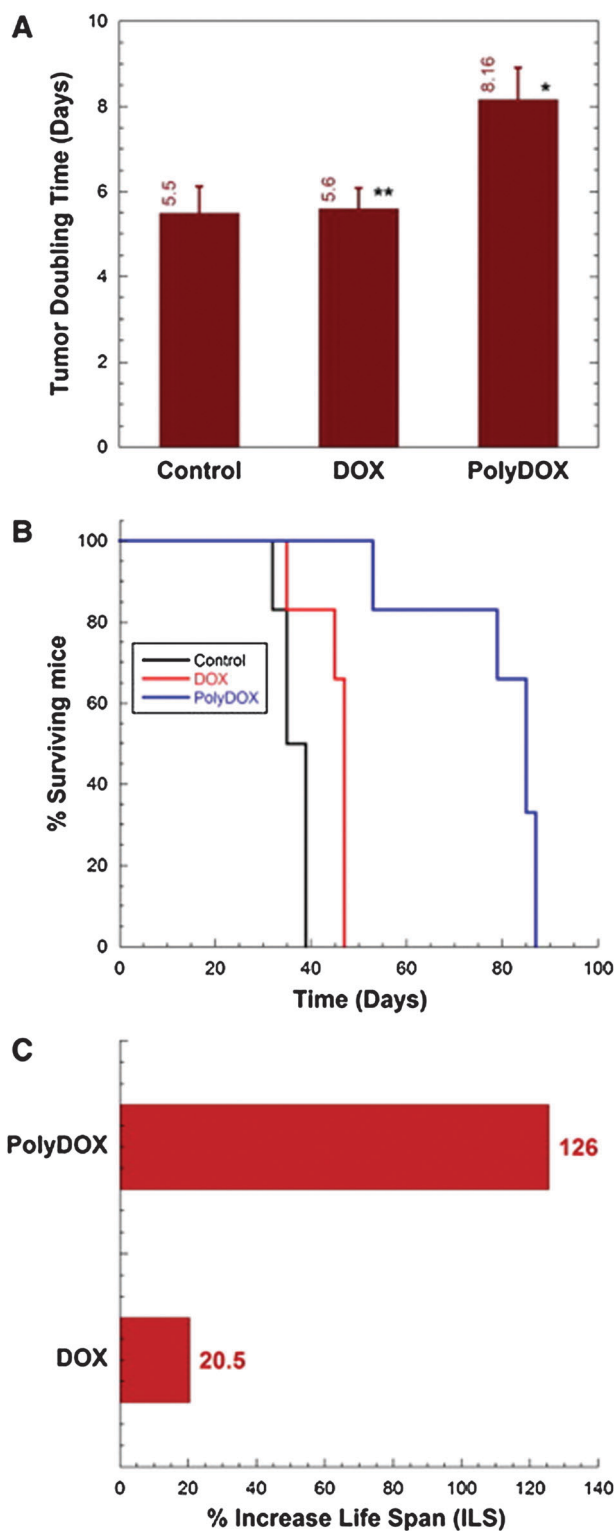


Fig. 46 Tumor volume doubling time (DT) of EAT-bearing mice treated with free DOX and PolyDOX at 5 mg kg^{-1} equivalent to free DOX ($*p < 0.01$ vs. DOX, $*p < 0.01$ vs. control, $**p > 0.05$ vs. control). The data represent mean of six animals \pm SD. (B) Kaplan–Meier survival curve of mice treated with DOX and PolyDOX. (C) Percent increase in life span (ILS) of mice treated with DOX and PolyDOX compared to control. PolyDOX-treated groups survived significantly longer as compared to control and DOX ($p < 0.001$) (reproduced with permission from ref. 378. Copyright 2012, Elsevier).

An example of RGD-conjugated nanocarriers which exhibited a significant anticancer activity *in vivo* without showing the systemic toxicity associated to conventional chemotherapies was reported by Hu and coworkers.²⁸⁶ MDA-MB-435 breast tumor-bearing mice were treated once a week with Ptx-loaded RGD-targeted micelles of PLA-*b*-PEG-RGD or control formulations. Functionalized micelles demonstrated a dramatic efficacy, resulting in complete tumor regression in five of eight animals at the end of the treatment and in a better survival than other treatments. Moreover, active targeting increased the apoptotic induction in tumor cells and prevented adverse effects on healthy tissues which were instead observed after administration of Cremophore[®] EL paclitaxel formulation.

A combined therapeutic approach, using two different RGD-targeted PLGA-*b*-PEG nanoparticles loaded with Ptx or the CDK inhibitor JNJ-7706621, was investigated in a fast growing transplantable liver tumor model.²⁸⁵ The two functionalized carriers were sequentially administered and resulted in inhibition of tumor growth to a greater extent than either treatment. Non-functionalized NPs were instead ineffective in reducing the tumor growth rate. A RGD-peptide mimetic was also investigated by the same group; however, although interesting results were obtained *in vitro*, this ligand did not induce any improvement of Ptx efficacy *in vivo*.³²⁴

The RGD targeting strategy was also explored for nanocarriers based on PCL or PCL derivatives.^{319–322} The RGD4C peptide was conjugated to micelles made of the PEO-*b*-PCL copolymer to which Dox was tethered *via* an amide bond [RGD4C-PEO-*b*-P(CL-Ami-Dox)] or a pH-sensitive hydrazone bond [RGD4C-PEO-*b*-P(CL-Hyd-Dox)].³²¹ Targeting potential and cytotoxicity of these nanocarriers were evaluated in both wild type and MDR MDA-435/LCC6 cells. Significant increase in the uptake of RGD-functionalized micelles compared to bare systems was observed in both cell lines. However, the presence of a hydrazone or an amide bond led to a different intracellular distribution of the released Dox, which was responsible for the different cytotoxic response of sensitive and resistant cells. MDA-435/LCC6^{wt} cells were more sensitive to RGD4C-PEO-*b*-P(CL-Hyd-Dox) micelles, which led to preferential nuclear accumulation of Dox. In contrast, RGD4C-PEO-*b*-P(CL-Ami-Dox) micelles were associated to mitochondrial drug localization and were thus more toxic in MDA-435/LCC6^{MDR}. The therapeutic potential of these micelles was evaluated *in vivo* in tumor models developed by inoculation of wild type or MDR cells. Each group was then treated with the formulation that caused the highest cytotoxic response *in vitro*. Targeted formulations showed the highest therapeutic efficacy with inhibition of tumor growth and longer life span compared to animals that received the non-functionalized micelles. Noteworthy, the accurate choice of the coupling strategy to conjugate the doxorubicin to the polymer backbone led to the formulation of drug delivery systems effective even in MDR tumors.

Moreover, with the aim of finding successful strategies to overcome the multidrug resistance, a combined dual targeting/dual therapy approach was explored.³²² Micelles were functionalized with both the RGD and TAT peptides as homing

devices. A siRNA against the P-gp was co-delivered with Dox, conjugated to the copolymer *via* the hydrazone bond. This complex nanosystem showed excellent results *in vitro* with high cytotoxicity in MDR resistant cells also. Although therapeutic efficacy was not demonstrated, the significant tumor accumulation observed *in vivo* represents a promising starting point to achieve this goal (Fig. 47).

The synthesis of triple-functionalized NPs based on PLGA-*b*-PLL-*b*-PEG for targeted and delivery of siRNA to tumors was reported by Zhou and coworkers.¹²⁵ These nanocarriers exhibited at the distal end of PEG chains iRGD (CRGDKGPDC) and two CPPs (*i.e.*, mHph1 and mAP). When these NPs were loaded with siRNA against PLK1, they provided knockdown of PLK1 expression in A549 cells (91.0%), which was similar to the inhibition seen with Lipofectamine RNAiMAX (94.4%). In addition, delivery siRNA against PLK1 significantly inhibited the *in vitro* proliferation of A549 cells. Intravenous injection of these nanoparticles significantly inhibited tumor growth and the expression of the PLK1 gene in the treatment group was 47% of the expression in the control group, even 7 days after the last treatment. Histologically, tumors from the control-treated group revealed a highly cellular mass with prominent nucleoli whereas tumors from animals treated with NPs loaded with siRNA against PLK1 revealed a much less cellular mass with a lower nuclear/cytoplasmic ratio, and a marked increase in the number of apoptotic cells (Fig. 48).

Chitosan as polymeric scaffold was employed to design RGD-functionalized nanocarriers for gene silencing purposes.³⁵² *In vitro*, these targeted nanoparticles labeled with Alexa555 were able to selectively target $\alpha_v\beta_3$ -positive ovarian cancer cell lines (SKOV3ip1) in a RGD concentration-dependent manner, while a significant lower internalization (−94,25%) was observed with non-RGD particles. In contrast, similar binding efficiency was observed in A2780ip2 cells ($\alpha_v\beta_3$ -negative) for both functionalized and non-RGD nanoparticles. To evaluate the enhanced targeted delivery *in vivo*, the authors quantified the siRNA-Alexa555 tumor accumulation 48 h after a single injection, observing a 3-fold higher accumulation of targeted nanoparticles compared to non-functionalized counterparts. A co-localization, of $\alpha_v\beta_3$ integrin and NP fluorescence signals, was detected in tumor slices stained with specific antibodies, confirming a specific targeting. Furthermore, once loaded with a periostin specific siRNA, the functionalized nanoparticles provided better tumor growth inhibition in SKOV3ip1 tumor-bearing mice than the non-functionalized counterpart (Fig. 49).

4.2.4.2. Other peptides. The phage display strategy has been exploited by various groups to screen peptides able to selectively bind a specific target. Short peptides were isolated and used to functionalize various types of nanocarriers. The Lyp-1 peptide is a 9-amino acid cyclic peptide able to selectively bind tumor cells and tumor-associated lymphatic vessels.¹³¹ Due to these targeting abilities, Lyp-1-targeted NPs have been exploited as nanocarriers for selective drug delivery to tumor and lymphatic metastasis. Proof of concept of the feasibility of this approach was provided *in vitro* and *in vivo* in a BxPC-3 lymphatic metastasis

model.²⁵² After administration of coumarin-6-loaded PLGA-*b*-PEG-Lyp-1 NPs, an efficient active targeting, which led to a marked accumulation in lymph nodes with metastasis, was observed by non-invasive *in vivo* imaging. These results make the Lyp-1 peptide extremely attractive to achieve a targeted delivery to lymphatic metastatic tumors.

A xenograft MDA-MB-231 human breast cancer model was used to assess the therapeutic efficacy of two different nanocarriers: (i) Dox-loaded pH-sensitive PLA-*b*-PEG-AP/PAE-*b*-PEG micelles functionalized with the AP peptide which specifically bind to the IL-4 receptor on breast cancer cells²⁶⁰ and (ii) Ptx-loaded PLA-*b*-PEG NPs functionalized with the K237 peptide specifically targeted to the VEGFR of tumor neovessels.²⁸⁷ In both studies, an excellent therapeutic anticancer activity was observed after systemic administration due to an increased cell accumulation *via* the receptor mediate mechanism. Noteworthy, in the latter case, the therapeutic effect was the consequence of the significant apoptosis of tumor neovasculature endothelial cells which led to large necrotic areas in the tumor due to the deprivation of the blood supply.²⁸⁷

Research was also focused on a new peptidic sequence (Gly-Ile-Arg-Leu-Arg-Gly, GIRLRG) which can selectively bind to receptors expressed only on cancer cells exposed to ionizing radiation therapy (XRT).¹³³ These receptors represent an interesting target to achieve a controlled delivery of chemotherapeutic drugs to XRT-exposed cells and enhance the effectiveness of XRT. The targeting GIRLRG peptide was identified by phage display technology and used to functionalize PVL-based cross-linked nanoparticles loaded with Ptx. Heterotopic breast and glioma mice tumor models were used for these *in vivo* studies. Mice were treated with 3 Gy XRT daily for 3 days and Ptx-loaded functionalized NPs were *i.v.* administered at the second day. Due to the specific binding to the GPR78 receptor, expressed only at the surface of irradiated cells, the GIRLRG peptide caused a specific accumulation of NPs in XRT-responding cells, which resulted in a greater reduction of the tumor growth rate compared to controls.

4.2.5. EGF-TARGETED NANOCARRIERS. Due to the overexpression of EGFR in a wide range of solid tumors, EGF-conjugated micelles of PCL-*b*-PEG or PVL-*b*-PEG have been formulated.^{70,304–306} In these nanocarriers, EGF exerts the double function of a specific targeting ligand as well as a therapeutic molecule due to its capacity to activate apoptosis in cancer cells expressing high levels of EGFR.^{429,430} The possibility of using drug-loaded micelles for a combined therapy was assessed *in vitro* in MDA-MB-468 (high EGFR expression) and MCF7 (low EGFR expression) breast cancer cells.³⁰⁴ A significant growth inhibitory effect was observed due to a synergic effect between EGF and the encapsulated anticancer drug, and to the ligand-mediated active targeting. Noteworthy, these EGF-micelles represent one of the first examples of nanocarriers able to induce a strong bystander effect because of their specific targeting capacity.⁴³¹ Pharmacokinetic and biodistribution studies were performed on breast cancer bearing mice and highlighted the influence of the density and structural integrity of the tumor neovasculature on the accumulation of nanocarriers. The influence of the micelle size was also investigated,

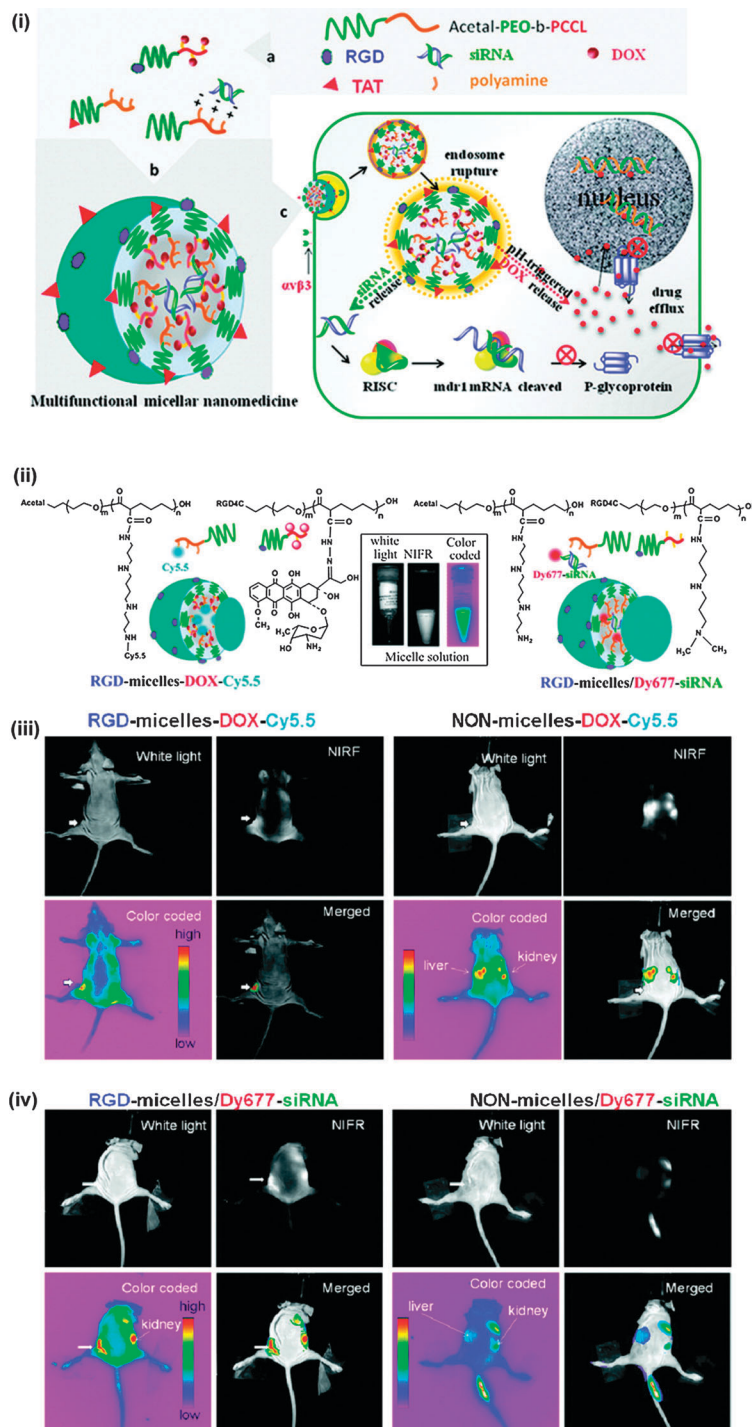


Fig. 47 (i) Rational design of a multifunctional micellar nanomedicine for targeted co-delivery of siRNA and DOX to overcome multidrug resistance. (a) Chemical structure of functionalized copolymers with ligands at the end of the PEO block and conjugated moieties on the PCL block. (b) Assembly of multifunctional micelles with DOX and siRNA in the micellar core and RGD and/or TAT on the micellar shell. (c) Schematic diagram showing the proposed model for the intracellular processing of targeted micelles in MDR cancer cells after receptor-mediated endocytosis, leading to cytoplasmic siRNA delivery followed by P-gp down-regulation on the cellular and nuclear membrane and endosomal DOX release, followed by DOX nuclear accumulation. (ii) Schematic illustration of polymer structures and assembled RGD-functionalized micelles containing NIRF imaging probes. The insets show images of one of those NIRF formulations. (iii) Athymic nude mice bearing MDA-MB-435/LCC6MDR1-resistant tumors injected with RGD- and NON-micelles-DOX-Cy5.5. (iv) Athymic nude mice bearing MDA-MB-435/LCC6MDR1-resistant tumors injected with RGD- and NON-micelles/Dy677-siRNA. MDA-MB-435/LCC6MDR1-resistant cells were transplanted subcutaneously into the right rear flanks of the mice, and tumor was approximately 0.1 cm³ 17 days after implant. The mice were imaged at 24 h after injection. The intensity of fluorescence is expressed by different colors, with pink reflecting the lowest intensity (background) and red reflecting the highest intensity. The tumor is indicated by the thick arrow (reproduced with permission from ref. 322. Copyright 2011, American Chemical Society).

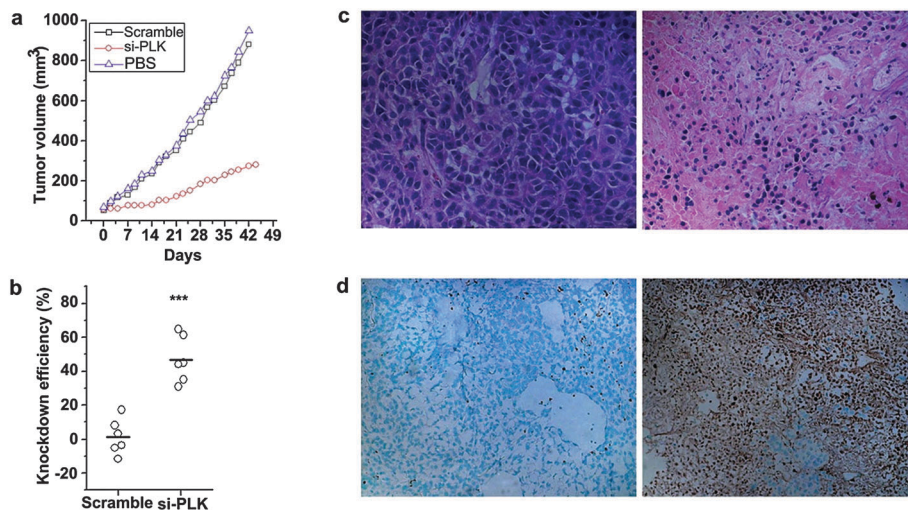


Fig. 48 (a) Antitumor effects of nanoparticles loaded with siRNA against PLK1. (b) Expression of the PLK1 gene in residual tumors. (c) H&E staining of the control tumor (left) and the siPLK1 treated tumor (right), 40× magnification. (d) TUNEL staining of the control tumor (left) and the siPLK1 treated tumor (right), 20× magnification (reproduced with permission from ref. 125. Copyright 2012, Elsevier).

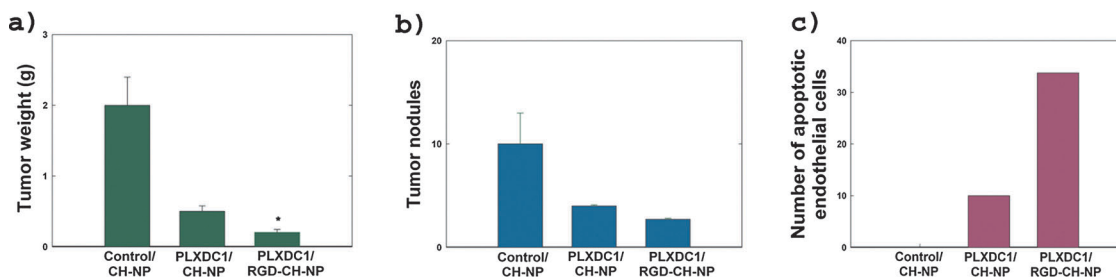


Fig. 49 Therapeutic efficacy of PLXDC1 siRNA/RGD-CH-NP, PLXDC1 siRNA/CH-NP or CH-NP in A2780 tumor-bearing mice: (a) and (b) antitumor effect; (c) apoptosis in tumor endothelial cells (data taken from ref. 352).

demonstrating that smaller micelles were easily uptaken, although a certain delay was observed when micelles were functionalized due to the so-called “binding site barrier effect”.^{305,306} Indeed, according to this effect, internalization of ligand-functionalized nanocarriers requires the successful binding to their target, which therefore halt their penetration in solid tumors compared with free molecules.⁴³²

4.2.6. TRANSFERRIN-TARGETED NANOCARRIERS. Transferrin is a glycoprotein which plays a key role in several biological functions of the organism. Among them, Tf shows the capacity to bind Fe³⁺ and interact with its corresponding receptors to induce the delivery of iron to the brain by a receptor-mediated mechanism. Therefore, Tf-functionalized nanocarriers have been exploited mainly to overcome the BBB and to achieve an efficient delivery to the CNS. However, Tf receptors are overexpressed also in solid tumors such as breast and prostate cancers. With the aim to reduce side effects associated to the conventional Cremophore[®] EL formulation, Ptx has been encapsulated into PLGA NPs decorated with Tf.²⁸⁹ The effectiveness of a single-dose intratumoral delivery of this formulation was evaluated *in vivo* in pancreatic xenograft tumor-bearing mice. A significant tumor inhibition and longer survival was achieved with Ptx loaded-Tf targeted NPs than with control NPs and Cremophore[®]

EL formulation, which was correlated to an increased NP uptake *via* the Tf receptor-mediated mechanism.

Significant results were also obtained using transferrin-targeted nanocarriers based on CDs for the delivery of anti-cancer siRNA. The ability of this nanoparticulate system to predominantly target tumor cells was first identified *in vitro*, where the co-administration with free Tf clearly reduced the uptake of the nanoparticles in HeLa cells.³⁶¹ The *in vivo* pharmacokinetics of these particles was studied using ⁶⁴Cu labeling for micro-PET imaging. The results highlighted that the presence of Tf at the surface of the nanocarrier had a negligible impact on the biodistribution and tumor accumulation kinetic, likely because of the EPR effect. However, bioluminescence analysis showed that the functionalization enhanced the siRNA intracellular localization. These results confirmed that targeting moieties did not noticeably affect the NP accumulation in tumor environment but contributed to the increase of the internalization in tumor cells.^{360,363} The activity of this non-viral nanocarrier system was assessed using different siRNAs to target specific tumor mutations. Anti-EWS-FLI1 siRNA was employed to combat Ewing's sarcoma, leading to impressive results. Three consecutive daily injections of targeted NPs resulted in a decreased tumor signal lasting for 2 to 3 days,

related to a 60% decrease of EWS-FLI1 expression by the tumor tissue while no effect was observed with scramble siRNA. Most notably, a long-term treatment regimen in which formulations were given twice a week, beginning the same day as injection of tumor cells (TC71-LUC), was evaluated. The targeted NPs dramatically inhibited the engraftment of tumor cells with 20% of the mice showing no tumor growth compared to 90–100% in control groups. Further analysis also confirmed the absence of immune response or major organs damage in the treated animals.³⁶⁶

Safety, systemic doses and pharmacokinetics of this CD-based nanocarrier, charged with anti-M2 subunit of ribonucleotide reductase siRNA (siR2B + 5), were widely investigated in non-human primates. When administered to cynomolgus monkeys at doses of 3 and 9 mg siRNA kg⁻¹, the NPs were well tolerated, while at 27 mg siRNA kg⁻¹, a significant toxicity was observed in the kidneys and in the liver. Analysis of complement factors did not reveal any change that could be clearly assigned to NPs injections doses even if a mild immune response was detected at the highest dose. Biodistribution and pharmacokinetic parameters were also investigated and identified.³⁶⁵ These results were considered very encouraging and led to a phase I clinical trial in patients with solid tumors (see Section 4.7 for more details).³⁶²

4.2.7. MAB TARGETED NANOCARRIERS. Upregulation of the epidermal growth factor receptors (EGFR) and the human epidermal growth factor receptor 2 (HER2) is associated to the development of tumors. Specific monoclonal antibodies able to target these tumor-associated receptors have been widely used for functionalization of biodegradable polyester-based drug delivery systems.^{209,211,233,240,247,269–271,274,294,297,308} Noteworthy, these Mabs not only provide an active targeting but can also exert a therapeutic activity by inhibiting the ligand–receptor interaction and consequently blocking the associated signaling pathway.

The PE38KDEL toxin was encapsulated in PLGA NPs decorated with anti-HER2 Mab (PE-NPs-HER) and its therapeutic efficacy was investigated in a HER2-overexpressing breast cancer model and compared to a control immunotoxine synthesized by conjugation of anti-HER2 Mab to PE38KDEL (PE-HER).²⁰⁹ Encapsulation of PE38KDEL in immuno NPs was associated to a reduced non-specific toxicity, compared with free PE38KDEL. Internalization of functionalized NPs *via* a receptor-mediated mechanism led to the release of the drug in the intracellular compartment, which prevented its interaction with specific receptors for protein toxins in normal tissues. In protective experiments, tumor development was inhibited in a dose dependent manner, without significant difference, after administration of both anti-HER2-PLGA NPs and PE-HER. Nevertheless, the potent antitumor activity of antibody-functionalized NPs compared to the control toxin was clearly demonstrated under therapeutic experiments.

A similar approach was described *in vitro* by using chitosan polymeric backbone decorated with anti-HER2 Mab encapsulating Gemcitabine (Gem) or Dox. An increased internalization of functionalized nanoparticles was observed in MiaPaca2,

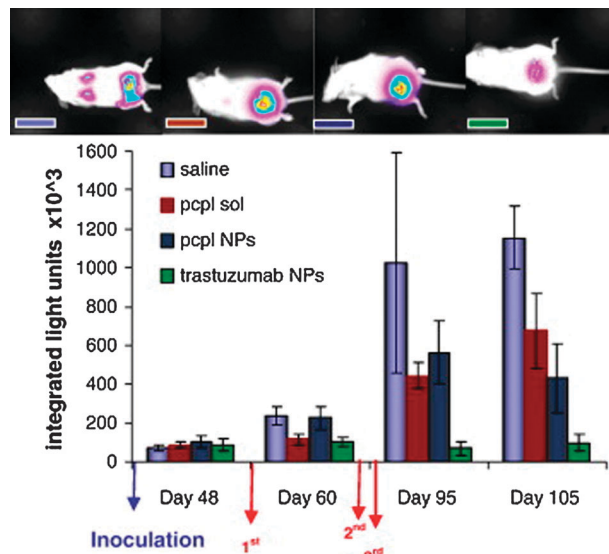


Fig. 50 Detection and quantification of tumor size in living mice by a luciferase assay using a CCD camera following 3 consecutive treatment injections of different pcpl formulations 54 days post cell inoculation. Paclitaxel palmitate loaded immuno NPs inhibit the tumor growth much more than the pcpl solution and pcpl NPs ($p < 0.05$). $N = 8$, values are mean \pm SE. Mice pictures were taken at day 95 (reproduced with permission from ref. 274. Copyright 2008, Elsevier).

PANC-1 and ovarian carcinoma cell line SKOV-3, compared with the HER2 deficient MCF7 cell line.^{347,351}

As an alternative to the conventional methods to evaluate the tumor progression, the non-invasive bioluminescence imaging was selected to assess *in vivo* the effectiveness of Ptx-palmitate-loaded anti-HER2 functionalized PLA-*b*-PEG NPs in an orthotopic model of prostate cancer developed by injection of PC-3.38/luc cells. A significant decrease in tumor growth rate was observed after administration of targeted formulation compared to controls as results of a tissue specific accumulation mediated by the Mab (Fig. 50).²⁷⁴

In vivo ligand-mediated targeted delivery of fluorescent rhodamine loaded PLA-PL-EGFRmAb NPs in a SMMC-7721 hepatocellular carcinoma xenograft mouse model was investigated by non-invasive imaging.²⁴⁰ In contrast with controls (free rhodamine and non-functionalized NPs), fluorescence intensities of tumor in groups treated with PLA-PL-EGFRmAb NPs was stronger and lasted for a longer time, thus confirming an active targeting of the tumor *via* the receptor–ligand recognition.

An optimized nanoparticulate system based on Heparin, encapsulating *CisPt* and decorated with a single chain antibody against EGFR, which contains the binding region able to recognize the receptor but lacks the Fc region, was reported.³⁶⁸ This approach led to several advantages compared to the use of the whole Ab: (i) a decrease in the molecular weight of the whole nanoassemblies, (ii) a decreased immunogenicity and (iii) a low accumulation in normal organs. Compared to free *CisPt*, the designed Heparin nanoparticles showed a prolonged blood circulation time, improved pharmacokinetics and significant enhancement of the anti-tumor activity, without leading to weight

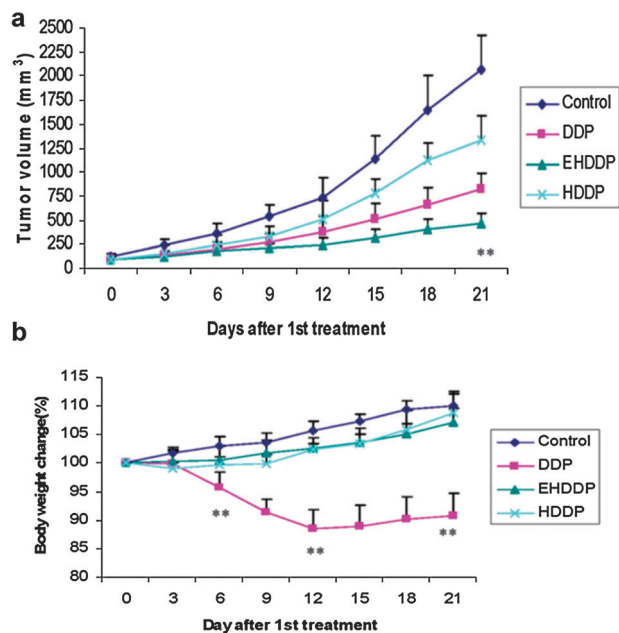


Fig. 51 Effects of free *CisPt* (DDP), DDP loaded heparin NPs (HDDP) and ScFvEGFR-decorated/DDP loaded heparin nanoparticles (EHDDP) on tumor growth and body weight. Tumor growth rate (A) and body weight change (%) (B) of nude mice treated with DDP, HDDP, and EHDDP nanoparticles (Pt 2.5 mg kg⁻¹, 5 injections, 3 day intervals, 6 mice per group). The data are shown as mean (SD, **p* < 0.05, ***p* < 0.01) (reproduced with permission from ref. 368. Copyright 2009, American Chemical Society).

loss or damage to the kidney and the spleen in nude mice bearing the H292 lung mucoepidermoid tumor (Fig. 51).

4.2.8. APTAMER-TARGETED NANOCARRIERS. Aptamers are DNA or RNA oligonucleotides that, through intramolecular interactions, fold into a unique conformation able to bind target ligands with specificity and affinity comparable to those observed for antibodies.¹⁸⁴

The A10 RNA aptamer that recognizes the extracellular domain of the prostate specific membrane antigen (PSMA) was widely exploited by Langer and coworkers to design PEGylated PLGA-*b*-PEG NP-aptamer bioconjugates.^{185,186,235,236,298} The anticancer activity of drug loaded nanocarriers was evaluated *in vivo* using a LNCaP mouse model of pancreatic cancer and compared with traditional chemotherapeutics (*i.e.*, Ptx, *CisPt*, Dtx). Intratumoral administration of Apt NPs-bioconjugates was significantly more efficient in tumor reduction than non-targeted NPs and controls due to efficient cell internalization after binding the PSMA protein onto the cell surface (Fig. 52). Interestingly, a significant reduction of systemic toxicity was also observed. The most efficient cell uptake both *in vitro* and *in vivo* was correlated to an optimal density of aptamers and PEG molecules at the surface of NPs, which modulated targeting and stealth properties, respectively.

A DNA aptamer (AS1411) which binds to nucleolin, a membrane protein highly expressed in cancer cells, was instead investigated by Guo and coworkers to mediate specific drug delivery to gliomas.²³⁷ Pharmacokinetics and biodistribution analysis of aptamer-functionalized Ptx-loaded PLA-*b*-PEG NPs

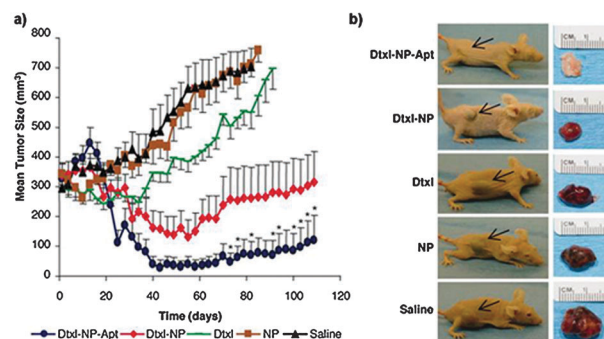


Fig. 52 (a) Comparative efficacy study in LNCaP s.c. xenograft nude mouse model of PCa. of a single intratumoral injection (day 0) of (i) saline (black); (ii) pegylated PLGA NP without drug (NP, brown); (iii) emulsified Dtxl (Dtxl, green), 40 mg kg⁻¹; (iv) Dtxl-encapsulated NPs (Dtxl-NP, red), 40 mg kg⁻¹; or (v) Dtxl-encapsulated NP-Apt bioconjugates (Dtxl-NP-Apt, blue), 40 mg kg⁻¹ evaluated over 109 days. *, Data points for the Dtxl-NP-Apt group that were statistically significant compared with all other groups (*p* < 0.05). (b) Representative mouse at the end point for each group is shown (Left) alongside images of excised tumors (Right). Black arrows point to the position of the implanted tumor on each mouse (reproduced with permission from ref. 186. Copyright 2006, PNAS).

clearly demonstrated an improved accumulation in C6 glioma cells due to specific aptamer–nucleolin interactions. Significant tumor inhibition and longer survival times were observed in subcutaneous and orthotopic glioma tumor models after intravenous administration of functionalized NPs (Fig. 53).

4.3. CNS delivery

The BBB is formed at the level of the endothelial cells of the cerebral capillaries and essentially composes the major interface between the blood and the brain.^{433,434} This barrier is the most important factor that limits drug delivery to the central nervous system. Indeed, even small therapeutic molecules are generally not able to cross the BBB. In recent years, many attempts were focused on the development of various approaches to overcome the limitations inherent to BBB passage. Among them, BBB-targeted surface-functionalized nanocarriers appeared to be an extremely attractive and promising strategy.

4.3.1. BRAIN CANCER

4.3.1.1. Peptide-functionalized nanocarriers. Candotoxin is a snake neurotoxin, which binds with high affinity the nicotine acetylcholine receptors (nAChRs). nAChRs are widely expressed on the capillary endothelium of the brain and are involved in a peptide-mediated delivery to the CNS of various molecules. Therefore, short candotoxin-derived peptides (CDX) have been exploited as targeting ligands to promote the transport to the brain of PEGylated PLA-*b*-PEG micelles.¹⁴⁷ The therapeutic potential of Ptx-loaded functionalized micelles was assessed using intracranial glioblastoma-bearing nude mice. nAChRs-mediated transport across the BBB was responsible for the efficiency of these micelles which led to a significant longer survival time compared to non-functionalized ones. Results clearly highlighted the higher potential of the peptide-targeted strategy in the management of brain tumors as well as other CNS diseases.

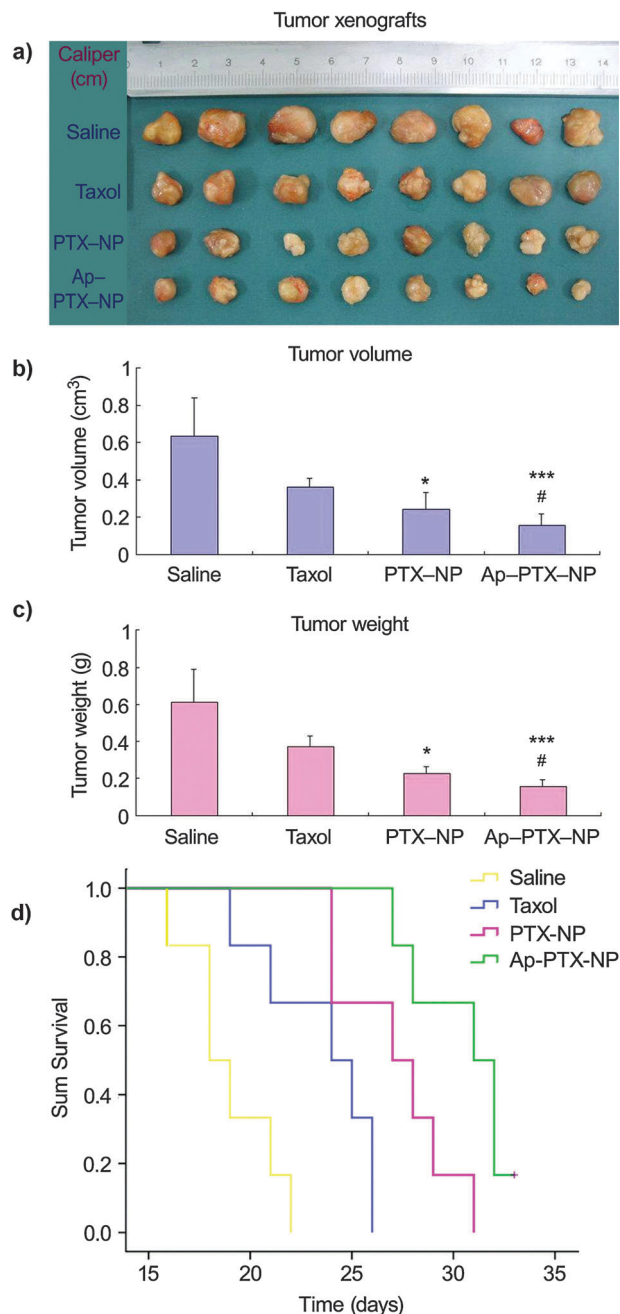


Fig. 53 Anti-tumor efficacy of Taxol[®], PTX-NP and Ap-PTX-NP on nude mice bearing glioma xenograft. (a) Tumor xenografts alignment of each group taken out from the sacrificed mice, (b) tumor volume and (c) tumor weight at the study end point. Significant differences found between the Ap-PTX-NP/PTX-NP and the Taxol[®] groups, and marked as * $p < 0.05$, *** $p < 0.001$ respectively. Significant differences found between the Ap-PTX-NP and the PTX-NP groups, and labeled with # $p < 0.05$. (d) Kaplan–Meier survival log-rank analysis of Wistar rats bearing intracranial C6 glioma ($n = 6$). The survived time of the animals received Ap-PTX-NP was significantly longer than that of those received PTX-NP ($p < 0.05$), Taxol[®] ($p < 0.01$) and saline ($p < 0.001$) (reproduced with permission from ref. 237. Copyright 2011, Elsevier).

With the aim of finding a new strategy for efficient delivery of drugs to the CNS, *in vivo* phage display was proposed to isolate peptides able to target the brain with high specificity

and thus potentially promote the passage across the BBB of drug delivery nanoconstructs. A 12 amino acids sequence, denoted Pep-TGN, was isolated by Li *et al.*¹⁵⁰ and covalently conjugated at the surface of PLGA-*b*-PEG NPs. As observed by NIR imaging, pep-TGP-functionalized NPs were able to cross the BBB with a significant accumulation in the brain compared to non-functionalized NPs, which mainly accumulated in the liver and the spleen. Higher uptake in the brain was achieved by increasing the Pep-TGP density at the surface of the NPs. Although extremely interesting results were obtained, much effort is needed to establish the exact mechanism by which the BBB passage is achieved.

By decorating the surface of PCL-*b*-PEG NPs both with the TGN peptide and the AS1411 DNA aptamer, Gao and coworkers engineered a double functionalized colloidal system, able to facilitate the NP transport in the brain and to selectively target gliomas cells.³⁰³ This aptamer binds with high affinity the nucleolin protein highly expressed at the surface of various tumor cells including gliomas. *In vivo* NIR imaging allowed monitoring distribution of fluorescent DiR-loaded NPs and showed that the highest accumulation in the glioma was observed with bi-functionalized NPs, thus confirming that the TGN peptide could facilitate the transport of the NPs from the blood to the brain and the AS1411 aptamer could recognize glioma cells and enrich NPs in the glioma. Mono-functionalized NPs caused instead a diffuse brain distribution of NPs without selectivity. Efficacy studies were performed by *i.v.* administration of Dtx-loaded NPs. Due to the specific glioma accumulation, bi-functionalized NPs resulted in higher survival time compared to non- or mono-functionalized NPs.

The low-density lipoprotein receptor-related protein (LRP) is highly expressed both at the BBB, which is involved in the transcytosis of several molecules, and at the surface of human gliomas cells. Therefore, the Angiopep-2, a small peptide able to bind the LRP, is extremely attractive for the design of dual-targeted drug delivery systems. This strategy has been applied to the development of Ptx-loaded Angiopep-targeted PCL-*b*-PEG NPs to achieve an improved passage of the BBB and an efficient accumulation in gliomas cells.^{309,310} This dual targeting was investigated *in vitro* and *in vivo*, whereby a marked anti-proliferative effect against U87 MG glioma cells was observed using a transwell co-culture model. Distribution studies clearly showed the penetration of angiopep-targeted NPs in the brain tissue *via* a receptor-mediated endocytosis and a specific accumulation both in glioma bed and infiltrating margins. Conversely, only a moderate accumulation was noticed using non-functionalized NPs which penetrated only by EPR effect.

4.3.1.2. Transferrin-targeted nanocarriers. An increased expression of Tf receptors has been found in various malignant brain tumors. This feature has been exploited to achieve a specific delivery to the CNS by designing Tf-functionalized PLA-²⁴⁸ and PCL-based nanocarriers,³¹¹ encapsulating Dtx and Dox, respectively. C6 glioma cells were used to provide an *in vitro* proof of concept of the feasibility of such systems as targeted drug carriers. Surface conjugation of Tf led to a higher

cell accumulation and enhanced cytotoxicity compared to non-functionalized systems. Biodistribution studies confirmed the possibility to target the brain through a receptor-mediated endocytosis, thus achieving CNS accumulation of functionalized nanocarriers for an extended period of time. Noteworthy, NPs formulated with the TGSP, although not functionalized, were able to accumulate to a certain extent in the brain, probably as a consequence of the P-gp transporter inhibition mediated by the TGPS.²⁴⁸

Encapsulation of Dox in PCL-*b*-PEG-Tf polymersomes resulted in a significant increase of mice survival time and a reduction of tumor volume in an orthotopic model of glioma.³¹¹ Immunohistological analysis of brain tumors clearly showed a marked apoptotic response in mice treated with doxorubicin loaded Tf-targeted polymersomes, while only a few apoptotic cells were detected in control groups.

4.3.1.3. Lactoferrin-targeted nanocarriers. Similarly to Tf, lactoferrin (Lf) is another iron-binding protein which has been investigated as targeting molecule to overcome the BBB and to promote the delivery of anticancer drugs to the brain.³⁰⁷ Pharmacokinetic and biodistribution of Lf-functionalized PCL-*b*-PEG polymersomes encapsulating both Dox and the potent MDR inhibitor tetrandrine were performed in an orthotopic glioma model in rats. NIR fluorescence images showed a higher accumulation of targeted DiR-loaded polymersomes in brain tumors compared to non-functionalized counterparts which confirmed the ability of Lf to facilitate the passage of Lf-conjugated systems across the BBB. Administration of Lf-targeted polymersomes loaded with the two therapeutic agents resulted in decrease of tumor growth rate and extended long-term survival compared to control treatments (Fig. 54) Combination of both active targeting and tetrandrine-mediated inhibition of MDR dramatically increased the therapeutic efficacy of Dox.

4.3.2. NEURODEGENERATIVE DISEASES

4.3.2.1. Chitosan-functionalized nanocarriers. Another possibility to deliver drugs to the brain relies on the adsorptive-mediated transcytosis (AMT) through the cerebral endothelium based on specific charge interactions.⁴³⁵ This pathway allows the efficient internalization of polycationic molecules after binding to the negatively charged cell membrane. Being

positively charged under physiological conditions, the trimethylated chitosan (TMC), a permanent quaternized chitosan derivative,⁴³⁶ might promote an active transport *via* the AMT mechanism and thus allow the brain internalization of TMC-modified NPs. This approach has been investigated to achieve an efficient delivery to the brain of the coenzyme Q10-loaded PLGA-TMC NPs.¹⁰³ Behavioral experiments carried out on an Alzheimer's disease (AD) transgenic animal model enabled assessment of the neuroprotective effect of these formulations after *i.v.* injection. The Morris water maze task demonstrated an improvement in the memory impairment after administration of coenzyme Q10-loaded PLGA-TMC NPs with a rise in learning ability and significant reduction of the escape latency compared to control animals. Analysis of brain parenchyma in AD mice clearly showed the presence of senile plaques. However, a progressive reduction of the number and the size of these plaques was observed after treatment with coenzyme Q10-loaded PLGA-TMC NPs. The concentration of A β was reduced and the deposition of A β fibrils was inhibited. This work clearly demonstrated that TMC-modified NPs crossed the BBB and it constitutes the first proof of the ability of the coenzyme Q10 to dissolve senile plaques *in vivo*. Nevertheless all these results are in conflict with the recent failure of highly promising phase III clinical trial showing that a dramatic reduction of amyloid peptides in the brain (obtained using monoclonal antibody, Solanezumab[®], Eli Lilly) is not associated with recovery of cognitive or functional state, thus underlining the complexity of the disease and the difficulty of animals-human translation.

4.3.2.2. Lectin-functionalized NPs. Intranasal administration has been proposed as an alternative strategy to cross the BBB and to achieve an efficient delivery of drugs to the CNS. Due to the specific capacity to bind to the glycosylated nasal mucosa, lectin-functionalized nanoparticles were formulated to enhance the nose to brain delivery of biodegradable NPs (PLA-*b*-PEG and PLGA-*b*-PEG). Different lectins were employed: (i) WGA,^{264,265} (ii) odorranalectin (OD),^{255,256} and (iii) solanum tuberosum lectin (SLT).²⁶⁷ OD is the smallest peptide with lectin-like properties and presents low immunogenicity while STS is attractive for its stability over a wide range of pHs (4–10) and temperatures (above 50 °C). Extensive studies were performed to investigate the pathways followed by these NPs after

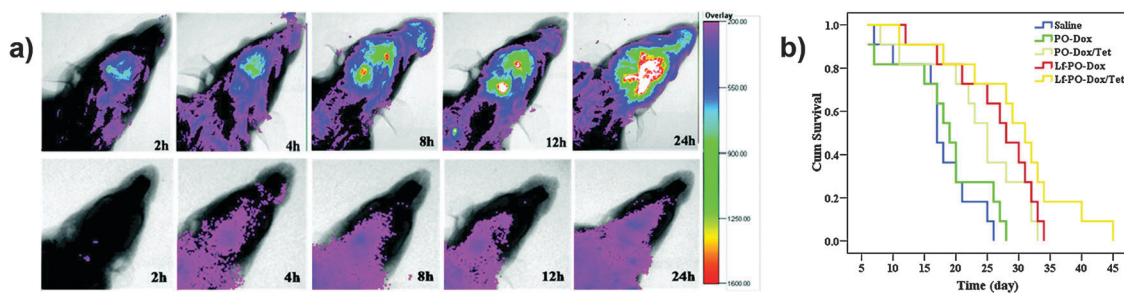


Fig. 54 (a) Brain fluorescence imaging of glioma model rats at a series of time points after *i.v.* injection of Lf-PO-DiR (the upper row) or PO-DiR (the lower row) at the dose of 0.5 mg kg⁻¹ of DiR ($n = 4$). (b) Percentage of survival (Kaplan–Meier plot) of glioma bearing rats after intravenous injection of 1.5 mg kg⁻¹ Dox on days 2, 5, 8, and 11 with different formulations ($n = 11$) (adapted with permission from ref. 307. Copyright 2010, American Chemical Society).

administration and to assess their potential toxicity. Significant brain accumulation was obtained after intranasal administration compared to intravenous injection. WGA-functionalized NPs were transported to the brain *via* an extracellular mechanism along the olfactory and trigeminal nerves in 2 h following nasal administration.^{266,267} All these NPs showed very low toxicity and represent a biocompatible platform to achieve a controlled delivery of drugs to the brain. Proof of concept of the therapeutic potential of this strategy has been provided by formulating drug loaded lectin-functionalized NPs.^{256,265} The neuroprotective effect of the vasoactive intestinal peptide (VIP) and the corticotrophin releasing factor urocortin was investigated on a Parkinson disease and a learning impairment animal model, respectively. Intranasal administration of the urocortin-loaded OD-targeted NPs was responsible for a significant therapeutic efficacy in a hemiparkinsonian rat model as demonstrated by a dramatically reduced rotational behavior.²⁵⁶ Similarly, VIP-loaded WGA targeted NPs exerted a neuroprotective effect with a significant improvement in learning in the Morris maze task, as a result of an increased cholinergic activity.²⁶⁵

4.3.2.3. Lactoferrin-targeted nanocarriers. Lf has been investigated as targeting molecule not only for the transport of chemotherapeutics to the CNS, but also of molecules which can exert a neuroprotective effect in various neurodegenerative diseases.^{261–263} Biodistribution studies, performed using coumarin-6 loaded PLA-*b*-PEG-Lf NPs, demonstrated an extensive distribution in the cortex, the *striatum substantia nigra*, the third ventricle and the periventricular regions. In these areas, the fluorescence associated to non-functionalized NPs was negligible. The possibility of using these Lf-functionalized NPs to deliver therapeutic molecules to the brain was also investigated in animal models of neurodegenerative diseases. A neuroprotective agent, urocortin, was encapsulated in Lf-targeted NPs, and their therapeutic efficacy was evaluated in a Parkinson model induced by unilateral intra-striatal infusion of 6-HODA in rats. Administration of urocortin-loaded Lf-targeted NPs caused a significant reduction of the apomorphine-induced rotational behavior, thus confirming a potential anti-parkinsonian activity. Intravenously injected urocortin could not cross the BBB, but the encapsulation in Lf-functionalized NPs led to a specific brain accumulation and an attenuation of the brain lesions induced by the 6-HODA. Similarly, S14G-humanin, a neuroprotective peptide able to inhibit Alzheimer's disease-associated apoptosis and amyloid- β related toxicity, was encapsulated in Lf-targeted PLA-*b*-PEG polymersomes. The therapeutic potential of this actively targeted drug delivery system was evaluated by immuno-histochemistry in rats treated with amyloid- $\beta_{25–35}$ to induce a model of AD. Intravenous administration of S14G-humanin-loaded Lf-targeted polymersomes caused an increase of the activity of the cholinesterase and remarkable inhibition of Bax expression and caspase-3-related neuronal apoptosis. All these results suggest the possibility to achieve an active targeting using Lf functionalized nanocarriers.²⁶³

4.3.2.4. Mab-targeted nanocarriers. Another strategy to target the Tf receptors located at the BBB and to promote the passage across the BBB consists in using specific anti-Tf Mab. Among them, the OX26, previously used to decorate the surface of lipid vesicular carriers and chitosan nanoparticles, has been chosen to functionalize PCL-*b*-PEG polymersomes and transport efficiently to the brain the neuroprotective peptide NC-1900.³¹² A rat model of learning and memory deficit was successfully developed by i.p. injection of scopolamine. Then, the Morris water maze task was used to assess the therapeutic potential of NC-1900-loaded OX-26 polymersomes. Even at the very low dose of 1 ng kg⁻¹ of NC-1900, functionalized nanocarriers induced an improvement of the spatial memory impairment with a significant shortening of the latency time, while the s.c. administration of the free drug at the same dose was totally ineffective. A progressive dose-dependent improvement was also observed, reaching a plateau at 10 ng kg⁻¹. Results obtained were promising and offered the possibility to enhance the transport and the bioavailability of various therapeutic peptides into the brain.

4.3.3. MISCELLANEOUS APPLICATIONS

4.3.3.1. FA-targeted nanocarriers for treatment of rheumatoid arthritis. FA-decorated chitosan NPs have been investigated as non-viral carrier for gene delivery of IL-1Ra (interleukin 1 receptor antagonist), a natural blocker of the inflammatory cytokine IL-1, which plays a crucial role in the progressive cartilage destruction and bone damage that characterize rheumatoid arthritis. Gene therapy offers the possibility to overcome the limitation of the conventional therapy (*i.e.* recombinant IL-1Ra), which requires high-yield daily subcutaneous injections to maintain the therapeutic serum levels. The active targeting approach was selected according to the fact that, interestingly, articular macrophages isolated from rats with adjuvant-induced arthritis overexpress folate and exhibit significantly higher binding capacity for folate conjugates than macrophages obtained from healthy rats.⁴³⁷ *In vitro*, the functionalized carrier did not demonstrate increased transfection efficacy compared with non-functionalized ones.³⁴¹ However, in an adjuvant induced arthritis (AIA) model in rats, treatment with IL-1Ra-loaded folate-functionalized chitosan NPs significantly inhibited elevated levels of IL-1 β , which is known to be a potent mediator of bone resorption, by acting as an osteoclast-activating factor.⁴³⁸ Therefore, blocking or lowering the activity of proinflammatory IL-1 β should protect against inflammatory bone resorption. This result was confirmed by the investigation of three different bone metabolism biomarkers, namely alkaline phosphatase (ALP), tartrate-resistant acid phosphatase (TRAP) and osteocalcin (OC). Indeed, functionalized NPs were able to reduce the activity of ALP and the number of TRAP-positive osteoclasts and to increase the osteoblastic levels of OC, confirming the partial disease recovery. Moreover, the particles induced a slight decrease of prostaglandin (PGE₂), indicating a reduction of inflammatory conditions.

4.3.3.2. Cell penetrating peptide-functionalized nanocarriers for HIV management. Functionalization of nanocarriers with cell

penetrating peptides has been proposed as a way to cross the BBB as an alternative to receptor-mediated transport.⁴³⁹ Among them, the TAT peptide is one of the widely used in the design of functionalized drug delivery nanoassemblies.¹²³ The capacity of this peptide to cross the BBB has been investigated to achieve an efficient delivery to the brain of ritonavir-loaded NPs and to increase the bioavailability of the anti-HIV drug.²⁹⁰ *In vivo* studies were performed on healthy mice and aimed at assessing the localization of NPs and the distribution of ritonavir in the brain as well as any potential adverse effect of the functionalized NPs on the BBB integrity. Results clearly demonstrated an efficient uptake of TAT-targeted NPs and a sustained release of ritonavir, reaching concentration that corresponds to the required therapeutic levels. Ritonavir first accumulated in the ventricles and then drug biodistribution changed with exposure time. Noteworthy, no modification of the BBB permeability was observed. Even though the use of CPPs represents a smart method to promote the crossing of the plasma membrane, the lack of cell/tissue specificity remains a significant limitation.

4.3.3.3. Functionalized nanocarriers for management of pain and depression. Considering that some naturally occurring peptides (*e.g.*, opioid peptides) are able to cross the BBB by receptor-mediated transport, the use of specific peptides for targeted delivery to the brain has been investigated by several groups. Different glycosylated simi-opioid heptapeptides (g7) were tethered at the surface of PLGA NPs to confer them the ability to cross the BBB.^{200,201,215} To perform pharmacological and biodistribution studies, loperamide and rhodamine-123, both unable to cross the BBB when injected intravenously, were encapsulated into these nanocarriers. The hot-plate test was used to measure the nociceptive threshold. The insurgence of the opioid effect as early as 30–60 min after NP injection clearly demonstrated the rapid penetration of the NPs into the brain. Moreover, a strong analgesic effect was assured for 5 h, thus demonstrating a sustained drug release. Dual surface functionalization with g7 peptide and sialic acid residues,²¹⁵ able to bind specific brain receptors, caused an even quicker analgesic effect (with 15 min post-injection) and a long lasting constant sedative effect was observed up to 15 h and then slowly decreased. Confocal microscopy analysis showed, at least qualitatively, the ability of targeted NPs to accumulate within the brain parenchyma and a prolonged residence until 15 days was observed for double targeted NPs.²¹⁵ The *in vitro* proof of concept concerning the possibility of using g7-functionalized NPs to deliver Zn²⁺ to the brain, whose altered concentration seemed to be associated to neuropsychological disorders such as depression, was also provided.¹⁷³

Functionalized NPs based on proteins such as HSA or gelatin were also selected as potential nanocarriers for BBB crossing and CNS delivery of active drugs such as loperamide.^{169,390,392,393} Their functionalization was achieved with apolipoproteins (*e.g.*, ApoE, A-I, B-100),^{169,390,392,393} insulin or anti-insulin receptor monoclonal antibody (29B4),¹⁶⁹ transferrin or anti-transferrin receptor monoclonal antibodies (OX26 or

R17217).³⁹³ In particular, HSA-PEG NPs decorated with apolipoproteins induced antinociceptive effects in the tail-flick test in ICR mice after *i.v.* injection. In contrast, nanoparticles linked to apolipoprotein E variants that do not recognize lipoprotein receptors failed to induce these effects.³⁹⁰ It was also shown that the delivery of drugs to the brain by means of HSA NPs, in addition to the Apo E and B pathway, may also be improved by the interaction of apolipoprotein A-I covalently attached to these nanoparticles with the scavenger receptor SR-BI located at the BBB.³⁹² Similar results were obtained with insulin, 29B4, Tf, OX26 or R17217 ligands.^{169,393}

4.3.3.4. Mab-targeted nanocarriers for treatment of cerebral ischemia. During the last few years, diverse therapeutic peptides able to specifically interfere with cerebral ischemia-derived cell death have been discovered. Caspase-3 plays an important role as mediator of cell death in acute and chronic neurological disorders. The Z-DEVD-FMK peptide, a specific inhibitor, is reported to significantly reduce vulnerability to the neuronal cell death following cerebral ischemia. Although very active, the peptide has to be administered intracerebroventricularly due to the lack of BBB-crossing ability and its limited (several minutes) plasma stability. To bypass all these restrictions, the group of Couvreur designed a nanocarrier system based on chitosan-g-PEG, encapsulating Z-DEVD-FMK and decorated with Tfr-specific monoclonal Ab (OX26, CD71) to promote the passage of the BBB.³⁵⁴ Fluorescence and TEM microscopy on brain slices demonstrated the penetration of functionalized nanocarriers to the brain parenchyma 2 h after intravenous administration in healthy mice (Fig. 55). The neuroprotective effect of the designed system was studied in a mouse focal cerebral ischemia model where the targeted nanocarriers significantly reduced the infarct volume ($43 \pm 4 \text{ mm}^3$) compared with the group receiving the peptide-free nanospheres ($50 \pm 4 \text{ mm}^3$). An even stronger effect was obtained by increasing the treatment dose, confirming a dose-dependent activity. Most notably, a significant recovery in neurological deficits score was identified 24 h after the reperfusion in animals treated with targeted NPs, while no effect was detected in control mice.³⁵³

4.4. Other applications

Despite the preferential application of targeted-nanomedicine to diagnosis and treatment of cancer and CNS diseases, a few studies describe the benefits of active targeting strategy directed toward other pathologies.

4.4.1. MANNAN-TARGETED NANOCARRIERS FOR VACCINATION. Mannan is a natural polysaccharide able to bind with high affinity the mannose receptors localized on antigen-presenting cells such as dendritic cells and macrophages. Targeting antigens to mannose receptors has been demonstrated to be an interesting strategy to enhance antigen uptake, processing and presentation, which resulted in improved antigen-specific T-cells response.⁹⁸ Mannan has therefore been proposed to functionalize the surface of antigen-loaded PLGA NPs, in order to enhance their effectiveness as vaccines. Proof of concept studies

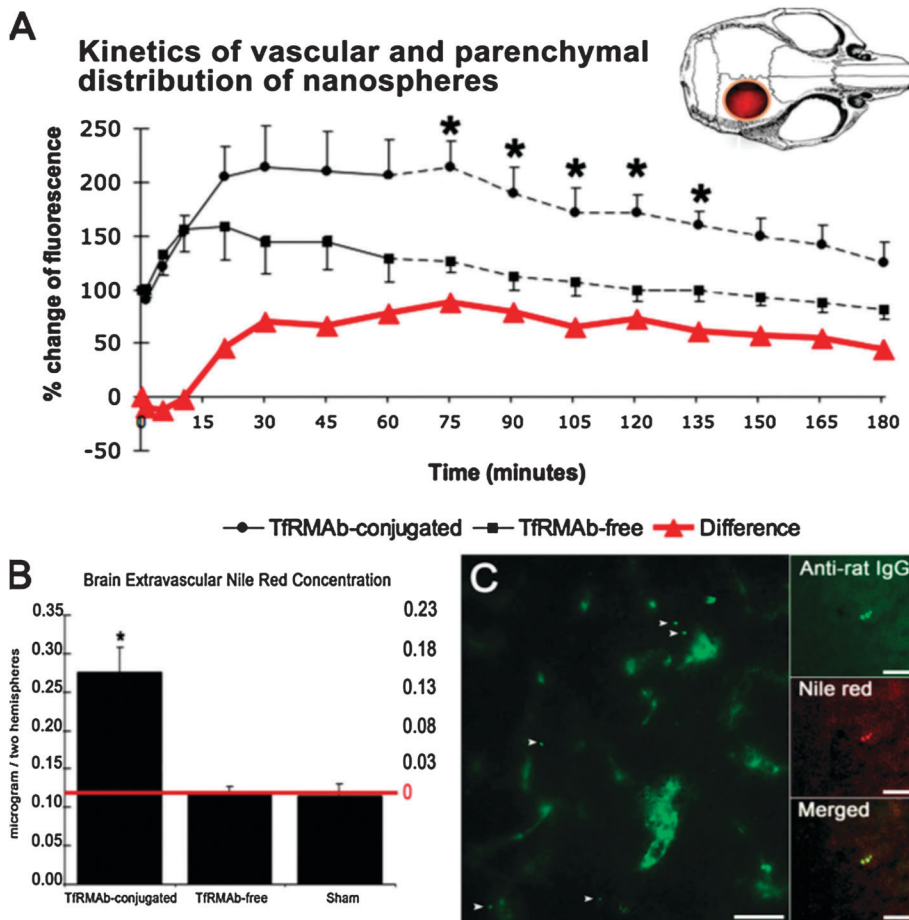


Fig. 55 (a) Nanospheres are rapidly transported to brain parenchyma after systemic administration. The graph illustrates the change in fluorescence recorded in the brain over the course of 3 h after injection of Nile red-loaded to TfrMAB-conjugated (●) or unconjugated (■) nanospheres. The difference between the two lines (red line) reflects the fluorescence coming from the nanospheres within the parenchyma and illustrates the time course of nanosphere penetrance to the brain. (b) Nile red concentration in brain post-vascular tissue increased only when TfrMAB-conjugated nanospheres were administered. The graph illustrates spectrophotometric measurements at 549 nm from brain homogenates obtained 1 h after injection of TfrMAB-conjugated or unconjugated nanospheres or from sham-operated mice. Only values above the horizontal red line, below which values correspond to the tissue background readings, were taken into consideration. * $p < 0.05$. (c) FITC-conjugated anti-rat IgG antibody (green) labeled the nanospheres bearing TfrMAB, clearly demonstrating that the nanospheres were dispersed within the extracellular space outside the vessel lumens. Vessels were visualized by nonspecific labeling obtained with a high concentration of the antibody. Some FITC-conjugated nanospheres exhibited green as well as red fluorescence because they had not released all the Nile red loaded within an hour (right). A lower concentration of the antibody was used to stain these sections; hence, vessels were not labeled (reproduced with permission from ref. 353. Copyright 2009, Society of Neuroscience).

has been obtained both *in vitro* and *in vivo* using the ovalbumin as model antigen. Vaccination was carried out in wild type C57BL/6 mice which received two subcutaneous injections of functionalized NPs or controls. These immunization experiments demonstrated the possibility to use MN-decorated nanoparticles to enhance both CD4⁺ and CD8⁺ T cell responses. Although the response of CD4⁺ T cells was predominant, opportune modulation of NPs physico-chemical properties could enhance their ability to stimulate CD8⁺ associated immune responses.²¹³

4.4.2. PEPTIDE-TARGETED NANOCARRIERS FOR DIABETES MANAGEMENT. A proof of concept for the development of islet targeting NPs for the immunomodulatory therapy of autoimmune type 1 diabetes was reported.²⁰² To achieve this goal, PLGA-*b*-PEG NPs were decorated with a cyclic peptide sequence able to target specifically the microvessels of the pancreatic islets and loaded with Genistein, a tyrosin kinase inhibitor agent, which impairs

leucocyte adhesion to activated endothelial cells. *In vivo* internalization studies, performed both in static and dynamic conditions (using a microfluidic system), showed the high affinity of peptide-functionalized NPs towards the islet capillary endothelial cells with up to 3-fold greater uptake compared to the skin capillary endothelial cells. Moreover, the significant inhibition of leucocyte adhesion to TNF-activated endothelium after incubation with genistein-loaded NPs was achieved at a 200-fold lower dose than with the free drug. A clear superior therapeutic effect was obtained by using these site-specific delivery systems, which might have implications not only for diabetes therapy but also for diagnostic screening of pre-diabetic subjects through incorporation of imaging agents that can permit real-time monitoring of pancreatic islets.

4.4.3. PEPTIDE-TARGETED NANOCARRIERS FOR THROMBOLYTIC THERAPIES. Targeted delivery of thrombolytic agents *via* peptide-functionalized

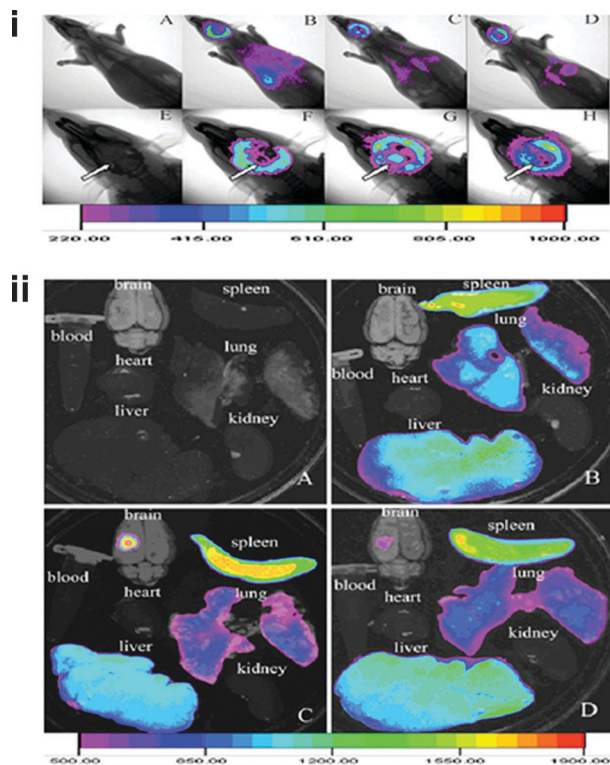


Fig. 56 Distribution of Dir-loaded EGFP-EGF1-NP and EGFP-NP *In vivo*. I. (A) Model rats treated by normal saline (2 ml kg^{-1}); (B) Control rats treated by Dir-loaded EGFP-EGF1-NP (80 mg kg^{-1}); (C) Model rats treated by Dir-loaded EGFP-EGF1-NP (80 mg kg^{-1}); (D) Model rats treated by Dir-loaded EGFP-NP (80 mg kg^{-1}); E, F, G, and H are the close-ups of the head part of figures A, B, C, and D. The white arrows show the regions illuminated by glass-fiber light and the light bar indicates fluorescence intensity, from low intensity (violet) to high intensity (red). II. Organ imaging results corresponding to A, B, C and D in I (reproduced with permission from ref. 254. Copyright 2010, Elsevier).

NPs has been proposed as an alternative strategy to overcome side effects associated with the antibody-mediated thrombolysis.²⁵⁴ Due to the fundamental role of the interaction between coagulation and tissue factors in the formation of intravascular thrombi, the EGF1 domain of the coagulation factor FVIIa was chosen as a targeting ligand due to its specific affinity to the tissue factor. Fusion protein EGF1-EGFP, expressed to achieve both targeting and *in vitro* imaging purposes, was conjugated at the surface of PLA-*b*-PEG NPs. The NIR Dir dye was encapsulated to monitor non-invasively the distribution of EGF1-EGFP-NPs in a model of cerebral thrombosis photochemically induced. Highest fluorescence was observed in the irradiated regions due to the specific interaction between the EGF1 and the expressed tissue factor. Although promising, the real thrombolytic potential *in vivo* still needs to be investigated (Fig. 56).

4.4.4. PEPTIDE-FUNCTIONALIZED NANOCARRIERS FOR INJURED VASCULATURE TARGETING. An interesting work proposed by Farokhzad and coworkers aimed at developing original PLA-based nanocarriers able to target the vessel basement membrane.¹³⁴ These nano-systems might be useful for targeted drug delivery in pathological conditions characterized by injured vasculature,

neo-angiogenesis and increased vascular permeability, such as cardiovascular and oncologic diseases. Heptapeptides specific to collagen IV, the most important component of the basal membrane, were screened by phage display biopanning and the peptide sequence YHWYGYTPQNVI (GE11 peptide) was selected to functionalize the surface of NPs named “nanoburrs”. In this core-shell hybrid lipid-polymer system, Ptx was covalently conjugated to PLA in order to provide a better-controlled sustained release. The affinity of peptide-targeted NPs was evaluated *ex vivo* and *in vivo* in different rat models of injured vasculature. Both intra-arterial and intravenous administration revealed the accumulation of the nanoburrs at the injured sites (Fig. 57). The controlled and prolonged drug release over 12 days observed *in vitro* could explain the obtained *in vivo* pharmacological efficacy.

4.4.5. PEPTIDE-FUNCTIONALIZED NANOCARRIERS FOR ATHEROSCLEROTIC LESION TARGETING. Cardiovascular diseases represent the leading cause of death in developed countries and atherosclerosis is a major contributor of myocardial and cerebral infarction. The formation and evolution of atherosclerotic plaques play pivotal role in the pathogenesis. Catheter-based intravascular ultrasound, CT and MRI imaging system was demonstrated to be effective for the study/analysis of the plaques. However, the recent advances of nanobiotechnology gave the chance for the development of novel specific probes for plaque imaging. A new atherosclerotic lesion-imaging probe was designed by conjugating a plaque homing peptide with chitosan-based nanoparticles.³³⁶ This smart probe demonstrated *in vitro* the ability to recognize activated bovine aortic endothelial cells (BAECs) but most notably showed a higher binding affinity to the atherosclerotic aorta of an *Ldlr*^{-/-} mouse than to the aorta of normal animals (Fig. 58). The reported system, coupled with different classes of contrast agents, could present an interesting tool for the development of an innovative imaging approach for the visualization of atherosclerotic plaques.

4.4.6. PEPTIDE-FUNCTIONALIZED NANOCARRIERS FOR TREATMENT OF HEARING LOSS. Due to the lack of effective therapeutic strategies for the treatment of sensorineural hearing loss, new approaches must be developed to achieve a controlled and targeted delivery of drugs to the inner ear. Tet-1 peptide-functionalized PCL-*b*-PEG polymersomes were proposed by Zhang and coworkers as novel nanocarriers to target the cochlear nerve and the spiral ganglion cells.³²⁶ This peptide was chosen for its capacity to specifically bind the neuronal GT1b receptors. Proof of concept was provided *in vivo* by transtympanic injection or cochleostomy. Only in the latter case, polymersomes accumulated in spiral ganglion cells and neurofilaments. Although no difference between functionalized and bare polymersomes was observed in the ganglion cells, the former showed axonal accumulation. Accumulation in neuronal soma was not detected; however, the specific targeting to axons could be opportunely exploited for controlled delivery of drugs.

4.4.7. MAB-FUNCTIONALIZED NANOCARRIERS FOR INFLAMED ENDOTHELIUM TARGETING. Sites of pathological inflammation are characterized by the overexpression of endothelial cell adhesion

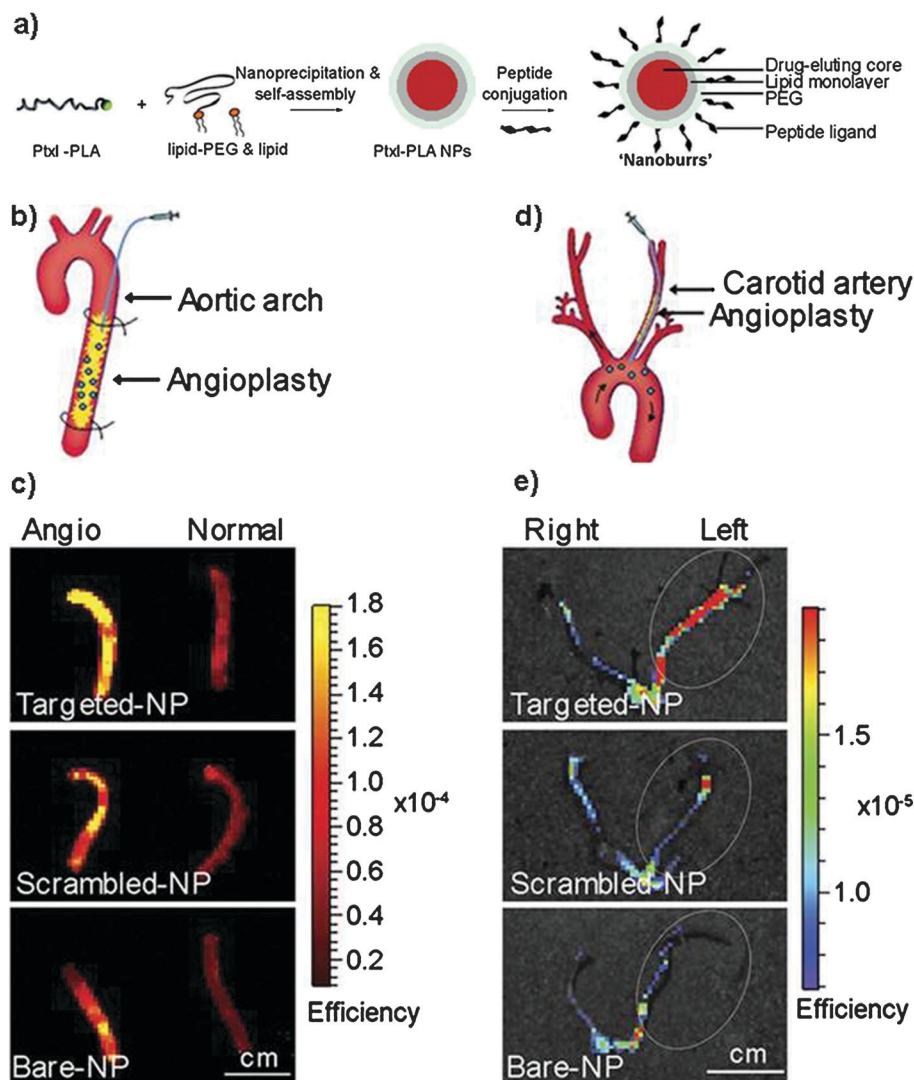


Fig. 57 (a) Schematic representation of nanoburrs synthesis by nanoprecipitation and self-assembly. Ptxl-PLA in acetone was added dropwise to a heated lipid solution, vortexed vigorously, and allowed to self-assemble for 2 h to form NPs. The NPs were peptide-functionalized using maleimide–thiol chemistry. Nanoburrs have a drug-eluting polymeric core, a lipid monolayer, a PEG layer, and peptide ligands to adhere to the exposed basement membrane during vascular injury. (b) *Ex vivo* delivery in an abdominal aorta injury model. Samples were delivered into the aorta segment for 5 min *in situ*. Non-adsorbed samples were flushed out by saline infusion for 15 min. (c) Fluorescence images overlaid on photographs of balloon-injured aortas incubated with nanoburrs, compared with scrambled-peptide and non-targeted NPs. (d) Carotid injury model. A catheter was inserted *via* the external carotid into the common carotid and advanced into the aortic arch. Samples were delivered at 1 mL min⁻¹ for 1 min and allowed to circulate for 1 h before the animals were killed. (e) Fluorescence images overlaid on photographs of carotid arteries incubated with nanoburrs, compared with scrambled-peptide and non-targeted NPs (reproduced with permission from ref. 134. Copyright 2010, PNAS).

molecules (ECAMs), which mediate the recruitment of leukocytes. Taking inspiration from the leukocyte-endothelial cell biochemistry, adhesive PEGylated PLA NPs, able to selectively adhere to the inflamed endothelium, were prepared by using as targeting ligands different Mabs specific to the most expressed ECAMs (*e.g.* E-selectin, P-selectin, vascular cell adhesion molecule 1 and intercellular adhesion molecule 1).²⁸¹ Specific adhesion of functionalized NPs to the inflamed endothelium was observed under *in vitro* flow conditions (that simulate fluid dynamic conditions present *in vivo*), as well as during *in vivo* studies, performed on cytokine or trauma-induced activated endothelium, which demonstrated the possibility to achieve both firm adhesion and rolling as a function of the selected ligand.

4.4.8. MAB-TARGETED NANOCARRIERS FOR IMMUNOMODULATION. Recognition of an antigen causes activation of naïve CD4⁺ T lymphocytes and their differentiation into effector cells (Teff) or regulatory cells (Treg). In this process, the composition of the microenvironment and in particular the type of cytokines plays a key role.⁴⁴⁰ The modulation of T cell development seems to be crucial for the therapy of immune-mediated diseases. In this context, Park and coworkers evaluated the possibility of specific and controlled delivery of the leukemia inhibitory factor (LIF) and IL-6 by their encapsulation in anti-CD4⁺-targeted PLGA NPs.²⁸⁴ *In vitro* preliminary studies revealed the ability of functionalized LIF-loaded NPs to inhibit the IL-6-mediated maturation of the CD4⁺ cells into the aggressive Th17

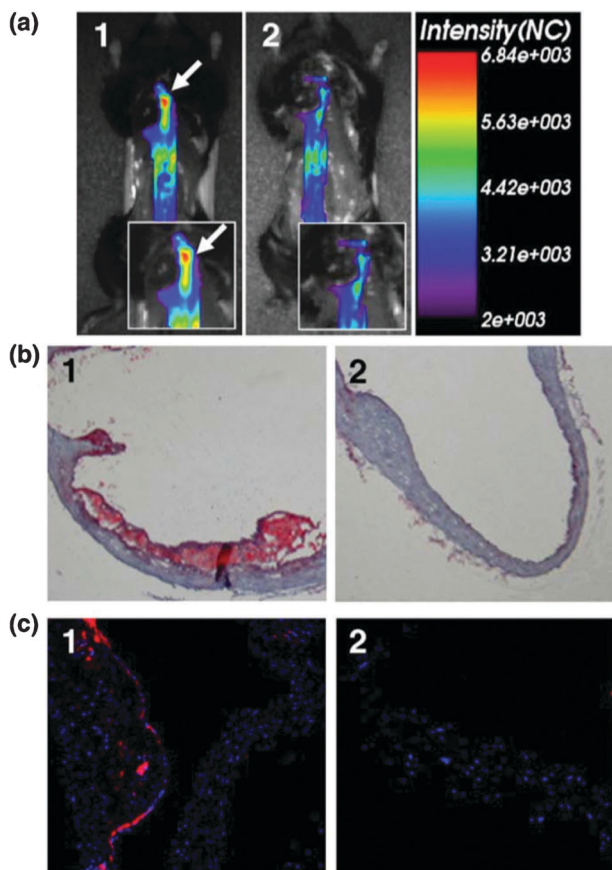


Fig. 58 *In vivo* imaging of atherosclerotic lesion targeting by AP-tagged Chitosan-Cy5.5 nanoparticles. (a) The representative NIR fluorescence image of the exposed aorta in an *Ldlr*^{-/-} mouse (1) and in a normal mouse (2). AP-tagged Chitosan-Cy5.5 nanoparticles (5 mg kg⁻¹) were injected *via* the lateral tail vein. After 6 h, the exposed aortas were imaged using the eXplore Optix system. (b) Oil Red O lipid staining of aortas in an *Ldlr*^{-/-} mouse (1) and in a normal mouse (2). (c) NIR fluorescence microscopy of aortas in an *Ldlr*^{-/-} mouse (1) and in a normal mouse (2) injected with AP-tagged Chitosan-Cy5.5 nanoparticles (reproduced with permission from ref. 336. Copyright 2008, Elsevier).

regulatory phenotype. Moreover, these NPs induced prolonged survival in a mouse model of heart allograft and increased the number of CD4⁺ Foxp3-expressing cells in a non-human primate *in vitro* model. The demonstrated tolerogenic effect might be further explored to achieve the development of cytokine-based therapies.

4.5. Oral drug delivery

4.5.1. WGA-TARGETED NANOCARRIERS FOR IMMUNOMODULATION. Although functionalized drug delivery systems have been mainly conceived for intravenous administration, surface functionalization can be exploited also to increase the bioavailability of drugs after oral administration. Thymopentin (TP5) is a synthetic pentapeptide generally used as an immunomodulating agent in the treatment of autoimmune diseases.^{441,442} However, due to its high water solubility, poor membrane permeability and a $t_{1/2}$ of 30 s, repeated *i.v.* injections are required to reach therapeutic concentrations. Thus, use of WGA-functionalized PLGA NPs was proposed as an alternative

approach for the oral delivery of thymopentin.^{203,204} Due to the capacity of WGA to specifically bind the intestinal mucosa, this ligand offers the possibility to design a promising bioadhesive drug delivery system. The retention of the WGA biorecognitive activity, after covalent conjugation to the PLGA, was assessed *in vitro* by haemagglutination test. *Ex vivo* studies, performed to evaluate the interaction of functionalized NPs with the different structures of the intestine, revealed a significant enhanced adhesion to the intestinal segments with or without Peyer's patches compared to control NPs without WGA conjugation. A significant accumulation in the small intestine, due to the improved bio-adhesion and lectin-induced cellular uptake, was confirmed also by *in vivo* biodistribution analysis. Noteworthy, the enhanced absorption led to a remarkable immunomodulating effect, which was associated to changes of the count of peripheral blood lymphocytes (CD4⁺ and CD8⁺). WGA conjugation clearly improved the oral adsorption of thymopentin and could be therefore exploited to improve uptake and bioavailability of other poorly absorbable drugs such as peptides and proteins. Interestingly, the bioadhesion capacity was only marginally influenced by the WGA density at the surface of the NPs. A minimal WGA amount was required to bind to intestinal mucosa but higher WGA density did not induce a proportional uptake enhancement.

4.5.2. PEPTIDE-TARGETED NANOCARRIERS FOR VACCINE DELIVERY. Oral administration of targeted nanoparticles was also proposed as novel strategy to deliver antigens to the M cells located in the intestinal mucosa and thus enhance the effectiveness of orally delivered vaccines.^{138,323} According to the expression of β 1 integrins on M cells, the GRGDS peptide was used as a targeting ligand to decorate the surface of PCL-based NPs loaded with ovalbumin as model antigen. Immunization experiment was performed on mice and IgG titers were determined 10 weeks after the first oral administration of GRGDS-targeted NPs. Unfortunately, despite the interesting theoretic approach, results were not satisfactory. Indeed, although a slight increase of the number of mice producing IgG after administration of the targeted formulation was observed, the mean concentration of serum IgG was not modified.

An M cell-homing peptide, isolated by phage display was instead conjugated at the surface of chitosan NPs by Yoo and coworkers.¹³⁸ Specific targeting to Peyer's patches region, where the M cells are abundant, was monitored *in vivo* after injection in a closed ideal loop.

4.5.3. VITAMIN B12-FUNCTIONALIZED NANOCARRIERS FOR INSULIN DELIVERY. The oral delivery of peptide/protein drugs still represents a major challenge due to their poor intrinsic permeability across the intestinal epithelium and the rapid degradation in the gastrointestinal tract. Insulin is being used for decades for the treatment of diabetes but the molecule does not immediately reach the liver post-subcutaneous administration. During the last few decades, several delivery mechanisms have been proposed for effective oral delivery of insulin including liposomes and polymeric nanocapsules.⁴⁴³ Although the reported systems provided interesting results, none of these led to a commercially viable product. Chalasani and coworkers

designed a dextran-based nanocarrier system decorated with vitamin B12,³⁷² a molecule with confirmed ability to promote the intestine up-take of pharmaceuticals.⁴⁴⁴ The efficacy of the obtained nanoparticles for the delivery of insulin was tested on a streptozotocin-induced and congenital diabetic mice model (NOD/J). The functionalized carriers demonstrated significant hypoglycemic action for a prolonged period (54 h) with doses (10 and 20 IU kg⁻¹) comparable to those clinically employed as well as an interesting dose-response effect that may offer the flexibility to adjust the doses for different conditions. Interestingly, the insulin delivery was found to be predominantly VB1-mediated, as the co-administration of VB12 in excess significantly reduced the hypoglycemic effect. The reported results demonstrated the efficacy of VB12 as a targeting moiety for intestinal delivery; however, the supremacy of these delivery systems compared to those clinically employed for insulin delivery needs to be proven.

4.6. Pulmonary delivery

Administration of drug-loaded nanocarriers *via* the pulmonary route represents an alternative to the parenteral one due to the high bioavailability of nanoparticulate systems in the lungs, their high retention *in situ* and their low capture by alveolar macrophages, providing their diameter is around 250 nm.⁴⁴⁵ Interesting results have been obtained after aerosol administration of EGF-functionalized gelatin NPs^{398–400} in an animal model of pulmonary metastasis induced by *i.v.* injection of A549 cells (Fig. 59).

Conjugation of FITC at the NPs surface enabled us to follow their biodistribution and to clearly demonstrate their capacity

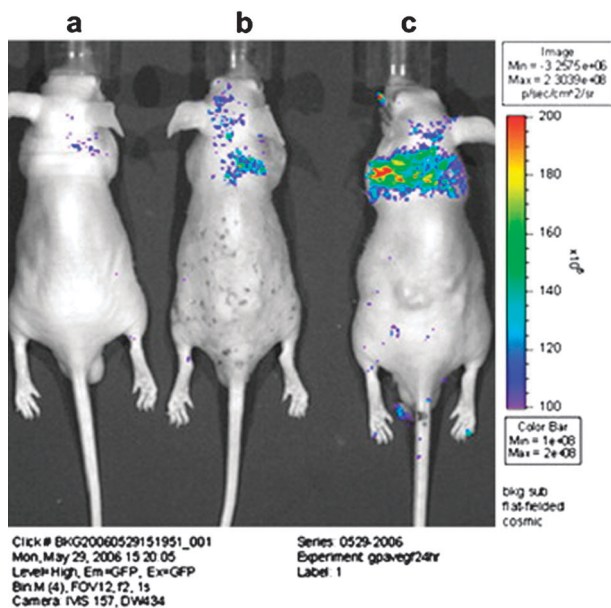


Fig. 59 The *in vivo* fluorescence images of tumor-induced mice following aerosol delivery 24 h later by treatment with different nanoparticles' solution: PBS-treated group (a), GP-AV-treated group (b), and GP-AV-bEGF conjugate-treated group (c). FITC green fluorescence spectra were obtained from live mice xenografted with the human lung adenocarcinoma cells (A549) (reproduced with permission from ref. 399. Copyright 2008, Elsevier).

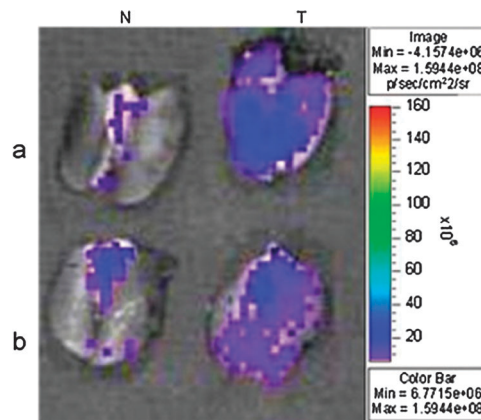


Fig. 60 Fluorescent image of lungs. The sites of color spot on the tissue were initiated by green fluorescence from FITC on the gelatin nanoparticles (GP-AV-bEGF). The cancerous lung had much higher fluorescent spots on it: (a) the result of 0.5 h after inhalation and (b) the image obtained 24 h later. (N: normal SCID mice; T: tumor inoculation by A549 cells in SCID mice) (reproduced with permission from ref. 398. Copyright 2007, Elsevier).

of specific targeting and accumulation in the lungs (Fig. 60).³⁹⁸ Therapeutic potential of *CisPt*-loaded EGF-functionalized NPs was evaluated after aerosol administration using the same tumor model. This treatment showed that inhaled nanoparticles could target EGFR-overexpressing cells to achieve high *CisPt* dosage in cancerous lungs.⁴⁰⁰ Furthermore, *CisPt*-loaded EGF-functionalized NPs were given through intra-tumoral injections to SCID mice in a subcutaneous model. This treatment showed a stronger anti-tumor activity and was less toxic than free *CisPt*. Indeed, NPs-treated mice showed slight body weight loss, whereas free drug treatment at the same dose caused a body weight loss of 20–30%.⁴⁰⁰

4.7. Clinical applications of targeted-nanocarriers

Despite the numerous promising results described previously, translations of designed targeted-nanocarriers from preclinical *in vivo* results to the clinical practice are rather scarce. Nevertheless, a successful example of clinical application of targeted nanoparticles has been recently reported by Langer, Farokzhad and coworkers.¹⁸⁸ Firstly, a systematic investigative physico-chemical study conducted to an optimized formulation of Dtx-loaded biodegradable PLA-*b*-PEG/PLGA-*b*-PEG NPs targeted towards PSMA *via* the use of the ACUPA molecule as a homing device. Then, pharmacokinetics, biodistribution and tolerability studies were investigated in multiple animal species, and several xenograft tumor models were used to evaluate their therapeutic potential. The promising results obtained in pre-clinical studies allowed starting a phase I human clinical trial in which patients with advanced or metastatic cancers were treated every three weeks with Dtx-loaded ACUPA-functionalized NPs administered by intravenous infusion. The preliminary data were highly promising and showed pharmacokinetic profiles similar to those observed during the preclinical trials and, in some patients, a reduction of tumor volume at doses of Dtx lower than those conventionally used in clinical therapeutic protocols.

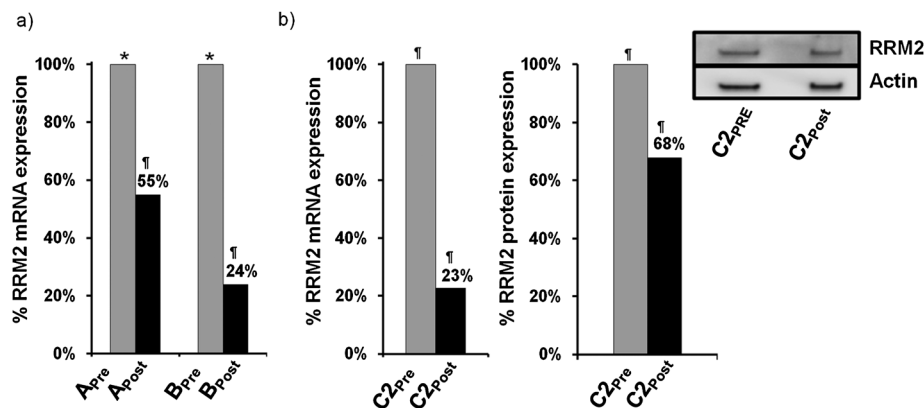


Fig. 61 RRM2 mRNA and protein expression in tumor tissue. (a) qRT-PCR analysis of RRM2 mRNA levels in samples from patients A and B before and after dosing. RRM2 mRNA levels are normalized to TATA box binding protein (TBP) mRNA levels. Results are presented as the percentage of the pre-dosing RRM2/TBP mRNA levels for each patient. (b) qRT-PCR and western blot analysis of RRM2 protein expression from patient samples C2pre and C2post. The bar graph shows the average volume of western blot bands from two independent experiments; one representative blot is pictured. Asterisk denotes archived samples; dagger symbol denotes samples obtained during the trial (reproduced with permission from ref. 362. Copyright (2010) Nature Publishing Group).

Recent advances have also been witnessed in the field of gene therapy using siRNA. Several clinical trials are now ongoing using siRNA for the treatment of severe diseases.⁴⁴⁶ An attractive concept was proposed by the group of Davis for the use TF-decorated CDs nanoparticles as siRNA tumor-specific carrier (CALAA-01). After positive outcomes in wide preclinical studies, the authors moved to human evaluations (Clinical trial NCT00689065, Calando Pharmaceuticals). In patients with metastatic melanoma, refractory to standard therapies were administered with targeted nanoparticles (18, 24 or 30 mg m⁻² siRNA) on days 1, 3, 8 and 10 in a 21-day cycle by a 30 min intravenous infusion. Tumor biopsies from post-treatment melanoma showed the presence of intracellularly localized NPs in amounts that correlated with doses of the administered nanocarriers. Most notably, a reduction was found in both the specific messenger RNA (M2 subunit of ribonucleotide reductase (RRM2)) and the protein (RRM2) levels when compared to pre-dosing tissues (Fig. 61).³⁶² A short Phase Ib study started in August 2011 was undertaken to find whether the therapeutic window of CALAA-01 could be further increased simply by changing the dosing schedule. In addition, these results demonstrated the feasibility of using both RNAi-based therapeutics and targeted NPs, and opened the door for future breakthrough therapeutics that could fight cancer and other diseases at the genetic level.

5. Concluding remarks

Due to the high flexibility offered by macromolecular synthesis methods, the almost infinite diversity of polymers in terms of nature, properties and composition, and their ease of functionalization, a broad range of functionalized nanoparticulate systems have been witnessed over the past decades. Complex macromolecular architectures and efficient coupling methods conjugated to the discovery of various biologically active ligands gave access to a wide collection of targeted systems. Their successful applications in many different pathologies (although cancer was the most representative) confirmed their

high potential and hold great promise concerning the development of future nanomedicines.

However, despite the wide enthusiasm associated with the presentation of every new and always more sophisticated targeted nanocarrier, much work still needs to be done before functionalized nanoparticulate systems could be effectively introduced into the medical practice. This can be mainly explained by several obstacles encountered before clinical trials are foreseen: (i) the difficulty to perform efficient scale-up of the nanocarrier formulation while maintaining all the parameters that would govern its *in vivo* fate and its therapeutic efficiency (*e.g.*, purity of the compounds and building blocks, colloidal stability, drug loading, ligand spatial organization, biological activity) and (ii) the commonly employed murine models that perhaps do not perfectly reflect the pathological conditions in humans. Consequently, an urgent need to tackle these problems would be to develop both some more robust and reproducible, scalable preparation methodologies to readily fulfill the need of clinical trials and some animal models that would give more reliable results closer to the clinic. Furthermore, as well demonstrated by Langer, Farokzhad and coworkers,¹⁸⁸ the assessment of the efficacy of functionalized nanocarriers in patients requires that safety, biodistribution and pharmacokinetic/pharmacodynamic parameters must be investigated in multiple animal species. The cost of such experimental protocols could represent a limit for translation of the laboratory-based nanotechnologies to clinical trials.

Abbreviations

6-HODA	6 Hydroxy dopamine
ACUPA	<i>S,S</i> -2-[5-Amino-1-carboxypentyl]-ureido]-pentanedioic acid
ACVA	4,4'-Azobis (4-cyanovaleric acid)
AD	Alzheimer's disease
ADR	Adriamycin
AEM	<i>N</i> -(2-Aminoethyl) maleimide

AMT	Adsorptive mediated transcytosis	MBS	<i>m</i> -Maleimidobenzoyl- <i>N</i> -hydroxysuccinimide ester
Asp	Aspartic acid	MCL	4-Maleate- ϵ -caprolactone
ATRP	Atom transfer radical polymerization	MDR	Multidrug resistance
Av	Avidin	MMC	Mitomycin C
BMP-2	Bone morphogenetic protein-2	MPBH	4-(4- <i>N</i> -maleimidophenyl)butyric acid hydrazid-HCl
BSA	Bovine serum albumin	MTX	Methotrexate
CD	Cyclodextrins	nAChR	Nicotine acetylcholine receptors
CDI	<i>N,N'</i> -carbonyldiimidazole	NAv	Neutravidin
CE	Capillary electrophoresis	NHS	<i>N</i> -Hydroxysuccinimide
CEA	Carcinoembryonic antigen	NP	Nanoparticle
<i>CisPt</i>	<i>Cis</i> platin	NSCL cancer	Non small cells lung cancer
CNS	Central nervous system	OD	Odorranalectin
CPADB	(4-Cyanopentanoic acid) dithiobenzoate	Oli-A	Oligomycin-A
CPP	Cell penetrating peptide	OMCCA	Octadecyl-4-(maleimido methyl) cyclohexane-carboxylic acid
CPK	Creatine phosphokinase	OQLCS	Octadecyl-quaternised lysine modified chitosan
CPT	Camptothecin	P(His- <i>co</i> -Phe)	Poly(l-histidine- <i>co</i> -phenylalanine)
DC	Dendritic cells	PAE	Poly β (amino-ester)
DCC	<i>N,N'</i> -Dicyclohexylcarbodiimide	PAsp	Poly(aspartic acid)
DiR	1,1'-Dioctadecyl-3,3,3',3'-tetramethyl indotricarbocyanine iodide	PBLA	Poly(benzyl-l-aspartic acid)
DMBA	7,12-Dimethylbenz[<i>a</i>]anthracene	PBLG	Poly(benzyl-l-glutamate)
DNA	Deoxyribonucleic acid	PCB	Poly(L-cysteinenisamide)
Dox	Doxorubicin	PCBS	Poly(L-cysteinebisamide- <i>g</i> -sulfadiazine)
DSS	Disuccinimidyl subernate	PCL	Poly(ϵ -caprolactone)
Dtx	Docetaxel	Pcpl	Paclitaxel palmitate
ϵ Cl	ϵ -Caprolactone	PD	Pharmacodistribution
EDC	1-Ethyl-3-(3-dimethylaminopropyl) carbodiimide hydrochloride	pDNA	Plasmid deoxyribonucleic acid
EGF	Epidermal growth factor	PED	Polyester dendron
EGFR	Epidermal growth factor receptor	PEEP	Poly(ethyl ethylene phosphate)
ELPbc	Elastin-like polypeptide diblock copolymer	PEG	Poly(ethylene glycol)
EMA	Ethyl methacrylate	PEGCA	Poly(ethylene glycol cyanoacrylate)
EMCS	<i>N</i> - ϵ -Maleimidocaproyl-oxysuccinimide ester	PEI	Polyethyleneimine
ENX	Enoxacin	PG	Propargylglycine
FA	Folic acid	PHDCA	Poly(hexadecyl cyanoacrylate)
FACS	Fluorescence-activated cell sorting	PHis	Polyhistidine
FBP	Folate-binding protein	PK	Pharmacokinetics
FTSC	Fluorescein-5-thiosemicarbazide	PLA	Poly lactide
GBM	Glioblastoma	PLGA	Poly(lactide- <i>co</i> -glycolide)
Gem	Gemcitabine	PLL	Poly-L-lysine
<i>H. pylori</i> .	<i>Helicobacter pylori</i>	PMPI	<i>p</i> -Maleimidophenylisocyanate
H40	Hyperbranched polyester Boltorn H40	PSD	Poly(methacryloyl sulfadimethoxine)
HA	Hyaluronan	PSMA	Prostate specific membrane antigen
HER2	Human epidermal growth factor receptor 2	PTD	Protein transduction domain
HPAE	Hyperbranched poly(amino-ester)	Ptx	Paclitaxel
HSA	Human serum albumine	QC	Quinacrine
I.p.	Intraperitoneal	ROP	Ring-opening polymerization
I.v.	Intravenous	SAv	Streptavidin
ICAM-1	Intercellular cell-adhesion molecule-1	SCK	Shell cross linked
ICR	Imprinting control region	SeI	Selegiline
LDH	Lactate dehydrogenase	SiRNA	Small interfering RNA
Lf	Lactoferrin	SPDP	<i>N</i> -succinimidyl-3-(2-pyridyldithio) propionate
LRP	Low-density lipoprotein receptor-related protein	SPR	Surface plasmon resonance
MAB	Monoclonal antibody	Sulfo-MBS	<i>m</i> -Maleimidobenzoyl- <i>N</i> -hydroxysulfosuccinimide ester
Mal	Maleimide	SMCC	Succinimidyl-4-(<i>N</i> -maleimidomethyl)cyclohexane-1-carboxylate
MAO-B	Monoamine oxidase-B		

Sulfo-SMCC	Sulfosuccinimidyl-4-(<i>N</i> -maleimidomethyl)cyclohexane-1-carboxylate	27 N. Kamaly, Z. Xiao, P. M. Valencia, A. F. Radovic-Moreno and O. C. Farokhzad, <i>Chem. Soc. Rev.</i> , 2012, 41 , 2971.
TAT	<i>Trans</i> activating transcription factor	28 D.-E. Lee, H. Koo, I.-C. Sun, J. H. Ryu, K. Kim and I. C. Kwon, <i>Chem. Soc. Rev.</i> , 2012, 41 , 2656.
TCEP	Tris(2-carboxyethyl)phosphine	29 W. T. Al-Jamal and K. Kostarelos, <i>Acc. Chem. Res.</i> , 2011, 44 , 1094.
TCHD	<i>Trans</i> cyclohexane-1,2-diol	30 R. H. Muller and C. M. Keck, <i>J. Biotechnol.</i> , 2004, 113 , 151.
Tf	Transferrin	31 D. Peer, J. M. Karp, S. Hong, O. C. Farokhzad, R. Margalit and R. Langer, <i>Nat. Nanotechnol.</i> , 2007, 2 , 751.
TFA	Trifluoro acetic acid	32 M. L. Adams, A. Lavasanifar and G. S. Kwon, <i>J. Pharm. Sci.</i> , 2003, 92 , 1343.
TGPS	<i>D</i> - α -Tocopheryl polyethylene glycol succinate	33 C. Oerlemans, W. Bult, M. Bos, G. Storm, J. Nijsen and W. Hennink, <i>Pharm. Res.</i> , 2010, 27 , 2569.
ThT	Thioflavin-T assay	34 V. Torchilin, <i>Pharm. Res.</i> , 2007, 24 , 1.
TLT	Transplantable liver tumor model	35 U. Kedar, P. Phutane, S. Shidhaye and V. Kadam, <i>Nanomedicine</i> , 2010, 6 , 714.
TMC	Trimethylated chitosan	36 H. Hillaireau and P. Couvreur, in <i>Polymers in Drug Delivery</i> , ed. I. F. Uchegbu and A. G. Schätzlein, Taylor & Francis, New York, 2006, pp. 101.
ToF-SIMMS	Time-of-flight secondary ion mass spectrometry	37 K. Letchford and H. Burt, <i>Eur. J. Pharm. Biopharm.</i> , 2007, 65 , 259.
UEA-I	<i>Ulex europaeus</i> agglutinin I	38 J. Liu, Y. Xiao and C. Allen, <i>J. Pharm. Sci.</i> , 2004, 93 , 132.
VEGF	Vascular endothelium growth factor	39 C. LoPresti, H. Lomas, M. Massignani, T. Smart and G. Battaglia, <i>J. Mater. Chem.</i> , 2009, 19 , 3576.
WGA	Wheat germ agglutinin	40 B. M. Discher, Y.-Y. Won, D. S. Ege, J. C.-M. Lee, F. S. Bates, D. E. Discher and D. A. Hammer, <i>Science</i> , 1999, 284 , 1143.
XPS	X-ray photoelectron spectroscopy	41 K. Kita-Tokarczyk, J. Grumelard, T. Haefele and W. Meier, <i>Polymer</i> , 2005, 46 , 3540.

Acknowledgements

The authors acknowledge the financial support of CNRS and the French Ministry of Research.

References

- O. C. Farokhzad and R. Langer, *ACS Nano*, 2009, **3**, 16.
- D. Brambilla, B. Le Droumaguet, J. Nicolas, S. H. Hashemi, L.-P. Wu, S. M. Moghimi, P. Couvreur and K. Andrieux, *Nanomedicine*, 2011, **7**, 521.
- I. Brigger, C. Dubernet and P. Couvreur, *Adv. Drug Delivery Rev.*, 2002, **54**, 631.
- W. R. Sanhai, J. H. Sakamoto, R. Canady and M. Ferrari, *Nat. Nanotechnol.*, 2008, **3**, 242.
- S. E. Erb, *Drug Delivery Syst.*, 2009, **24**, 63.
- K. Riehemann, S. W. Schneider, T. A. Luger, B. Godin, M. Ferrari and H. Fuchs, *Angew. Chem., Int. Ed.*, 2009, **48**, 872.
- M. L. Hans and A. M. Lowman, *Curr. Opin. Solid State Mater. Sci.*, 2002, **6**, 319.
- J. Panyam and V. Labhasetwar, *Adv. Drug Delivery Rev.*, 2003, **55**, 329.
- L. Brannon-Peppas, *Int. J. Pharm.*, 1995, **116**, 1.
- R. Sinha, G. J. Kim, S. Nie and D. M. Shin, *Mol. Cancer Ther.*, 2006, **5**, 1909.
- H. Cabral, N. Nishiyama and K. Kataoka, *Acc. Chem. Res.*, 2011, **44**, 999.
- K. S. Soppimath, T. M. Aminabhavi, A. R. Kulkarni and W. E. Rudzinski, *J. Controlled Release*, 2001, **70**, 1.
- P. Couvreur and C. Vauthier, *Pharm. Res.*, 2006, **23**, 1417.
- G. B. Sukhorukov, A. L. Rogach, B. Zebli, T. Liedl, A. G. Skirtach, K. Köhler, A. A. Antipov, N. Gaponik, A. S. Sussha, M. Winterhalter and W. J. Parak, *Small*, 2005, **1**, 194.
- F. Zhang, E. Lees, F. Amin, P. Rivera_Gil, F. Yang, P. Mulvaney and W. J. Parak, *Small*, 2011, **7**, 3113.
- S. Laurent, D. Forge, M. Port, A. Roch, C. Robic, L. Vander Elst and R. N. Muller, *Chem. Rev.*, 2008, **108**, 2064.
- S. S. Kelkar and T. M. Reineke, *Bioconjugate Chem.*, 2011, **22**, 1879.
- R. Mout, D. F. Moyano, S. Rana and V. M. Rotello, *Chem. Soc. Rev.*, 2012, **41**, 2539.
- K. Miyata, N. Nishiyama and K. Kataoka, *Chem. Soc. Rev.*, 2012, **41**, 2562.
- N. Lee and T. Hyeon, *Chem. Soc. Rev.*, 2012, **41**, 2575.
- M. Perfezou, A. Turner and A. Merkoci, *Chem. Soc. Rev.*, 2012, **41**, 2606.
- J. L. Vivero-Escoto, R. C. Huxford-Phillips and W. Lin, *Chem. Soc. Rev.*, 2012, **41**, 2673.
- E. C. Dreaden, A. M. Alkilany, X. Huang, C. J. Murphy and M. A. El-Sayed, *Chem. Soc. Rev.*, 2012, **41**, 2740.
- J. Khandare, M. Calderon, N. M. Dagia and R. Haag, *Chem. Soc. Rev.*, 2012, **41**, 2824.
- M. Elsabahy and K. L. Wooley, *Chem. Soc. Rev.*, 2012, **41**, 2545.
- S. Mizrahy and D. Peer, *Chem. Soc. Rev.*, 2012, **41**, 2623.
- N. Kamaly, Z. Xiao, P. M. Valencia, A. F. Radovic-Moreno and O. C. Farokhzad, *Chem. Soc. Rev.*, 2012, **41**, 2971.
- D.-E. Lee, H. Koo, I.-C. Sun, J. H. Ryu, K. Kim and I. C. Kwon, *Chem. Soc. Rev.*, 2012, **41**, 2656.
- W. T. Al-Jamal and K. Kostarelos, *Acc. Chem. Res.*, 2011, **44**, 1094.
- R. H. Muller and C. M. Keck, *J. Biotechnol.*, 2004, **113**, 151.
- D. Peer, J. M. Karp, S. Hong, O. C. Farokhzad, R. Margalit and R. Langer, *Nat. Nanotechnol.*, 2007, **2**, 751.
- M. L. Adams, A. Lavasanifar and G. S. Kwon, *J. Pharm. Sci.*, 2003, **92**, 1343.
- C. Oerlemans, W. Bult, M. Bos, G. Storm, J. Nijsen and W. Hennink, *Pharm. Res.*, 2010, **27**, 2569.
- V. Torchilin, *Pharm. Res.*, 2007, **24**, 1.
- U. Kedar, P. Phutane, S. Shidhaye and V. Kadam, *Nanomedicine*, 2010, **6**, 714.
- H. Hillaireau and P. Couvreur, in *Polymers in Drug Delivery*, ed. I. F. Uchegbu and A. G. Schätzlein, Taylor & Francis, New York, 2006, pp. 101.
- K. Letchford and H. Burt, *Eur. J. Pharm. Biopharm.*, 2007, **65**, 259.
- J. Liu, Y. Xiao and C. Allen, *J. Pharm. Sci.*, 2004, **93**, 132.
- C. LoPresti, H. Lomas, M. Massignani, T. Smart and G. Battaglia, *J. Mater. Chem.*, 2009, **19**, 3576.
- B. M. Discher, Y.-Y. Won, D. S. Ege, J. C.-M. Lee, F. S. Bates, D. E. Discher and D. A. Hammer, *Science*, 1999, **284**, 1143.
- K. Kita-Tokarczyk, J. Grumelard, T. Haefele and W. Meier, *Polymer*, 2005, **46**, 3540.
- G. Battaglia and A. J. Ryan, *J. Am. Chem. Soc.*, 2005, **127**, 8757.
- T. P. Lodge, B. Pudil and K. J. Hanley, *Macromolecules*, 2002, **35**, 4707.
- R. Gurny, N. A. Peppas, D. D. Harrington and G. S. Banker, *Drug Dev. Ind. Pharm.*, 1981, **7**, 1.
- A. Sanchez, J. L. Vila-Jato and M. J. Alonso, *Int. J. Pharm.*, 1993, **99**, 263.
- J.-P. Plard and D. Bazile, *Colloids Surf., B*, 1999, **16**, 173.
- J.-C. Leroux, E. Allémann, F. De Jaeghere, E. Doelker and R. Gurny, *J. Controlled Release*, 1996, **39**, 339.
- H. Fessi, F. Puisieux, J. P. Devissaguet, N. Ammoury and S. Benita, *Int. J. Pharm.*, 1989, **55**, R1.
- S. Stainmesse, H. Fessi, J. P. Devissaguet, F. Puisieux and C. Theis, *US*, 1989-374246, 1992, p. 8.
- O. Thioune, H. Fessi, J. P. Devissaguet and F. Puisieux, *Int. J. Pharm.*, 1997, **146**, 233.
- J.-W. Nah, Y.-W. Paek, Y.-I. Jeong, D.-W. Kim, C.-S. Cho, S.-H. Kim and M.-Y. Kim, *Arch. Pharmacol. Res.*, 1998, **21**, 418.
- P. Calvo, C. Remuñán-López, J. L. Vila-Jato and M. J. Alonso, *J. Appl. Polym. Sci.*, 1997, **63**, 125.
- Z. L. Tyrrell, Y. Shen and M. Radosz, *Prog. Polym. Sci.*, 2010, **35**, 1128.
- M. Yokoyama, P. Opanasopit, T. Okano, K. Kawano and Y. Maitani, *J. Drug Targeting*, 2004, **12**, 373.
- S. Elhasi, R. Astaneh and A. Lavasanifar, *Eur. J. Pharm. Biopharm.*, 2007, **65**, 406.
- C. E. Mora-Huertas, H. Fessi and A. Elaissari, *Int. J. Pharm.*, 2010, **385**, 113.
- J. J. Marty, R. C. Oppenheim and P. Speiser, *Pharm. Acta Helv.*, 1978, **53**, 17.
- K. Langer, S. Balthasar, V. Vogel, N. Dinauer, H. von Briesen and D. Schubert, *Int. J. Pharm.*, 2003, **257**, 169.
- C. Weber, C. Coester, J. Kreuter and K. Langer, *Int. J. Pharm.*, 2000, **194**, 91.
- K. Strebhardt and A. Ullrich, *Nat. Rev. Cancer*, 2008, **8**, 473.
- J. Shi, Z. Xiao, N. Kamaly and O. C. Farokhzad, *Acc. Chem. Res.*, 2011, **44**, 1123.
- M. R. Dreher, W. Liu, C. R. Michelich, M. W. Dewhirst, F. Yuan and A. Chilkoti, *J. Natl. Cancer Inst.*, 2006, **98**, 335.
- H. Maeda, J. Wu, T. Sawa, Y. Matsumura and K. Hori, *J. Controlled Release*, 2000, **65**, 271.
- A. K. Iyer, G. Khaled, J. Fang and H. Maeda, *Drug Discovery Today*, 2006, **11**, 812.
- K. Greish, *J. Drug Targeting*, 2007, **15**, 457.
- A. Gabizon, R. Catane, B. Uziely, B. Kaufman, T. Safra, R. Cohen, F. Martin, A. Huang and Y. Barenholz, *Cancer Res.*, 1994, **54**, 987.
- T.-Y. Kim, D.-W. Kim, J.-Y. Chung, S. G. Shin, S.-C. Kim, D. S. Heo, N. K. Kim and Y.-J. Bang, *Clin. Cancer Res.*, 2004, **10**, 3708.

- 68 T. Ishida and H. Kiwada, *Int. J. Pharm.*, 2008, **354**, 56.
- 69 E. Gullotti and Y. Yeo, *Mol. Pharmaceutics*, 2009, **6**, 1041.
- 70 F. Zeng, H. Lee and C. Allen, *Bioconjugate Chem.*, 2006, **17**, 399.
- 71 M. E. Gindy, S. Ji, T. R. Hoye, A. Z. Panagiotopoulos and R. K. Prud'homme, *Biomacromolecules*, 2008, **9**, 2705.
- 72 E. Jule, Y. Nagasaki and K. Kataoka, *Bioconjugate Chem.*, 2003, **14**, 177.
- 73 Y. B. Patil, U. S. Toti, A. Khair, L. Ma and J. Panyam, *Biomaterials*, 2009, **30**, 859.
- 74 D. Sutton, N. Nasongkla, E. Blanco and J. Gao, *Pharm. Res.*, 2007, **24**, 1029.
- 75 C. Zhan, B. Gu, C. Xie, J. Li, Y. Liu and W. Lu, *J. Controlled Release*, 2010, **143**, 136.
- 76 P. S. Low, W. A. Henne and D. D. Doorneweerd, *Acc. Chem. Res.*, 2008, **41**, 120.
- 77 Y. Lu, E. Segal, C. P. Leamon and P. S. Low, *Adv. Drug Delivery Rev.*, 2004, **56**, 1161.
- 78 G. Russell-Jones, K. McTavish, J. McEwan, J. Rice and D. Nowotnik, *J. Inorg. Biochem.*, 2004, **98**, 1625.
- 79 D. Goren, A. T. Horowitz, D. Tzemach, M. Tarshish, S. Zalipsky and A. Gabizon, *Clin. Cancer Res.*, 2000, **6**, 1949.
- 80 J. F. Ross, P. K. Chaudhuri and M. Ratnam, *Cancer*, 1994, **73**, 2432.
- 81 W. Yang, Y. Cheng, T. Xu, X. Wang and L. P. Wen, *Eur. J. Med. Chem.*, 2009, **44**, 862.
- 82 G. J. Russell-Jones, S. W. Westwood and A. D. Habberfield, *Bioconjugate Chem.*, 1995, **6**, 459.
- 83 G. J. Kelloff, J. A. Crowell, E. T. Hawk, V. E. Steele, R. A. Lubet, C. W. Boone, J. M. Covey, L. A. Doody, G. S. Omenn, P. Greenwald, W. K. Hong, D. R. Parkinson, D. Bagheri, G. T. Baxter, M. Blunden, M. K. Doeltz, K. M. Eisenhauer, K. Johnson, G. G. Knapp, D. G. Longfellow, W. F. Malone, S. G. Nayfield, H. E. Seifried, L. M. Swall and C. C. Sigman, *J. Cell. Biochem.*, 1996, **63**, 54.
- 84 Y. Porat, A. Abramowitz and E. Gazit, *Chem. Biol. Drug Des.*, 2006, **67**, 27.
- 85 K. Ono, K. Hasegawa, H. Naiki and M. Yamada, *J. Neurosci. Res.*, 2004, **75**, 742.
- 86 F. Yang, G. P. Lim, A. N. Begum, O. J. Ubeda, M. R. Simmons, S. S. Ambegaokar, P. P. Chen, R. Kaye, C. G. Glabe, S. A. Frautschy and G. M. Cole, *J. Biol. Chem.*, 2005, **280**, 5892.
- 87 J. Tetrad and J. Langston, *Science*, 1989, **245**, 519.
- 88 M. Sano, C. Ernesto, R. G. Thomas, M. R. Klauber, K. Schafer, M. Grundman, P. Woodbury, J. Growdon, C. W. Cotman, E. Pfeiffer, L. S. Schneider and L. J. Thal, *N. Engl. J. Med.*, 1997, **336**, 1216.
- 89 C. Ehrhardt, C. Kneuer and U. Bakowsky, *Adv. Drug Delivery Rev.*, 2004, **56**, 527.
- 90 E. E. Simanek, G. J. McGarvey, J. A. Jablonowski and C. H. Wong, *Chem. Rev.*, 1998, **98**, 833.
- 91 H. Fleisch, *Metab. Bone Dis. Relat. Res.*, 1981, **3**, 279.
- 92 T. M. Allen, *Nat. Rev. Cancer*, 2002, **2**, 750.
- 93 A. A. Reinke and J. E. Gestwicki, *Chem. Biol. Drug Des.*, 2007, **70**, 206.
- 94 M. Goto, H. Yura, C.-W. Chang, A. Kobayashi, T. Shinoda, A. Maeda, S. Kojima, K. Kobayashi and T. Akaike, *J. Controlled Release*, 1994, **28**, 223.
- 95 J. H. Han, Y. K. Oh, D. S. Kim and C. K. Kim, *Int. J. Pharm.*, 1999, **188**, 39.
- 96 Y.-I. Jeong, S.-J. Seo, I.-K. Park, H.-C. Lee, I.-C. Kang, T. Akaike and C.-S. Cho, *Int. J. Pharm.*, 2005, **296**, 151.
- 97 R. A. Dwek, *Chem. Rev.*, 1996, **96**, 683.
- 98 T. Keeler, V. Ramakrishna and M. W. Fanger, *Expert Opin. Biol. Ther.*, 2004, **4**, 1953.
- 99 K. L. White, T. Rades, R. H. Furneaux, P. C. Tyler and S. Hook, *J. Pharm. Pharmacol.*, 2006, **58**, 729.
- 100 E. A. Turley, P. W. Noble and L. Y. Bourguignon, *J. Biol. Chem.*, 2002, **277**, 4589.
- 101 R. E. Eliaz and F. C. Szoka, *Cancer Res.*, 2001, **61**, 2592.
- 102 M. G. Ismail, C. Stanca, H. R. Ha, E. L. Renner, P. J. Meier and G. A. Kullak-Ublick, *Hepatol. Res.*, 2003, **26**, 343.
- 103 Z. H. Wang, Z. Y. Wang, C. S. Sun, C. Y. Wang, T. Y. Jiang and S. L. Wang, *Biomaterials*, 2010, **31**, 908.
- 104 S. Kelm, R. Brossmer, R. Isecke, H. J. Gross, K. Strenge and R. Schauer, *Eur. J. Biochem.*, 1998, **255**, 663.
- 105 C. Lemarchand, R. Gref, C. Passirani, E. Garcion, B. Petri, R. Müller, D. Costantini and P. Couvreur, *Biomaterials*, 2006, **27**, 108.
- 106 R. C. Ladner, A. K. Sato, J. Gorzelany and M. de Souza, *Drug Discovery Today*, 2004, **9**, 525.
- 107 H. Koo, M. S. Huh, I.-C. Sun, S. H. Yuk, K. Choi, K. Kim and I. C. Kwon, *Acc. Chem. Res.*, 2011, **44**, 1018.
- 108 M. de Jong, W. A. P. Breeman, D. J. Kwekkeboom, R. Valkema and E. P. Krenning, *Acc. Chem. Res.*, 2009, **42**, 873.
- 109 M. A. Clark, B. H. Hirst and M. A. Jepson, *Adv. Drug Delivery Rev.*, 2000, **43**, 207.
- 110 Y. Nagata and M. M. Burger, *J. Biol. Chem.*, 1974, **249**, 3116.
- 111 J. Li, H. Wu, J. Hong, X. Xu, H. Yang, B. Wu, Y. Wang, J. Zhu, R. Lai, X. Jiang, D. Lin, M. C. Prescott and H. H. Rees, *PLoS One*, 2008, **3**, e2381.
- 112 I. Damjanov, *Lab. Invest.*, 1987, **57**, 5.
- 113 C. Bies, C. M. Lehr and J. F. Woodley, *Adv. Drug Delivery Rev.*, 2004, **56**, 425.
- 114 A. E. Clausen, C. E. Kast and A. Bernkop-Schnurch, *Pharm. Res.*, 2002, **19**, 602.
- 115 E. Ruoslahti, *Annu. Rev. Cell Dev. Biol.*, 1996, **12**, 697.
- 116 C. C. Kumar, *Curr. Drug Targets*, 2003, **4**, 123.
- 117 P. C. Brooks, R. A. Clark and D. A. Cheresch, *Science*, 1994, **264**, 569.
- 118 R. Haubner, R. Gratas, B. Diefenbach, S. L. Goodman, A. Jonczyk and H. Kessler, *J. Am. Chem. Soc.*, 1996, **118**, 7461.
- 119 R. Haubner, W. Schmitt, G. Hoelzemann, S. L. Goodman, A. Jonczyk and H. Kessler, *J. Am. Chem. Soc.*, 1996, **118**, 7881.
- 120 L. Hetian, A. Ping, S. Shumei, L. Xiaoying, H. Luowen, W. Jian, M. Lin, L. Meisheng, Y. Junshan and S. Chengchao, *J. Biol. Chem.*, 2002, **277**, 43137.
- 121 K. M. Stewart, K. L. Horton and S. O. Kelley, *Org. Biomol. Chem.*, 2008, **6**, 2242.
- 122 K. S. Rao and V. Labhasetwar, *J. Biomed. Nanotechnol.*, 2006, **2**, 173.
- 123 V. P. Torchilin, *Adv. Drug Delivery Rev.*, 2008, **60**, 548.
- 124 J.-M. Choi, M.-H. Ahn, W.-J. Chae, Y.-G. Jung, J.-C. Park, H.-M. Song, Y.-E. Kim, J.-A. Shin, C.-S. Park, J.-W. Park, T.-K. Park, J.-H. Lee, B.-F. Seo, K.-D. Kim, E.-S. Kim, D.-H. Lee, S.-K. Lee and S.-K. Lee, *Nat. Med.*, 2006, **12**, 574.
- 125 J. Zhou, T. R. Patel, M. Fu, J. P. Bertram and W. M. Saltzman, *Biomaterials*, 2012, **33**, 583.
- 126 V. P. Torchilin, *Adv. Drug Delivery Rev.*, 2012, DOI: 10.1016/j.addr.2012.09.031.
- 127 E. Koren, A. Apte, R. R. Sawant, J. Grunwald and V. P. Torchilin, *Drug Delivery*, 2011, **18**, 377.
- 128 G. Drin, S. Cottin, E. Blanc, A. R. Rees and J. Temsamani, *J. Biol. Chem.*, 2003, **278**, 31192.
- 129 R. Pasqualini and E. Ruoslahti, *Nature*, 1996, **380**, 364.
- 130 G. P. Smith and V. A. Petrenko, *Chem. Rev.*, 1997, **97**, 391.
- 131 P. Laakkonen, K. Porkka, J. A. Hoffman and E. Ruoslahti, *Nat. Med.*, 2002, **8**, 751.
- 132 T. Oyama, K. F. Sykes, K. N. Samli, J. D. Minna, S. A. Johnston and K. C. Brown, *Cancer Lett.*, 2003, **202**, 219.
- 133 R. J. Passarella, D. E. Spratt, A. E. van der Ende, J. G. Phillips, H. M. Wu, V. Sathiyakumar, L. Zhou, D. E. Hallahan, E. Harth and R. Diaz, *Cancer Res.*, 2010, **70**, 4550.
- 134 J. M. Chan, L. Zhang, R. Tong, D. Ghosh, W. Gao, G. Liao, K. P. Yuet, D. Gray, J.-W. Rhee, J. Cheng, G. Golomb, P. Libby, R. Langer and O. C. Farokhzad, *Proc. Natl. Acad. Sci. U. S. A.*, 2010, **107**, 2213.
- 135 C. Eigenbrot, *Curr. Protein Pept. Sci.*, 2002, **3**, 287.
- 136 H. Y. Hong, H. Y. Lee, W. Kwak, J. Yoo, M. H. Na, I. S. So, T. H. Kwon, H. S. Park, S. Huh, G. T. Oh, I. C. Kwon, I. S. Kim and B. H. Lee, *J. Cell. Mol. Med.*, 2008, **12**, 2003.
- 137 V. J. Yao, M. G. Ozawa, M. Trepel, W. Arap, D. M. McDonald and R. Pasqualini, *Am. J. Pathol.*, 2005, **166**, 625.
- 138 M.-K. Yoo, S.-K. Kang, J.-H. Choi, I.-K. Park, H.-S. Na, H.-C. Lee, E.-B. Kim, N.-K. Lee, J.-W. Nah, Y.-J. Choi and C.-S. Cho, *Biomaterials*, 2010, **31**, 7738.
- 139 J. Mendelsohn, *Endocr.-Relat. Cancer*, 2001, **8**, 3.
- 140 Z. Li, R. Zhao, X. Wu, Y. Sun, M. Yao, J. Li, Y. Xu and J. Gu, *FASEB J.*, 2005, **19**, 1978.
- 141 H. Yusuf-Makagiansar and T. J. Sahaan, *Pharm. Res.*, 2001, **18**, 329.
- 142 T. R. Daniels, E. Bernabeu, J. A. Rodriguez, S. Patel, M. Kozman, D. A. Chiappetta, E. Holler, J. Y. Ljubimova, G. Helguera and M. L. Penichet, *Biochim. Biophys. Acta, -Gen. Subj.*, 2012, **1820**, 291.

- 143 E. Wagner, D. Curiel and M. Cotten, *Adv. Drug Delivery Rev.*, 1994, **14**, 113.
- 144 C. Fillebeen, L. Descamps, M. P. Dehouck, L. Fenart, M. Benaissa, G. Spik, R. Cecchelli and A. Pierce, *J. Biol. Chem.*, 1999, **274**, 7011.
- 145 R. Polt and M. M. Palian, *Drug Future*, 2001, **26**, 561.
- 146 A. F. Casy and R. T. Parfitt, *J. Clin. Pharmacol.*, 1988, **28**, 191.
- 147 C. Zhan, B. Li, L. Hu, X. Wei, L. Feng, W. Fu and W. Lu, *Angew. Chem., Int. Ed.*, 2011, **50**, 5482.
- 148 M. Demeule, A. Regina, C. Che, J. Poirier, T. Nguyen, R. Gabathuler, J. P. Castaigne and R. Beliveau, *J. Pharmacol. Exp. Ther.*, 2008, **324**, 1064.
- 149 M. Demeule, J. C. Currie, Y. Bertrand, C. Che, T. Nguyen, A. Regina, R. Gabathuler, J. P. Castaigne and R. Beliveau, *J. Neurochem.*, 2008, **106**, 1534.
- 150 J. Li, L. Feng, L. Fan, Y. Zha, L. Guo, Q. Zhang, J. Chen, Z. Pang, Y. Wang, X. Jiang, V. C. Yang and L. Wen, *Biomaterials*, 2011, **32**, 4943.
- 151 J. Kreuter, D. Shamenkov, V. Petrov, P. Ramge, K. Cychutek, C. Koch-Brandt and R. Alyautdin, *J. Drug Targeting*, 2002, **10**, 317.
- 152 M. J. Coloma, H. J. Lee, A. Kurihara, E. M. Landaw, R. J. Boado, S. L. Morrison and W. M. Pardridge, *Pharm. Res.*, 2000, **17**, 266.
- 153 S. C. Benn, I. Ay, E. Bastia, R. J. Chian, S. A. Celia, R. B. Pepinsky, P. S. Fishman, R. H. Brown, Jr. and J. W. Francis, *J. Neurochem.*, 2005, **95**, 1118.
- 154 E. V. Surovtseva, A. H. Johnston, W. Zhang, Y. Zhang, A. Kim, M. Murakoshi, H. Wada, T. A. Newman, J. Zou and I. Pyykkö, *Int. J. Pharm.*, 2012, **424**, 121.
- 155 J. K. Liu, Q. Teng, M. Garrity-Moses, T. Federici, D. Tanase, M. J. Imperiale and N. M. Boulis, *Neurobiol. Dis.*, 2005, **19**, 407.
- 156 S. Roy, A. H. Johnston, T. A. Newman, R. Glueckert, J. Dudas, M. Bitsche, E. Corbacella, G. Rieger, A. Martini and A. Schrott-Fischer, *Int. J. Pharm.*, 2010, **390**, 214.
- 157 A. V. Kabanov, V. P. Chekhonin, V. Y. Alakhov, E. V. Batrakova, A. S. Lebedev, N. S. Melik-Nubarov, S. A. Arzhakov, A. V. Levashov, G. V. Morozov, E. S. Severin and V. A. Kabanov, *FEBS Lett.*, 1989, **258**, 343.
- 158 V. P. Torchilin, A. N. Lukyanov, Z. Gao and B. Papahadjopoulos-Sternberg, *Proc. Natl. Acad. Sci. U. S. A.*, 2003, **100**, 6039.
- 159 M. Buschle, M. Cotten, H. Kirlappos, K. Mechtler, G. Schaffner, W. Zauner, M. L. Birnstiel and E. Wagner, *Hum. Gene Ther.*, 1995, **6**, 753.
- 160 R. Nahta and F. J. Esteva, *Cancer Lett.*, 2006, **232**, 123.
- 161 Y. Zhou, D. C. Drummond, H. Zou, M. E. Hayes, G. P. Adams, D. B. Kirpotin and J. D. Marks, *J. Mol. Biol.*, 2007, **371**, 934.
- 162 F. Mitjans, D. Sander, J. Adan, A. Sutter, J. M. Martinez, C. S. Jaggle, J. M. Moyano, H. G. Kreysch, J. Piulats and S. L. Goodman, *J. Cell Sci.*, 1995, **108**, 2825.
- 163 B. C. Trauth, C. Klas, A. M. Peters, S. Matzku, P. Moller, W. Falk, K. M. Debatin and P. H. Krammer, *Science*, 1989, **245**, 301.
- 164 L. Beketic-Oreskovic, B. Sarcevic, B. Malenica and D. Novak, *Neoplasma*, 1993, **40**, 69.
- 165 R. L. J. Kadouche, *USA*, 2006.
- 166 J. Boye, T. Elter and A. Engert, *Ann. Oncol.*, 2003, **14**, 520.
- 167 F. V. Ona, N. Zamcheck, P. Dhar, T. Moore and H. Z. Kupchik, *Cancer*, 1973, **31**, 324.
- 168 A. Serrano-Pozo, C. M. William, I. Ferrer, E. Uro-Coste, M. B. Delisle, C. A. Maurage, C. Hock, R. M. Nitsch, E. Masliah, J. H. Growdon, M. P. Frosch and B. T. Hyman, *Brain*, 2010, **133**, 1312.
- 169 K. Ulbrich, T. Knobloch and J. Kreuter, *J. Drug Targeting*, 2011, **19**, 125.
- 170 Z. M. Qian, H. Li, H. Sun and K. Ho, *Pharmacol. Rev.*, 2002, **54**, 561.
- 171 J. Lesley, R. Schulte and J. Woods, *Exp. Cell Res.*, 1989, **182**, 215.
- 172 S. M. Ranuncolo, V. Ladeda, S. Specterman, M. Varela, J. Lastiri, A. Morandi, E. Matos, E. Bal de Kier Joffe, L. Puricelli and M. G. Pallotta, *J. Surg. Oncol.*, 2002, **79**, 30.
- 173 A. M. Grabrucker, C. C. Garner, T. M. Boeckers, L. Bondioli, B. Ruozi, F. Forni, M. A. Vandelli and G. Tosi, *PLoS One*, 2011, **6**, e17851.
- 174 G. Horneff, G. R. Burmester, F. Emmrich and J. R. Kalden, *Arthritis Rheum.*, 1991, **34**, 129.
- 175 M. Everts, A. J. Schraa, L. F. M. H. de Leij, D. K. F. Meijer and G. Molema, in *Drug Targeting*, Wiley-VCH Verlag GmbH, 2001, pp. 171.
- 176 E. Horak, T. Heitner, M. K. Robinson, H. H. Simmons, J. Garrison, M. Russeva, P. Furmanova, J. Lou, Y. Zhou, Q. A. Yuan, L. M. Weiner, G. P. Adams and J. D. Marks, *Cancer Biother. Radiopharm.*, 2005, **20**, 603.
- 177 M. Peipp, H. Kupers, D. Saul, B. Schlierf, J. Greil, S. J. Zunino, M. Gramatzki and G. H. Fey, *Cancer Res.*, 2002, **62**, 2848.
- 178 P. Carter, *Nat. Rev. Cancer*, 2001, **1**, 118.
- 179 A. A. Gabizon, H. Shmeeda and S. Zalipsky, *J. Liposome Res.*, 2006, **16**, 175.
- 180 A. Orlova, M. Magnusson, T. L. Eriksson, M. Nilsson, B. Larsson, I. Hoiden-Guthenberg, C. Widstrom, J. Carlsson, V. Tolmachev, S. Stahl and F. Y. Nilsson, *Cancer Res.*, 2006, **66**, 4339.
- 181 Z. Xiao, E. Levy-Nissenbaum, F. Alexis, A. Lupták, B. A. Teply, J. M. Chan, J. Shi, E. Digga, J. Cheng, R. Langer and O. C. Farokhzad, *ACS Nano*, 2012, **6**, 696.
- 182 S. E. Lupold, B. J. Hicke, Y. Lin and D. S. Coffey, *Cancer Res.*, 2002, **62**, 4029.
- 183 W. Hwang do, H. Y. Ko, J. H. Lee, H. Kang, S. H. Ryu, I. C. Song, D. S. Lee and S. Kim, *J. Nucl. Med.*, 2010, **51**, 98.
- 184 A. D. Ellington and J. W. Szostak, *Nature*, 1990, **346**, 818.
- 185 O. C. Farokhzad, S. Jon, A. Khademhosseini, T.-N. T. Tran, D. A. LaVan and R. Langer, *Cancer Res.*, 2004, **64**, 7668.
- 186 O. C. Farokhzad, J. Cheng, B. A. Teply, I. Sherifi, S. Jon, P. W. Kantoff, J. P. Richie and R. Langer, *Proc. Natl. Acad. Sci. U. S. A.*, 2006, **103**, 6315.
- 187 K. P. Maresca, S. M. Hillier, F. J. Femia, D. Keith, C. Barone, J. L. Joyal, C. N. Zimmerman, A. P. Kozikowski, J. A. Barrett, W. C. Eckelman and J. W. Babich, *J. Med. Chem.*, 2009, **52**, 347.
- 188 J. Hrkach, D. Von Hoff, M. Mukkaram Ali, E. Andrianova, J. Auer, T. Campbell, D. De Witt, M. Figa, M. Figueiredo, A. Horhota, S. Low, K. McDonnell, E. Peeke, B. Retnarajan, A. Sabnis, E. Schnipper, J. J. Song, Y. H. Song, J. Summa, D. Tompsett, G. Troiano, T. Van Geen Hoven, J. Wright, P. LoRusso, P. W. Kantoff, N. H. Bander, C. Sweeney, O. C. Farokhzad, R. Langer and S. Zale, *Sci. Transl. Med.*, 2012, **4**, 128ra39.
- 189 F. Re, C. Airoidi, C. Zona, M. Masserini, B. La Ferla, N. Quattrocchi and F. Nicotra, *Curr. Med. Chem.*, 2010, **17**, 2990.
- 190 L. Nobs, F. Buchegger, R. Gurny and E. Allemann, *J. Pharm. Sci.*, 2004, **93**, 1980.
- 191 R. P. Haugland, *The Handbook A Guide to Fluorescent Probes and Labeling Technologies*, 2005.
- 192 P. Crosasso, P. Brusa, F. Dosio, S. Arpicco, D. Pacchioni, F. Schuber and L. Cattel, *J. Pharm. Sci.*, 1997, **86**, 832.
- 193 W. R. Algar, D. E. Prasuhn, M. H. Stewart, T. L. Jennings, J. B. Blanco-Canosa, P. E. Dawson and I. L. Medintz, *Bioconjugate Chem.*, 2011, **22**, 825.
- 194 A. Warnecke and F. Kratz, *Bioconjugate Chem.*, 2003, **14**, 377.
- 195 J.-F. Lutz, *Angew. Chem., Int. Ed.*, 2007, **46**, 1018.
- 196 V. Hong, S. I. Presolski, C. Ma and M. G. Finn, *Angew. Chem., Int. Ed.*, 2009, **48**, 9879.
- 197 M. Moro, M. Pelagi, G. Fulci, G. Paganelli, P. Dellabona, G. Casorati, A. G. Siccardi and A. Corti, *Cancer Res.*, 1997, **57**, 1922.
- 198 S. Y. Mao, *Methods Mol. Biol.*, 2010, **588**, 49.
- 199 T. Yoshikawa and W. M. Pardridge, *J. Pharmacol. Exp. Ther.*, 1992, **263**, 897.
- 200 L. Costantino, F. Gandolfi, G. Tosi, F. Rivasi, M. A. Vandelli and F. Forni, *J. Controlled Release*, 2005, **108**, 84.
- 201 G. Tosi, A. V. Vergoni, B. Ruozi, L. Bondioli, L. Badioli, F. Rivasi, L. Costantino, F. Forni and M. A. Vandelli, *J. Controlled Release*, 2010, **145**, 49.
- 202 K. Ghosh, M. Kanapathipillai, N. Korin, J. R. McCarthy and D. E. Ingber, *Nano Lett.*, 2011, **12**, 203.
- 203 Y. Yin, D. Chen, M. Qiao, Z. Lu and H. Hu, *J. Controlled Release*, 2006, **116**, 337.
- 204 Y. Yin, D. Chen, M. Qiao, X. Wei and H. Hu, *J. Controlled Release*, 2007, **123**, 27.
- 205 Y. Mo and L.-Y. Lim, *J. Pharm. Sci.*, 2004, **93**, 20.
- 206 Y. Mo and L.-Y. Lim, *J. Controlled Release*, 2005, **108**, 244.
- 207 Y. Mo and L.-Y. Lim, *J. Controlled Release*, 2005, **107**, 30.
- 208 P. A. McCarron, W. M. Marouf, D. J. Quinn, F. Fay, R. E. Burden, S. A. Olwill and C. J. Scott, *Bioconjugate Chem.*, 2008, **19**, 1561.
- 209 H. Chen, J. Gao, Y. Lu, G. Kou, H. Zhang, L. Fan, Z. Sun, Y. Guo and Y. Zhong, *J. Controlled Release*, 2008, **128**, 209.

- 210 P. Kocbek, N. Obermajer, M. Cegnar, J. Kos and J. Kristl, *J. Controlled Release*, 2007, **120**, 18.
- 211 S. Acharya, F. Dilnawaz and S. K. Sahoo, *Biomaterials*, 2009, **30**, 5737.
- 212 W. Hyung, H. Ko, J. Park, E. Lim, S. B. Park, Y.-J. Park, H. G. Yoon, J. S. Suh, S. Haam and Y.-M. Huh, *Biotechnol. Bioeng.*, 2008, **99**, 442.
- 213 S. Hamdy, A. Haddadi, A. Shayeganpour, J. Samuel and A. Lavasanifar, *Pharm. Res.*, 2011, **28**, 2288.
- 214 S.-W. Choi and J.-H. Kim, *J. Controlled Release*, 2007, **122**, 24.
- 215 G. Tosi, L. Costantino, F. Rivasi, B. Ruozi, E. Leo, A. V. Vergoni, R. Tacchi, A. Bertolini, M. A. Vandelli and F. Forni, *J. Controlled Release*, 2007, **122**, 1.
- 216 S. H. Kim, J. H. Jeong, K. W. Chun and T. G. Park, *Langmuir*, 2005, **21**, 8852.
- 217 F. Esmacili, M. H. Ghahremani, S. N. Ostad, F. Atyabi, M. Seyedabadi, M. R. Malekshahi, M. Amini and R. Dinarvand, *J. Drug Targeting*, 2008, **16**, 415.
- 218 Y. Liu, K. Li, J. Pan, B. Liu and S.-S. Feng, *Biomaterials*, 2010, **31**, 330.
- 219 J. Kim, J. E. Lee, S. H. Lee, J. H. Yu, J. H. Lee, T. G. Park and T. Hyeon, *Adv. Mater.*, 2008, **20**, 478.
- 220 H. Zhao and L. Y. L. Yung, *Int. J. Pharm.*, 2008, **349**, 256.
- 221 Y. Nie, Z. Zhang, L. Li, K. Luo, H. Ding and Z. Gu, *J. Mater. Sci.: Mater. Med.*, 2009, **20**, 1849.
- 222 M. E. Werner, J. A. Copp, S. Karve, N. D. Cummings, R. Sukumar, C. Li, M. E. Napier, R. C. Chen, A. D. Cox and A. Z. Wang, *ACS Nano*, 2011, **5**, 8990.
- 223 M. E. Werner, S. Karve, R. Sukumar, N. D. Cummings, J. A. Copp, R. C. Chen, T. Zhang and A. Z. Wang, *Biomaterials*, 2011, **32**, 8548.
- 224 Y. B. Patil, S. K. Swaminathan, T. Sadhukha, L. Ma and J. Panyam, *Biomaterials*, 2010, **31**, 358.
- 225 P. M. Valencia, M. H. Hanewich-Hollatz, W. Gao, F. Karim, R. Langer, R. Karnik and O. C. Farokhzad, *Biomaterials*, 2011, **32**, 6226.
- 226 D. Kim, E. S. Lee, K. T. Oh, Z. G. Gao and Y. H. Bae, *Small*, 2008, **4**, 2043.
- 227 E. S. Lee, K. Na and Y. H. Bae, *J. Controlled Release*, 2003, **91**, 103.
- 228 C. Chittasupho, S.-X. Xie, A. Baoum, T. Yakovleva, T. J. Siahaan and C. J. Berkland, *Eur. J. Pharm. Sci.*, 2009, **37**, 141.
- 229 N. Zhang, C. Chittasupho, C. Duangrat, T. J. Siahaan and C. Berkland, *Bioconjugate Chem.*, 2007, **19**, 145.
- 230 V. Sanna, G. Pintus, A. M. Roggio, S. Punzoni, A. M. Posadino, A. Arca, S. Marceddu, P. Bandiera, S. Uzzau and M. Sechi, *J. Med. Chem.*, 2011, **54**, 1321.
- 231 Z. Wang and P. C. Ho, *Small*, 2010, **6**, 2576.
- 232 Z. Wang, W.-K. Chui and P. C. Ho, *Pharm. Res.*, 2009, **26**, 1162.
- 233 J. S. Lee, T. Groothuis, C. Cusan, D. Mink and J. Feijen, *Biomaterials*, 2011, **32**, 9144.
- 234 J. Cheng, B. A. Teply, I. Sherifi, J. Sung, G. Luther, F. X. Gu, E. Levy-Nissenbaum, A. F. Radovic-Moreno, R. Langer and O. C. Farokhzad, *Biomaterials*, 2007, **28**, 869.
- 235 F. Gu, L. Zhang, B. A. Teply, N. Mann, A. Wang, A. F. Radovic-Moreno, R. Langer and O. C. Farokhzad, *Proc. Natl. Acad. Sci. U. S. A.*, 2008, **105**, 2586.
- 236 S. Dhar, N. Kolishetti, S. J. Lippard and O. C. Farokhzad, *Proc. Natl. Acad. Sci. U. S. A.*, 2011, **108**, 1850.
- 237 J. Guo, X. Gao, L. Su, H. Xia, G. Gu, Z. Pang, X. Jiang, L. Yao, J. Chen and H. Chen, *Biomaterials*, 2011, **32**, 8010.
- 238 H. Wang, P. Zhao, W. Su, S. Wang, Z. Liao, R. Niu and J. Chang, *Biomaterials*, 2010, **31**, 8741.
- 239 C.-H. Wang and G.-H. Hsiue, *Bioconjugate Chem.*, 2005, **16**, 391.
- 240 P. Liu, Z. Li, M. Zhu, Y. Sun, Y. Li, H. Wang and Y. Duan, *J. Mater. Sci.: Mater. Med.*, 2010, **21**, 551.
- 241 W. Cao, J. Zhou, Y. Wang and L. Zhu, *Biomacromolecules*, 2010, **11**, 3680.
- 242 W. Cao, J. Zhou, A. Mann, Y. Wang and L. Zhu, *Biomacromolecules*, 2011, **12**, 2697.
- 243 D. Kim, Z. G. Gao, E. S. Lee and Y. H. Bae, *Mol. Pharmaceutics*, 2009, **6**, 1353.
- 244 J. Pan and S.-S. Feng, *Biomaterials*, 2008, **29**, 2663.
- 245 J. Wang, W. Liu, Q. Tu, J. Wang, N. Song, Y. Zhang, N. Nie and J. Wang, *Biomacromolecules*, 2010, **12**, 228.
- 246 Z. Zhang, S. Huey Lee and S.-S. Feng, *Biomaterials*, 2007, **28**, 1889.
- 247 J. Zhao, Y. Mi, Y. Liu and S. S. Feng, *Biomaterials*, 2012, **33**, 1948.
- 248 C. W. Gan and S.-S. Feng, *Biomaterials*, 2010, **31**, 7748.
- 249 H.-F. Liang, S.-C. Chen, M.-C. Chen, P.-W. Lee, C.-T. Chen and H.-W. Sung, *Bioconjugate Chem.*, 2006, **17**, 291.
- 250 H.-F. Liang, C.-T. Chen, S.-C. Chen, A. R. Kulkarni, Y.-L. Chiu, M.-C. Chen and H.-W. Sung, *Biomaterials*, 2006, **27**, 2051.
- 251 L. Milane, Z. Duan and M. Amiji, *Mol. Pharmaceutics*, 2010, **8**, 185.
- 252 G. Luo, X. Yu, C. Jin, F. Yang, D. Fu, J. Long, J. Xu, C. Zhan and W. Lu, *Int. J. Pharm.*, 2010, **385**, 150.
- 253 J. S. Guthi, S.-G. Yang, G. Huang, S. Li, C. Khemtong, C. W. Kessinger, M. Peyton, J. D. Minna, K. C. Brown and J. Gao, *Mol. Pharmaceutics*, 2009, **7**, 32.
- 254 H. Mei, W. Shi, Z. Pang, H. Wang, W. Lu, X. Jiang, J. Deng, T. Guo and Y. Hu, *Biomaterials*, 2010, **31**, 5619.
- 255 Z. Wen, Z. Yan, R. He, Z. Pang, L. Guo, Y. Qian, X. Jiang and L. Fang, *Drug Delivery*, 2011, **18**, 555.
- 256 Z. Wen, Z. Yan, K. Hu, Z. Pang, X. Cheng, L. Guo, Q. Zhang, X. Jiang, L. Fang and R. Lai, *J. Controlled Release*, 2011, **151**, 131.
- 257 U. S. Toti, B. R. Guru, A. E. Grill and J. Panyam, *Mol. Pharmaceutics*, 2010, **7**, 1108.
- 258 N. Nasongkla, E. Bey, J. Ren, H. Ai, C. Khemtong, J. S. Guthi, S.-F. Chin, A. D. Sherry, D. A. Boothman and J. Gao, *Nano Lett.*, 2006, **6**, 2427.
- 259 F. Alexis, P. Basto, E. Levy-Nissenbaum, A. F. Radovic-Moreno, L. Zhang, E. Pridgen, A. Z. Wang, S. L. Marein, K. Westerhof, L. K. Molnar and O. C. Farokhzad, *ChemMedChem*, 2008, **3**, 1839.
- 260 X. L. Wu, J. H. Kim, H. Koo, S. M. Bae, H. Shin, M. S. Kim, B.-H. Lee, R.-W. Park, I.-S. Kim, K. Choi, I. C. Kwon, K. Kim and D. S. Lee, *Bioconjugate Chem.*, 2010, **21**, 208.
- 261 K. Hu, J. Li, Y. Shen, W. Lu, X. Gao, Q. Zhang and X. Jiang, *J. Controlled Release*, 2009, **134**, 55.
- 262 K. L. Hu, Y. B. Shi, W. M. Jiang, J. Y. Han, S. X. Huang and X. G. Jiang, *Int. J. Pharm.*, 2011, **415**, 273.
- 263 Y. Yu, Z. Pang, W. Lu, Q. Yin, H. Gao and X. Jiang, *Pharm. Res.*, 2012, **29**, 83.
- 264 X. Gao, W. Tao, W. Lu, Q. Zhang, Y. Zhang, X. Jiang and S. Fu, *Biomaterials*, 2006, **27**, 3482.
- 265 X. Gao, B. Wu, Q. Zhang, J. Chen, J. Zhu, W. Zhang, Z. Rong, H. Chen and X. Jiang, *J. Controlled Release*, 2007, **121**, 156.
- 266 Q. Liu, Y. Shen, J. Chen, X. Gao, C. Feng, L. Wang, Q. Zhang and X. Jiang, *Pharm. Res.*, 2012, **29**, 546.
- 267 J. Chen, C. Zhang, Q. Liu, X. Shao, C. Feng, Y. Shen, Q. Zhang and X. Jiang, *J. Drug Targeting*, 2012, **20**, 174.
- 268 C. K. Huang, C. L. Lo, H. H. Chen and G. H. Hsiue, *Adv. Funct. Mater.*, 2007, **17**, 2291.
- 269 L. Nobs, F. Buchegger, R. Gurny and E. Allemann, *Bioconjugate Chem.*, 2005, **17**, 139.
- 270 A. Cirstoiu-Hapca, L. Bossy-Nobs, F. Buchegger, R. Gurny and F. Delie, *Int. J. Pharm.*, 2007, **331**, 190.
- 271 A. Cirstoiu-Hapca, F. Buchegger, L. Bossy, M. Kosinski, R. Gurny and F. Delie, *Eur. J. Pharm. Sci.*, 2009, **38**, 230.
- 272 Y. Zheng, B. Yu, W. Weecharangsan, L. Piao, M. Darby, Y. Mao, R. Koyanova, X. Yang, H. Li, S. Xu, L. J. Lee, Y. Sugimoto, R. W. Brueggemeier and R. J. Lee, *Int. J. Pharm.*, 2010, **390**, 234.
- 273 Q. Xu, Y. Liu, S. Su, W. Li, C. Chen and Y. Wu, *Biomaterials*, 2012, **33**, 1627.
- 274 N. Debotton, M. Parnes, J. Kadouche and S. Benita, *J. Controlled Release*, 2008, **127**, 219.
- 275 X. Yang, J. J. Grailler, I. J. Rowland, A. Javadi, S. A. Hurley, D. A. Steeber and S. Gong, *Biomaterials*, 2010, **31**, 9065.
- 276 V. A. Sethuraman and Y. H. Bae, *J. Controlled Release*, 2007, **118**, 216.
- 277 V. Sethuraman, M. Lee and Y. Bae, *Pharm. Res.*, 2008, **25**, 657.
- 278 C.-M. J. Hu, S. Kaushal, H. S. T. Cao, S. Aryal, M. Sartor, S. Esener, M. Bouvet and L. Zhang, *Mol. Pharmaceutics*, 2010, **7**, 914.
- 279 A. O. Saeed, J. P. Magnusson, E. Moradi, M. Soliman, W. Wang, S. Stolnik, K. J. Thurecht, S. M. Howdle and C. Alexander, *Bioconjugate Chem.*, 2011, **22**, 156.
- 280 J. Lu, M. Shi and M. S. Shoichet, *Bioconjugate Chem.*, 2008, **20**, 87.
- 281 H. S. Sakhalkar, M. K. Dalal, A. K. Salem, R. Ansari, J. Fu, M. F. Kiani, D. T. Kurjiaka, J. Hanes, K. M. Shakesheff and D. J. Goetz, *Proc. Natl. Acad. Sci. U. S. A.*, 2003, **100**, 15895.
- 282 S. A. Townsend, G. D. Evrony, F. X. Gu, M. P. Schulz, R. H. Brown, Jr and R. Langer, *Biomaterials*, 2007, **28**, 5176.
- 283 J. Park, T. Mattessich, S. M. Jay, A. Agawu, W. M. Saltzman and T. M. Fahmy, *J. Controlled Release*, 2011, **156**, 109.

- 284 J. Park, W. Gao, R. Whiston, T. B. Strom, S. Metcalfe and T. M. Fahmy, *Mol. Pharmaceutics*, 2010, **8**, 143.
- 285 F. Danhier, B. Ucakar, N. Magotteaux, M. E. Brewster and V. Préat, *Int. J. Pharm.*, 2010, **392**, 20.
- 286 Z. Hu, F. Luo, Y. Pan, C. Hou, L. Ren, J. Chen, J. Wang and Y. Zhang, *J. Biomed. Mater. Res., Part A*, 2008, **85A**, 797.
- 287 D.-H. Yu, Q. Lu, J. Xie, C. Fang and H.-Z. Chen, *Biomaterials*, 2010, **31**, 2278.
- 288 Y. Nagasaki, K. Yasugi, Y. Yamamoto, A. Harada and K. Kataoka, *Biomacromolecules*, 2001, **2**, 1067.
- 289 S. K. Sahoo, W. Ma and V. Labhasetwar, *Int. J. Cancer*, 2004, **112**, 335.
- 290 K. S. Rao, M. K. Reddy, J. L. Horning and V. Labhasetwar, *Biomaterials*, 2008, **29**, 4429.
- 291 X. Banquy, G. g. Leclair, J.-M. Rabanel, A. Argaw, J.-F. o. Bouchard, P. Hildgen and S. Giasson, *Bioconjugate Chem.*, 2008, **19**, 2030.
- 292 T. Hammady, J.-M. Rabanel, R. S. Dhanikula, G. Leclair and P. Hildgen, *Eur. J. Pharm. Biopharm.*, 2009, **72**, 418.
- 293 K. Yasugi, T. Nakamura, Y. Nagasaki, M. Kato and K. Kataoka, *Macromolecules*, 1999, **32**, 8024.
- 294 M. Shi, K. Ho, A. Keating and M. S. Shoichet, *Adv. Funct. Mater.*, 2009, **19**, 1689.
- 295 H. S. Yoo and T. G. Park, *J. Controlled Release*, 2004, **96**, 273.
- 296 P. Liu, X. Qi, Y. Sun, H. Wang, Y. Li and Y. Duan, *J. Nanosci. Nanotechnol.*, 2011, **11**, 10760.
- 297 Y. Liu, K. Li, B. Liu and S.-S. Feng, *Biomaterials*, 2010, **31**, 9145.
- 298 S. Dhar, F. X. Gu, R. Langer, O. C. Farokhzad and S. J. Lippard, *Proc. Natl. Acad. Sci. U. S. A.*, 2008, **105**, 17356.
- 299 V. R. Sinha, K. Bansal, R. Kaushik, R. Kumria and A. Trehan, *Int. J. Pharm.*, 2004, **278**, 1.
- 300 S. Ponsart, J. Coudane and M. Vert, *Biomacromolecules*, 2000, **1**, 275.
- 301 Y. Zhang, J. Li, M. Lang, X. Tang, L. Li and X. Shen, *J. Colloid Interface Sci.*, 2011, **354**, 202.
- 302 J. Liu, Q. Zhang, E. E. Remsen and K. L. Wooley, *Biomacromolecules*, 2001, **2**, 362.
- 303 H. Gao, J. Qian, S. Cao, Z. Yang, Z. Pang, S. Pan, L. Fan, Z. Xi, X. Jiang and Q. Zhang, *Biomaterials*, 2012, **33**, 5115.
- 304 H. Lee, M. Hu, R. M. Reilly and C. Allen, *Mol. Pharmaceutics*, 2007, **4**, 769.
- 305 H. Lee, H. Fonge, B. Hoang, R. M. Reilly and C. Allen, *Mol. Pharmaceutics*, 2010, **7**, 1195.
- 306 H. Lee, B. Hoang, H. Fonge, R. Reilly and C. Allen, *Pharm. Res.*, 2010, **27**, 2343.
- 307 Z. Pang, L. Feng, R. Hua, J. Chen, H. Gao, S. Pan, X. Jiang and P. Zhang, *Mol. Pharmaceutics*, 2010, **7**, 1995.
- 308 T. Noh, Y. H. Kook, C. Park, H. Youn, H. Kim, E. T. Oh, E. K. Choi, H. J. Park and C. Kim, *J. Polym. Sci., Part A: Polym. Chem.*, 2008, **46**, 7321.
- 309 H. Xin, X. Jiang, J. Gu, X. Sha, L. Chen, K. Law, Y. Chen, X. Wang, Y. Jiang and X. Fang, *Biomaterials*, 2011, **32**, 4293.
- 310 H. Xin, X. Sha, X. Jiang, L. Chen, K. Law, J. Gu, Y. Chen, X. Wang and X. Fang, *Biomaterials*, 2012, **33**, 1673.
- 311 Z. Pang, H. Gao, Y. Yu, L. Guo, J. Chen, S. Pan, J. Ren, Z. Wen and X. Jiang, *Bioconjugate Chem.*, 2011, **22**, 1171.
- 312 Z. Pang, W. Lu, H. Gao, K. Hu, J. Chen, C. Zhang, X. Gao, X. Jiang and C. Zhu, *J. Controlled Release*, 2008, **128**, 120.
- 313 N. Nasongkla, X. Shuai, H. Ai, B. D. Weinberg, J. Pink, D. A. Boothman and J. Gao, *Angew. Chem., Int. Ed.*, 2004, **43**, 6323.
- 314 X. Yang, W. Deng, L. Fu, E. Blanco, J. Gao, D. Quan and X. Shuai, *J. Biomed. Mater. Res., Part A*, 2008, **86A**, 48.
- 315 J. Yang, E.-J. Cho, S. Seo, J.-W. Lee, H.-G. Yoon, J.-S. Suh, Y.-M. Huh and S. Haam, *J. Biomed. Mater. Res., Part A*, 2008, **84A**, 273.
- 316 Y.-C. Wang, X.-Q. Liu, T.-M. Sun, M.-H. Xiong and J. Wang, *J. Controlled Release*, 2008, **128**, 32.
- 317 E. K. Park, S. B. Lee and Y. M. Lee, *Biomaterials*, 2005, **26**, 1053.
- 318 E. K. Park, S. Y. Kim, S. B. Lee and Y. M. Lee, *J. Controlled Release*, 2005, **109**, 158.
- 319 X.-B. Xiong, A. Mahmud, H. Uludağ and A. Lavasanifar, *Biomacromolecules*, 2007, **8**, 874.
- 320 X.-B. Xiong, A. Mahmud, H. Uludağ and A. Lavasanifar, *Pharm. Res.*, 2008, **25**, 2555.
- 321 X.-B. Xiong, Z. Ma, R. Lai and A. Lavasanifar, *Biomaterials*, 2010, **31**, 757.
- 322 X.-B. Xiong and A. Lavasanifar, *ACS Nano*, 2011, **5**, 5202.
- 323 M. Garinot, V. Fiévez, V. Pourcelle, F. Stoffelbach, A. des Rieux, L. Plapied, I. Theate, H. Freichels, C. Jérôme, J. Marchand-Brynaert, Y.-J. Schneider and V. Préat, *J. Controlled Release*, 2007, **120**, 195.
- 324 F. Danhier, B. Vroman, N. Lecouturier, N. Crockart, V. Pourcelle, H. Freichels, C. Jérôme, J. Marchand-Brynaert, O. Feron and V. Préat, *J. Controlled Release*, 2009, **140**, 166.
- 325 J. Rieger, H. I. n. Freichels, A. Imberty, J.-L. Putaux, T. Delair, C. Jérôme and R. Auzely-Velty, *Biomacromolecules*, 2009, **10**, 651.
- 326 Y. Zhang, W. Zhang, A. H. Johnston, T. A. Newman, I. Pyykko and J. Zou, *Int. J. Nanomed.*, 2012, **7**, 1015.
- 327 R. Gref, P. Couvreur, G. Barratt and E. Mysiakine, *Biomaterials*, 2003, **24**, 4529.
- 328 T. Liu, Y. Qian, X. Hu, Z. Ge and S. Liu, *J. Mater. Chem.*, 2012, **22**, 5020.
- 329 X. Yang, J. J. Grailer, S. Pilla, D. A. Steeber and S. Gong, *Bioconjugate Chem.*, 2010, **21**, 496.
- 330 M. Prabaharan, J. J. Grailer, S. Pilla, D. A. Steeber and S. Gong, *Biomaterials*, 2009, **30**, 3009.
- 331 S. Chen, X.-Z. Zhang, S.-X. Cheng, R.-X. Zhuo and Z.-W. Gu, *Biomacromolecules*, 2008, **9**, 2578.
- 332 X. Li, Y. Qian, T. Liu, X. Hu, G. Zhang, Y. You and S. Liu, *Biomaterials*, 2011, **32**, 6595.
- 333 S. Santra, C. Kaittanis and J. M. Perez, *Mol. Pharmaceutics*, 2010, **7**, 1209.
- 334 C. Zhang, L. Zhao, Y. Dong, X. Zhang, J. Lin and Z. Chen, *Eur. J. Pharm. Biopharm.*, 2010, **76**, 10.
- 335 V. B. Morris, C. K. S. Pillai and C. P. Sharma, *Polym. Int.*, 2011, **60**, 1097.
- 336 K. Park, H. Y. Hong, H. J. Moon, B. H. Lee, I. S. Kim, I. C. Kwon and K. Rhee, *J. Controlled Release*, 2008, **128**, 217.
- 337 S. M. Alex, M. R. Rekha and C. P. Sharma, *Int. J. Pharm.*, 2011, **410**, 125.
- 338 A. Zou, M. Huo, Y. Zhang, J. Zhou, X. Yin, C. Yao, Q. Zhu, M. Zhang, J. Ren and Q. Zhang, *J. Pharm. Sci.*, 2012, **101**, 627.
- 339 H. Wang, P. Zhao, X. Liang, X. Gong, T. Song, R. Niu and J. Chang, *Biomaterials*, 2010, **31**, 4129.
- 340 S. J. Yang, F. H. Lin, K. C. Tsai, M. F. Wei, H. M. Tsai, J. M. Wong and M. J. Shieh, *Bioconjugate Chem.*, 2010, **21**, 679.
- 341 J. C. Fernandes, H. Wang, C. Jreysaty, M. Benderdour, P. Lavigne, X. Qiu, F. M. Winnik, X. Zhang, K. Dai and Q. Shi, *Mol. Ther.*, 2008, **16**, 1243.
- 342 S. Mansouri, Y. Cuie, F. Winnik, Q. Shi, P. Lavigne, M. Benderdour, E. Beaumont and J. C. Fernandes, *Biomaterials*, 2006, **27**, 2060.
- 343 J. Ji, D. Wu, L. Liu, J. Chen and Y. Xu, *Polym. Bull.*, 2012, **68**, 1707.
- 344 Z. Hou, C. Zhan, Q. Jiang, Q. Hu, L. Li, D. Chang, X. Yang, Y. Wang, Y. Li, S. Ye, L. Xie, Y. Yi and Q. Zhang, *Nanosci. Res. Lett.*, 2011, **6**, 563.
- 345 Y. Zu, Q. Zhao, X. Zhao, S. Zu and L. Meng, *Int. J. Nanomed.*, 2011, **6**, 3429.
- 346 J. M. Shen, X. M. Guan, X. Y. Liu, J. F. Lan, T. Cheng and H. X. Zhang, *Bioconjugate Chem.*, 2012, **23**, 1010.
- 347 G. Arya, M. Vandana, S. Acharya and S. K. Sahoo, *Nanomedicine*, 2011, **7**, 859.
- 348 J. Lee, K.-S. Yun, C. S. Choi, S.-H. Shin, H.-S. Ban, T. Rhim, S. K. Lee and K. Y. Lee, *Bioconjugate Chem.*, 2012, **23**, 1174.
- 349 D. Rahmat, M. I. Khan, G. Shahnaz, D. Sakloetsakun, G. Perera and A. Bernkop-Schnurch, *Biomaterials*, 2012, **33**, 2321.
- 350 A. Lin, Y. Liu, Y. Huang, J. Sun, Z. Wu, X. Zhang and Q. Ping, *Int. J. Pharm.*, 2008, **359**, 247.
- 351 P. Yousefpour, F. Atyabi, E. Vashghani-Farahani, A. A. Movahedi and R. Dinarvand, *Int. J. Nanomed.*, 2011, **6**, 1977.
- 352 H. D. Han, L. S. Mangala, J. W. Lee, M. M. K. Shahzad, H. S. Kim, D. Shen, E. J. Nam, E. M. Mora, R. L. Stone, C. Lu, S. J. Lee, J. W. Roh, A. M. Nick, G. Lopez-Berestein and A. K. Sood, *Clin. Cancer Res.*, 2010, **16**, 3910.
- 353 H. Karatas, Y. Aktas, Y. Gursoy-Ozdemir, E. Bodur, M. Yemisci, S. Caban, A. Vural, O. Pinarbasli, Y. Capan, E. Fernandez-Megia, R. Novoa-Carballal, R. Riguera, K. Andrieux, P. Couvreur and T. Dalkara, *J. Neurosci.*, 2009, **29**, 13761.
- 354 Y. Aktas, M. Yemisci, K. Andrieux, R. N. Gursoy, M. J. Alonso, E. Fernandez-Megia, R. Novoa-Carballal, E. Quiñoá, R. Riguera, M. F. Sargon, H. H. Çelik, A. S. Demir, A. A. Hincal, T. Dalkara, Y. Çapan and P. Couvreur, *Bioconjugate Chem.*, 2005, **16**, 1503.

- 355 S. Sahu, S. Mallick, S. Santra, T. Maiti, S. Ghosh and P. Pramanik, *J. Mater. Sci.: Mater. Med.*, 2010, **21**, 1587.
- 356 S. K. Sahu, S. Maiti, T. K. Maiti, S. K. Ghosh and P. Pramanik, *Macromol. Biosci.*, 2011, **11**, 285.
- 357 C. Li, T. Guo, D. Zhou, Y. Hu, H. Zhou, S. Wang, J. Chen and Z. Zhang, *J. Controlled Release*, 2011, **154**, 177.
- 358 M. E. Davis and M. E. Brewster, *Nat. Rev. Drug Discovery*, 2004, **3**, 1023.
- 359 N. C. Bellocq, S. H. Pun, G. S. Jensen and M. E. Davis, *Bioconjugate Chem.*, 2003, **14**, 1122.
- 360 D. W. Bartlett, H. Su, I. J. Hildebrandt, W. A. Weber and M. E. Davis, *Proc. Natl. Acad. Sci. U. S. A.*, 2007, **104**, 15549.
- 361 D. W. Bartlett and M. E. Davis, *Bioconjugate Chem.*, 2007, **18**, 456.
- 362 M. E. Davis, J. E. Zuckerman, C. H. Choi, D. Seligson, A. Tolcher, C. A. Alabi, Y. Yen, J. D. Heidel and A. Ribas, *Nature*, 2010, **464**, 1067.
- 363 S. H. Pun, F. Tack, N. C. Bellocq, J. Cheng, B. H. Grubbs, G. S. Jensen, M. E. Davis, M. Brewster, M. Janicot, B. Janssens, W. Floren and A. Bakker, *Cancer Biol. Ther.*, 2004, **3**, 641.
- 364 D. W. Bartlett and M. E. Davis, *Biotechnol. Bioeng.*, 2008, **99**, 975.
- 365 J. D. Heidel, Z. Yu, J. Y.-C. Liu, S. M. Rele, Y. Liang, R. K. Zeidan, D. J. Kornbrust and M. E. Davis, *Proc. Natl. Acad. Sci. U. S. A.*, 2007, **104**, 5715.
- 366 S. Hu-Lieskovan, J. D. Heidel, D. W. Bartlett, M. E. Davis and T. J. Triche, *Cancer Res.*, 2005, **65**, 8984.
- 367 M. E. Davis, *Mol. Pharmaceutics*, 2009, **6**, 659.
- 368 X. H. Peng, Y. Wang, D. Huang, H. J. Shin, Z. Chen, M. B. Spewak, H. Mao, X. Wang, Z. G. Chen, S. Nie and D. M. Shin, *ACS Nano*, 2011, **5**, 9480.
- 369 X. Wang, J. Li, Y. Wang, K. J. Cho, G. Kim, A. Gjyzezi, L. Koenig, P. Giannakakou, H. J. Shin, M. Tighiouart, S. Nie, Z. G. Chen and D. M. Shin, *ACS Nano*, 2009, **3**, 3165.
- 370 Y. Wang, J. Xiang and K. Yao, *Biomacromolecules*, 2010, **11**, 3531.
- 371 Y. Cao, Y. Gu, H. Ma, J. Bai, L. Liu, P. Zhao and H. He, *Int. J. Biol. Macromol.*, 2010, **46**, 245.
- 372 K. B. Chalasani, G. J. Russell-Jones, A. K. Jain, P. V. Diwan and S. K. Jain, *J. Controlled Release*, 2007, **122**, 141.
- 373 X. Wang, J. Li, Y. Wang, L. Koenig, A. Gjyzezi, P. Giannakakou, E. H. Shin, M. Tighiouart, Z. Chen, S. Nie and D. M. Shin, *ACS Nano*, 2011, **5**, 6184.
- 374 X. Yang, J. J. Grailer, I. J. Rowland, A. Javadi, S. A. Hurley, V. Z. Matson, D. A. Steeber and S. Gong, *ACS Nano*, 2010, **4**, 6805.
- 375 K. K. Upadhyay, A. N. Bhatt, E. Castro, A. K. Mishra, K. Chuttani, B. S. Dwarakanath, C. Schatz, J.-F. Le Meins, A. Misra and S. Lecommandoux, *Macromol. Biosci.*, 2010, **10**, 503.
- 376 K. K. Upadhyay, A. N. Bhatt, A. K. Mishra, B. S. Dwarakanath, S. Jain, C. Schatz, J.-F. Le Meins, A. Farooque, G. Chandraiah, A. K. Jain, A. Misra and S. Lecommandoux, *Biomaterials*, 2010, **31**, 2882.
- 377 K. K. Upadhyay, J. F. L. Meins, A. Misra, P. Voisin, V. Bouchaud, E. Ibarboure, C. Schatz and S. Lecommandoux, *Biomacromolecules*, 2009, **10**, 2802.
- 378 K. K. Upadhyay, A. K. Mishra, K. Chuttani, A. Kaul, C. Schatz, J.-F. Le Meins, A. Misra and S. Lecommandoux, *Nanomedicine*, 2012, **8**, 71.
- 379 E. S. Lee, Z. Gao, D. Kim, K. Park, I. C. Kwon and Y. H. Bae, *J. Controlled Release*, 2008, **129**, 228.
- 380 E. S. Lee, K. Na and Y. H. Bae, *Nano Lett.*, 2005, **5**, 325.
- 381 Y. Bae, W.-D. Jang, N. Nishiyama, S. Fukushima and K. Kataoka, *Mol. Biosyst.*, 2005, **1**, 242.
- 382 L. Li, J. K. Kim, K. M. Huh, Y.-k. Lee and S. Y. Kim, *Carbohydr. Polym.*, 2012, **87**, 2120.
- 383 L. Li, K. Huh, Y.-K. Lee and S. Kim, *Macromol. Res.*, 2010, **18**, 153.
- 384 Z. Poon, S. Chen, A. C. Engler, H.-i. Lee, E. Atas, G. von Maltzahn, S. N. Bhatia and P. T. Hammond, *Angew. Chem., Int. Ed.*, 2010, **49**, 7266.
- 385 A. J. Simnick, C. A. Valencia, R. Liu and A. Chilkoti, *ACS Nano*, 2010, **4**, 2217.
- 386 J. Huang, C. Bonduelle, J. Thévenot, S. Lecommandoux and A. Heise, *J. Am. Chem. Soc.*, 2012, **134**, 119.
- 387 S. Santra and J. M. Perez, *Biomacromolecules*, 2011, **12**, 3917.
- 388 F. Kratz, *J. Controlled Release*, 2008, **132**, 171.
- 389 R. Xu, M. Fisher and R. L. Juliano, *Bioconjugate Chem.*, 2011, **22**, 870.
- 390 K. Michaelis, M. M. Hoffmann, S. Dreis, E. Herbert, R. N. Alyautdin, M. Michaelis, J. Kreuter and K. Langer, *J. Pharmacol. Exp. Ther.*, 2006, **317**, 1246.
- 391 P. Magadala and M. Amiji, *AAFS J.*, 2008, **10**, 565.
- 392 J. Kreuter, T. Hekmatara, S. Dreis, T. Vogel, S. Gelperina and K. Langer, *J. Controlled Release*, 2007, **118**, 54.
- 393 K. Ulbrich, T. Hekmatara, E. Herbert and J. Kreuter, *Eur. J. Pharm. Biopharm.*, 2009, **71**, 251.
- 394 H. Wartlick, K. Michaelis, S. Balthasar, K. Strebhardt, J. Kreuter and K. Langer, *J. Drug Targeting*, 2004, **12**, 461.
- 395 S. Wagner, F. Rothweiler, M. G. Anhorn, D. Sauer, I. Riemann, E. C. Weiss, A. Katsen-Globa, M. Michaelis, J. Cinatl Jr, D. Schwartz, J. Kreuter, H. von Briesen and K. Langer, *Biomaterials*, 2010, **31**, 2388.
- 396 M. G. Anhorn, S. Wagner, J. r. Kreuter, K. Langer and H. von Briesen, *Bioconjugate Chem.*, 2008, **19**, 2321.
- 397 I. Steinhauser, B. Spänkuch, K. Strebhardt and K. Langer, *Biomaterials*, 2006, **27**, 4975.
- 398 C.-L. Tseng, T.-W. Wang, G.-C. Dong, S. Yueh-Hsiu Wu, T.-H. Young, M.-J. Shieh, P.-J. Lou and F.-H. Lin, *Biomaterials*, 2007, **28**, 3996.
- 399 C.-L. Tseng, S. Y.-H. Wu, W.-H. Wang, C.-L. Peng, F.-H. Lin, C.-C. Lin, T.-H. Young and M.-J. Shieh, *Biomaterials*, 2008, **29**, 3014.
- 400 C.-L. Tseng, W.-Y. Su, K.-C. Yen, K.-C. Yang and F.-H. Lin, *Biomaterials*, 2009, **30**, 3476.
- 401 S. Balthasar, K. Michaelis, N. Dinauer, H. von Briesen, J. Kreuter and K. Langer, *Biomaterials*, 2005, **26**, 2723.
- 402 A. Taheri, R. Dinarvand, F. Atyabi, F. Nouri, F. Ahadi, M. H. Ghahremani, S. N. Ostad, A. T. Borougeni and P. Mansoori, *J. Biomed. Nanotechnol.*, 2011, **7**, 743.
- 403 A. Taheri, R. Dinarvand, F. S. Nouri, M. R. Khorramzadeh, A. T. Borougeni, P. Mansoori and F. Atyabi, *Int. J. Nanomed.*, 2011, **6**, 1863.
- 404 Z. Shen, W. Wei, H. Tanaka, K. Kohama, G. Ma, T. Dobashi, Y. Maki, H. Wang, J. Bi and S. Dai, *Pharmacol. Res.*, 2011, **64**, 410.
- 405 X.-H. Tian, F. Wei, T.-X. Wang, P. Wang, X.-N. Lin, J. Wang, D. Wang and L. Ren, *Int. J. Nanomed.*, 2012, **7**, 1031.
- 406 Z.-Y. Wang, Y. Zhao, L. Ren, L.-H. Jin, L.-P. Sun, P. Yin, Y.-F. Zhang and Q.-Q. Zhang, *Nanotechnology*, 2008, **19**, 445103.
- 407 R. B. Umamaheshwari and N. K. Jain, *J. Drug Targeting*, 2003, **11**, 415.
- 408 S. Ji, J. Xu, B. Zhang, W. Yao, W. Xu, W. Wu, Y. Xu, H. Wang, Q. Ni, H. Hou and X. Yu, *Cancer Biol. Ther.*, 2012, **13**, 206.
- 409 P. Couvreur, B. Kante, M. Roland, P. Guiot, P. Bauduin and P. Speiser, *J. Pharm. Pharmacol.*, 1979, **31**, 331.
- 410 V. Lenaerts, P. Couvreur, D. Christiaensleyh, E. Joiris, M. Roland, B. Rollman and P. Speiser, *Biomaterials*, 1984, **5**, 65.
- 411 J. Nicolas and P. Couvreur, *Wiley Interdiscip. Rev.: Nanomed. Nanobiotechnol.*, 2009, **1**, 111.
- 412 B. Stella, S. Arpicco, M. T. Peracchia, D. Desmaële, J. Hoebeke, M. Renoir, J. d'Angelo, L. Cattel and P. Couvreur, *J. Pharm. Sci.*, 2000, **89**, 1452.
- 413 B. Stella, V. Marsaud, S. Arpicco, G. Geraud, L. Cattel, P. Couvreur and J.-M. Renoir, *J. Drug Targeting*, 2007, **15**, 146.
- 414 Y. Gao, W. Gu, L. Chen, Z. Xu and Y. Li, *J. Controlled Release*, 2007, **118**, 381.
- 415 G. Wangwen, X. Zhenghong, G. Yu, C. Lingli and L. Yaping, *Nanotechnology*, 2006, **17**, 4148.
- 416 Y. Li, Y. Zhang, D. Yang, J. Hu, G. Lu and X. Huang, *J. Polym. Sci., Part A: Polym. Chem.*, 2010, **48**, 2084.
- 417 H. C. Kolb, M. G. Finn and K. B. Sharpless, *Angew. Chem., Int. Ed.*, 2001, **40**, 2004.
- 418 J. Nicolas, F. Bensaid, D. Desmaële, M. Grogna, C. Detrembleur, K. Andrieux and P. Couvreur, *Macromolecules*, 2008, **41**, 8418.
- 419 D. Brambilla, J. Nicolas, B. Le Droumaguet, K. Andrieux, V. Marsaud, P.-O. Couraud and P. Couvreur, *Chem. Commun.*, 2010, **46**, 2602.
- 420 B. Le Droumaguet, H. Souguir, D. Brambilla, R. Verpillot, J. Nicolas, M. Taverna, P. Couvreur and K. Andrieux, *Int. J. Pharm.*, 2011, **416**, 453.
- 421 D. Brambilla, R. Verpillot, M. Taverna, L. De Kimpe, B. Le Droumaguet, J. Nicolas, F. Mantegazza, M. Canovi, M. Gobbi, M. Salmona, V. Nicolas, W. Scheper, P. Couvreur and K. Andrieux, *Anal. Chem.*, 2010, **82**, 10083.
- 422 B. Le Droumaguet, J. Nicolas, D. Brambilla, S. Mura, A. Maksimenko, L. De Kimpe, E. Salvati, C. Zona, C. Airoidi,

- M. Canovi, M. Gobbi, M. Noiray, B. La Ferla, F. Nicotra, W. Scheper, O. Flores, M. Masserini, K. Andrieux and P. Couvreur, *ACS Nano*, 2012, **6**, 5866.
- 423 D. Brambilla, R. Verpillot, B. Le Droumaguet, J. Nicolas, M. Taverna, J. Kňa, B. Lettiero, S. H. Hashemi, L. De Kimpe, M. Canovi, M. Gobbi, V. Nicolas, W. Scheper, S. M. Moghimi, I. Tvaroška, P. Couvreur and K. Andrieux, *ACS Nano*, 2012, **6**, 5897.
- 424 Y. Li, M. Ogris, E. Wagner, J. Pelisek and M. Ruffer, *Int. J. Pharm.*, 2003, **259**, 93.
- 425 N. Parker, M. J. Turk, E. Westrick, J. D. Lewis, P. S. Low and C. P. Leamon, *Anal. Biochem.*, 2005, **338**, 284.
- 426 H. Gelderblom, J. Verweij, K. Nooter and A. Sparreboom, *Eur. J. Cancer*, 2001, **37**, 1590.
- 427 E. Harper, W. Dang, R. G. Lapidus and R. I. Garver, Jr., *Clin. Cancer Res.*, 1999, **5**, 4242.
- 428 T. Meyer, J. F. Marshall and I. R. Hart, *Br. J. Cancer*, 1998, **77**, 530.
- 429 D. K. Armstrong, S. H. Kaufmann, Y. L. Ottaviano, Y. Furuya, J. A. Buckley, J. T. Isaacs and N. E. Davidson, *Cancer Res.*, 1994, **54**, 5280.
- 430 A. R. Kamer, P. G. Sacks, A. Vladutiu and C. Liebow, *Int. J. Mol. Med.*, 2004, **13**, 143.
- 431 M. A. Chaudhry, *Mutat. Res.*, 2006, **597**, 98.
- 432 J. N. Weinstein, R. R. Eger, D. G. Covell, C. D. Black, J. Mulshine, J. A. Carrasquillo, S. M. Larson and A. M. Keenan, *Ann. N. Y. Acad. Sci.*, 1987, **507**, 199.
- 433 N. J. Abbott, A. A. Patabendige, D. E. Dolman, S. R. Yusof and D. J. Begley, *Neurobiol. Dis.*, 2010, **37**, 13.
- 434 J. Correale and A. Villa, *Neurochem. Res.*, 2009, **34**, 2067.
- 435 U. Bickel, T. Yoshikawa and W. M. Pardridge, *Adv. Drug Delivery Rev.*, 2001, **46**, 247.
- 436 M. Amidi, S. G. Romeijn, G. Borchard, H. E. Junginger, W. E. Hennink and W. Jiskoot, *J. Controlled Release*, 2006, **111**, 107.
- 437 M. J. Turk, G. J. Breur, W. R. Widmer, C. M. Paulos, L. C. Xu, L. A. Grote and P. S. Low, *Arthritis Rheum.*, 2002, **46**, 1947.
- 438 M. Gowen, D. D. Wood, E. J. Ihrie, M. K. McGuire and R. G. Russell, *Nature*, 1983, **306**, 378.
- 439 V. P. Torchilin, *Biopolymers*, 2008, **90**, 604.
- 440 L. Zhou, M. M. Chong and D. R. Littman, *Immunity*, 2009, **30**, 646.
- 441 M. G. Bernengo, G. C. Doveil, M. Meregalli, A. Appino and R. Massobrio, *Br. J. Dermatol.*, 1988, **119**, 207.
- 442 R. Colle, T. Ceschia, A. Colatutto and F. Biffoni, *Curr. Ther. Res. Clin. E*, 1988, **44**, 1045.
- 443 M. A. Kisel, L. N. Kulik, I. S. Tsybovsky, A. P. Vlasov, M. S. Vorob'yov, E. A. Kholodova and Z. V. Zabarovskaya, *Int. J. Pharm.*, 2001, **216**, 105.
- 444 G. Russell-Jones, S. Westwood, P. Farnworth, J. Findlay and H. Burger, *Bioconjugate Chem.*, 1995, **6**, 34.
- 445 S. A. Shoyeal and S. Cawthorne, *Adv. Drug Delivery Rev.*, 2006, **58**, 1009.
- 446 D. Castanotto and J. J. Rossi, *Nature*, 2009, **457**, 426.